University of Glasgow

Li, Ang (2011) *Investigating the roles of Fascin and Rac1 in cell migration, invasion and metastasis.*
PhD thesis.

http://theses.gla.ac.uk/2849/

Copyright and moral rights for this thesis are retained by the author

A copy can be downloaded for personal non-commercial research or study, without prior permission or charge

This thesis cannot be reproduced or quoted extensively from without first obtaining permission in writing from the Author

The content must not be changed in any way or sold commercially in any format or medium without the formal permission of the Author

When referring to this work, full bibliographic details including the author, title, awarding institution and date of the thesis must be given

Glasgow Theses Service
http://theses.gla.ac.uk/
theses@gla.ac.uk

Investigating the roles of Fascin and Rac1 in cell migration, invasion and metastasis

Ang Li

Beatson Institute for Caner Research

Glasgow University

Faculty of Medicine

A Thesis submitted for Degree of Doctor of Philosophy

July 2011

Abstract

Cell migration and invasion is a central process in embryonic development, wound healing and immune responses. Errors during this process have serious consequences, including mental retardation, vascular disease, tumor formation and metastasis. An understanding of the mechanism by which cells migrate and invade may lead to the development of novel therapeutic strategies for controlling, for example, cancer metastasis.

Fascin is an actin-bundling protein involved in filopodia assembly and cancer invasion and metastasis of multiple epithelial cancer types. In this thesis, I have investigated the role of fascin in invadopodia formation, which are invasive finger-like protrusions that cancer cells use to invade into and degrade extracellular matrix. I demonstrated that fascin and its actin bundling activity are required for the assembly of the actin cytoskeleton at invadopodia as well as for the degradation of matrix. Fascin is a very stable component of invadopodia and its presence enhance the stability of actin structures at invadopodia. Furthermore, fascin is required for invasive migration into collagen I-Matrigel gels particularly in cell types that use an elongated mesenchymal type of motility in 3D. These data provide a potential molecular mechanism for how fascin increases the invasiveness of cancer cells.

During embryogenesis, melanoblasts proliferate and migrate ventrally through the developing dermis and epidermis as single cells. In the second part of this thesis, I examined the importance of small Rho GTPase Rac1 on melanoblast migration during development. I demonstrate that targeted deletion of Rac1 in the melanoblasts of developing mice causes defects in migration, cell cycle progression and cytokinesis. Rac1 null cells migrate markedly less efficiently, but surprisingly global steering, crossing the dermal/epidermal junction and homing to hair follicles are normal. Melanoblasts navigate in the epidermis using two classes of protrusion: short stubs and long pseudopods. Short stubs are driven by actin assembly, but unexpectedly are independent of Rac1, Arp2/3 complex, myosin or microtubules. Rac1 positively regulates

the frequency of initiation of long pseudopods, which promote migration speed and directional flexibility. Scar/WAVE and Arp2/3 complex drive actin assembly for long pseudopod extension, which is also microtubule dependent. Myosin contractility balances the extension of long pseudopods by effecting retraction and allowing force generation for movement through the complex 3D epidermal environment. In addition, I demonstrated that expression of activated N-Ras did not affect migration and proliferation of melanoblast during embryogensis. However, Rac1 is required for constitutively active N-Ras induced dermal melanocytes survival in mice.

Declaration

I declare that all of the work in this thesis was performed personally. No part of this work has been submitted for consideration as part of any other degree or award.

Acknowledgments

I would like to take this opportunity to express my appreciation to Prof. Laura Machesky for giving me the chance to study for this PhD. As a supervisor, she was always there to help, listen and support me whatever the cost; I could not have wished for a kinder or more considerate supervisor. As a role model, her enthusiasm towards science has certainly encouraged me to march forward in the field of biology after this PhD. I would like to thank Prof. Owen Sansom, Prof. Robert Insall and my advisor Dr. Kurt Anderson for their continuous enthusiasm and discussions.

Thanks to all R2 and R6 members, past and present, and to all the lovely friends I have made at the Beatson for their help, support. Without them, my PhD time would have been far less colorful. A big thank you to all of the support staff throughout the Beatson Institute for their invaluable help, especially Margaret and Tom for teaching me everything I know about microscopy.

Thanks to my parents, BaoHeng Li and Hong Li, who have worked very hard in order to send their son for higher education. I will always be in debt to their unconditional love. Also my lovely girl friend Grace Xu, who has helped me through the ups and downs of the last three years, and without whom life would be a much poorer place.

Finally, I would like to thank Cancer Research UK for the four years of funding, without which I would not have been able to complete this thesis.

Publication arising from this work included within this thesis

Li A, Dawson JC, Forero-Vargas M, Spence HJ, Yu X, König I, Anderson K, Machesky LM. The actin-bundling protein fascin stabilizes actin in invadopodia and potentiates protrusive invasion. *Curr Biol.* 2010 Feb 23;20(4):339-45.

Machesky LM, **Li A**. Fascin: Invasive filopodia promoting metastasis. *Commun Integr Biol.* 2010 May;3(3):263-70.

Scott RW, Hooper S, Crighton D, **Li A**, König I, Munro J, Trivier E, Wickman G, Morin P, Croft DR, Dawson J, Machesky LM, Anderson KI, Sahai EA, Olson MF. LIM kinases are required for invasive path generation by tumor and tumor-associated stromal cells. *J Cell Biol.* 2010 Oct 4;191(1):169-85.

Li A, Ma Y, Yu X, Mort R, Lindsay C, Insall RH, Chernoff J, Snapper SB, Jackson I, Larue L, Sansom O, Machesky LM. Rac1 drives melanoblast organization during mouse development by orchestrating pseudopod-driven motility and cell cycle progression. *Dev Cell* in press.

Abbreviations

Abi	Abl-kinase interacting protein
ADAM	A Disintegrin And Metalloproteinase
ADP	Adenosine diphosphate
AhR	Aryl hydrocarbon receptor
Arp2/3	Actin related protein 2/3
ATP	Adenosine Triphosphate
Brdu	5-Bromo-2′-deoxyuridine
BSA	Bovine serum albumin
$CaCl_2$	Calcium chloride
Cdc42	Cell division control protein 42 homolog
Cre	Cre recombinase
CREB	cAMP response element-binding
Cyfip	Cytoplasmic fragile-X mental retardation interacting protein
CO_2	Carbon dioxide
DAB	3.3'-diaminobenzidine
DAPI	4',6-diamidino-2-phenylindole
DC	Dendritic cells
DCT	Dopachrome tautomerase
DMEM	Dulbecco's Modified Eagle Medium
DMSO	Dimethyl sulfoxide
Dock	Dedicator of cytokinesis
ECM	Extracellular matrix
Ena/VASP	Enabled/vasodilator-stimulated phosphoprotein
ERK	Extracellular signal-regulated kinase
FAK	Focal adhesion kinase
FBS	Foetal Bovine Serum
FLIM	Fluorescence lifetime imaging microscopy
FRAP	Fluorescence recovery after photobleaching
FRET	Fluorescence resonance energy transfer
G	Glycine
GAP	GTPase activating protein
GAPDH	Glyceraldehyde 3-phosphate dehydrogenase
GDI	Guanine nucleotide dissociation inhibitor
GDP	Guanosine diphosphate
GEF	Guanine nucleotide exchange factor
GFP	Green fluorescent protein
GTP	Guanosine triphosphate
H_2O	Water
HBSS	Hank's Buffered Salt Solution
HBS	HEPES buffered saline
HCl	Hydrochloric acid
HNSCC	Head and neck squamous cell carcinoma
H-Ras	Transforming protein p21
HSPC300	Haematopoietic stem/progenitor cell protein 300
IRSP53	Insulin receptor substrate protein 53
IRTKS	Insulin receptor tyrosine kinase substrate
JNK	c-Jun N-terminal kinases

Kit	Kit receptor tyrosine kinase
KitL	Kit ligand
K-Ras	V-Ki-ras2 Kirsten rat sarcoma viral oncogene homolog
MAP	Mitogen-activated protein kinase
MARCKS	Myristoylated alanine-rich C-kinase substrate
mDia	Diaphanous-related formin
MT1-MMP	Membrane-type 1 matrix metalloproteinase
miRNA	microRNA
Mitf	Microphthalmia-associated transcription factor
mRNA	Massager RNA
Nap1	NAK-associated protein 1
NaCl	Sodium chloride
NADPH	Nicotinamide adenine dinucleotide phosphate-oxidase
NaOH	Sodium hydroxide
NF-κB	Nuclear factor kappa-light-chain-enhancer of activated B cells
NH_4CL	Ammonium chloride
N-Ras	Neuroblastoma RAS viral oncogene homolog
N-WASP	Neural Wiskott-Aldrich syndrome protein
OHT	4-hydroxytamoxifen
p53	Tumor protein 53
Pak	p21 activated kinase
PanIN	Pancreatic Intraepithelial Neoplasia
PBS	Phosphate Buffered Saline
PDAC	Ancreatic ductal adenocarcinoma
PE	PBS/EDTA
PI3K	Phosphatidylinositol 3-kinases
PIP2	Phosphatidylinositol 4,5-bisphosphate
PKC	Protein kinase C
Q	Glutamine
Rac	Ras-related C3 botulinum toxin substrate
Ras	RAt sarcoma
RFP	Red fluorescent protein
Rho	Ras homolog gene family
ROCK	Rho kinase
RT	Room temperature
S	Serine
SAPK	Stress-activated protein kinase
Sox10	SRY (sex determining region Y)-box 10
SCID	Severe combined immune deficiency
Src	Sarcoma
shRNA	Small hairpin RNA
siRNA	Small interfering RNA
SNAI2	Snail homolog 2
SNARE	Soluble N-ethylmaleimide sensitive fusion protein attachment protein receptor
TAE	Tris-acetate-EDTA
TE	Tris-EDTA
TBST	TBS Tween
TNF	Tumour necrosis factor

TPA	Phorbol 12-myristate 13-acetate
TSP	Thrombospondin
WASP	Wiskott-Aldrich syndrome protein
WAVE	WASP family verprolin homologous
X-Gal	5-bromo-4-chloro-3-indolyl-β-D-galactopyranoside

Table of Contents

List of Figures and Tables

Chapter I
Introduction

1.1 Actin based cell motility

1.1.1 2D Cell migration

The directional migration of cancer cells largely relies on the actin cytoskeleton and its regulatory proteins, and indeed, cell motility genes are often found to be upregulated at certain stages during the metastasis progression (Machesky, 2008; Nürnberg et al., 2011). During migration on 2D surface, cells in response to an external signal, which leads to the generation of protrusions in the direction of migration such as lamellipodia and filopodia. In malignant cancer cells, another kind of actin-based protrusion termed invadopodia are generated from ventral surface of a cell and have proteolytic activity toward extracellular matrix (Figure 1.1). Within these protrusions, the actin cytoskeleton is dynamically remodelled into different kinds of protrusive structures that lie just beneath the plasma membrane and force generated by these protrusive structures pushes the plasma membrane forward which coupled with adhesion of this leading edge to the substrate drives cell migration.

1.1.2 Actin polymerization

The protrusive force of leading edge extension is generated by polymerization of globular actin (G-actin) subunits to form a double helical polymer called an actin filament (F-actin) (Pollard and Cooper, 2009). Based on the arrowhead-like appearance created by decoration with the moter domain of myosin, one end is called the barbed end and the other the pointed end (Small et al., 1978). The initial stage of actin polymerization is called nucleation. This process is a rate-limiting step due to the considerable instability of actin oligomers. Once the nucleus (trimer) is formed, actin polymerization proceeds quickly at the plus or barbed end and dissociation of actin monomers is favored at minus or pointed end (Bugyi and Carlier, 2010; Pollard and Cooper, 2009). This kinetic asymmetry between the two ends is achieved by ATP hydrolysis. The ATP in actin filaments is hydrolyzed to ADP. Because the

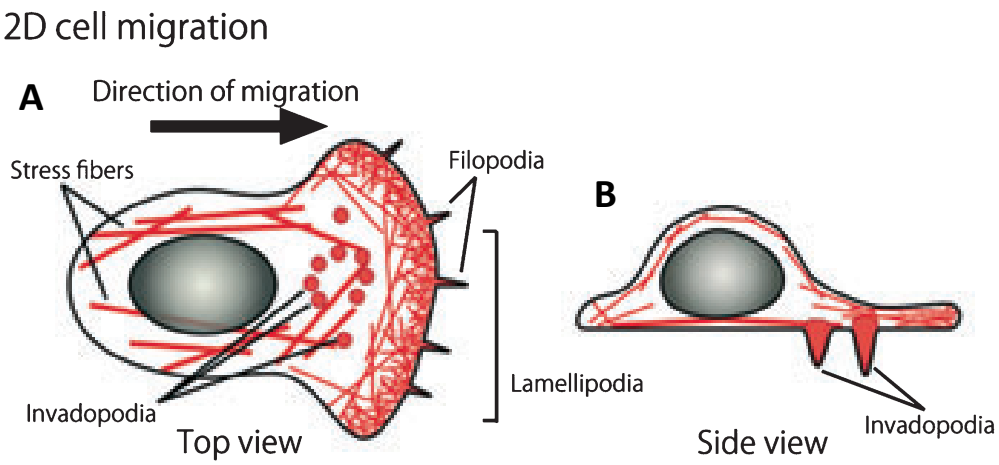

Figure 1.1 Actin-based structures in metazoan cells.
A metazoan cell migrate on a 2D surface. Characteristic actin structures are commonly seen in many cell types. They generally form lamellipodia, filopodia, and stress fibers. whereas invadopodia are recognised as large actin dots. (B) side view of a cell, emphasizing that invadopodia are ventral. Figure adapted from (Kurisu and Takenawa, 2010).

ADP-actin has lower binding affinity to the filaments end than ATP-actin and hydrolysis of ATP in the F-actin is irreversible, consequently, depolymerization is favoured at pointed end. Subsequently, ADP-actin monomers released from old filaments then undergo nucleotide exchange for next round of polymerization. Furthermore, because the barbed end of actin filaments face toward the cell plasma membrane, thus under cellular conditions, incorporation of new actin subunits at the barbed end provides mechanical force for the generation of membrane protrusions in migrating cells. In vivo, spontaneous formation of actin nuclei is disfavored due to the strong kinetic barrier and the large concentrations of monomer binding/sequestering proteins in cells (e.g. thymosin beta 4 and profilin). Therefore, F-actin polymerization is regulated by several actin nucleators from a number of different families and is assisted by various proteins that bind to actin monomers or to filament ends.

1.1.3 Lamellipodia

Actin powers protrusions by polymerizing just under the plasma membrane. One of the filament geometries is the formation of branched actin filaments, which lead to generation of sheet-like protrusions consist of highly branched short actin filaments at cell leading edge, termed lamellipodia, which are important in cell motility and cell spreading (Figure 1.2) (Nobes et al., 1995; Ridley et al., 1992). The major actin nucleator within lamellipodia is Arp2/3, an assembly of 7 subunits that include two actin related proteins Arp2 and Arp3 and five non-Arp components, p41/ARPC1, p34/ARPC2, p21/ARPC3, p20/ARPC4 and p16/ARPC5, which was the first actin nucleation factor to be identified (Machesky et al., 1994). Arp2/3 complex binds to the preexisting 'mother' filaments and promotes the formation of new 'daughter' filaments branching at a 70^{o} angle from preexisting filaments. Other regulators of actin dynamics at leading edge of lamellipodia include ADF/cofilin, which bind G-actin monomers and depolymerize actin filaments through severing and increasing off-rate for actin monomers from the pointed end, thus maintain the G-actin monomer pool for polymerization at the plus end (McGough et al.,

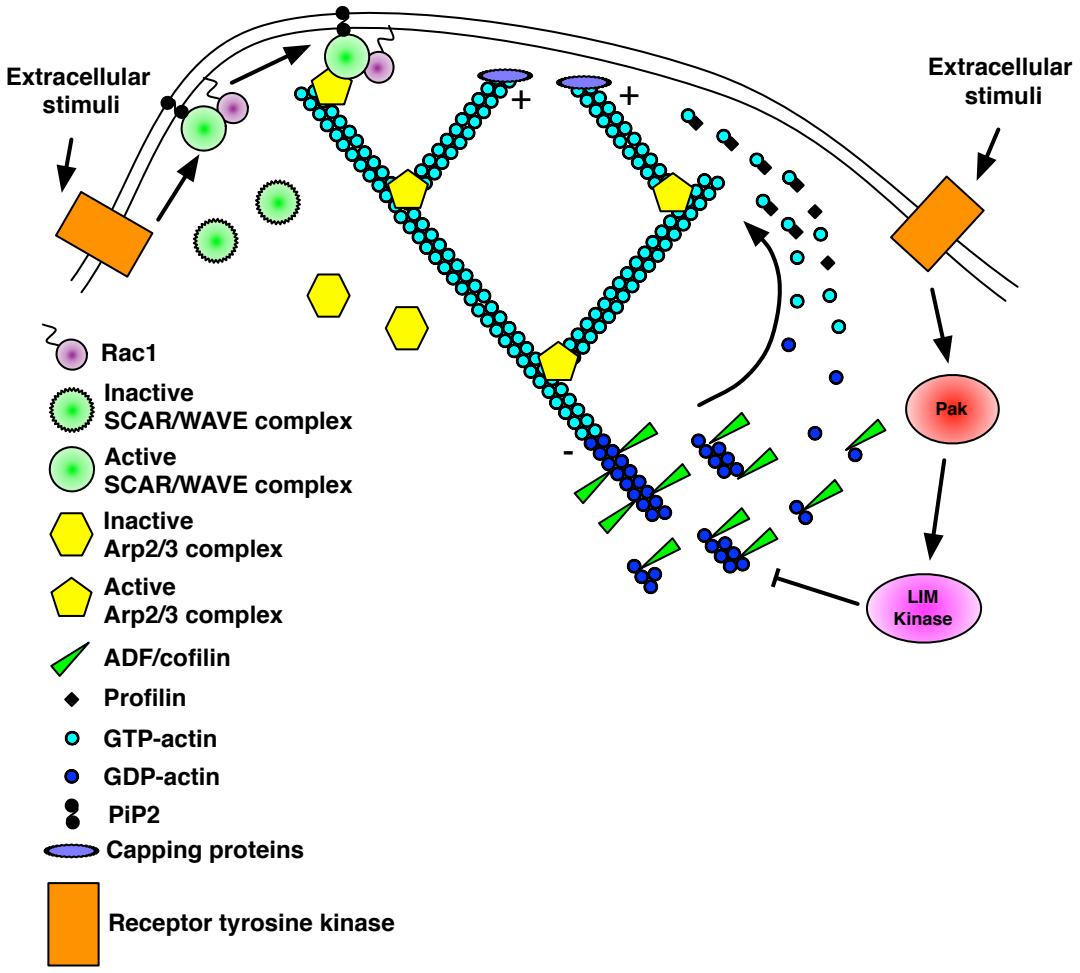

Figure 1.2 The regulation of lamellipodia formation.
Simple schematic diagram of the regulation of actin polymerisation leading to lamellipodia formation. Scar/WAVE complex is recruited to the plasma membrane, possibly via the small GTPase Rac1 in response to a variety of signals. where it activates Arp2/3 complex to polymerize actin filaments at the free barbed ends off the sides of actin filaments near the plasma membrane. Branches grow and push against the plasma membrane. ADP bound actin filaments were depolymerized by binding of ADF/cofilin and actin monomers undergo a rapid cycling from ADP to ATP bound forms that is promoted by profilin. Rac or Cdc42 acts via group I Paks to stimulate LIMK, which inhibit cofilin-induced actin depolymerization, allowing increased accumulation of polymerized actin at the leading edge of cells.

1997). Other proteins include profilin, which binds and incorporates G-actin from the cytoplasmic pool to the growing barbed ends of the actin filaments. Capping protein, which binds to the barbed end of actin filaments. Capping protein restricts actin polymerization and affects the balance between branched and unbranched networks. Therefore, it optmizes the rate of motility by promoting more frequent filament nucleation by the Arp2/3 complex (Akin and Mullins, 2008; Dos Remedios et al., 2003; Le Clainche and Carlier, 2008).

As Arp2/3 complex itself has little nucleation activity, nucleation-promoting factors (NPFs) are thus required to initiate a new actin filament via activation of Arp2/3 complex (Campellone and Welch, 2010). The main NPFs to activate Arp2/3 complex are the WASP family proteins, of which the best known are N-WASP and SCAR/WAVE complex. SCAR/WAVE complex, which consists of five subunits (SCAR/WAVE, HSPC300, Abi, Nap1, and Cyfip) has been shown to be the major NPF to activate Arp2/3 complex in lamellipodia. SCAR/WAVE complex interacts with Arp2/3 complex and G-actin via Scar/WAVE verprolin central acidic domain (VCA) domain and this facilitates Arp2/3 catalytic activity (Insall and Machesky, 2009). SCAR/WAVE complex also acts as a scaffold that directly or indirectly link Arp2/3 complex activity to various regulatory proteins such as the Rho family of small GTPases. SCAR/WAVE complex interacts with the small GTPase Rac1 (described below) via Cyfip and it has been proposed to be recruited to the plasma membrane at sites of lamellipodial assembly by Rac1, thus allow signaling to catalyze rapid filament growth (Innocenti et al., 2004; Kunda et al., 2003).

However, this dendritic branched network model of actin filament organization in the protruding lamellipodia is recurrently being challenged. Victor Small and colleagues used cryo-electron tomograms and negatively stained cytoskeletons to visulaise actin networks in the lamellipodia in frozen 'live' cells (Urban et al., 2010). They demonstrate that actin filaments at the leading edge diverge at various angles and are unbranched. The authors propose a new model for lamellipodial protrusion and suggest that Arp2/3 nucleates actin filaments on the membrane and rides on the filament pointed end after nucleation initiated by WAVE complex until being released and recycled at the lamellipodium tip. They propose that tetramers of VASP, a barbed end binding

protein that can compete with capping protein, mediates elongation of long unbranched filaments adjacent to the plasma membrane (Urban et al., 2010).

1.1.4 Filopodia

In addition to lamellipodia, filopodia are slender cytoplasmic projections that extend beyond the leading edge of lamellipodia in migrating cells. They are made up of bundles of parallel actin filaments, which grow at the tip end (Oldenbourg et al., 2000). They can form focal adhesions with the substratum and are believed to function as directional sensors (Zheng et al., 1996). Earlier work suggested that N-WASP localizes to filopodia and that activation of N-WASP by the small Rho GTPase Cdc42 leads to filopodia formation (Nobes et al., 1995; Stradal et al., 2004). Thus, it has been proposed that filopodia are generated by the reorganization of an Arp2/3 complex generated actin network (Figure 1.3). Proteins that mediate filament elongation such as VASP and formins bind to actin filaments in lamellipodia and come together to form a filopodial tip complex that elongates a group of actin filaments (Figure 1.3) (Gupton and Gertler, 2007). The filopodial tip complex initiates filament cross-linking by recruiting and activating fascin (described below), which then allows the bundling process to keep pace with elongation and guarantees efficient pushing which then forming a filopodium. However, deletion of N-WASP does not inhibit filopodia formation (Snapper et al., 2001). Furthermore, inhibition of Arp2/3 or WAVE complex only minimally affects filopodial protrusion (Steffen et al., 2006) . In addition, a recent study reported filopodia formation in $Cdc42^{-/-}$ fibroblastoid cells (Czuchra et al., 2005), but another paper disputes this and demonstrates a crtitical role for Cdc42 in filopodia formation in mouse embryonic fibroblast (Yang et al., 2006). Alternatively, it is proposed that filopodia are initiated by *de novo* nucleation of actin filaments presumably close to the plasma membrane, driven by the action of formins, which have been localised to filopodia tips for generating unbranched actin filaments (Gupton and Gertler, 2007). These assemblies of parallel nascent filopodial actin filaments are cross-linked by actin-bundling

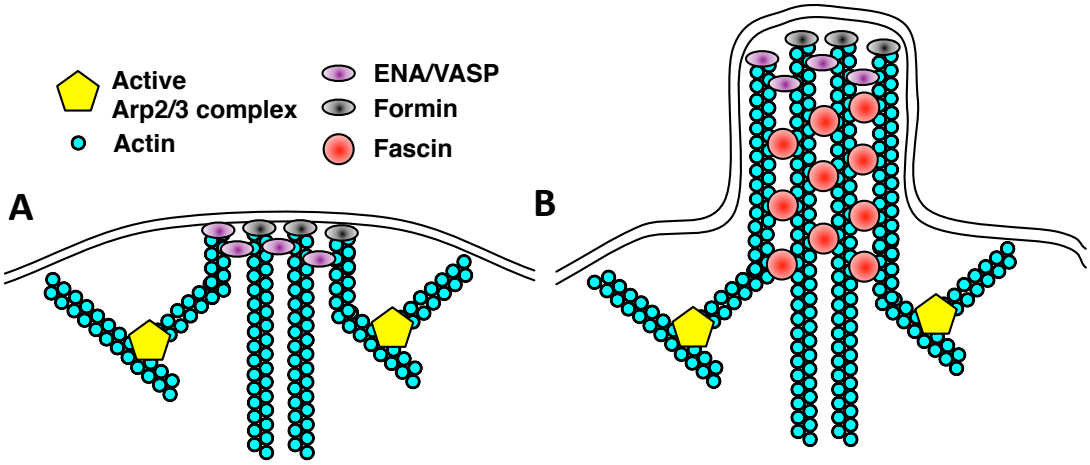

Figure 1.3 The regulation of filopodia formation.
Simple schematic diagram of the regulation of actin polymerisation leading to filopodia formation. (A) A subset actin filaments of the ARP2/3 ceomplex nucleated dendritic network are targeted for continued elongation by the formin and/or by ENA/VASP proteins. Formin also nucleates the formation of new, unbranched actin filaments. ENA/VASP proteins can also function as initial F-actin-crosslinking proteins in the tip of an elongating filopodium. (B) The incorporation of the actin crosslinking protein fascin in the shaft of the filopodium generates a stiff actin filament bundle. Formins and/or by ENA/VASP are localized in the 'tip complex' and controls the barbed-end elongation of the filaments.

proteins for force generation.

1.1.5 Invadopodia

1.1.5.1 Introduction to Invadopodia

Invadopodia are finger like protrusions especially formed in invasive, tumoral, or transformed cells when they are grown on a thin layer of ECM (eg. gelatin or fibronectin). Invadopodia are observed as proteolytcally active protrusions that extend from the ventral surface of the cell, into the surrounding matrix, cause the focal pericellular degradation of ECM (Figure 1.4A). Invadopodia have highly dynamic actin that resembles actin comets when viewed with GFP-actin in time lapse (Baldassarre et al., 2006). Invadopodia are normally close to the nucleus and proximal to the Golgi complex (Baldassarre et al., 2003). At ultrastructural level, invadopodia have been suggested to be large convolutions of cell membrane with long membrane extensions into the matrix, and these protrusions originate from the larger invagination at the ventral surface of cell with diameters range from hundreds of nm to a few μm (Baldassarre et al., 2003; Bowden et al., 1999). Under the fluoresce microscope, invadopodia appear as actin-rich formations with underlying holes of ECM degradation, and by using this kind of assay, several actin associated proteins, some special proteases and other cellular components are identified to be important for the formation of invadopodia over the past decade.

1.1.5.2 Regulation of invadopodia formation

Previous studies have implicated the N-WASP-Arp2/3-cortactin-dynamin2 complex as a key player in invadopodia formation (Figure 1.4B) (Artym et al., 2006; Ayala et al., 2008; Baldassarre et al., 2003; Buccione et al., 2004; Gimona and Buccione, 2006). Interestingly, only N-WASP, but not WAVE proteins were identified within invadopodia (Lorenz et al., 2004; Yamaguchi and Condeelis, 2007; Yamaguchi et al., 2005). In addition, expression of

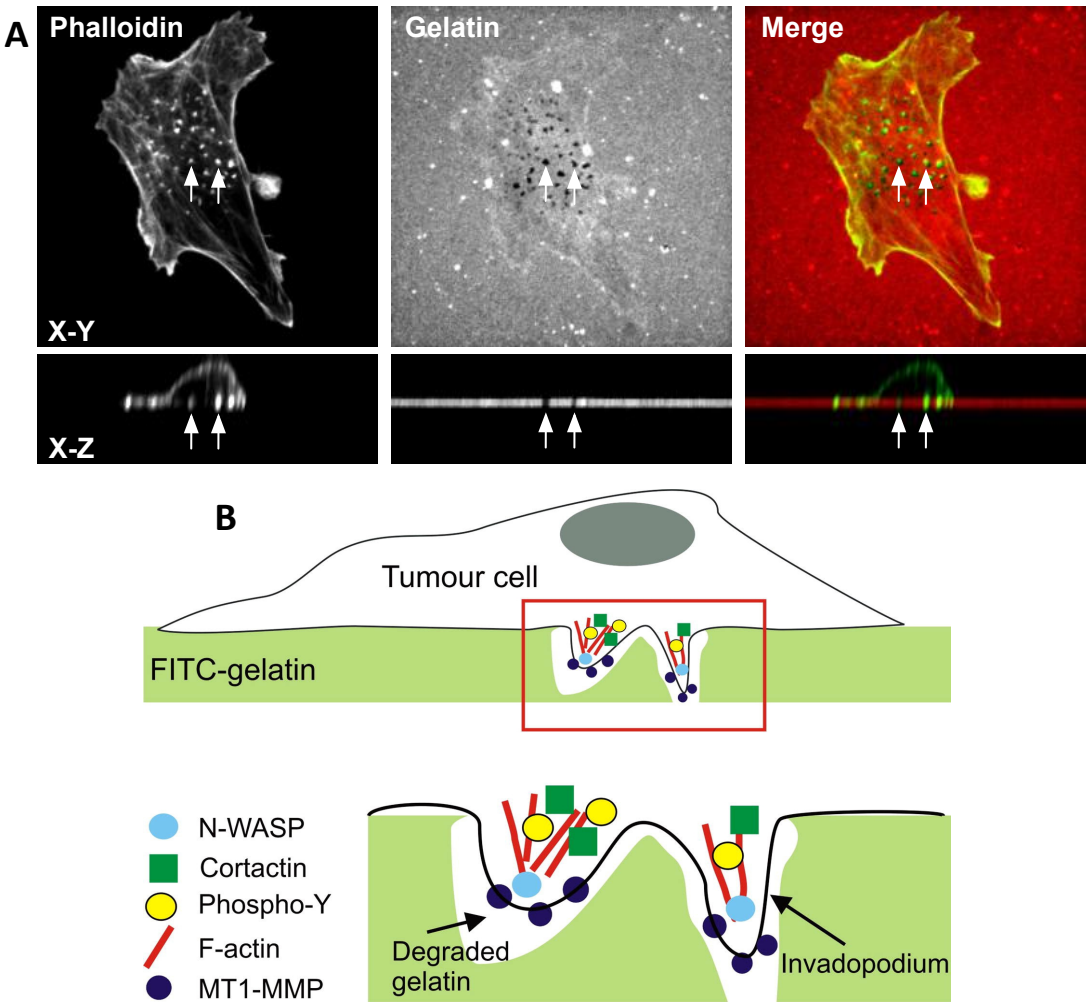

Figure 1.4 The regulation of invadopodia formation.
(A) MDA-MB-231 human breast adenocarcinoma cells cultured on Alexa594-gelatin coated glass coverslips were stained with Alexa488-phalloidin. Bottom images are XZ sections showing a cell with an invadopodium collected with a confocal microscope. Invadopodia and gelatin degradation were white arrowed. (B) Schematic diagram showing tumour cell with formation of invadopodia on a film of crosslinked gelatin. Degradation of gelatin by invadopodia-associated MT1-MMP results in the formation of fluorescence negative cavities beneath cells that can be visualised by confocal fluorescence microscopy. Invadopodia are enriched with actin branches regulated by N-WASP, Arp2/3 complex and cortactin. Figure B adapted from (Stylli et al., 2008).

dominant-active mutant of Cdc42 or Rac enhanced dot-like and diffused fibronectin degradation respectively in RPMI17951 melanoma cells (Nakahara et al., 2003). N-WASP drives formation of branched actin assembly via activation of the Arp2/3 complex. Expression of a truncated "dominant-negative" N-WASP strongly inhibited formation of invadopodia as well as ECM degradation (Mizutani et al., 2002). Cortactin and dynamin-2 may function as scaffolds to bring together a multifunctional protein complex, such as Arp2/3 complex and N-WASP, to coordinate cortical actin assembly/disassembly and protease secretion in a highly polarized manner (Artym et al., 2006; Clark and Weaver, 2008; Clark et al., 2007). Cortactin is a Src substrate that interacts with F-actin and can stimulate actin polymerization by direct interaction with the Arp2/3 complex. Cortactin is frequently used as a marker of invadopodia, due to its strong localization to these structures. Furthermore, research using live cell imaging to study the dynamics of invadopodia formation suggested that cortactin localization marks the early stage of invadopodia assembly (Artym et al., 2006). Furthermore, invadopodia are sites of tyrosine phosphorylation and require Src kinase signaling (Bowden et al., 2006). Adhesion receptors including many kinds of integrins and CD44, are also found enriched at invadopodia (Mueller et al., 1999). However, proteins that are important in focal adhesion complexes, such as vinculin, are not localized at invadopodia, indicating the specialized role of integrins at invadopodia compared with their function in focal adhesion complexes (Machesky, 2008). Notably, consistent with their matrix degradation activity, invadopodia are enriched in soluble proteases, such as MMP2, MMP9 and transmembrane metalloproteinases MT1-MMP (Clark and Weaver, 2008). Live-cell imaging showed that the ECM degradation happened almost simultaneously with the recruitment of MT1-MMP to the sites of invadopodia (Artym et al., 2006). There also must be a mechanism for the trafficking of proteases to the cell surface at invadopodia. Indeed, a potential mechanism for MMP delivery to invadopodia has emerged recently with the discovery of the role of the exocyst complex and SNARE proteins in MT1-MMP trafficking and invadopodia formation (Liu et al., 2009; Poincloux et al., 2009; Sakurai-Yageta et al., 2008; Steffen et al., 2008).

It has become now accepted that invadopodia initiation is due to engagement of cell surface integrins by substrate components. This was shown first for $\alpha_5\beta_1$ and $\alpha_3\beta_1$ integrins (Mueller et al., 1999), despite the specific integrin combination might be cell-type dependent. α3β1 integrin activation can promote Src dependent tyrosine phosphorylation of p190RhoGAP (Nakahara et al., 1998), which in turn affected the actin cytoskeleton, through the Rho family GTPases, thus activating membrane-protrusive and proteolytic activity, leading to invadopodia formation and cell invasion.

The actin filament organization during the formation of invadopodia, however, is still not clear, it may be possible that a precursor structure containing the N-WASP-Arp2/3-cortactin-dynamin2 complex results on the formation of a small branched actin network (Artym et al., 2006). The later development of invadopodia may involve both the insertion of new membrane material into the plasma membrane as suggested by the close spatial relationship between the Golgi complex and invadopodia, and also actin polymerization (Baldassarre et al., 2003). There are two possibilities regarding to the growth of actin-rich core in the invadopodia (Linder, 2007; Vignjevic and Montagnac, 2008). The first possibility is the continued growth of branched actin network initiated by the N-WASP and Arp2/3 complex though the whole invadopodia. The second possibility could be a process resembling the convergent growth of filopodia. This may involve the recruitment of actin bundling proteins, such as fascin, to crosslink the actin filaments that extend from the branched actin networks into bundles to push the plasma membrane. The latter possibility is supported by the observation that N-WASP was only active at the base of invadopodia (Lorenz et al., 2004), and Ena/VASP and diaphanous related formins mDia2 are required for invadopodia formation (Lizárraga et al., 2009; Philippar et al., 2008).

The correlation between invadopodia and structures found when cancer cells invade in a 3D matrix is not yet well understood. Recent studies showed that during initial step of metastasis, invasive cancer cells use invadopodia degrade a holes as they force through the basement membrane using a machinery based on Arp2/3 nucleated actin assembly and N-WASP-cortactin in a 3D experimental setting (Hotary et al., 2006; Schoumacher et al., 2010).

1.1.6 Podosomes

Podosomes were first identified within monocytic cells such as macrophages, dendritic cells and osteoclasts (Marchisio et al., 1984). Similar to invadopodia, podosomes also present as dot-like structures at the ventral cell surface, which are enriched in F-actin, (N-)WASP, Arp2/3 complex and cortactin (Buccione et al., 2004). The presence of actin polymerization proteins such as Arp2/3 complex and WASP differentiate podosomes from focal adhesions (Marchisio et al., 1988). Podosomes also show a ring consisting of adhesion plaque proteins such as paxillin, vinculin, talin, α-actinin, Src, and tyrosine-phosphorylated proteins surrounding the actin cores. The ultrastructure of dentritic cell podosome is recently been solved by transmission electron microscopy (Gawden-Bone et al., 2010), which contain actin foci surrounded by a specialised ring region that is rich in material containing paxillin, thus confirm the light microscopy data. In contrast, invadopodia seem to lack these ring structures (Gimona et al., 2008). Typically, cells form numerous (20-100) podosomes of roughly uniform size (1-2 μm diameter), but only few (1-10) invadopodia of varying size. In addition, podosomes are rapidly turned over, as fast as 2-4 mins whereas invadapodia are thought to be longer lived, can extend up to over 1 h (Linder, 2007). Podosomes are able to form widespread but only shallow zones of degradation, probably through their high number and fast turnover. In contrast, the longer-lived invadopodia form more aggressive, deeper matrix degradation. Little is known about the precise function of podosomes. In myeloid cells, podosomes are necessary for directional movement and trans-cellular diapedesis at sites of inflammation (Calle et al., 2006). In osteoclasts, podosomes are thought to aid in the creation of sealing rings associated with the area of bone resorption. A role in adhesion is considered due to the similarities between podosomes and focal adhesions. The dynamic nature of podosomes suggested that they might transfer membrane tension along the substrate, as the lamellipodium extends forwards (Buccione et al., 2004).

1.1.7 3D Cell migration: Mesenchymal vs Amoeboid

1.1.7.1 Introduction to 3D cell migration

Tumour cell invasion occurs in 3 dimensions. The behavior of cells in 3D has been studied within reconstituted extracellular matrices such as collagen and matrigel. Tumour cells can migrate using both actin-based protrusions and myosin-based contractile activities in 3D (Sahai, 2005; Wolf et al., 2003a), which have been described as mesenchymal type motility and amoeboid type motility (Figure 1.5).

1.1.7.2 Mesenchymal type motility

Mesenchymal cell migration as used by MDA-MB-231 carcinoma cells or HT1080 fibrosarcoma cells (Wolf et al., 2007), involves a long and narrow morphology aligned with the direction of migration**.** Mesenchymal cells move by the formation of actin-rich pseudopodia at the leading edge, driven by Rho GTPases Rac and Cdc42. Rac activity is required for protrusive actin polymerization and Cdc42 is important in defining polarity, largely through its positioning of the microtubule-organising centre between the nucleus and the leading edge. In addition, integrin clusters attach to the ECM and matrix metalloprotease activity is required for ECM degradation and navigating the cell through dense matrix (Friedl and Wolf, 2003).

1.1.7.3 Ameoboid type motility

Cells moving in an amoeboid mode, such as MTLn3 rat mammary adenocarcinoma and A375MM human melanoma cells (Sanz-Moreno et al., 2008; Wyckoff et al., 2006), are more rounded and more reliant on Rho and ROCK activity and acto-myosin contraction to remodel the cytoskeleton and propel them through gaps between matrix fibres. Cell using ameoboid type of migration normally squeeze through existing gaps in the ECM without clustering integrins or concentrating proteinases to sites of adhesion (Wolf et

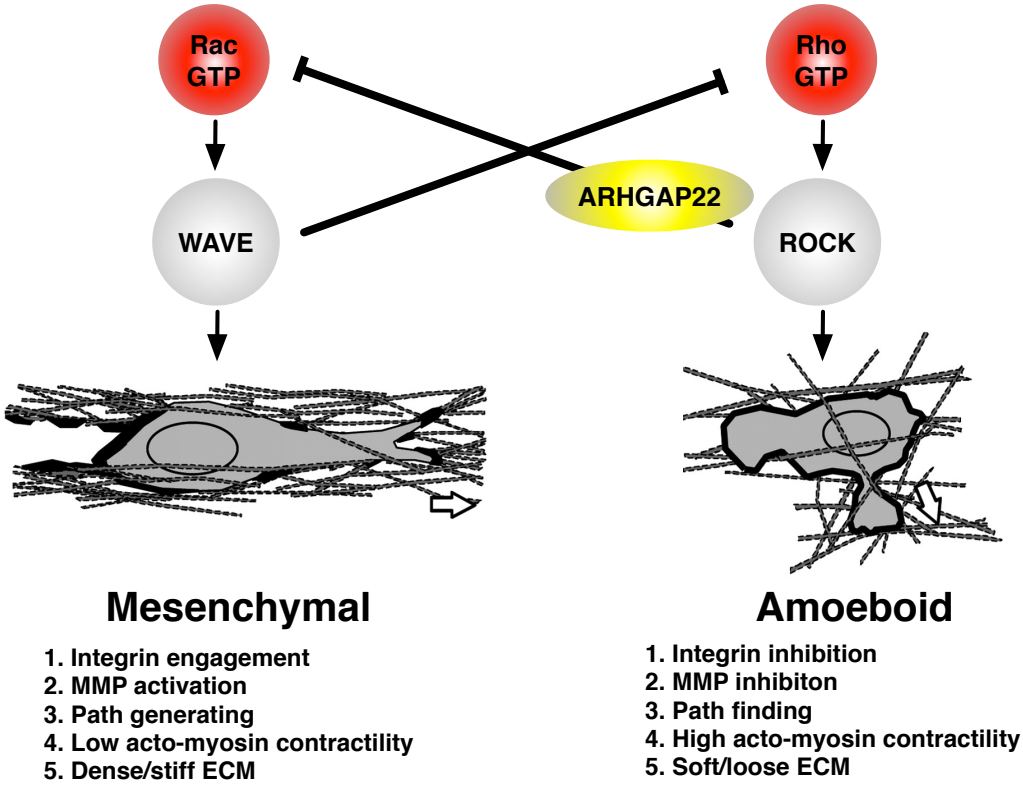

Figure 1.5 Reciprocal regulation between Rho and Rac during mesenchymal or amoeboid motility styles.
Rac, which drives oriented mesenchymal motility, leading edge protrusion and lamellipodia formation. Mesenchymal cells also use integrins to actively contact the ECM and use MMP to proteolytically degrade ECM to generate path for migration. Rho activation is responsible for amoeboid motility, a non-oriented movement which enables the cell to squeeze between gaps of ECM, which is integrin and MMP independent. mesenchymal or amoeboid motility are interchangable. Activated RhoA is able to inhibit Rac through the ARHGAP2, while Rac1 activates WAVE2 which in turn inhibits RhoA. Figure adapted from (Wolf et al., 2003).

al., 2003a), indicating that amoeboid type migration is ECM degradation independent (Sahai and Marshall, 2003; Wolf et al., 2003a). This is similar to the mechanism used by lymphocyte (Wolf et al., 2003b). In addition, The low levels of attachments to ECM made by amoeboid cells is believed to allow them to move faster through 3D environments than their mesenchymal counterparts (Paňková et al., 2010)

1.1.7.4 Regulation of mesenchymal and ameoboid type motility

It has been shown that tumour cells can invade using either amoeboid or mesenchymal type of movement, interchanging between the two depending on the up or down regulation of specific molecular pathways governing the mode of motility (Figure 1.5). For instance, activation of the Rac through a complex containing adaptor molecule NEDD9 and a Rac GEF DOCK3 is required for mesenchymal migration in A375MM cells. Rac signals through WAVE2 to direct mesenchymal movement and suppress amoeboid movement through decreasing myosin light chain phosphorylaton (Sanz-Moreno et al., 2008). It has also recently been proposed that Rab5 may play a role in the process of amoeboid to mesenchymal transition of cancer cells by influence the trafficking of Rac (Palamidessi et al., 2008). Conversely, in amoeboid movement, Rho-kinase signaling activates a Rac GAP, ARHGAP22, which inactivate Rac and suppress mesenchymal movement (Sanz-Moreno et al., 2008). In addition, a Cdc42 GEF DOCK10 and expression of dominant active Cdc42 can enhance the amoeboid migration and cell invasion by suppress Rac activity. Furthermore, the Cdc42 effectors N-WASP and Pak2 are required for the maintenance of the rounded-amoeboid phenotype in melanoma cells (Gadea et al., 2008). However, blocking Cdc42 also results in loss of mesenchymal morphology, suggest that Cdc42 is also involved in mesenchymal morphology.

When mesenchymal HT1080 and MDA-MB-231 cells were subject to protease inhibitors in 3D collagen matrix, they changed from mesenchymal morphology to amoeboid morphology (Wolf et al., 2003a). It is likely that

tumour cells can compensate to environmental factors by change the style of migration through different activation and effectors pathways.

1.2 Cancer metastasis

1.2.1 Metastasis is a multifaceted process

Metastasis is the ability of cancer cells to spread from their tissue of origin to other parts of the body via the bloodstream or the lymphatic system. It is a critical step in cancer progression and is a major cause of human cancer death (Sporn, 1997). Metastatic development is a multi-step process involving the acquisition of invasive behaviour, escape from the primary tumour, invasion into the surrounding tissue, transit in the circulatory system, and finally the establishment of secondary tumours at new sites (Figure 1.6) (Chambers et al., 2002). A primary step in the metastatic cascade is the detachment of cancer cells from a solid tumour mass, which is mediated by their decreased adhesive potential and dedifferentiation of epithelial cells toward a mesenchymal state. This process is termed epithelial-mesenchymal transition (EMT) (Thiery et al., 2009). One of the most important changes during this process is the down-regulation of E-cadherin, which under normal circumstances provides a bridge between adjacent epithelial cells and serves as a scaffold for anti-growth signalling to its downstream effectors such as β-catenin and TCF transcription factor (Christofori and Semb, 1999). As cell-cell junction proteins are suppressed, individual epithelial cancer cells start to separate from other cells that normally form a sheet-like structure. These cells become more elongated fibroblast-like and gain invasive features such as the up regulation of N-cadherin, fibronectin, metalloproteinases, and decrease in the abundance of protease inhibitors and altered expression of intergrins that preferentially bind the degraded stromal components produced by extracellular proteases (Lozano et al., 2003). Therefore, cells become differently polarised and rearrange their actin cytoskeleton with the formation of specific membrane protrusions. Matrix-degrading proteases are secreted at cell at leading edge to allow the cell to degrade and navigate through the basement membrane and extracellular matrix. Cancer cells get into the blood

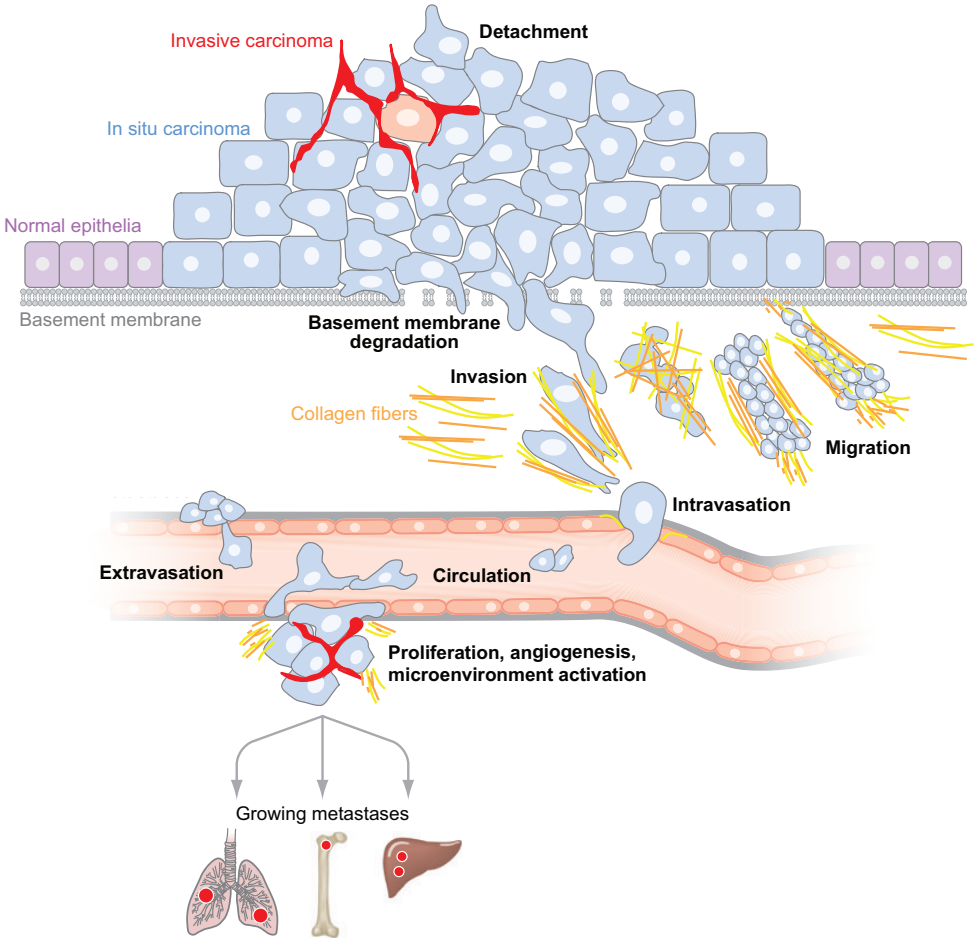

Figure 1.6 The main steps in the formation of a metastasis. Formation of metastases is a multistep process, involving loss of differentiation, enhanced proliferation and angiogensis. The active invasion of a subset of cancer cells then escape the primary tumour through the surrounding matrix, enter the circulation which they travel to the distant sites of the body, where they extravasate to populate new niches and form secondary lesions. Figure adapted from (Bacac and Stamenkovic, 2008).

vessel via process called intravasation. Once trapped in the vessel, cancer cells must be able to avoid anoikis (A form of programmed cell death which is induced by anchorage-dependent cells detaching from the surrounding ECM), oppose hydrostatic shear forces that could lead to physical damage and they also need to evade being targeted by immune surveillance probably via interaction with platelets, lymphocytes and other blood cells. As only a few cancer cells can finally survive and be able to escape from the vasculature via process called extravasation. This process requires adherence and invasion through endothelium and basement membrane into the new tissue. Surviving cancer cells can either undergo proliferation within the blood vessel to form a small tumour that can then physically disrupt the endothelium or, probably following leukocytes in a process similar to diapedesis (a process that leukocytes secrete proteases to degrade the basement membrane and allowing them to escape from the blood vessel) to eventually invade into the new tissue to establish growth as a metastasis. Within the new tissue, metastatic tumor cells will frequently undergo reversion from a mesenchymal phenotype back to something that is more similar to the original tumor.

1.2.2 Cell migration and invasion in cancer metastasis

Cell migration and invasion are required at multiple steps of metastasis – during invasion through the basement membrane and extracellular matrix toward blood or lymphatic vessels, into and out of a vascular or lymphatic vessel, and invading into the new tissue in distant organs. In addition, they are also important in many physiological events such as embryogenesis, morphogenesis, neurogenesis, angiogenesis, wound healing and inflammation. For instance, during embryogenesis, the directed migration of highly motile neural crest cells involves modulation of expression of the cell-cell adhesion molecule cadherin (Kuriyama and Mayor, 2008). Such change is commonly seen in invasive cancer cells undergo EMT and a lack of cadherins correlates with cancer cells that start to migrate. In addition, invasion is critical for leukocytes transmigrate through the endothelial cell layer from the bloodstream to invade to the sites of infection during inflammation (Madri and

Graesser, 2000). Moreover, the cellular similarities between wound healing and tumor cell invasion have been noted for some time and recent comparison of gene expression between these two cellular process further confirm these similarities at genetic level (Chang et al., 2004; Pedersen et al., 2003). Therefore, tumor cell migration and invasion are believed to be processes where normal cellular behaviors occur in a mis-regulated manner and in an inappropriate context.

1.3 Fascin: the actin bundling protein

1.3.1 Introduction to fascin

Fascin was originally characterized as a 55kDa actin-binding and bundling protein purified from extracts of sea urchin oocytes and coelomocytes and is later found to be highly conserved throughout evolution with the identification of orthologues in a number of other species, including the related Drosophila singed protein (Bryan et al., 1993; Kane, 1975). Fascin is an actin cross-linking protein, which bundles adjacent actin filaments using two actin-binding sites located at N- and C-terminus of the proteins. Fascin is found in membrane ruffles, microspikes, and stress fibers and is important for the assembly of filopodia. It localises along the length of filopodia and regulates the formation and dynamics of actin bundles (Vignjevic et al., 2006; Vignjevic et al., 2003).

1.3.2 Strcuture of fascin

The mammalian genome encodes 3 isoforms of fascin. Fascin 1 (The isoform studied in this thesis) is widely expressed in mesenchymal and nervous tissues (De Arcangelis et al., 2004). Fascin 2 is specifically expressed in retina and ear hair cell stereocilia (Chou et al., 2011; Shin et al., 1999; Wada et al., 2003; Wada et al., 2001), whereas fascin 3 is expressed only in testis (Tubb et al., 2002). The structure of fascin is unique among actin binding proteins. Fascin has four β-trefoil folds, with each β-trefoil comprising six two-

stranded β-hairpins. Previous mutagenesis studies indicate that the actin-binding sites are located at the amino terminus in the first beta-trefil domain between aa33–47, and the other lies between aa277–493 (Figure 1.7) (Cant and Cooley, 1996; Ono et al., 1997). The recent structural analysis, however, implicated that the N and C termini constitute one of the actin-binding sites with both termini located in the same cleft. A stretch of residues (29–42) at the N-terminus has similarity to an actin-binding site of MARCKS and also faces the trefoil 1–4 cleft suggesting that this cleft represents one of the actin-binding sites (Chen et al., 2010). It has also been proposed that F-actin binding in this cleft between trefoils 1 and 4 could induce a conformational change at the opposite end of fascin, between trefoils 2 and 3, that might alter the actin-binding activity and result in cooperative binding to F-actin (Sedeh et al., 2010).

1.3.3 Expression and regulation of fascin

Fascin is principally expressed in nervous system, somites and mesenchyme during mammalian embryonic development (De Arcangelis et al., 2004). In adult human tissues, fascin is expressed in vascular endothelial cells, neuronal cells, and fibroblasts as well as dendritic cells but is not expressed in most normal epithelia (Zhang et al., 2008). Fascin is upregulated both at mRNA and protein level in many different types of cancers, including colon, prostate, breast, stomach and oral squamous cell carcinoma (Machesky and Li, 2010). In colon cancer, fascin is identified as a downstream target of β-catenin-TCF signaling and is preferentially expressed at the invasive fronts of tumors and is thought to be upregulated only during the active phase of metastasis and then downregulated again when a new metastasis is established as a tumor (Vignjevic et al., 2007). However, a recent detailed promoter analysis has revealed that fascin expression levels are regulated by the CREB and AhR transcription factors, but did not support a specific role for β-catenin regulation of expression in fascin positive carcinoma cells (Hashimoto et al., 2009). How this may be related to increased expression in cancers is not yet understood. Interestingly, recent studies demonstrate that

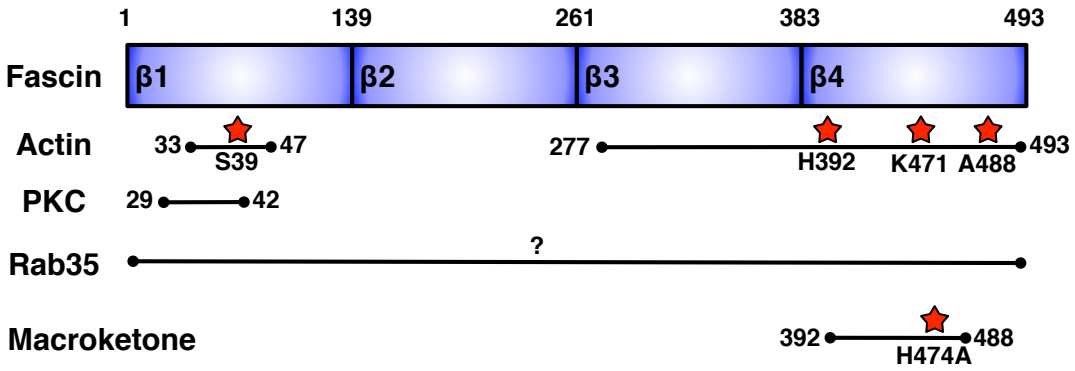

Figure 1.7 Fascin strcuture.
Schematic representation of fascin: β-trefoil domains 1–4 and binding partners and the domains involved on interactions. Mutantions on residues marked with star lead to the loss of binding with each partner.

fascin mRNA is negatively regulated by miRNA 145 both in normal (Quintavalle et al., 2010) and cancer cells (Chiyomaru et al., 2010; Kano et al., 2010), suggesting a new source of regulation of fascin at the transcriptional level.

In addition to actin, fascin also binds to several other proteins that can regulate its activity. Fascin binds directly to PKC and is a substrate for PKC phosphorylation on serine 39 (S39), this turns off the actin bundling activity via the actin binding site at the N-terminus (Figure 1.7 and 1.8) (Ono et al., 1997). FRET/FLIM revealed the interaction of fascin and active PKC within protrusions and filopodia of migrating cells and this complex is regulated by the activity of the small GTPase Rac via Pak (Parsons and Adams, 2008). Interestingly, recent studies indicated that phosphorylation of fascin negatively correlated with the poor survival in patients with esophageal squamous cell carcinoma; this suggests the importance of fascin S39 phosphorylation in cancer progression (Zhao et al., 2010). Extracellular signals and ECM components can also regulate the phosphorylation status of fascin in cells and thus affect its actin bundling propensity (Figure 1.8) (Adams, 2004a; Kureishy et al., 2002) . In *Drosophila*, fascin homologue *singed* binds directly to the small GTPase Rab35 that is known to be involved in intracellular vesicle trafficking. Rab35 is postulated to recruit and activate fascin to sites of actin assembly, and this is dependent upon both GTP-bound Rab35 and fascin S39 phosphorylation status (Figure 1.8) (Zhang et al., 2009). A recent study showed that the bacterial macrolide compound migrastatin, which is an organic compound which naturally occurs in the *Streptomyces platensis* bacteria, have shown to have potential in treating cancer, as it inhibits the metastasis of cancer cells (Shan et al., 2005). More recently, macroketone, the synthetic substance based on the fourteen-membered lactone ring found in the bacterial antibiotic migrastatin, have been shown bind to one of the actin-binding sites on fascin and therefore inhibit fascin activity and tumour cell metastasis *in vivo* (Chen et al., 2010a).

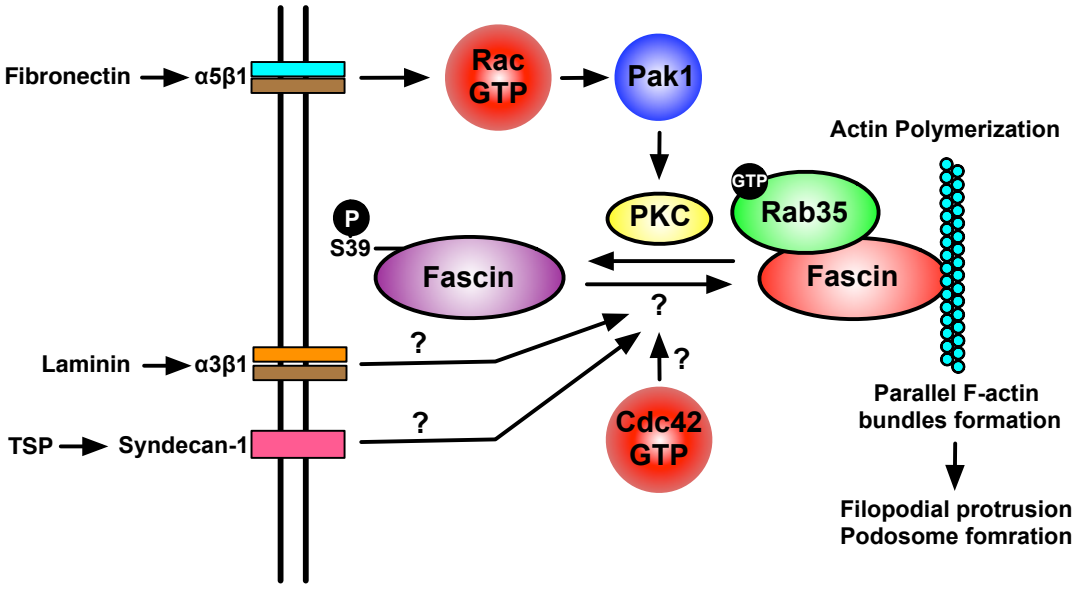

Figure 1.8 Regulation of fascin.
Schematic representation of regulation of fascin activity and its role in cytoskeletal reorganization and cell motility. ECM components control fascin-based protrusions. TSP and laminin acts through syndecan-1 and α3β1 integrins to promote the bundling of F-actin by fascin. Fascin interaction with GTP bound Rab35 is required for trafficking and localization of fascin. In contrast, ligation of α5β1 integrins by fibronectin disfavors fascin protrusions by activating Rac which acts via Pak1 to increase the content of S39- phosphorylated fascin as a result of PKC activity, and modulates the assembly of focal adhesions as a result of the interaction of S39-phosphorylated fascin-1 with the regulatory domain of PKC. How dephosphorylation of S39 is regulated is unknown.

1.3.4 Biological function of fascin

Fascin has an important role in filopodia formation and dynamics (Jayo and Parsons, 2010) and in biochemical experiments it forms very stable actin bundles and displays slow dissociation kinetics (Aratyn et al., 2007). Fascin forms both polarized parallel bundles and side-branched actin structures in vitro, which agrees with its localization in both lamellipodia and filopodia of cells (Tseng et al., 2001). Depletion of fascin in B16 melanoma cells or human colon carcinoma cells led to a loss of filopodial protrusions (Vignjevic et al., 2006; Vignjevic et al., 2007). Depletion of fascin in colon carcinoma SW480 cells also led to a decrease in migration and a reduction in focal adhesion dynamics (Hashimoto et al., 2007). In glioma cells, fascin knockdown decreased migration and transwell invasion of cells and decreased invasion into brain slices ex-vivo (Hwang et al., 2008). Fascin expression has been shown to correlate with tumor growth and metastasis in a few studies. Hashimoto et al. found that fascin knockdown significantly reduced tumour growth and metastasis in sub-cutaneous xenografts of SW480 colon cancer cells (Hashimoto et al., 2007). Another recent study showed that fascin knockdown reduced the metastasis and tumor growth of DU145 cells implanted in the prostate of Severe comined immunodenficient (SCID) mice and high fascin expression correlated with a low probability of disease-free survival (Darnel et al., 2009). Expression of fascin in HT29 colon cancer cells also increased the formation of lung tumours following tail vein injection of SCID mice (Vignjevic et al., 2007). Fascin localises to the actin-rich core of podosomes in smooth muscle cells where it promotes adhesion stability and migration (Quintavalle et al., 2010). Conversely, more recent study using fascin1-null mature dendritic cells showed that fascin is required for podosomes disassembly, suggesting a cell type specific role of fascin in regulating podosome formation (Yamakita et al., 2011).

Surprisingly, fascin deficient mice were recently shown to be viable and fertile with no gross developmental abnormalities other than minor defects in neuronal cell behaviour (Yamakita et al., 2009). In addition, Fascin-1 null

fibroblasts protruded filopodia about half as often as normal fibroblasts and those filopodia were shorter and had a shorter lifespan (Yamakita et al., 2009), suggest that fascin is not essential for filopodia formation, but may be more important for filopodia stabilization.

Conversely, the *Drosophila* singed mutant animals are female sterile and display aberrant assembly of F-actin-rich structures during bristle extension, which also depend on Rab35 to localize fascin to specific subcellular sites for F-actin bundling (Zhang et al., 2009). In addition, fascin is required for polarization and migration of the *Drosophila* macrophage equivalent cells, hemocytes (Zanet et al., 2009). Fascin localised to and stabilize dynamic actin-rich microspikes within hemocytes during migration. Interestingly, the highly conserved PKC substrate serine site in the N-terminus (S52 in drosophila) was not required for motility *in vivo*, suggest other regulatory mechanisms upstream of fascin may exist in different organisms.

1.4 Rac and Rho family GTPase

1.4.1 Introduction to Rho GTPase

The Rho family GTPase comprises a subset of the larger Ras superfamily of small GTPases. Small GTPases are generally 20-25 kDa signalling molecules, which act as molecular switches and involved in multiple signaling pathways leading to cell adhesion, migration proliferation and transformation (Wennerberg et al., 2005). There are approximately 20 members of the Rho family that can be divided into 6 subgroups base on their amino acid sequence identity, structural motifs and biological functions (Figure 1.9) (Heasman and Ridley, 2008; Wherlock and Mellor, 2002). The most extensively characterized members of Rho family GTPas are Cdc42, Rac1 and RhoA. Their roles on actin cytoskeleton have been demostrated via microinjection of active forms (Hall, 1998). This has led to the identification that Rho GTPases play an important role in filopodia, lamellipodia, and stress fibre formation respectively in different type of cells.

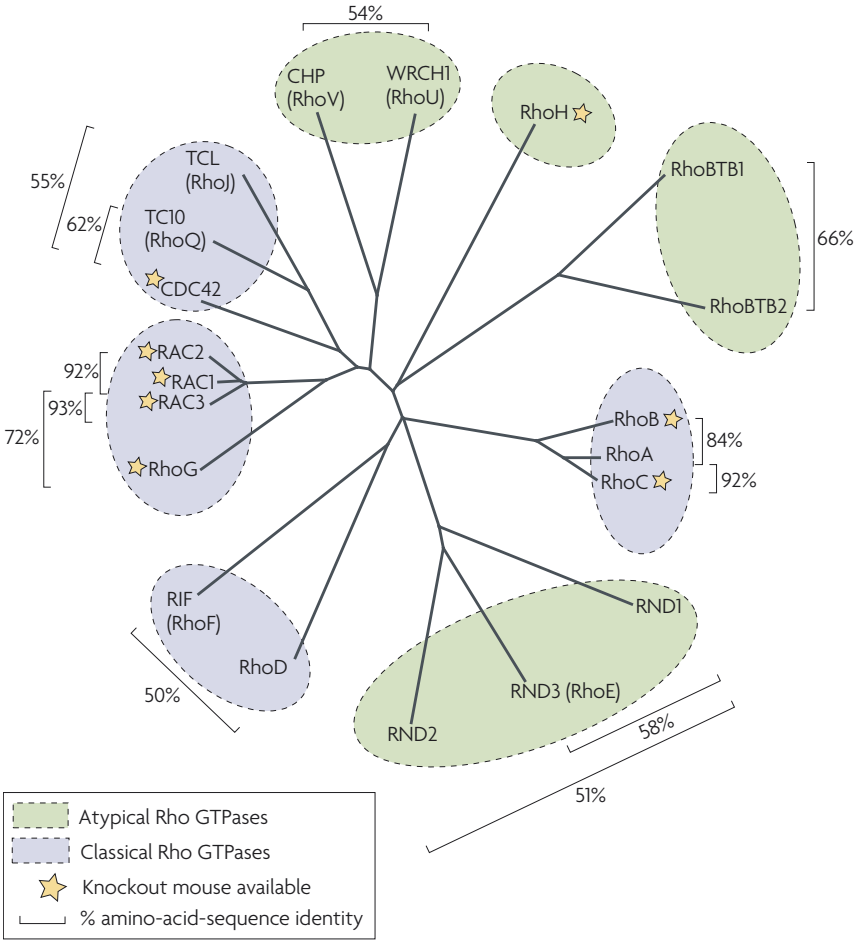

Figure 1.9 Mamalian Rho GTPase family.
On the basis of primary amino acid sequence identity, closely related proteins can be further grouped within the family (colour patches). Sequences were aligned using the ClustalW algorithm and sequence distances displayed as unrooted dendrograms in TreeView. EMBOSS pairwise alignment was used to calculate the percentage of amino-acid-sequence identity within subfamilies. The classical Rho GTPases include the Rho, Rac, CDC42 and RhoF and RhoD subfamilies and these all cycle between active GTP-bound forms and inactive GDP-bound forms. The atypical Rho GTPases comprise the RhoBTB, Rnd, RhoU and RhoV subfamilies and RhoH. These proteins are all effectively GTP-bound and are thought to be regulated by other mechanisms, including phosphorylation and protein levels. Figure adapted from sarah mammalian Rho GTpase. Figure adapted from (Heasman and Ridley, 2008).

1.4.2 Regulation of Rho GTPase

Most Rho GTPases shuttle between an inactive GDP-bound state and an active GTP-bound state while some others thought to be regulated by expression level, localization and posttranslational modification (Figure 1.10). This exchange cycle between GDP and GTP cycle is control by 3 types of regulating protein: GEFs, GAPs and GDIs. In response to diverse extracellular stimuli, GEFs activate GTPases by stabilising their nucleotide free form and stimulating the exchange of GDP to GTP (Rossman et al., 2005). Binding of GTP to Rho GTPases induces a conformational change that allows GTPases to interact with and activate downstream effectors. GAPs, on the other hand, act as negative regulators of Rho GTPases by enhacing the intrinsic hydrolytic activity of GTP-bound GTPases and thereby promoting the transition into GDP-bound form, which results in termination of signaling (Tcherkezian and Lamarche-vane, 2007). GDIs is able to form cytosolic complexes with most members of the Rho family thus block the spontaneous dissociation of GDP and prevent the interaction with GEFs, which in turn limit the function of GTPases by sequestering them from the active pool (Dovas and Couchman, 2005).

1.4.3 Introduction to Rac

Based on sequence similarity, the Rac1 subfamily comprises four proteins: Rac1, Rac2, Rac3 and RhoG. All Rac proteins are able to stimulate the formation of lamellipodia and membrane ruffles, RhoG promotes formation of lamellipodia via activating Rac GEF: DOCKs (Dovas and Couchman, 2005; Wennerberg and Der, 2004). The three Rac isoforms have different expression patterns despite their high sequence similarity. Rac1 is ubiquitously expressed, whereas Rac2 expression is mostly restricted to cells of haematopoietic origin and Rac3 mRNA is most abundant in the brain (Didsbury et al., 1989; Haataja et al., 1997; Heasman and Ridley, 2008).

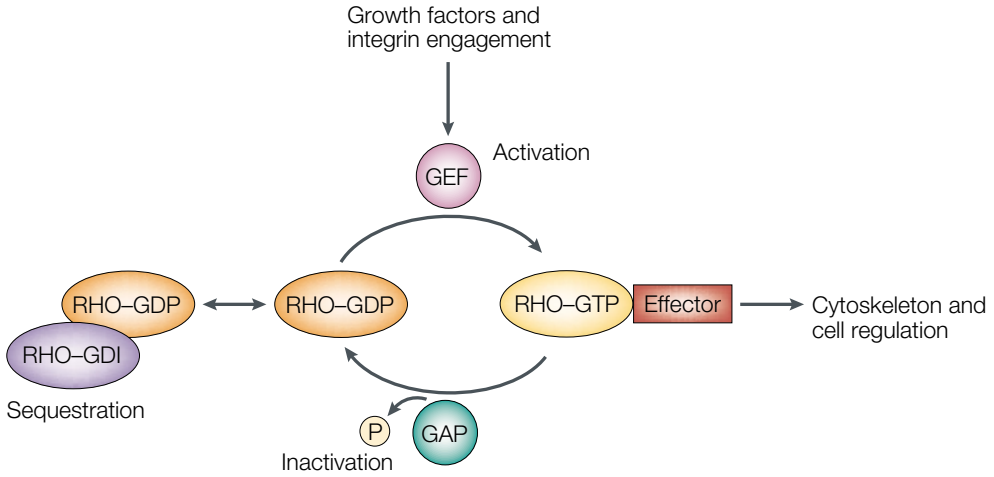

Figure 1.10 Regulation of Rho GTPase.
Rho proteins can bind either GTP or GDP. When bound to GDP, they can be sequestered in the cytoplasm by binding to GDIs. The exchange of GDP for GTP is stimulated by GEFs, and is often associated with translocation of Rho proteins to plasma membranes. Where GTP-bound Rho proteins interact with a variety of effecters alter their ability to regulate cell behaviour. GAPs act as negative regulators of Rho GTPases by enhacing the intrinsic hydrolytic activity of GTP-bound GTPases and thereby promoting the transition into GDP-bound form, which results in termination of signalling. Figure adapted from (Sahai and Marshall, 2002).

1.4.4 Biological function of Rac

It has been shown in multiple cell types including macrophages, T cells, epithelial cells and fibroblasts that expression dominant-negative RAC1 inhibits lamellipodia extension and migration (Heasman and Ridley, 2008; Ridley, 2001). Similarly, RAC1-null fibroblasts, schwann cells, endothelial cells and platelets have impaired lamellipodia formation (McCarty et al., 2005b; Nodari et al., 2007; Tan et al., 2008; Vidali et al., 2006). Surprisingly, RAC1-null macrophages can still form membrane ruffles and migrate at a similar speed to wild-type cells. However, they have an elongated morphology and fail to spread, which implies that they are defective in lamellipodia extension (Wells et al., 2004; Wheeler et al., 2006).

Rac regulates formation of lamellipodia through several signaling ways (Figure 1.11). First, Rac can activate Arp2/3 complex through WAVE complex (Kunda et al., 2003). Second, Rac can increase the availability of actin monomers for incorporation into actin filaments by regulating cofilin via Pak and LIM kinase (Edwards et al., 1999).

In addition to the involvement in the regulation of the actin cytoskeleton organization, Rac1 also plays a role in the cell-cycle progression in both G1/S (Olson et al., 1995; Vidali et al., 2006) and G2/M phase (Michaelson et al., 2008; Moore et al., 1997) in different cell types. Rac activity is also required for the activation of the JNK/SAPK, and p38 MAP kinase and TNF induced p42/44 MAP kinase cascades (Coso et al., 1995; Minden et al., 1994; Williams et al., 2008). Rac can regulate the activity of NADPH oxidase resulting in the production of superoxide radicals (Diekmann et al., 1994) and the activation of NF-κB (Perona et al., 1997; Williams et al., 2008). In addition, Rac1 activity is involved in tight junction biogenesis (Jou and Nelson, 1998; Mertens et al., 2005), cadherin-mediated cell-cell adhesion (Braga et al., 2000; Braga et al., 1999; Braga et al., 1997; Takaishi et al., 1997) and integrin-mediated cell-matrix adhesion (Hotchin and Hall, 1995; Nobes and Hall, 1995; Price et al., 1998). In cancer, Rac1 is essential for H-Ras-induced

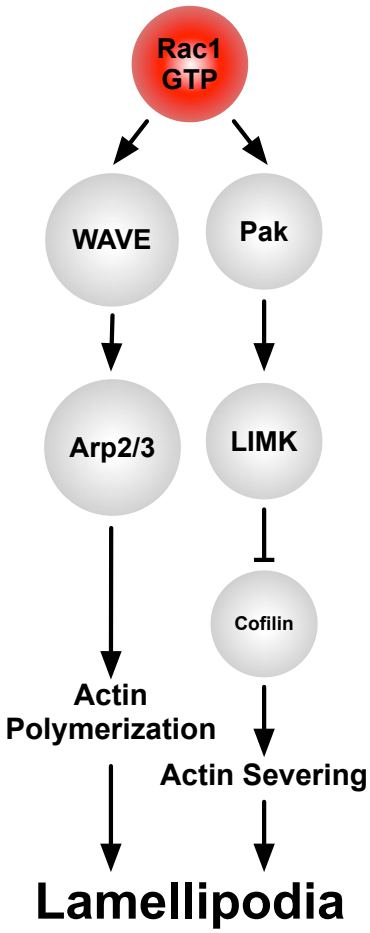

Figure 1.11 Rac regulate formation of lamellipodia
Left: Rac promote actin polymerization by activating Arp2/3 complex through WAVE complex. Right: Rac-mediated activation of PAK phosphorylates LIM kinase, which phosphorylates and inhibits cofilin, thereby regulating actin-filament turnover and actin filament severing.

transformation of NIH3T3 fibroblasts in vitro (Qiu et al., 1995), and expression of constitutively activated mutants of Rac1 is sufficient for their malignant transformation. Interestingly, Rac induced activation of Pak, JNK or induction of lamellipodia, was neither necessary nor sufficient for Rac1 transforming activity, suggest multiple pathways may contribute to Rac1-induced cellular transformation (Westwick et al., 1997).

In vivo, expression of dominant negative Rac inhibits protrusion formation and collective migration of oocyte border cells in *Drosophila* egg chamber (Bianco et al., 2007; Duchek et al., 2001; Geisbrecht and Montell, 2004; Murphy and Montell, 1996; Wang et al., 2010). Likewise, sequestration of Rac activity in zebrafish germ cells inhibits actin brush formation, cell polarity and migration (Kardash *et al.*, 2010). In mouse, global Rac1 knockout was embryonic lethal and developing embryos do not progress past E9.5, with a high incidence of apoptotic cell death in the mesoderm during gastrulation (Sugihara et al., 1998), therefore tissue specific knockout of Rac have been widely used to study Rac1 function. Deletion of Rac1 induced by wnt-1 Cre in murine neural crest cells showed non-requirement of Rac1 for migration of neural crest cells to initial target structures, but strong proliferation defect (Fuchs *et al.*, 2009). Deletion of Rac1 in developing nervous with nestin Cre showed increased apoptosis and Rac1-deficient cerebellar granule neurons showed impaired migration and axon formation. In addition, Rac1 is required for protrusion formation and collective migration of anterior visceral endoderm cells to the developing anterior side of the embryo between days E5.5-6.0 during body axis specification. However, Rac1 is dispensable for proliferation in this system (Migeotte et al., 2010). Epidermal deletion of Rac1 in keratinocyte revealed an important role of Rac in maintaining the adult epidermal stem cell compartment (Benitah et al., 2005).

In contrast to Rac1, Rac2 knockout mice revealed normal development but neutrophilic, phagocytic and lymphocytic defects (Croker et al., 2002; Li et al., 2000; Roberts et al., 1999). Comparison of defects in hematopoietic cell function, observed after single and double deletion of Rac1 and Rac2, demonstrated both overlapping and distinct roles of these two related

GTPases in hematopoietic cells (Benvenuti et al., 2004; Gu et al., 2003; Walmsley et al., 2003). Similarly, The Rac3 protein is specifically expressed in the nervous system and Rac3-deficient mice have no obvious anatomical or physiological defects (Corbetta et al., 2005). However, more recent study using Rac1 and Rac3 double knockout mice revealed Rac1 and Rac3 play complementary roles during late stages of neuronal and brain development (Corbetta et al., 2009).

1.5 Melanoblast migration

1.5.1 Introduction to melanoblast migration

Mammalian melanoblasts are the precursor cells of melanin producing melanocytes; they arise from the neural crest. During embryogenesis, melanoblasts migrate away from the neuroepithelium in an extraordinary journey with cycles of migration and proliferation to eventually populate the skin and hair follicles (Figure 1.12) (Kelsh et al., 2009).

In mouse, neural crest cells undergo two migration pathways. Those that migrate in the space between the somites and the neural tube (ventral pathway) give rise to neuronal and glial cells, whereas those that migrate between the somite and the non-neural ectoderm (dorsolateral pathway) differentiate into melanoblasts (Serbedzija et al., 1990). Studies indicated that this melanogentic fate is detemined by expression of Kit (The major tyrosine kinase receptor in melanocytes) in neural crest cells before the migration (Wilson et al., 2004). Melanoblasts reside in an area just near the neural tube, called the migration staging area, where they receive proliferation and survival signals from Kit-ligand (KitL), the ligand of Kit. Between E8.5 and E10.5, their migration is dorsolateral and induced by transient expression of KitL in dermatome (Figure 1.12). After E10.5 they begin to progress ventrally toward the face, ventral abdomen and the developing limbs (Figure 1.12). They also undergo a migration in the z-plane, as they emerge upward through the developing dermis and into the epidermis at around E13.5 (Figure 1.12)

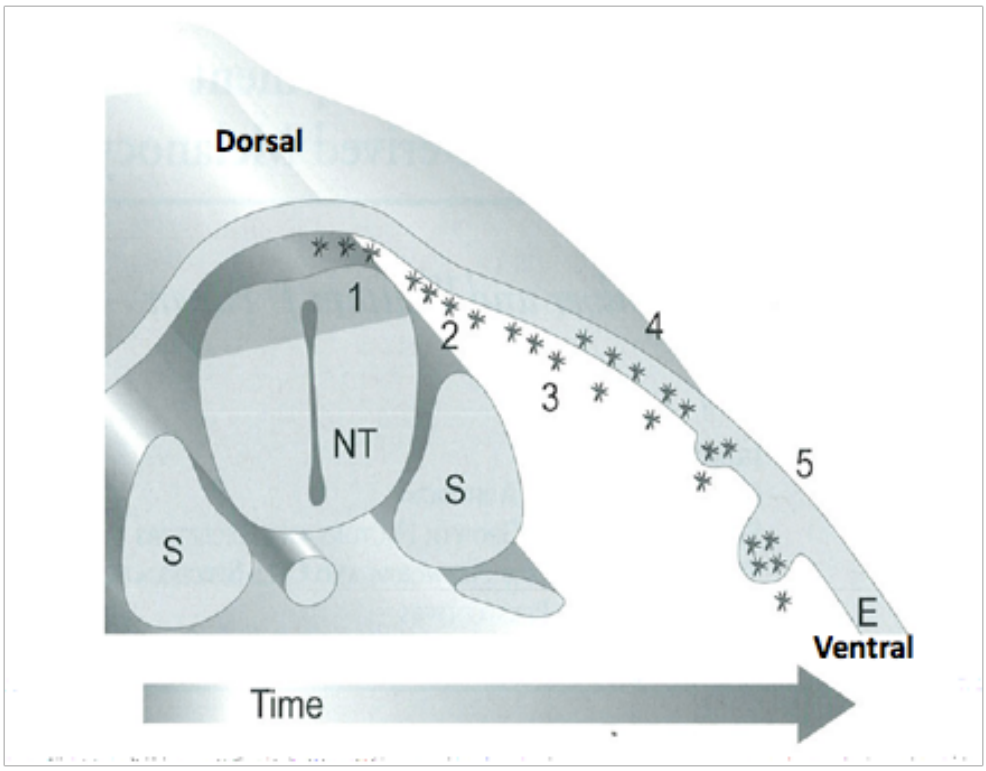

Figure 1.12 Melanoblast dorsolateral migration pathway.
(1) Melanoblasts emerge from the dorsal neural tube at around embryonic day 8.5. Melanoblasts migrate along the dorsolateral pathway between the dermatome and the overlying ectoderm, and from E10.5 migrate ventrally through the developing dermis (2-3). At E14.5, they begin to invade the overlying epidermis (4) and then migrate into the developing hair follicles at E15.5 (5). NT: Neural tube, S: Somite. Figure adapted from (Silver et al., 2006).

(Mayer, 1973). Over the next few days they enter developing hair follicles (Figure 1.12). At birth, melanocytes are observed in both the epidermis and hair follicles, but within a few days, epidermal melanoblasts disappear, leaving only those in the hair follicles, which differentiate and produce melanin by around P4 (Jordan and Jackson, 2000; Mayer, 1973). As a consequence, the skin in the adult mouse is mostly unpigmented. In contrast, human melanocytes normally located in the bottom layer of the skin's epidermis, which comprise from 5% to 10% of the cells in the basal layer of epidermis.

1.5.2 Regulaton of melanoblast migration

To date several genes have been identified which are associated with coat-color abnormalities in mice, indicating defects in melanoblast migration, proliferation and survival (Baxter et al., 2004; Bennett and Lamoreux, 2003; Kelsh et al., 2009). Some of these genes are also associated with neural crest and melanocyte disorders in humans. These genes include transcription factors: Mitf (Grüneberg, 1953; Hodgkinson et al., 1993; Hughes et al., 1993), SNAI2 (Perez-Losada et al., 2002), Sox10 (Britsch et al., 2001); Receptor tyrosine kinase Kit and its ligand KitL (Cable et al., 1995; Geissler et al., 1988; Mackenzie et al., 1997; Wehrle-Haller and Weston, 1995); G-protein coupled endothelin-3 receptor/ligand pair (Baynash et al., 1994; Hosoda et al., 1994) and secreted protease of the ADAM family of metalloproteinase ADAMTS20 (Silver et al., 2008).

For instance, signaling to Kit via KitL is known to trigger proliferation and survival via activation of Ras and downstream MAPK/ERK signaling (Mackenzie et al., 1997; Smalley, 2009; Steel et al., 1992; Yoshida et al., 2001), and has been speculated to be involved in motility (Jordan and Jackson, 2000; Peters et al., 2002). Application of Kit function blocking antibody to mouse embryo was able to block proper melanoblast development (Nishimura et al., 2002; Yoshida et al., 1996). Furthermore, ectopic expression of Kitl in the basal layer of the skin promotes dermal melanoblasts survival (Kunisada et al., 1998).

Endothelin-3 signaling functions are necessary for the development of melanoblasts. Endothelin-3 is not required for melanogentic fate specification, but is needed for migration and survival of melanoblasts between E10.5 and E12.5 (Shin et al., 1999), and is also required for melanoblast development in the epidermis beyond E12.5 (Yoshida et al., 1996). Similar to KitL, ectopic expression of endothelin-3 in keratinocytes driven by keratin 5 promoter also result increased melanoblast proliferation and pigmented skin harboring dermal melanocytes, suggest a important role of endothelin-3 in Kit independent survival of melanocytes (Garcia et al., 2007).

In addition to signaling molecules, melanoblast migration at different stages is tightly regulated by expression of cell-cell adhesion molecules (Pla et al., 2001). For example, E-cadherin and P-cadherin are expressed in complementary regions of the developing skin and are required to maintain the correct organization of the epidermis, dermis and hair follicle. In general, E-cadherin is expressed by keratinocytes of the epidermis; P-cadherin is expressed by keratinocytes of the hair matrix, but not in the dermis. Similarly, Melanoblasts that migrate in dermis neither express E-cadherin nor P-cadherin (Nishimura et al., 1999). Expression of E-cadherin is required for melanoblasts invading the epidermis, and localization of melanoblasts to the hair matrix requires P-cadherin expression (Nishimura et al., 1999).

1.6 Thesis aim

I aimed to investigate the role of two important cytoskeletal proteins, fascin-1, an actin bundling protein and Rac1, a signalling small GTPase in cell migration and cancer. The actin cytoskeleton and cytoskeletal control are crucial in development and cancer invasion/metastasis and understanding the function of these key proteins in both normal and cancer cells will aid future development of diagnostic and therapeutic cancer research.

The aims of my project are:

1. To investigate the potential role of fascin on invadopodia formation.
2. To investigate the potential role of fascin in cancer cell invasion.

3. To investigate the potential role of Rho GTPase Rac1 on melanoblast proliferation and migration during mouse embryogensis.
4. To investigate the potential role of Rho GTPase Rac1 in activated N-Ras Q61K induced melanocyte hyperproliferation.

Chapter II
Materials and Methods

2.1 Materials

2.1.1 Reagents and Solutions

Compound/Reagents	Type	Source
Y-27632	Rho kinase inhibitor	Dr. M, Olson, Beatson institute.
Latrunculin A	Actin polymerization inhibitor	Sigma
IPA-3	Pak1/2/3 inhibitor	Dr. J. Chernoof, Fox Chase Cancer Centre
LIMKi	LIM kinase inhibitor	Dr. M. Olson, Beatson institute.
U0126	MEK1/2 inhibitor	Cell signalling
Blebbistatin	Myosin II inhibitor	Sigma
GM6001	Metalloprotease inhibitor	Merck chemicals
CK312	Arp2/3 complex inhibitor (Negative Control)	Merck chemicals
CK869	Arp2/3 complex inhibitor	Merck chemicals
Nocodazole	Tubulin polymerization inhibitor	Sigma
Taxol	Microtubules stabilizer	Sigma
EGF	Growth factor	Sigma
Complete matrigel	ECM	BD biosciences
Growth factor reduced matrigel	ECM	BD biosciences
Rat Tail Collagen I (High concentration)	ECM	BD biosciences
PureCol Bovine Collagen	ECM	Advanced Biomatrix
Human Fibronectin	ECM	BD biosciences
Mouse laminin	ECM	BD biosciences
Ampicillin		Sigma

Kanamycin		Sigma
DNA Ladders	1kb	Invitrogen
6xDNA loading dye		New Englend Biolabs
Ethidium bromide		Invitrogen
Fetal Bovine Serum		Autogen Bioclear
Hybond-P PVDF membrane		GE Healthcare
DMEM		Gibco
F-12K Nutrient Mixture, Kaighn's Modification		Gibco
Luria Broth Agar	LB + 1.5% agar	Beatson Institute Central Services
Luria Broth	1% w/v bacto-tryptone, 86nM NaCl, 0.5% yeast extract	Beatson Institute Central Services
L-Glutamine (200mM)		Gibco
NuPAGE Novex Bis-Tris Mini Gels	10%, 12% and 4-12% gel percentage	Invitrogen
NuPAGE Sample Reducing Agent (10X)		Invitrogen
NuPAGE Sample Buffer (4X)		Invitrogen
NuPAGE MOPS SDS Running Buffer		Invitrogen
NuPAGE Transfer Buffer		Invitrogen
PE	PBS + 1mM EDTA	Beatson Institute Central Services
Penicillin-Streptomycin		Gibco
Primocin		InvivoGen
PBS	170mM NaCl, 3.3mM KCl, 1.8mM Na2HPO4, 10.6mM H2PO4	Beatson Institute Central Services
TBST	10mM Tris-HCl, pH 7.4, 150mM NaCl	Beatson Institute Central Services

TAE	40mM Tris, 0.1% glacial acetic acid, 1mM EDTA	Beatson Institute Central Services
TE	10mM Tris-HCl, pH 8.0, 1mM EDT A	Beatson Institute Central Services
Trypsin		Gibco
X-gal	5'-bromo-4-chloro-3-indolyl-D-galactopyranoside	Promega
Collagenase type I		Gibco
Collagenase type IV		Gibco
Cell dissociation buffer		Gibco
Sulfo-NHS-SS-biotin		Pierce Chemical
NeutrAvidin agarose resin		Thermo Scientific
RNase free water		Qiagen
Medium 254		Cascade Biologics
Human melanocyte growth supplement-2, TPA free		Cascade Biologics
TPA		Sigma
Geneticin		Gibco
10XDMEM		Gibco
OptiMEM		Gibco
Annealing buffer	100 mM NaCl and 50 mM HEPES pH 7.4	In house
QIAprep Maxiprep Kit		Qiagen
2x HBS	50 mM HEPES, 250 mM NaCl, 1.5 mM NaHPO4, pH 7.1	In house
RIPA buffer	50 mM Tris-HCl, 150 mM NaCl, 1% NP-40 and 0.25% Na-deoxycholate	In house
7.5% bicarbonate		GIBCO

BSA		Sigma
Melanin bleach kit		Polyscience Inc.
Brdu		Sigma
Puromycin		Invivogen
Protease inhibitor cocktail		Pierce
Halt phosphatase inhibitor cocktail		Pierce
SeeBlue Plus2 Pre-Stained Standard		Invitrogen
4-Hydroxytamoxifen		Sigma
Image-iT FX Signal Enhancer		Invitrogen
Citrate buffer, ph 6.4		Dako
Peroxidase block		Dako
X-Gal buffer	2 mM MgCl2, 0.02% NP-40, 2 mM K3Fe(CN)6 and 2 mM K4Fe(CN)6) containing 2 mg/ml X-Gal	In house
Detergent buffer	2 mM MgCl2, 0.02% NP-40 and 0.01% sodium deoxycholate in PBS, pH 7.5	In house
HBSS		Gibco
Prolong Gold Antifade reagent		Invitrogen
Antibody Diluent		Dako
Polybrene		Sigma
NeutrAvidin Agarose Resin		Thermo Scientific
TNE buffer	50mM Tris HCl pH7.5, 150mM NaCl, 1% Triton X-100 and 1mM EDTA	In house

Table 1 – Reagents and Solution

2.1.2 Antibodies and Dyes

Antibody	Dilution	Source
Mouse anti-Fascin (55K2)	WB – 1:500; IF – 1:100	Dako
Mouse anti-Fascin (SPM133)	IF – 1:100	Abcam
Rabbit anti-Fascin	IHC– 1:200	ATLAS antibodies
Mouse anti-Cortactin (4F11)	IF – 1:200	Millipore
Mouse anti-Rac1 (ARC03)	WB – 1:500; IF – 1:100	Cytoskeleton Inc.
Mouse anti-Myc (9E10)	IF – 1:200	Dr. L. Machesky
Rabbit anti-Pak1/2/3	WB – 1:500	Cell Signalling
Rabbit anti-Pak1	WB – 1:500	Cell Signalling
Rabbit anti-Pak2	WB – 1:500	Cell Signalling
Rabbit anti-Phospho Pak1 (Ser199/204)/Pak2 (Ser 192/197)	WB – 1:500	Cell Signalling
Rabbit anti-p34-Arc	WB – 1:500; IF – 1:200	Millipore
Rabbit anti-actin	WB – 1:500	Sigma
Mouse anti-Cdc42	WB – 1:500	Santa Cruz
Mouse anti-E-cadherin	WB – 1:500; IF – 1:100	BD bioscience
Mouse anti-ZO-1	WB – 1:500; IF – 1:100	Invitrogen
Rabbit anti-Collagen IV	IF – 1:100	Abcam
Rabbit anti-Phospho-Cofilin (Ser3)	WB – 1:500	Cell Signalling
Rabbit anti-Phospho-Myosin Light Chain 2 (Ser19),	WB – 1:500	Cell Signalling
Rabbit anti-GAPDH	WB – 1:500	Cell Signalling

Rabbit PhosphoHistone H3 (Ser10)	IF – 1:100	Cell Signalling
Rabbit anti-phospho-Erk1/2 (Thr202/Tyr204)	WB – 1:500	Cell Signalling
Rabbit anti-ERK1/2	WB – 1:500	Cell Signalling
Mouse anti-β1 integrin	WB – 1:500	Millipore
Mouse anti-active Rac1-GTP	IF – 1:100	NewEast Bioscience
Goat anti-DCT (D-18)	WB – 1:500; IF – 1:100; IHC – 1:5000	Santa Cruz
Goat anti-WAVE1	WB – 1:500	Santa Cruz
Rabbit anti-WAVE2	WB – 1:500	Santa Cruz
Mouse anti-BrdU	IF – 1:100	BD Bioscience
Rabbit anti-cleaved Caspase-3 (Asp175)	IF – 1:100	Cell Signalling
Mouse anti-vinculin	WB – 1:500	Millipore
Rabbit anti-Ki67 (SP6)	WB – 1:500; IF – 1:100	Neomarkers
Mouse anti-tubulin	WB – 1:500; IF – 1:100	Sigma
Mouse anti-Paxillin	WB – 1:500; IF – 1:100	Sigma
Rabbit anti-N-WASP	WB – 1:500	ATLAS antibodies
Mouse Anti-Abi1	IF – 1:100	Caltag medsystems
Rabbit anti-Nap1	WB – 1:500	Millipore
Mouse anti-MT1-MMP (3G4.2)	WB – 1:500	Millipore
Mouse anti-BrdU	FC-1:50	Dako
Anti-mouse IgG HRP linked	WB – 1:5000	Cell Signalling
Anti-Rabbit IgG HRP linked	WB – 1:5000	Cell Signalling
Anti-Goat IgG HRP linked	WB – 1:5000	Cell Signalling
Alexa Fluor 594 donkey anti-mouse IgG	IF – 1:500	Molecular Probes

Alexa Fluor 594 donkey anti-rabbit IgG	IF – 1:500	Molecular Probes
Alexa Fluor 488 donkey anti-goat IgG	IF – 1:500	Molecular Probes
Alexa Fluor 488 donkey anti-rabbit IgG	IF – 1:500	Molecular Probes
Alexa Fluor 488 donkey anti-mouse IgG	IF – 1:500	Molecular Probes
Alexa Fluor 488 goat anti-mouse IgG	IF – 1:500; FC – 1:50	Molecular Probes
Alexa Fluor 488 goat anti-rabbit IgG	IF – 1:500	Molecular Probes
Alexa Fluor 594 goat anti-mouse IgG	IF – 1:500	Molecular Probes
Alexa Fluor 594 goat anti-rabbit IgG	IF – 1:500	Molecular Probes
Alexa Fluor 647 goat anti-mouse IgG	IF – 1:500	Molecular Probes
Alexa Fluor 647 goat anti-rabbit IgG	IF – 1:500	Molecular Probes
Alexa Fluor 350 goat anti-mouse IgG	IF – 1:500	Molecular Probes
Rhodamine Phalloidin	IF – 1:200	Molecular Probes
Calcein AM	5μM	Molecular Probes

WB: Western Blot **IF:** Immunofluorescence

IHC; Immunohistochemistry **FC:** Flow cytometry

Table 2 – Antibodies and Dyes

2.1.3 DNA Constructs

Construct	**Type**	**Source**
LMP	Retroviral shRNA vector	Dr. J. Norman
eCFP-C1- *H. sapiens* fascin	Transient expression vector	Dr. J. Adams

eGFP-C1- *H. sapiens* fascin S39A	Transient expression vector	Dr. J. Adams
eGFP-C1- *H. sapiens* fascin S39E	Transient expression vector	Dr. J. Adams
eGFP-C2- *X. tropicalis* fascin	Transient expression vector	Dr. J. Adams
eGFP-C2- *X. tropicalis* fascin S33A	Transient expression vector	Dr. J. Adams
eGFP-C2- *X. tropicalis* fascin S33D	Transient expression vector	Dr. J. Adams
mCherry-C2- *X. tropicalis* fascin	Transient expression vector	This study
mCherry-C2- *X. tropicalis* fascin S33A	Transient expression vector	This study
mCherry-C2- *X. tropicalis* fascin S33D	Transient expression vector	This study
mCherry-C2	Transient expression vector	Dr. J. Norman
eGFP-C1	Transient expression vector	Dr. L. Machesky
GFP-mDia2	Transient expression vector	Dr. S. Narumiya
GFP-mDia2	Transient expression vector	Dr. S. Narumiya
IRSP53-myc	Transient expression vector	Dr. L. Machesky
IRTKS-myc	Transient expression vector	Dr. L. Machesky
GFP-N-WASP	Transient expression vector	Dr. T. Takenawa
GFP-Cortactin	Transient expression vector	Dr. R. Buccinone
GFP-p21-ARC	Transient expression vector	Dr. L. Machesky
GFP-actin	Transient expression vector	Dr. M. Parsons

RFP-actin	Transient expression vector	Dr. M. Parsons
GFP-Lifeact	Transient expression vector	Dr. R. Wedlich-Soldner
RFP-Lifeact	Transient expression vector	Dr. R. Wedlich-Soldner

Table 3 – DNA Constructs

2.1.4 Enzymes and kits

Kit	**Supplier**
Amaxa Nucleofection Kit	Lonza
Glutathione sepharose beads	Thermo Scientific
Hyperfect	Qiagen
Lipofectamine 2000	Invitrogen
QIAquick Gel Extraction Kit	Qiagen
Restriction enzymes and reaction buffers	New England Biolabs
SimplyBlue SafeStain	Invitrogen
Rapid DNA Ligation Kit	Roche
SuperSignal West Pico Chemiluminescent Substrate	Thermo Scientific
Phusion High-Fidelity DNA Polymerase	New England Biolabs
Precision Red Advanced Protein Assay	Cytoskeleton Inc.
QIAquick PCR purification kit	Qiagen
QIAprep Spin Miniprep Kit	Qiagen
Melanin bleach kit	Polyscience Inc.
Vectastain ABC kit	Vector laboratories, Inc.
Alkaline phosphatase substrate kit	Vector laboratories, Inc.

EnVision Detection Systems Peroxidase/DAB, Rabbit/Mouse	Dako

Table 4 – Enzymes and Kits

2.2 Methods

2.2.1 Cell Culture

2.2.1.1 Origin of cell lines

A375MM human melanoma cells were obtained from R. Buccione (Consorzio Mario Negri Sud, Chieti, Italy). CHL-1 and WM266.4 human melanoma cells and Phonenix-Ampho retroviral packaging cells were obtained from B. Ozanne (Beatson Institute, Glasgow, UK). MV3 human melanoma cells were obtained from G. van Muijen (University of Nijmegen, Nijmegen, The Netherlands). SCC-9 human oral cancer cells and MDA-MB-231 human breast adenocarcinoma cells were obtained from ATCC. Adult epidermal melanocyte (A melanocytes) and neonatal melanocyte (N melanocytes) were obtained from (Cascade Biologics) and cultured according to the manufacturer's instructions. Primary mouse melanocytes were established as described below.

2.2.1.2 Maintenance of cell lines

All cell lines were routinely grown in tissue culture treated 100 mm dishes (Falcon) at 37°C in a humidified atmosphere containing 5% CO_2. All techniques were performed in sterile conditions. All cell lines were cultured in DMEM containing 2mM glutamine and 10% FBS, except SCC9 cells were cultured in DMEM/F-12 medium (1:1) containing 2mM glutamine, 400 ng/ml hydrocortisone and 10% FBS. Fresh media was added every 3-4 days. Cells were passaged when subconfluent, typically every 3 days with a 1:10 split ratio. After aspirating the medium and washing with PE buffer, 0.1 ml PE buffer with 0.25% trypsin was added and after approximately 3 min cells were

resuspended in 10 ml fresh medium, 1 ml of which was added to 19 ml fresh medium in a new 10 mm dish. Human primary melanocytes were cultured in medium 254 with human melanocyte growth supplement-2, PMA free and split when subconfluent and the medium was changed every 3 days. Cells were passaged as described above.

2.2.1.3 Storage of cell lines

Cells were stored in liquid nitrogen. Cells were trypsinised as described above and pelleted by centrifugation. Cells were resuspended in medium supplemented as described but with 20 % FCS and 10 % DMSO. Resuspended cells were placed in cryotubes, wrapped in cotton wool and frozen at -70°C overnight before transferring to liquid nitrogen. Cells were thawed by placing cryotubes in a 37°C water bath. Cells were diluted in 10 ml fresh medium, pelleted by centrifugation, resuspended in 10 ml fresh medium and placed in a new 10 mm dish. Medium was changed once the next day.

2.2.1.4 Establishment of primary mouse melanocyte cell lines

Method for obtaining primary mouse melanocytes was previously reported (Larue et al., 1992). Briefly, 1 day old Rac1 f/f Tyr::CreERT2+/o Ink4a-Arf-/- (#3 and #4) or Rac1 f/f Tyr::CreERT2o/o Ink4a-Arf-/- (#2) littermate mice were stunned and decapitated and briefly sterilized by rinsing twice in ice-cold 70 % ethanol for 5 s and twice in ice-cold PBS for 5 s. The skin, typically 1 cm^2, was removed and cut into small pieces with scissors and forceps and incubated in 2 ml of collagenase type 1 and 4 at 37°C, 5 % CO_2 for 40 min. The epidermis and dermis were separated and transferred to 10 ml wash buffer, centrifuged at 1100 rpm at room temperature for 5 min and resuspended in 2 ml cell dissociation buffer. After incubating at 37 °C 5 % CO_2 for 10 mins, the tissue was repeatedly put through 18 g and then 20 g needles to further dissociate and then resuspended and left to settle in 10 ml wash buffer for 10 mins. The supernatant was centrifuged at 1100 rpm for 5 min and resuspended in 2 ml PBS and the cells counted. Cells were centrifuged as before and plated at a density of 1 x 10^6 per well of a 6-well tissue culture plate in melanocyte growth

medium F-12 containing 200 nM TPA and 100 µg/ml primocin. After 2 days in culture, G418 was added to the culture medium at 50 µg/ml for 3 d every week in order to selectively impair the growth of fibroblasts and keratinocytes. Melanocytes were passaged at around 50% confluence. All experiments were done with melanocytes that were spontaneously immortalized (Ink4a-Arf$^{-/-}$ background (Sviderskaya et al., 2002)) and kept in culture for between 3 and 4 months. Controls were done to ensure that OHT did not affect the morphology of cells not carrying inducible Rac1 deletion e.g. Tyr::CreER negative cell lines. Pure populations of melanocytes were normally achieved after 1.5 months culture of N-Ras^{Q61K} positive cells and after 4 months culture of N-Ras^{Q61K} negative cells.

2.2.2 Molecular Cloning

2.2.2.1 Agarose gel electrophoresis

Agarose was added to 1xTAE buffer at between 1 and 2 % depending on the size of the DNA to be visualized. Agarose in 1xTAE buffer was heated and Ethidium Bromide added at 0.5 µg/ml prior to solidification in a gel tray. DNA samples and 1 kb ladder in 1xDNA loading buffer were loaded on to the gel and electrophoresis performed at 100V in 1xTAE buffer. DNA bands were visualized using a UV transilluminator. The DNA bands of interest were cut and purified using QIAquick PCR purification kit according to the Manufacture's instructions.

2.2.2.2 Restriction enzyme digests

Restriction enzyme digests contained 1x appropriate enzyme buffer, approximately 10 µg DNA and 5-10 U of restriction enzyme were used per microgram DNA, made up to volume of 20 µl with distilled water. Reactions were incubated for 2 hour at 37°C.

2.2.2.3 Ligations

Ligations were performed using the Rapid DNA Ligation Kit. An approximate 2 fold molar excess of insert DNA to vector DNA was diluted in DNA Dilution Buffer to a final volume of 9 µl. This was combined with 1xT4 DNA Ligation Buffer was to a final volume of 10 µl and 5 U T4 DNA ligase was added. The ligation reaction was incubated at room temperature for 1.5 h before transforming competent bacteria.

2.2.2.4 Generation of mCherry-C2- *X. tropicalis* fascin constructs

mCherry-*X. tropicalis* fascin, *X. tropicalis* fascin S33A and *X. tropicalis* fascin S33D constructs was generated by subcloning *X. tropicalis* fascin, *X. tropicalis* fascin S33A and *X. tropicalis* fascin S33D from EGFP-C2 vector to mCherry-C2 vector using *BamHI /XhoI* restriction sites.

2.2.2.5 Transformation of competent cells

Competent *E. Coli* DH5a cells were stored at –70°C and thawed on ice. Plasmid DNA, typically 20 ng, was gently mixed with 100 µl of cells and incubated for 15 minutes on ice. Cells were then heat-shocked at 42°C for 45 seconds and placed back on ice for 1 min. 1ml L-broth was added and cells were incubated with shaking at 37°C for 1 h, 250 rpm. 200 µl of the transformation mixture was spread over pre-warmed LB agar plates containing 50 µg/ml ampicillin or kanamycin depend on the vector and incubated overnight at 37°C.

2.2.2.6 Design of shRNA constructs

Oligos siRNA sequences were designed based on siRNA sequence (see below). The resulting sequences were entered into an online shRNA oligo construction tool

(http//katahdin.cshl.org:9331/homepage/sirna/rnai.cgi?type=shrna) to design complimentary 110 nucleotide oligos suitable for ligation into the vector LMP.

2.2.2.7 Oligos for shRNA constructs

Primer	Sequence
Fascin SEQ1 F	TCGAGAAGGTATATTGCTGTTGACAGTGAGCGCAACTG GAAATAGCGAAATAAATAGTGAAGCCACAGATGTATTTA TTTCGCTATTTCCAGTTTTGCCTACTGCCTCGG
Fascin SEQ1 R	AATTCCGAGGCAGTAGGCAAAACTGGAAATAGCGAAAT AAATACATCTGTGGCTTCACTATTTATTTCGCTATTTCCA GTTGCGCTCACTGTCAACAGCAATATACCTTC
Fascin SEQ2 F	TCGAGAAGGTATATTGCTGTTGACAGTGAGCGCCACGG GCACCCTGGACGCCAATAGTGAAGCCACAGATGTATTG GCGTCCAGGGTGCCCGTGATGCCTACTGCCTCGG
Fascin SEQ2 R	AATTCCGAGGCAGTAGGCATCACGGGCACCCTGGACG CCAATACATCTGTGGCTTCACTATTGGCGTCCAGGGTG CCCGTGGCGCTCACTGTCAACAGCAATATACCTTC
Fascin SEQ3 F	TCGAGAAGGTATATTGCTGTTGACAGTGAGCGACAGCT GCTACTTTGACATCGATAGTGAAGCCACAGATGTATCGA TGTCAAAGTAGCAGCTGGTGCCTACTGCCTCGG
Fascin SEQ3 R	AATTCCGAGGCAGTAGGCACCAGCTGCTACTTTGACAT CGATACATCTGTGGCTTCACTATCGATGTCAAAGTAGCA GCTGTCGCTCACTGTCAACAGCAATATACCTTC
Fascin SEQ4 F	TCGAGAAGGTATATTGCTGTTGACAGTGAGCGCCTGAG CCTTATTTCTCTGGAATAGTGAAGCCACAGATGTATTCC AGAGAAATAAGGCTCAGATGCCTACTGCCTCGG
Fascin SEQ4 R	AATTCCGAGGCAGTAGGCATCTGAGCCTTATTTCTCTGG AATACATCTGTGGCTTCACTATTCCAGAGAAATAAGGCT CAGGCGCTCACTGTCAACAGCAATATACCTTC

Table 5 – Oligo sequences for shRNA constructs

2.2.2.8 Annealing shRNA oligos

Oligos were dissolved in sterile, nuclease-free water to a concentration of 3 mg/ml. The annealing reaction consisted of 1 µl each oligo in 48 µl annealing buffer. The mixture was incubated for 4 min at 90°C and then for 10 minutes at 72°C. The samples were cooled to 4°C and stored until ligation into vector LMP, which was digested with *XhoI/EcoR1* restriction enzymes.

2.2.2.9 Screening of transformants

Individual colonies of bacteria were used to inoculate 5 ml LB media containing 50 µg/ml ampicillin or kanamycin as appropriate and cultured overnight at 37 °C. Plasmid DNA was prepared using the QIAprep Spin Miniprep Kit and analyzed for the presence of desired insert by restriction digest and subsequent visualization by gel electrophoresis. Samples that tested positive were sequenced using appropriate sequencing primers. After sequence confirmation, plasmid DNA was used to transform fresh bacteria and 100 ml cultures were used to prepare DNA using QIAprep Maxiprep Kit (some procedures performed by Beatson Research Services).

2.2.2.10 Primers for sequencing

Primer	Sequence
pRETROSUPER forward	CCCTTGAACCTCCTCGTTCGACC
pRETROSUPER reverse	GAGACGTGCTACTTCCATTTGTC

Table 6 – Primers for sequenceing

2.2.3 Transfection

2.2.3.1 Transient transfection of plasmid DNA

For transient transfection of plasmid DNA using Lipofectamine 2000, cells were set up at an appropriate density in culture dishes (e.g. $1x10^5$ per well of a 6well dish for A375MM and CHL-1 cells). 16-24 hours later DNA was transfected according to the manufacturer's instructions. Both DNA (~5-10µg) and Lipofectamine 2000 were diluted in OptiMEM, incubated at RT for 5min, then combined and incubated for a further 20min before being added directly to the cells. Expression was then tested for after 24-48 hours.

Cells were also transfected by nucleofection. Cells were pelleted by centrifugation, resuspended to 2 x 10^6 cells per ml in the appropriate nucleofection reagent and 100 µl added to a 1.5 ml tube containing 5 µg DNA. Cells and DNA were pipetted into a nucleofection cuvette and placed in a nucleofection device (Lonza) and subjected to the appropriate program. Pre-warmed media was added to the cuvette and cells were carefully pipetted into a 100mm culture plate containing 10 ml medium and cultured under standard conditions.

2.2.3.2 siRNA transfections

On receiving of siRNA, RNase free water was used to dilute siRNA to 20µm. For siRNA experiments, $4x10^4$ (A375MM), $8x10^4$ (MV3 and CHL-1), $1.2x10^5$ (MDA-MB-231) and $1.5x10^5$ (primary mouse melanocyte) cells were treated with 50 to 100nmol/L of specific siRNA with Hyperfect, The cells were then grown for 2 days in 6 well tissue culture plate. The cells were then trypsinised and counted, replated and retransfected at the above concentration. This process was repeated again at 4 days, and the cells finally used for an experiment at 6 days.

2.2.3.3 siRNA sequence for RNA interference

Gene	Accession No.	Company, Cat No.	Target Sequence
AllStars Negative Control siRNA		Qiagen, 1027281	Nvegative control siRNA
Mm_Pak2_1	NM_177326	Qiagen, SI01368654	AAGAGATTATGGAGAAATTAA
Mm_Pak2_2	NM_177326	Qiagen, SI01368668	AAAGAAGGAATTGATCATTAA
Mm_Nap1_1	NM_016965	Dharmacon, J-041033-09	GGAGCAAGTGACCGAGAAT
Mm_Nap1_2	NM_016965	Dharmacon, J-041033-011	TTGAAAAGGATGACGATAA
Mm_Pak1	NM_011035	Dharmacon, L-048101-00-0005	ON-TARGETplus SMARTpool
Mm_p34	XM_001000089	Dharmacon, L-043464-01-0005	ON-TARGETplus SMARTpool
Mm_N-WASP	NM_028459	Dharmacon, L-055607-01-0005	ON-TARGETplus SMARTpool
Hs_Fascin1_1	NM_003088	Dharmacon, J-019576-07	GAGCATGGCTTCATCGGCT
Hs_Fascin1_2	NM_003088	Qiagen, SI00421799	CACGGGCACCCTGGACGCCAA
Hs_p34	NM_005731	Qiagen, SI02661414	AAGGATTCCATTGTGCATCAA
Hs_MT1-MMP	NM_004995	Dharmacon, L-004145-00-0005	ON-TARGETplus SMARTpool
Hs_N-WASP	NM_003941	Dharmacon, L-006444-00-0005	ON-TARGETplus SMARTpool

Table 7 – siRNA oligo sequences

2.2.3.4 Retroviral Infections

$2x10^6$ Phonenix-Ampho retroviral packaging cells were plated in a 100 mm dish and the following day cells were transfected using calcium chloride precipitation method. 5µg DNA in 440µl distilled H_2O was mixed with 500 µl 2 x HBS and 60 µl 2M $CaCl_2$ dropwise with vigorous shaking followed by precipitation for 30 minutes at 37°C and dropwise addition to Phonenix Ampho cells. Viral supernatant was harvested at 12 h intervals, purified through a 0.45 µm filter and added to target cells at 1 $x10^5$ cells/well in 6 well dish with addition of polybrene at a final concentration of 5 µg/ml. After 3 rounds of infection over 36 hrs, target cells were passaged into 100 mm dishes and 48 hours later selected with puromycin at 1 µg/ml (MDA-MB-231) and 3 µg/ml (CHL-1). All retrovirally produced cell lines were generated on at least 2 separate occasions to ensure the resulting phenotypes were consistent and, unless otherwise stated, all resulting cell populations were pools of selected colonies.

2.2.3.5 FACS of GFP or mRFP positive cell populations

A375MM cells stably expressing RFP-Lifeact, CHL-1 cells stably expressing GFP/RFP, GFP/RFP -*X. tropicalis* fascin, GFP/RFP -*X. tropicalis* fascin S33A, GFP/RFP -*X. tropicalis* fascin S33D and GFP-Lifeact were selected with 2mg/ml Geneticin. Cell pellets of 1 $x10^6$ were resuspended in 1 ml PBS and put through a 40 µm strainer. Cells expressing RFP or GFP were then sorted using Becton-Dickinson FACSAria. Typically, the brightest 10 % of the positive cell population were isolated for experimental use. The FacScan was operated by Tom Gilbey, Beatson Institute.

2.2.4 Protein immunoblotting

2.2.4.1 Protein extraction from cells or tissue

Fresh tissue or cells in tissue culture dishes were washed with ice cold PBS and lysed in RIPA buffer with protease inhibitor cocktail and Halt phosphatase inhibitor cocktail for 10 min on ice. Cells were scraped and tissue were homogenized with glass tissue grinder on ice and the lysates were transferred to ice cold 1.5 ml tubes and then centrifuged at 13,000 rpm for 5 minutes at 4 ^{o}C. The relatve protein concentration of the resulting supernatent was then determined using Precision Red Advanced Protein Assay Reagent and stored at –70 ^{o}C.

2.2.4.2 Separation of proteins by polyacrylamide gel electrophoresis (SDS-PAGE)

NuPAGE LDS Sample Buffer (4X) and NuPAGE Reducing Agent (10X) were used to dilute protein samples to give a 1x solution and heated at 95 ^{o}C for 3 minutes. Samples were resolved on precast NuPAGE Novex Bis-Tris Mini Gels (10% or 4%-12% depend on size of protein of interest) according to molecular weight by electrophoresis in gel tanks with 1 x NuPAGE MOPS SDS Running Buffer at 200V for approximately 50 mins until the dye front had reached the bottom of the gel. 10ul of SeeBlue Plus2 Pre-Stained Standard was load on side as molecular weight marker.

2.2.4.3 Western blotting

Proteins, separated by polyacrylamide gel electrophoresis, were transferred from the gel to PVDF membrane between Whatman 3MM paper at 250mA for 150 min in 1x NuPAGE transfer buffer. Membranes were blocked in TBST, 3 % BSA for 1 hour at room temperature and incubated with primary antibody at the appropriate dilution, time and temperature as advised by the manufacturer. Membranes were washed 3 times with TBST for 5 minutes, incubated with the appropriate secondary antibody in TBST, 3% BSA for 1 hour at room temperature and washed 3 times with TBST for 5 minutes. All incubations and washes were performed with gentle agitation. Proteins on

membranes were visualized using supersignal west femto maximum sensitivity substrate or supersignal west pico chemiluminescent substrate. The images were recorded and processed using GeneSnap software and Bio-imaging system. (Syngene). Western blots shown in figures are representative of typical results obtained on multiple occasions for each experiment shown. Quantification of western blots for siRNA experiments was done using Image J to outline the bands on the blots and calculate the pixel density compared with the non-targeting control.

2.2.5 Cell surface biotinylation assay

Cell surface proteins were biotinylated by incubating the cells with 0.5 mg/ml sulfo-NHS-SS-biotin on ice for 15 mins. Cells were then quenched with 50mM NH_4Cl and washed with ice cold PBS. Cells were lysed RIPA buffer and cleared cell lysate containing 400 µg total protein from each sample was incubated with NeutrAvidin Agarose Resin to pull down biotinylated proteins. The samples were then analyzed by immunoblotting for E-cadherin. Western shown in figures is representative of typical results obtained on multiple occasions for each experiment shown.

2.2.6 Effector Domain Pulldown Assays

The relative levels of GTP-bound RhoA, Rac, or Cdc42 were determined by an effector pulldown assay as described previously (Vidali et al., 2006). Briefly, primary melanocytes incubated with DMSO or 1 µM OHT as described in 2.14 were lysed in a buffer containing 50mM Tris HCl PH7.5, 1mM EDTA, 1% Triton X-100, 150 mM NaCl and protease inhibitor cocktail, and the lysates were probed with glutathione-agarose immobilized GST-Rhotekin (for RhoA) or GST-PAK1-PBD (for Cdc42 or Rac) domain (Cytoskeleton Inc). Bound proteins were analyzed by immunoblotting with anti-RhoA, -Rac1/2/3, or -Cdc42 monoclonal antibodies. Quantification of relative level of active RhoA or Cdc42 was done using ImageJ to outline the bands on the blots and calculate the pixel density compared with the DMSO treated control.

2.2.7 Fluorescent gelatin degradation assay (Invadopodia assay)

Gelatin from Porcine skin (Sigma) was labelled with Alexa Fluor 594 using Protein labeling kit (Invitrogen) according to manufacturer's protocol. Coverslips were acid-washed and coated with 50 µg/ml poly-L-lysine for 15 min, washed with PBS, and crosslinked with 0.5% glutaraldehyde for 15 min. The coverslips were then inverted on an 80 µl drop of 1mg/ml Alexa Fluor 594 conjugated or Oregon Green 488-conjugated gelatin or FITC-conjugated collagen type I for 10 min. After washing three times with PBS, the coverslips were then quenched with 5 mg/ml sodium borohydride for 3 mins followed by another three time washing with PBS. Finally, coverslips were sterilized with 70% ethanol for 5 min and incubated in complete growth medium for 1 hour before use. To assess the ability of cells to form invadopodia, cells were cultured on cross-linked fluorescent conjugated matrix for 16 hours for A375MM and 3 hours for MDA-MB-231 cells. CHL-1 cells were incubated overnight on cross-linked fluorescent conjugated matrix in presence of 5µM GM6001 MMP inhibitor and invadopodia were assessed 2 hours after washout of the inhibitor. The area of degradation was quantified using an Image J plug-in written for this purpose (Manuel Forero-Vargas, unpublished data). Quantification of area of degradation was done in at least three independent experiments in duplicate for each assay.

2.2.8 Three dimensional collagen I degradation assay

3D collagen degradation assay was performed as described previously (Wolf et al., 2003a; Wolf et al., 2007), with modifications. $1x10^6$ CHL-1 cells treated with NT, fascin, N-WASP, MT1-MMP siRNA or 5µM GM6001 MMP inhibitor or cells expressing both NT or fascin siRNA and mCherry-*X. tropicalis* fascin, *X. tropicalis* fascin S33A or *X. tropicalis* fascin S33D in 150 phenol red free medium were mixed with 150 µl rat tail collagen I containing 3 µl DQ FITC-labeled type I collagen monomers (2%), 16 µl 10xMEM and 11 µl 7.5% bicarbonate in well of 24 well plate. Mix polymerizes after 2 to 5 min at 20°C.

Put immediately in incubator. When collagen is cloudy, add each 300 µl phenolred-free medium. After 40 h of culture, solid-phase collagen including cells was pelleted by centrifuge at 13,000 rpm for 5 minutes at 4 ^{o}C, and the supernatant containing released FITC-collagen fragments was analyzed spectrofluorimentically with excitation at 490 nm and emission at 520 nm (QuantaMasterTM 40 spectrofluorometer; Photon technology international). The degradation of fibrillar collagen for each sample was calculated as fluorescence released from DQ FITC-labeled type I collagen monomers subtracted by background fluorescence, which was calculated by pelleting nondigested cell-free collagen lattices. Quantification of degradation was done in at least three independent experiments in duplicate for each assay.

2.2.9 Inverted Invasion Assay

2.2.9.1 Set up of invasion assay

Inverted invasion assays were performed as described previously (Caswell et al., 2007). Collagen I (PureCol Bovine Collagen, 3mg/ml) was concentrated to 10mg/ml using vivaspin 15R (Sartorius Stedim Biotech). 8 part of concentrated collagen I was then mixed with 1 part of 10xMEM and pH adjusted to 7.4 ± 0.2 by addition of 0.1M NaOH. An aliquot of matrigel, stored at -70 ^{o}C, was thawed on ice and diluted 1:1 with ice-cold PBS. Then, 70 µl of mixture of collagen I and matrigel yielding a final collagen concentration of approximately 4.4 mg/ml and a final Matrigel concentration of approximately 2.2 mg/ml was polymerized in transwell inserts containing 8µm pore-size micropore polycarbonate membrane filter (Corning) within a 24 well tissue culture plate (Falcon) for 2 hr at 37°C. Inserts were then inverted, 100 µl of cell suspension at a concentration of 5 x 10 per ml of medium was pipetted on to the underside of the transwell filter, the base of the 24 well plate was carefully replaced and the cells allow to adhere for 5 hours at 37°C. Transwell inserts were then placed in 1ml serum-free medium in 24 well plate, and 100µl normal growth medium was placed on top of the matrix, providing a chemotactic gradient. For experiments involving chemical inhibitors, appropriate inhibitors were added to both the serum free medium below the

transwell and the medium above the matrigel plug.

2.2.9.2 Quantification of invasion assay

72 hours after seeding, invading cells were stained by placing 500 µl of serum free medium containing 4 µM calcein AM above and below transwell invasion assays and incubating for 2 hours at 37 ^{o}C and cells that did not cross the transfilter were removed with tissue and the remaining cells were visualized by confocal microscopy using a 10 x objective at an excitation wavelength of 488 nm and emission wavelength of 515 nm; serial optical sections were captured at 10 µm intervals upwards from the underside of the transwell filter. The fluorescence intensity for each section was then measured using a plug-in (Area calculator) in ImageJ, which allocates each pixel an intensity value and allows a threshold intensity level to be set, below which pixels are not displayed. The threshold intensity of the images was set in order to register only cells that lay within each individual optical section. Finally, the percentage of invading cells was calculated as the fluorescence intensity of cells invaded above 20 µg against the total fluorescence intensity of all cells within the images of sections taken. At least three independent experiments in duplicate for each sample were carried out.

2.2.10 Transfilter migration assay

Transwell inserts (Corning) were coated with 20 µg/ml human placenta laminin overnight, which then blocked with 1mg/ml BSA for 1 hour and wash three times with PBS. For A375MM and MDA-MB-231 cells, 6x10^{4} cells in 500µl serum free medium were seeded into the top chambers of a 24-well, 8µm pore-size micropore polycarbonate membrane filter (Corning), and the lower chambers were filled with 1ml DMEM containing 10% FBS as a chemoattractant and incubated for 12 h at 37°C. For MV3 and CHL cells 3x10^{4} cells in 500µl serum were seeded and incubated for 12 hours at 37°C. Cells remaining on the upper surface of the transfilter were then carefully

removed with a cotton swab, and the membranes were fixed and stained with DAPI and rhodamine phalloidin. Migration was quantified by counting the migrated cells (DAPI staining) in 5 random 20x magnification fields per filter. At least three independent experiments in duplicate for each sample were carried out.

2.2.11 2D anchorage-dependent cell growth assay

Primary melanocytes were incubated with DMSO or 1 μM OHT for 5 days and then cultured in medium without DMSO or OHT for another two days. At day 0, $1x10^4$ cells were plated in each well of 6 well plates, and number of cells were trypsinized and counted every two days (for primary melanocytes) from one well of 6 well plates for 8 day using CASY Cell Counter (Roche Innovats). For cancer cells (A375MM, MDA-MB-231, MV3 and CHL-1), at day 0, $1x10^4$ cells were plated in each well of 6 well plates. Cells were then trypsinized and the number of cells was counted every day for 5 days. Each point (Mean ± SEM) is derived from the mean of hemocytometer count of cells from three replicate dishes from three independent experiments.

2.2.12 3D anchorage-independent cell growth assay (Agar growth assay)

1.5 ml of 0.7% SeaPlaque agarose/F-12/10% FBS was added to each well of 6-well dishes, which incubate at RT for 1 hour. 1×10^4 cells were plated in 1 ml of 0.35% SeaPlaque agarose/DME/10% FBS on the top. Once solidified, the agarose was covered with 2.5 ml DME/10% FBS, which was changed twice weekly. Digital images were captured 4 wk later at room temperature with a microscope (Axiovert Stemi 200C; Carl Zeiss, Inc.) using a 1.0× objective with a Canon 1000D camera processed with ImageJ. Number of colony in soft agar was quantified by determining the number of colonies >0.5 mm in diameter 4 wk after plating. Relative size of colony was determined by measuring the diameter of 20 biggest colonies in each sample. Three replicate dishes from three independent experiments were quantified.

2.2.13 Flow cytometry

Cells were pre-incubated for 2 hr with 10 uM BrdU and fixed in 70% ethanol/30% PBS overnight at -20 °C. Cells were then pellet, washed with PBS and bleached with melanin bleach kit. Cells were treated with pretreatment solution A for 2 min and followed with extensive wash with PBS and incubated with solution B for 1 min. After washes with PBS, cells were incubated with 4N HCl for 15 min and stained with mouse Anti-BrdU antibody (Dako, 1 in 40) in PBT (0.1% BSA+0.01% Tween 20 in PBS) for 30 min and followed with Alexa-488 conjugated goat anti-mouse secondary antibody (1 in 50) in PBT for 30 min. After washes, cells were stained with propidium iodide (1 mg/ml) and RNaseA (250 µg/ml) for 30 min before processed on BD FASC-Calibur (BD bioscicence).

2.2.14 Immunofluorescence

Cells cultured on crosslinked gelatin coverslips were fixed and processed for immunofluorescence. For 2D or 3D staining with antibody to fascin, β-actin or cells expressing GFP-fascin, cells were fixed with -20^{o}C methanol at -20^{o}C for 10 min and blocked for 30 min with Image-iT FX Signal Enhancer. For all other staining, cells were fixed in 4% formaldehyde and permeabilized for 4 min in 0.1% Triton X-100 in PBS and blocked with Image-iT FX Signal Enhancer for 30 min and incubated with primary antibody for 1 hours (overnight for 3D staining). Cells were washed 3 times for 5 min (30 min for 3D staining) in PBS and primary antibodies were detected with the use of appropriate species- and class- specific Alexa350, Alexa488, Alexa594 and Alexa647-conjugated secondary antibodies for 30 min (overnight for 3D staining). Samples were then examined using Olympus FV1000 inverted laser scanning confocal microscope or Nikon A1 inverted laser scanning confocal microscope or using a Zeiss Axioskop2 microscope equipped with a digital camera C4742-95 (Hamamatsu).

2.2.15 Live cell imaging

2.2.15.1 Live cell imaging of invadopodia dynamics

A375MM cells stably expressing RFP-Lifeact were transfected with control or fascin siRNA and cultured on Oregon Green 488-conjugated crosslinked gelatin overnight in presence of 5μM GM6001 MMP inhibitor. 1 hour after washout of the inhibitor, cells were recorded in a humidified CO2 chamber at 37 ^{o}C with an inverted fluorescence microscope (Nikon) with a motorized stage. Timelapse images were captured using Metamorph software (Molecular Devices) every 5 min for 15 h.

2.2.15.2 Live cell imaging of cell morphology during invasion

CHL-1 cells stably expressing GFP-Lifeact were plated on a glass bottom microwell 35mm petri dish (MatTek Cor.) at 2x10^{5} and starved overnight. The medium was then aspirated and 200μl of a mixture of collagen I-Matrigel (prepared as described in 2.2.9.1) was applied on top of cell monolayer and the gel was allowed to polymerize in 37 ^{o}C for 2 hours. The normal growth medium was added to the dish and samples were incubated for 48 hours. Cell that has invaded into the gel was imaged. Timelapse images were captured every 10 mins for 10 h using an Olympus FV1000 confocal microscope in a 37 ^{o}C chamber with 5% CO_2.

2.2.15.3 Live cell imaging of cell migration on 2D surface

For 2D melanocytes imaging, cells were plated overnight in glass bottomed dishes, which were coated with 10 μg/ml fibronectin for 1 h at 37 °C, and then incubated with 1% bovine serum albumin for 20 min. Time-lapse video microscopy was performed using a Nikon TE2000 microscope in a 37°C chamber with 5% CO_2.

2.2.15.4 Live cell imaging of cell morphology on 3D collagen I matrix

For live imaging of melanocytes on 3D think layer of collagen, Fibrillar rat-tail Collagen I was prepared from a 3 mg/ml as described in **2.11**, 500 ul was then set in wells of 12 well plate for 1 h at 37 °C. Cells were seeded on top of collagen in medium and allowed to adhere for 24 hr. Time-lapse video microscopy was performed using a Nikon TE2000 microscope in a 37°C chamber with 5% CO_2. For evaluation of the percentage of elongated cells, a cell was considered elongated when its longest dimension was twice the shortest.

2.2.15.5 Fluorescence recovery after photobleaching (FRAP)

FRAP was conducted using the following settings: pixel dwell time 4 µs/px, picture resolution 256 x 256, 2 % 488 nm or 561 nm laser power. GFP or mRFP signals at invadopodia were bleached using 45 % 405 nm laser power, 4-µs/pixel dwell time for 1 region of interest frame. Images were captured every 0.428s. Recovery of the signal was measured using the region analysis tool of the Olympus FV1000 viewer software and averaged in Excel. The resulting data was corrected for imaging dependent intensity loss (non-specific bleaching) and then normalized to the pre-bleached images. Each normalized single curve was then exported into SigmaPlot (Systat Inc.) for exponential curve fitting. Data were fit using the following exponential functions: y = y0 + a • (1 – e-bt). The half-time of recovery for each curve was calculated using the formula ln2 / b, where b was obtained from the exponential curve fit. The percentage of recovery was calculated using formula: Xm = F (∞)/F (I). Where F (I) denotes the average fluorescence intensity before photobleaching for each normalized curve, F (∞) refers to the average fluorescence intensity derived from the plateau for each normalized curve.

2.2.16 Ex-vivo imaging of melanoblast migration

Experiment set up was previously reported with modifications (Mort et al.,

2010). Briefly, a freshly dissected E15.5 embryonic skin sample was sandwiched between a nucleopore membrane (Whatman) and a gas permeable Lumox membrane in Greiner Lumox culture dish (Greiner Bio-One GmbH) so that the epidermial side of skin was in contact with lummox membrane. To immobilize the sample, Growth Factor Reduced Matrige was used to cover the whole assembly and incubate at 37°C for 10 min. Culture medium (Phenol red free DMEM supplied with 10% FBS and 100 µg/ml primocin was finally added. For drug treatment, drugs were added to Matrigel and medium 1 hr before imaging. All the drugs were used at 10µM, except CK869 and CK312, which was used at 20 µM, latrunculin A was used at 0.3µM and nocodazole was used at 1µM. Timelapse images were captured using an Olympus FV1000 or Nikon A1 confocal microscope in a 37°C chamber with 5% CO_2 at 20x magnification objective or 60x magnification objective for 5 hr.

2.2.17 Histology and staining of tissue

2.2.17.1 Immunohistochemistry (IHC)

Formalin-fixed paraffin-embedded sections were deparaffinized and rehydrated by passage through xylene and a grade alcohol series. Antigen retrieval was performed by incubation of sections in microwave-heated 1x citrate buffer, pH 6.4 in a pressure cooker (see 2.2.17.2). For IHC using alkaline phosphatase substrate kit, sections were blocked in 10% serum for 1 hr and then sections were washed three times with 1xTBST and incubated with primary antibody at RT. Sections were washed three times with 1xTBST and incubated with secondary antibody for 1 hr and after 5 min wash with 1x TBST, signal for secondary antibody was amplified using Vectastain ABC kit. The staining was visualized with alkaline phosphatase substrate kit according to manufacture's introduction (Vector laboratories, Inc.) and hematoxylin was used as the nuclear counterstain. For IHC using Envision kit, sections were blocked with peroxidase block for 5 min. the sections were washed and incubated with primary antibody diluted in antibody dilute. The sections were

then washed three times with 1xTBST and incubated with peroxidase labeled polymer. After three times wash in 1xTBST, the staining was visualized with Liquid DAB + substrate-chromogen solution according to manufacture's introduction. Slides were counterstained with haematoxylin, prior to being dehydrated in increasing concentrations of ethanol and mounted. For immunofluorescence on embryo sections, after antigen retrieval, sections were blocked with 5% serum for 1 hr and incubated with primary antibody overnight at 4 °C. Sections were then washed three times in PBS and incubated with fluorescent conjugated secondary antibodies for 1 h at RT and mounted with Prolong Gold Antifade reagent. For BrdU assay, mice were i.p. injected with 2.5 mg BrdU for either 2 hr or 24 hr before embryo dissection. For hematoxylin and eosin stain stainings, all steps were done according to standard protocols were performed by C. Nixon and colleagues, Beatson Institute.

2.2.17.2 Miarowave antigen retrieval

Microwave antigen retrieval was performed by pre-heating 1500ml Citrate buffer pH 6.4 in an open pressure cooker for ~15minutes until boiling. Slides were then placed into the solution and heated with the lid on until the pressure was optimised. Slides were then heated for a further 3-4 minutes, before being removed and allowed to cool at room temperature for 30 minutes.

2.2.17.3 Whole-mount X-Gal staining of embryos

Embryos or the dorsal skin from new born pups were fixed in 0.25% glutaraldehyde in PBS at 4 °C for 40 min, washed in detergent buffer and stained overnight in X-Gal buffer containing 2 mg/ml X-Gal in dimethylformamide. For quantification of the epidermis-dermis distribution of melanoblasts in embryos, X-Gal stained embryos were paraffin-embedded, sectioned and counterstained with hematoxylin or eosin.

2.2.17.4 Whole-mount immunofluorescence staining of embryos or skin explants

For whole mount immunofluorescence, embryos or skin explants were fixed in 4% paraformaldehyde at 4 °C overnight. Embryos or skin explants were then washed 3X in PBS containing 1% Triton for 30 min and incubated in blocking buffer (PBS 1% triton+ 10% FBS 0.2% sodium azide) for 1 hr at RT. Embryos or skin explants were washed another two times with blocking buffer and incubated in blocking buffer containing primary antibody for 4 days at 4 °C. Embryos or skin explants were washed 3X in blocking buffer for 1 hr and 3x in PBS 1% Triton for 10 min. Embryos or skin explants were then incubated with secondary antibody in blocking buffer for 4 days at 4 °C. Embryos or skin explants were washed 3x in PBS 1% Triton for 10 min and stored in dark at 4 °C.

2.2.18 Generation, maintenance and treatment of mouse colonies

2.2.18.1 Transgenic mice

All experiments were performed according to UK Home Office regulations. The Rac1 floxed mice in C57BL6/J background were previously described (Walmsley et al., 2003). Tyrosinase Cre A (Tyr::Cre) mice in C57BL6/J background were previously described (Delmas et al., 2003). The Tyr::Cre transgene is integrated on the X chromosome (Delmas et al., 2003). Therefore, only Rac1 f/f Tyr::Cre$^{+/o}$ males were analyzed as Rac1 null, which will carry one copy of Tyr::Cre and Rac1 f/f Tyr::Cre$^{+/o}$ female were excluded from this study. Tyr::Cre deletion of Rac1 caused a shakiness of the mice that required culling at around 3 week of age. This is likely due to some expression of the Cre in the neuronal lineage (L. Larue, and R. Mort, unpublished). There are no phenotypes associated with Rac1 f/+ Tyr::Cre$^{+/o}$ animals. Therefore, heterozygous genotype with genotypes: Rac1 +/+ Tyr::Cre$^{+/o}$, Rac1 +/+ Tyr::Cre$^{o/o}$, Rac1 f/+ Tyr::Cre$^{o/o}$ served as control for this study. LacZ/EGFP (Z/EG) mice in C57BL6/J background were previously described (Novak et al., 2000), N-WASP floxed mice in 129SvEv background

were previously described (Snapper et al., 2001) which were backcrossed for 6 generations with C57BL6/J mice. DCT-LacZ (DCT::LacZ) mice in mixed background were previously described (Mackenzie *et al.*, 1997). Tyrosinase Cre-ERT2 (Tyr::Cre-ERT2) in C57BL6/J background were described in (Yajima et al., 2006). GFP-Lifeact floxed mice were generated by David Stevenson and Douglas Strathdee (Beatson institute) and INK4a-deficient mice in C57BL6/J background were described in (Ackermann et al., 2005; Serrano et al., 1996).

2.2.18.2 Gentotyping

Genomic DNA was prepared from tail or skin biopsies and genotyping of the transgene was performed as previously described (McClive and Sinclair, 2001; Serrano et al., 1996) and by the company Transnetyx (Memphis, TN).

2.2.19 Quantifications

2.2.19.1 Melanoblast/mealnocyte migration speed, euclidean distance and persistence

For melanoblast migration in skin explants, individual cell was tracked manually using ImageJ, Manual Tracking plugin, with distance/time measurements taken every 5 min for 3 hr. For melanocyte migration on 2D surface, individual cell was tracked manually every 10min for 15 hr. The migration speed (cell path/time), euclidean distance (the net movement that cell made), and persistence (euclidean distance/ cell path) were calculated using Chemotaxis Tool plugin. More then 60 cells were examined for each skin explants and mean value was taken, and each experiment was repeated with at least 3 skin explants. Mean values ± s.e.m and statistical analysis were calculated and plotted using Graphpad Prism (Graphpad Software). Two-tailed unpaired t-tests were conducted to determine significance.

2.2.19.2 Quantification of Number of Filopodia-Like Protrusions

XY-series of sample stained with rhodamine phalloidin and DAPI were captured at 0.5μm Z-spacings. The total number of filopodia like protrusions (judged to be extending from the cell periphery) in each Z-stack was determined. The number of filopodia-like protrusions per cell was then determined by calculating the total number of filopodia like protrusions against the total number of cells (DAPI staining) in the Z-stack. Each siRNA treated cell population was analyzed in 3 random 20x magnification fields and duplicate in three independent experiments.

Chapter III
The Actin-Bundling Protein Fascin Stabilizes Actin in Invadopodia and Potentiates Protrusive Invasion

3.1 Summary

One of the defining features of invasive tumor cells is that they can degrade ECM and invade through the use of invadopodia. Previous studies have shown a role for fascin, an actin-bundling protein, in metastasis and invasion as well as tumour progression in several types of cancer. This work led to the discovery that fascin is an integral component of invadopodia in multiple cancer cell types and that fascin is required for the assembly of the actin cytoskeleton in these structures as well as for the degradation of matrix. The phosphorylation state of fascin at S39, a PKC site, contributes to its regulation at invadopodia. Fascin is a very stable component of invadopodia and its presence enhance the stability of actin structures at invadopodia. Thus we propose a major role for fascin in invasive migration in addition to its already established role in the formation of filopodia. Furthermore, fascin is required for invasive migration into collagen I-Matrigel gels particularly in cell types that use an elongated mesenchymal type of motility in 3D.

3.2 Introduction

Fascin is an evolutionarily conserved actin bundling protein important for filopodia dynamics in primary cells (Yamakita et al., 2009) and several types of cancer cells (Adams, 2004; Hashimoto et al., 2006; Vignjevic et al., 2006). Fascin forms stable bundles with slow dissociation kinetics in vitro (Tseng et al., 2001) and is regulated by phosphorylation of serine 39 by protein kinase C (Adams, 2004b). Fascin is not expressed in normal epithelia but is often upregulated in epithelial cancers and is associated with a poor prognosis and higher grade (Hashimoto et al., 2004; Vignjevic et al., 2007).

Invadopodia are protrusions on the ventral surface of cells that have matrix degrading activity and adhesive functions (Buccione et al., 2009). Tumor cells on a thin matrix in vitro form invadopodia rich in actin and other actin assembly proteins such as Arp2/3 complex and N-WASP (Baldassarre et al., 2006b; Yamaguchi et al., 2005). In vivo, tumor cells are thought to form structures resembling invadopodia (Wang et al., 2005; Wyckoff et al., 2007)

but their function in metastasis isn't clear. Invadopodia have highly dynamic actin that is assembled by both Arp2/3 complex and formins (Baldassarre et al., 2006; Lizarraga et al., 2009; Yamaguchi et al., 2005); they also contain components of membrane trafficking machinery such as dynamin and cortactin (Buccione et al., 2009) and have been compared with focal adhesions and podosomes (Buccione et al., 2004; Gimona et al., 2008).

Mammalian cells migrate using both actin-based protrusions and myosin-based contractile activities. Tumor cells moving in a 3D matrix employ two major modes of motility: mesenchymal type motility in which cells are elongated and protrusive and use protease activity to navigate through dense matrix and amoeboid movement in which cells are more rounded and use acto-myosin contractility to squeeze through the matrix in a bleb-like fashion (Friedl and Wolf, 2003; Wolf et al., 2003a).

In this Chaper, I have described a noval role of fascin as an integral component of invadopodia and that it is important for the stability of actin in invadopodia. I further implicated fascin in invasive migration into collagen I-Matrigel gels and particularly in cell types that use an elongated mesenchymal type of motility in 3D. This work provides a potential molecular mechanism for how fascin increases the invasiveness of cancer cells.

3.3 Results

3.3.1 Fascin expression in human melanocyte and melanoma cells

Multiple studies have reported a low or absence of fascin expression in normal epithelial tissue but highly upregulated in more aggressive and metastatic epithelial cancers and that high fascin expression is a significant independent prognostic indicator of poor outcome (Hashimoto et al., 2005; Machesky and Li, 2010). We therefore tested if this is the case for human melanoma. We first investigated the expression of fascin in a panel of human melanoma cell lines as well as normal primary human melanocytes by

western blot. Fascin expression was observed in all human melanoma cell lines and normal neonatal and adult epidermis melanocyte cells (Figure 3.1). Overall, no significant difference in fascin expression between human melanocyte and melanoma cells.

3.3.2 Fascin Localize at filopodia and dorsal microspikes in A375MM melanoma cells

A375MM melanoma cells are derived from the metastases of metastatic melanoma, thus are highly invasive (Kozlowski et al., 1984). To study the effect of fascin in human melanoma cell invasion, the distribution of fascin was analyzed in a A375MM cells. Phalloidin staining of A375MM cells revealed the formation of both filopodia at cell periphery and microspikes on the dorsal surface (Figure 3.2A). Immunostaining with fascin antibody (Figure 3.2B) or exogenous expression of GFP-fascin showed a localization of fascin at both peripheral filopodia and dorsal microspikes (Figure 3.2C, E). Fascin-enriched filopodia can also be observed on the ventral surface of cell body using total internal reflection fluorescence microscopy (Figure 3.2D). However, exogenous expression of GFP-fascin in A375MM cells did not obviously alter the general cell morphology.

3.3.3 Fascin is important for filopodia formation in A375MM melanoma cells

To investigate the function of fascin in filopodia, we used two independent siRNA to knock down fascin in A375MM cells by 90% and 85% respectively (Figure 3.3 A and B). We found that fascin knockdown did not affect cell proliferation (Figure 3.3 C). For both siRNA, fascin knockdown, however, results in a more than 1.6 fold reduction in the formation of peripheral filopodia without affecting the cell spreading and formation of lamellipodia (Figure 3.4 A and B). In addition, we also observed the decrease in the formation of microspikes in the dorsal surface of the cell with the remaining spikes appearing buckled (Data not shown). These findings are consistent with a

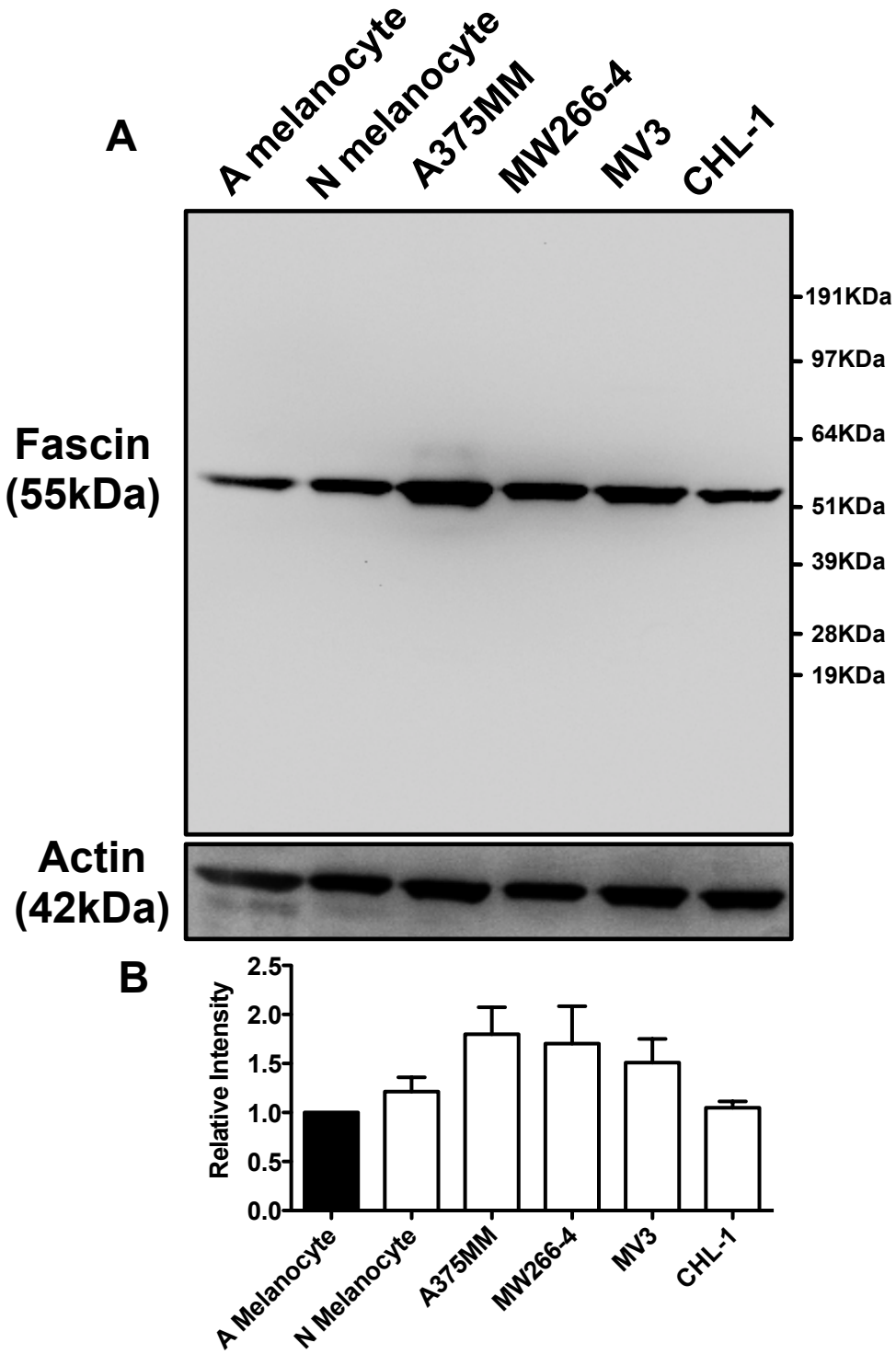

Figure 3.1. Fascin Is Expressed in Melanocytes and Melanoma Cells

(A) Western blot analysis of fascin expression in human (A melanocyte: adult epidermal melanocyte; N melanocyte: neonatal melanocyte; A375MM melanoma; MW266-4 melanoma; MV3 melanoma; CHL-1 melanoma cell lines. Actin was probed as loading control. (B) Western blots were quantified and the relative intensity of fascin signal was normalised to total actin. The results shown are the means ±SEM of three independent experiments.

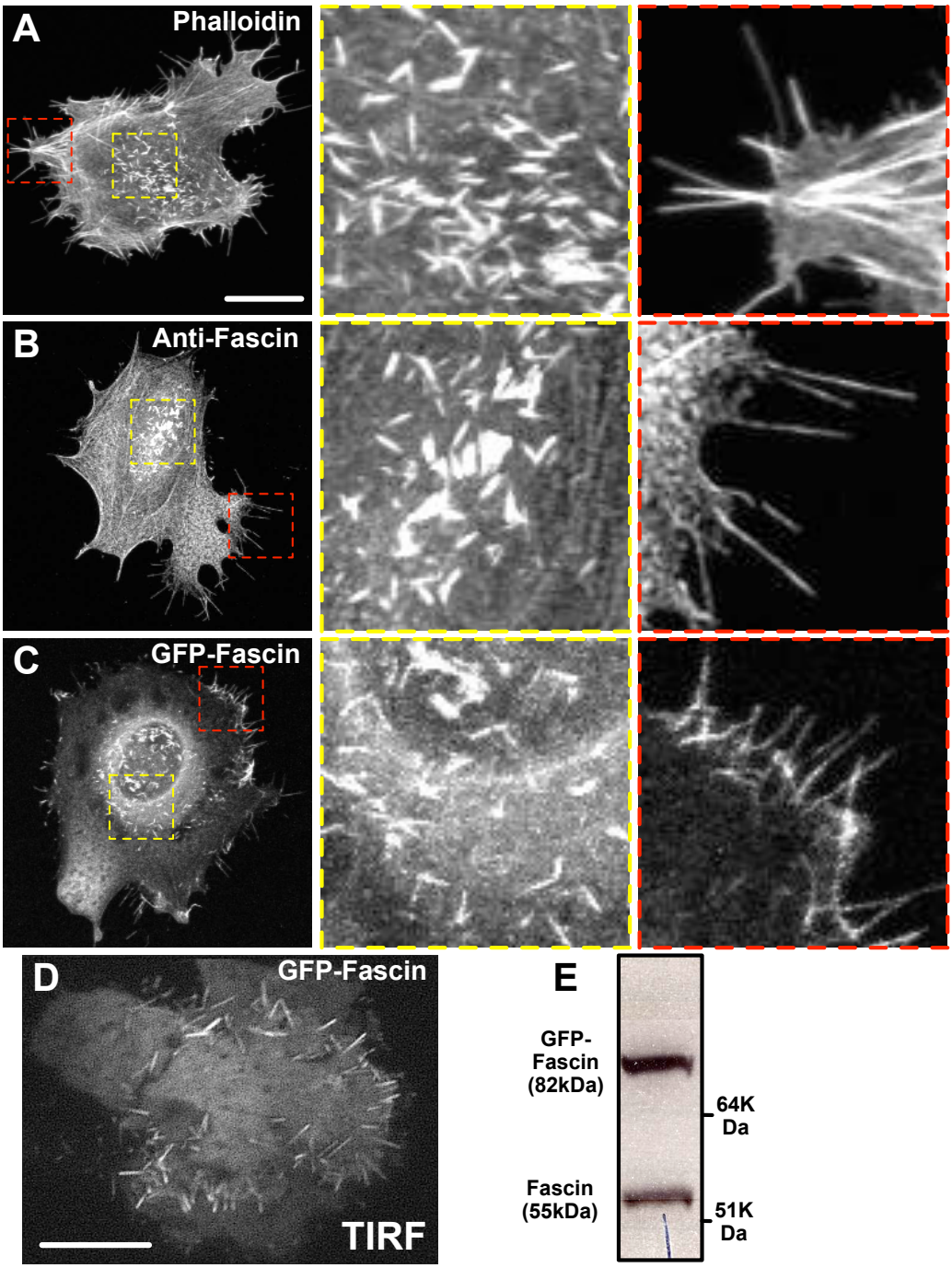

Figure 3.2. Localisation of fascin at filopodia in A375MM cells
Combined Z-stack images (1μm) of A375MM cells adherent on gelatin and stained with phalloidin (A) or anti-fascin (B) or expression of GFP-fascin (C) develop numerous filopodia at the periphery and microspikes on the dorsal surface and fascin localized at both peripheral filopodia and dorsal microspikes. (D) Total internal reflection microscopy images of A375MM cell expresses GFP-Fascin. Scale bar is 10μm. (E) western blot showing A375MM cells transfected with human GFP-fascin. Immunoblot was probed with fascin antibody.

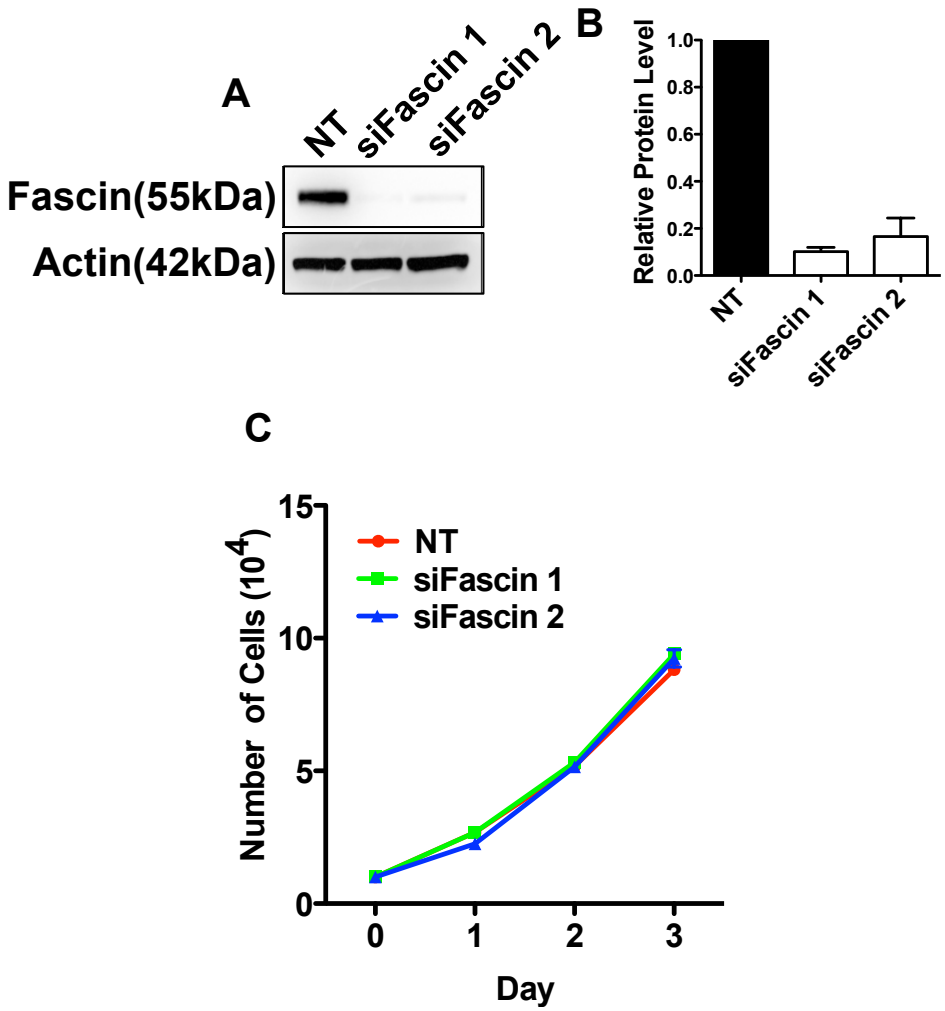

Figure 3.3 Fascin knockdown does not alter cell growth rate in A375MM melanoma cells

(A) Cell lysates from A375MM human melanoma cells transiently transfected with non-targeting pool control siRNA (NT) or fascin siRNA (sifascin 1 and sifascin 2) were analyzed by immunoblotting and probed for fascin. Membranes were also probed with actin antibody as a loading control. (B) Relative fascin expression level was qantified from 4 individual blots. (C) $1x10^4$ A375MM cells express NT or fascin siRNA were plated in each well of 6 well plates, and number of cells was counted every day for 3 days. Each point (Mean ± SEM) is derived from the mean of hemocytometer count of cells from three replicate dishes from two independent experiments.

previous report (Vignjevic et al., 2006) using B16F1 mouse melanoma cells and suggest that fascin is required for filopodia formation in A375MM cells and may help to maintain the filopodia stiffness. To further confirm the specificity of fascin knockdown phenotype on filopodia formation, we set up rescue experiment by expressing the GFP-tagged *X. tropicalis* fascin (GFP-Xtfascin) refractory to RNAi in fascin siRNA treated cells (Hashimoto et al., 2007). Fascin knockdown cells transfected with GFP-Xtfascin resulted formation of numerous filopodia on both cell periphery (Figure 3.4A, B. western blot of protein expression refer to Figure 3.20A) and dorsal side (Data not shown) with the number of filopodia statistically the same as control cells. Therefore, fascin knockdown phenotype could be rescued by expression of GFP-Xtfascin cDNA.

3.3.4 Fascin is localized at invadopodia in A375MM melanoma cells.

Early studies indicated that fascin is highly expressed in the invasive front when cancer cells start to invade into the local surrounding tissue (Hashimoto et al., 2005; Machesky and Li, 2010; Vignjevic et al., 2007). Invadopodia are finger-like proteolytically active protrusions that extend from the ventral surface of the cell into the surrounding matrix, causing the focal pericellular degradation of ECM to promote cell invasion (Ayala et al., 2006; Buccione et al., 2009; Weaver, 2006; Yamaguchi et al., 2006). Therefore we examined whether fascin was localized to invadopodia. Interestingly, immunofluorescence with two different antibodies to target endogenous fascin showed colocalization of fascin with actin and p34-Arc (ARPC2), a subunit of Arp2/3 complex, at invadopodia (Figure 3.5 A and B). In addition, GFP-fascin also colocalized with cortactin at invadopodia (Figure 3.5 C). Thus, fascin clearly localizes at invadopodia in A375MM cells.

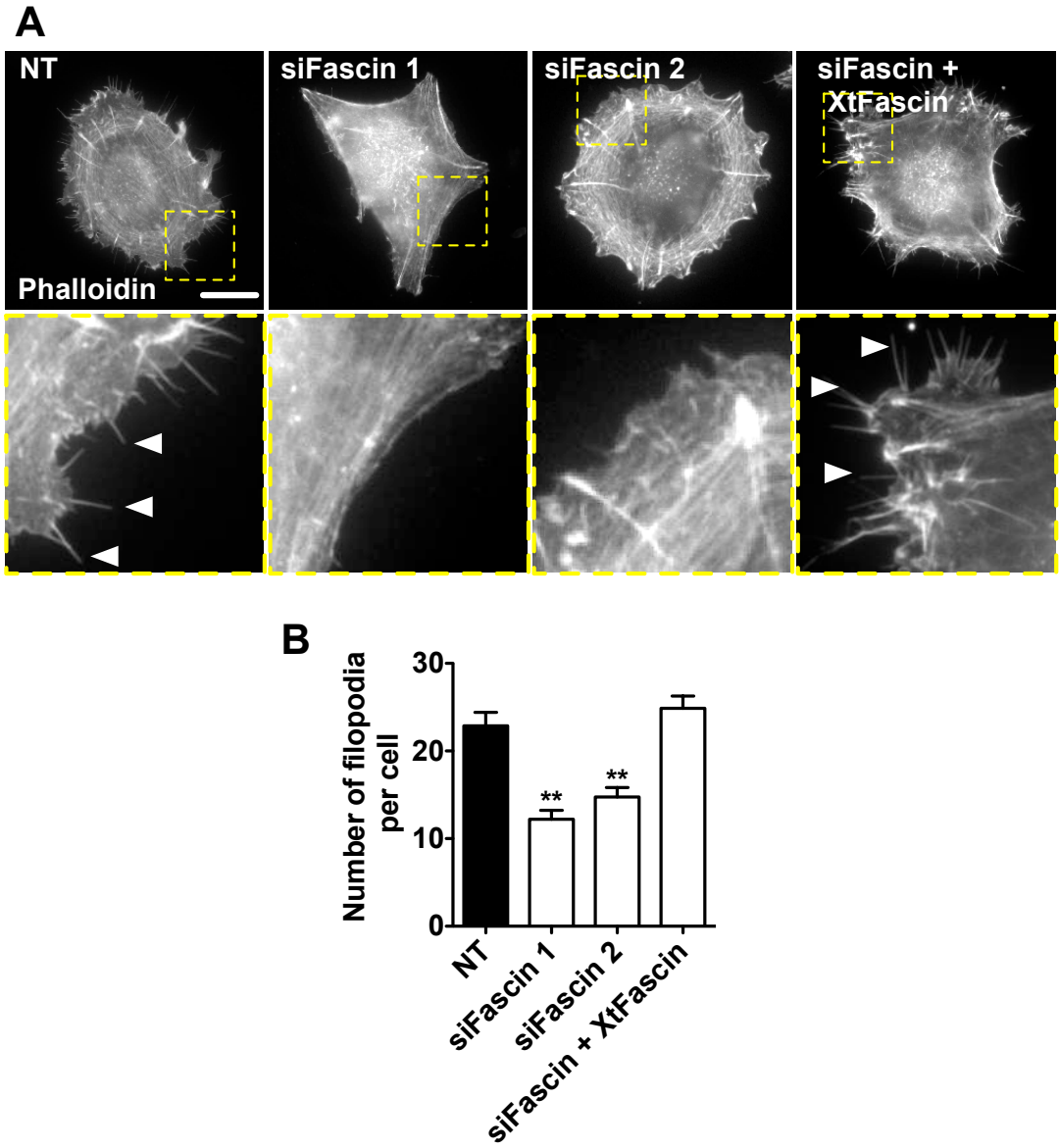

Figure 3.4. Fascin knockdown reduces filopodia formation in A375MM cells
(A) F-actin organization in A375MM cells. A375MM cells transfected with fascin siRNAs (siFascin 1 and siFascin 2) adherent on gelatin were fixed and stained with rhodamine phalloidin. Fascin knockdown cells showed fewer peripheral filopodia compared to cells transfected with control NT siRNA and cells expressing both Fascin siRNA (siFascin 1) and rescued with GFP-*X.tropicalis* fascin. Examples of filopodia are arrowed. Bars, 10μm.
(B) Quantification of filopodia. The number of peripheral fiopodia was counted from 90 phalloidin stained cells in three independent experiments. Error bars: Mean ± SEM. **, P< 0.01 compared to control cells by t-test.

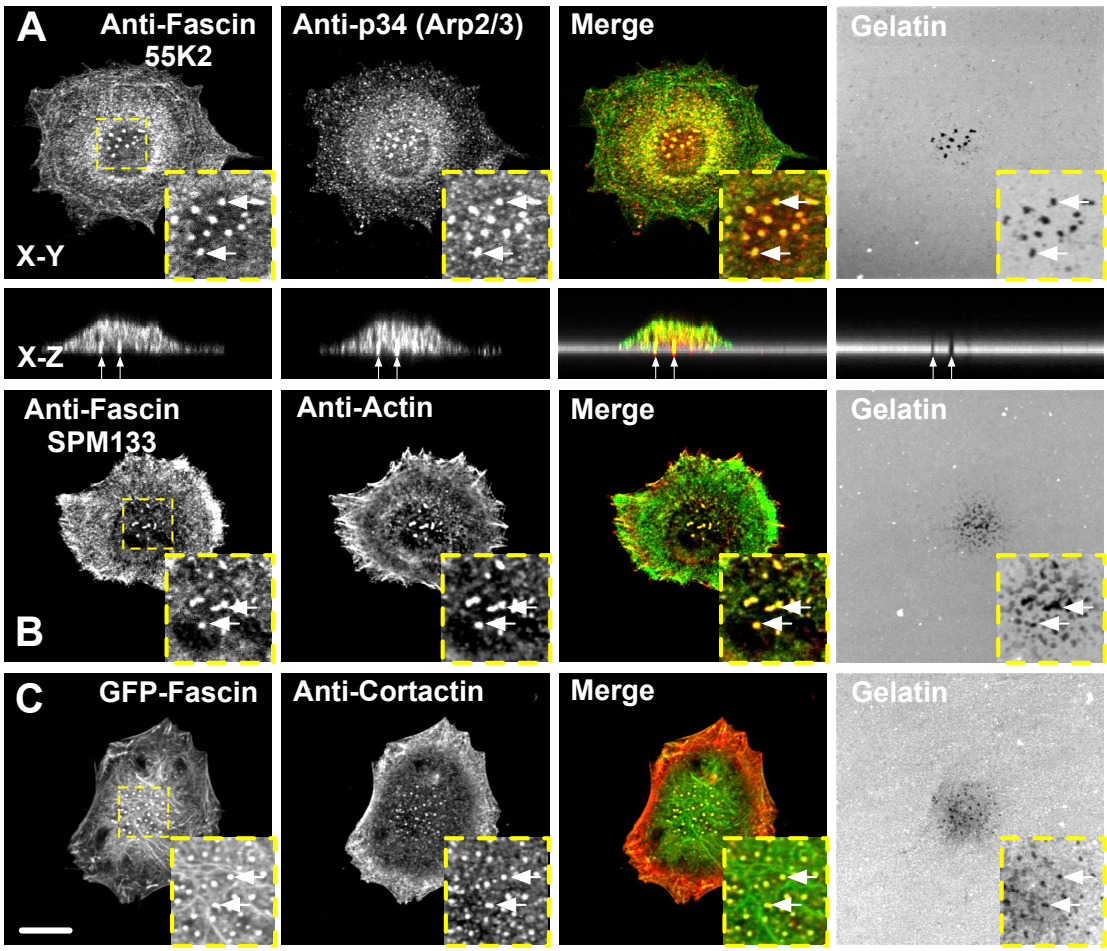

Figure 3.5. Fascin localize to invadopodia in A375MM melanoma cells
(A) A375MM cells on Oregon Green 488 gelatin matrix (shown as grey) immunolabeled with anti-fascin (55K2) and anti-p34-Arc (Arp2/3 complex). Both X-Y and X-Z view were showen. Individual invadopodia were white arrowed (B) A375MM cells on Oregon Green 488 gelatin matrix immunolabeled with anti-fascin (primary SPM133) and anti-actin. (C) A375MM cells expressing GFP-fascin on Alexa594 labelled gelatin matrix immunolabeled with anti-cortactin. Example invadopodia are arrowed. Scale bar is 10μm.

3.3.5 Fascin is localized throughout the comet structure of invadopodia and localization of filopodia proteins at invadopodia.

A recent study of invadopodia dynamics revealed a comet-like organization resembling bacteria-propelling actin tails with cortactin and Arp2/3 complex distributed throughout the comet structure, while N-WASP was only concentrated at the "head" section (Baldassarre et al., 2006). Consistent with that study, we also observed numerous comet tails, which appeared tethered near the head with a dynamic tail that spins, at degradation sites in A375MM cells, somewhat reminiscent of a corkscrew (Movie 1 Part 1). Only large invadopodia appeared as obvious comets (Figure 3.6). We found that Arp2/3 complex, cortactin, and fascin localized throughout comet heads and tails (Figure 3.6A, B, C and Movie 1 Part 2 and 3), whereas N-WASP concentrated mostly in the head (Figure 3.6D Part 4 and 5), which may be recruited to and activated at comet heads by phosphoinositides (Figure 3.6). In addition to fascin, IRSP53, IRTKS and mDia2, which are proteins that promote the formation of filopodia (Millard et al., 2007; Scita et al., 2008; Yang et al., 2007), also localized at invadopodia in A375MM (Figure 3.7). Taken together, these data suggested that invadopodia might be a hybrid structure containing both actin branches and bundles.

3.3.6 Fascin is required for invadopodia formation and ECM degradation in human A375MM melanoma cells.

To determine whether fascin function is necessary for invadopodia formation, RNA interference was used to knock down fascin in A375MM cells. A375MM cells expressing control or fascin siRNA were cultured on crosslinked Oregon Green 488-conjugated gelatin or FITC-conjugated collagen I matrix for 16 hours. Cells were then fixed and stained for actin and cortactin to visualize the invadopodia puncta (Figure 3.8A). The area of degradation was quantified using a semi-automated ImageJ plugin (created by John Dawson and Manuel Forero-Vargas, Birmingham University). The total areas of degradation per

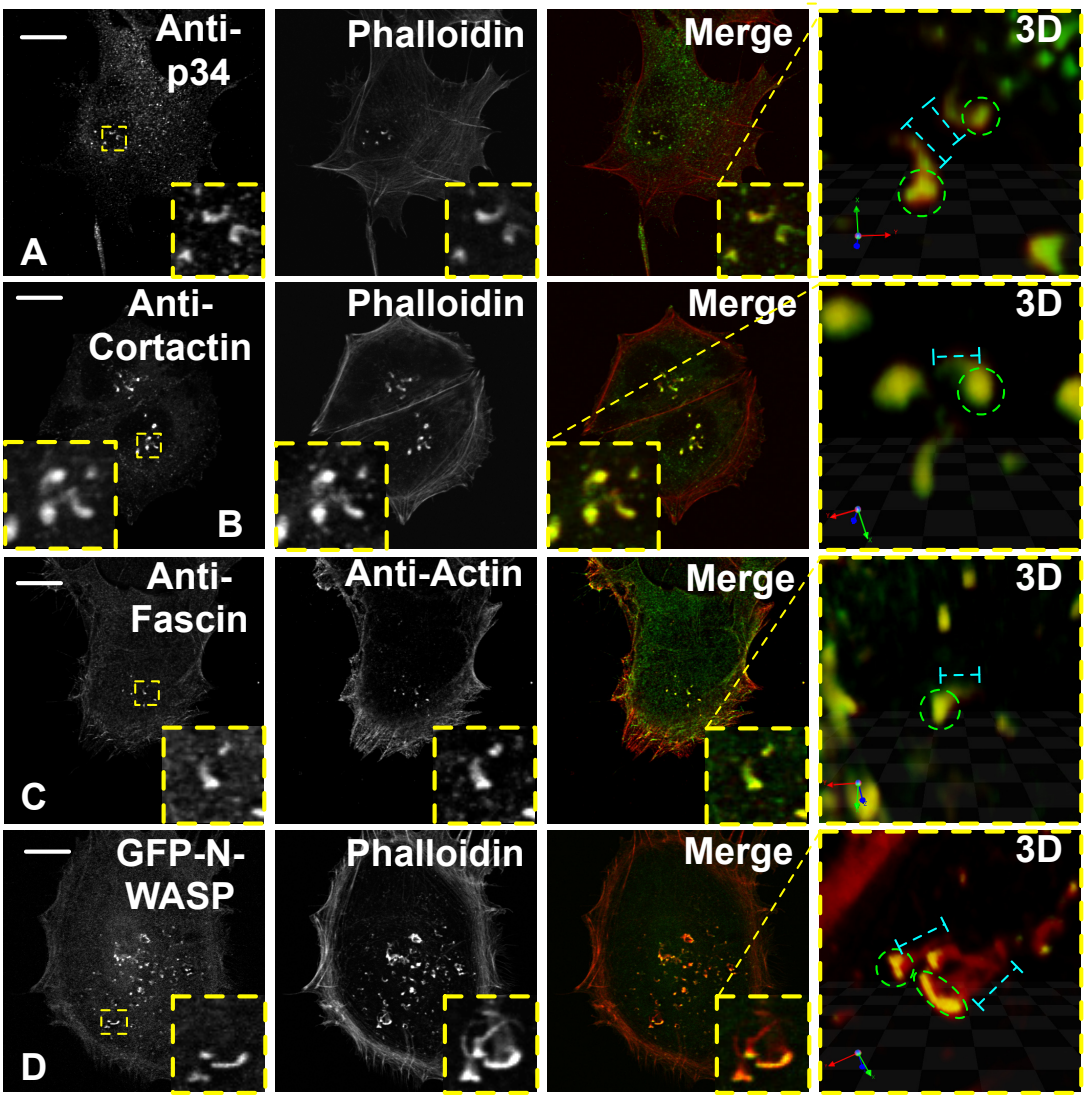

Figure 3.6. Localization of different proteins at invadopodia-associated actin comets
(A-D) A375MM cells were incubated on crosslinked gelatin matrix for 16 hours and then fixed and proteins were localized as labeled on the panels. 3D reconstruction of individual actin comets are shown with head indicated by green dashed circles and tail indicated by cyan dashed line. All scale bars are 10μm.

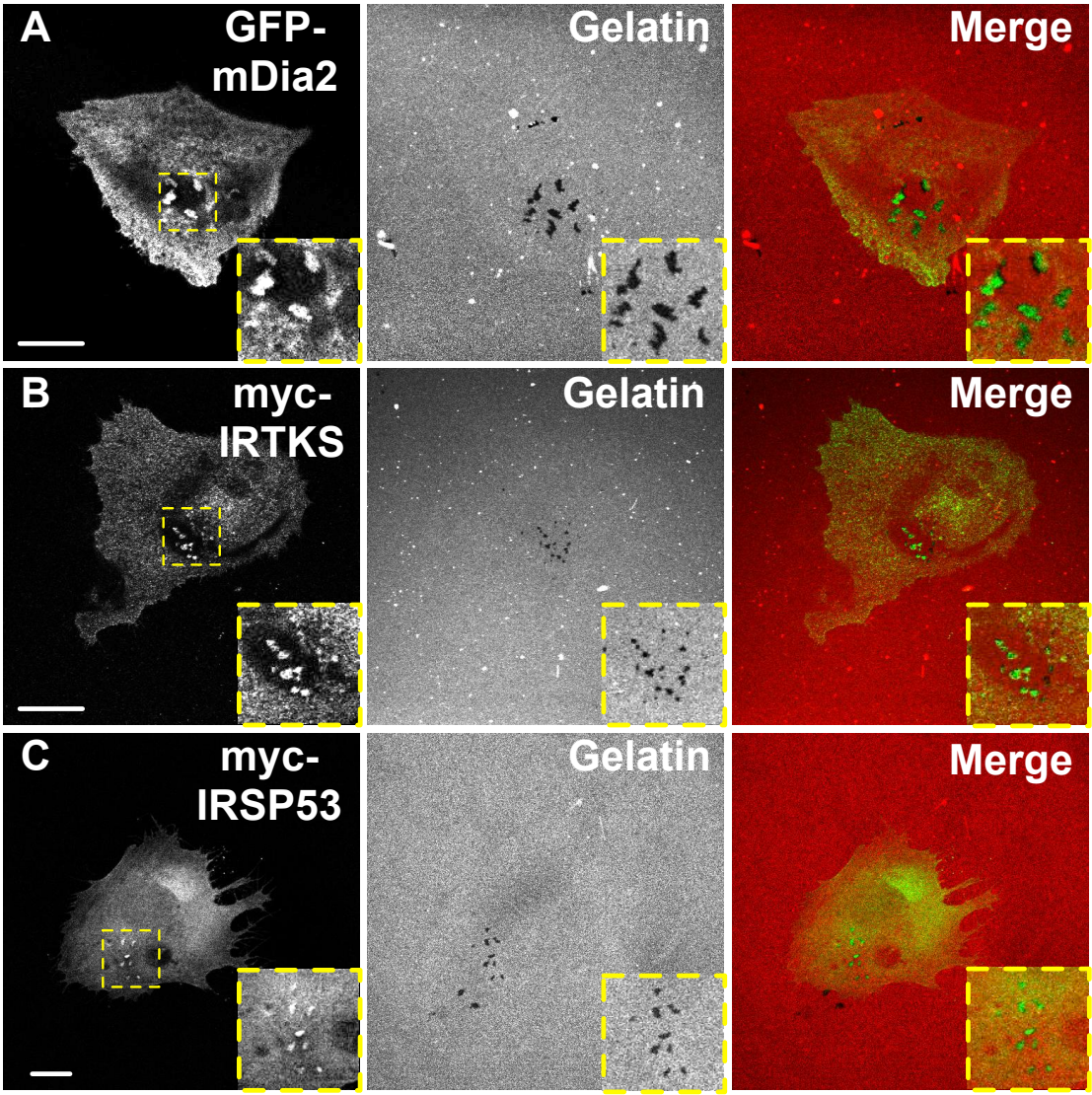

Figure 3.7. Localization of filopodia proteins at invadopodia
A375MM transiently transfected with GFP-mDia2 (A), myc-IRTKS (B) and myc-IRSP53 (C) was incubated on crosslinked Alexa594 conjugated gelatin matrix for 16 hours and fixed. Myc-IRTKS and myc-IRSP53 transfected cells were stained with 9E10 myc antibody followed by secondary Alexa488 conjugated antibody. Cells expressing low levels of myc-IRSP53 were selected for testing the localization. Examples of invadopodia are arrowed. Bars, 10μm.

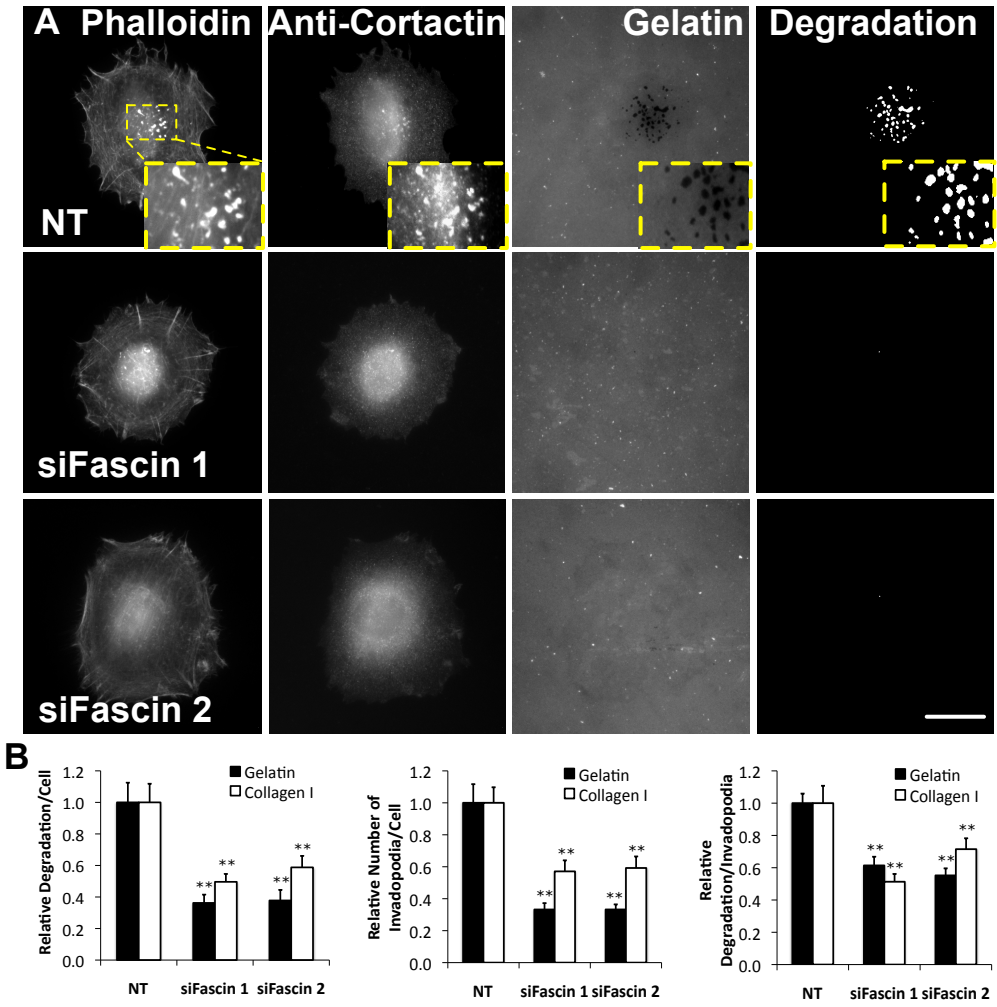

Figure 3.8. Fascin is required for the formation of invadopodia in A375MM cells. (A) Representative images from in vitro matrix degradation assay. Cells transfected with NT control or fascin siRNAs (siFascin 1 and siFascin 2) on Oregon Green 488 matrix (shown as grey) and stained with rhodamine phalloidin and anti-cortactin to localize invadopodia. the scale bar is 10μm. (B) Left: relative area of degradation per cell on gelatin (black) and collagen I (white). Middle: number of invadopodia per cell on gelatin (black) and collagen I (white). Right: area of degradation per invadopod of the ten biggest degradations per cell on gelatin (black) and collagen I (white). All error bars indicate mean ± standard error of the mean (SEM). **p < 0.01 by t test. Invadopodia were defined as puncta enriched for actin, cortactin, and gelatin degradation.

cell in fascin-depleted cells were reduced by more than two-fold compared with control cells (Figure 3.8B). To determine whether there was a change in the size of individual invadopodia, we also measured the area of degradation from individual invadopodia from control and fascin knockdown cells. Fascin depletion in A375MM cells results in about 1.6-fold reduction the area of degradation of individual invadopodia (Figure 3.8B). Finally, there was more than three-fold reduction in the number of invadopodia per cell in fascin knockdown cells (Figure 3.8B). Together, this data indicates that fascin is important for invadopodia formation by affecting both the number and size of invadopodia in A375MM cells and this effect is not matrix specific.

3.3.7 Fascin is localized at peripheral membrane ruffles and invadopodia in human CHL-1 melanoma cells.

In order to determine whether the effect of fascin on invadopodia formation is cell type specific, CHL-1, another human melanoma cell line, which has a moderate level of fascin expression was used (Figure 3.1). Moreover, the morphology of this cell line was distinct to A375MM, with cells showing a highly ruffling morphology but very few filopodia like protrusions. In contrast to A375MM cells, CHL-1 cells barely form any filopodia and immunostaining of endogenous fascin with antibody or transient expression of GFP-fascin in CHL-1 cells showed the colocalization of fascin with actin or p34-Arc in peripheral membrane ruffles (Figure 3.9A). Importantly, We found the colocalization of endogenous fascin or GFP-fascin with actin or p34-Arc at invadopodia (Figure 3.9A,B) indicates that fascin localization at invadopodia is not cell type specific.

3.3.8 Fascin is required for invadopodia formation and ECM degradation in human CHL-1 melanoma cells.

To test whether the endogenous fascin is important for invadopodia function, fascin levels were depleted by transiently transfecting cells with two individual

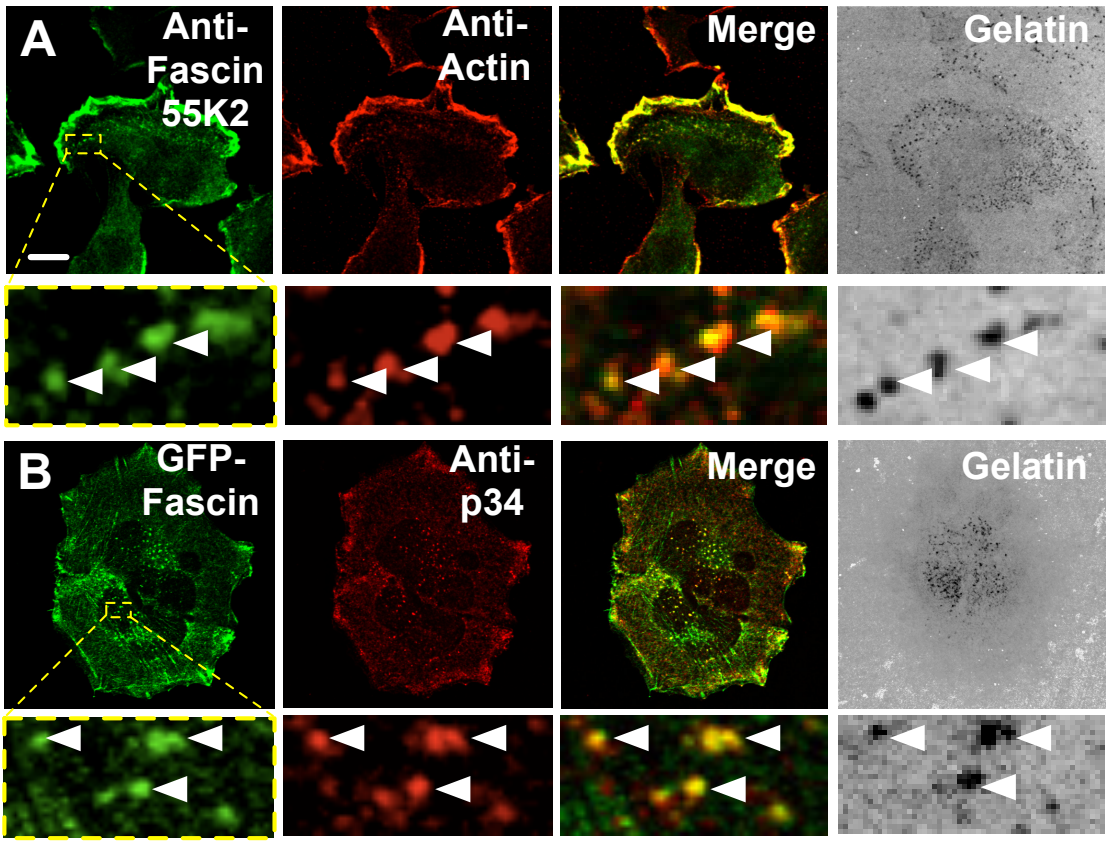

Figure 3.9. Fascin localize to invadopodia in CHL-1 melanoma cells
(A) CHL-1 human melanoma cells on Oregon Green 488 gelatin matrix (gray) with anti-fascin (55K2) and anti-actin. (B) CHL-1 cells expressing GFP-fascin on Alexa594 gelatin matrix (gray) stained with anti-p34-Arc (ARPC2). Arrows show individual invadopodia. .Scale bar is 10μm.

siRNA in CHL-1 cells (Figure 3.10A). No dramatic change in cell growth was observed (Figure 3.10B). Moreover, no huge morphology change was observed in CHL-1 cells on tissue culture plastic, although CHL-1 cells were slightly more spread and less ruffling in the absence of fascin (Data not shown).

Because CHL-1 cells were very efficient to form invadopodia as compared to A375 cells, which the whole area under the cells was often degraded after culture overnight on crosslinked gelatin (Figure 3.11B), which makes the quantification of degradation by individual invadopodia become impossible. Interestingly, A357MM cells only form invadopdia under the centre of the cell body (Figure 3.12A), which has been reported previously to be close to Golgi complex (Baldassarre et al., 2003) and this close spatial relationship with the Golgi complex is believed to be important for invadopodia function. However invadopodia formed by CHL-1 cells were all over the cell body (Figure 3.11B), suggesting that it may not be necessary for invadopodia or degradations to be close to the Golgi complex in all cell types.

To explore the role of fascin in invadopodia formation in CHL-1 cells, we used a different protocol. In this case, cells express NT or fascin siRNA were plated on crosslinked gelatin or collagen I overnight in presence of 5μm of metalloprotease inhibitor GM6001. Cell capacity to form invadopodia was then assessed by wash off the GM6001 for 2 h. Fascin depletion in CHL-1 cells results in a significant reduction in the area of degradation per cell as well as area of degradation of individual invadopodia on both crosslinked gelatin and collagen I matrix. In addition, we observed a significant decrease in the number of invadopodia per cell in fascin knockdown cells (Figure 3.12B, C). Furthermore, N-WASP depletion in CHL-1 also reduces invaodpodia formation (Figure 3.12 A-C). Together, this data indicates that fascin is important for invadopodia formation by affecting both the number and size of invadopodia in CHL-1 cells. This effect thus is not matrix specific and is conserved in melanoma cells.

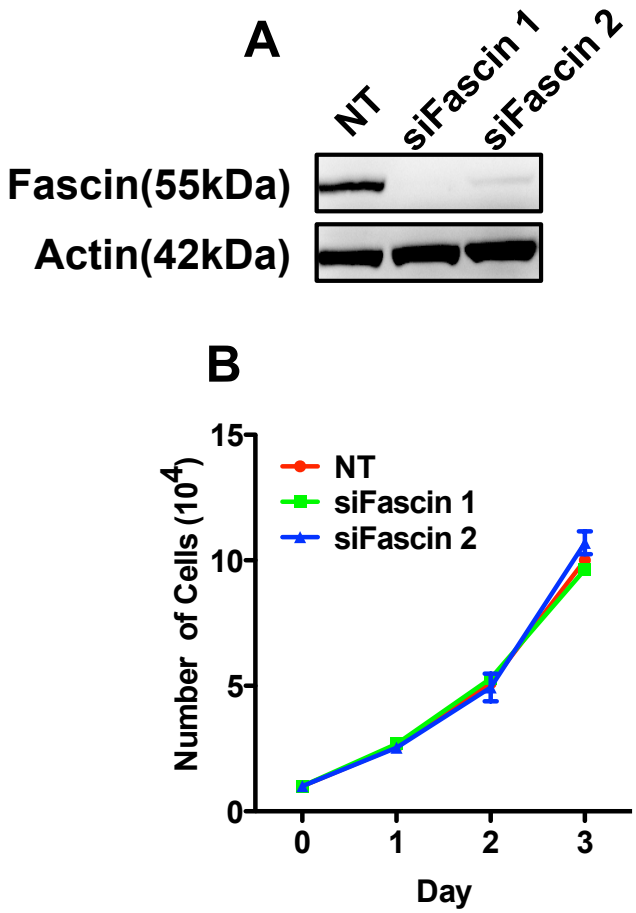

Figure 3.10 Fascin knockdown does not alter cell growth rate in CHL-1 melanoma cells

(A) Cell lysates from CHL-1 human melanoma cells transiently transfected with non-targeting pool control siRNA (NT) or fascin siRNA (sifascin 1 and sifascin 2) were analyzed by immunoblotting and probed for fascin. Membranes were also probed with actin antibody as a loading control. (B) $1x10^4$ CHL-1 cells express NT or fascin siRNA were plated in each well of 6 well plates, and number of cells was counted every day for 3 days. Each point (Mean ± SEM) is derived from the mean of hemocytometer count of cells from three replicate dishes from two independent experiments.

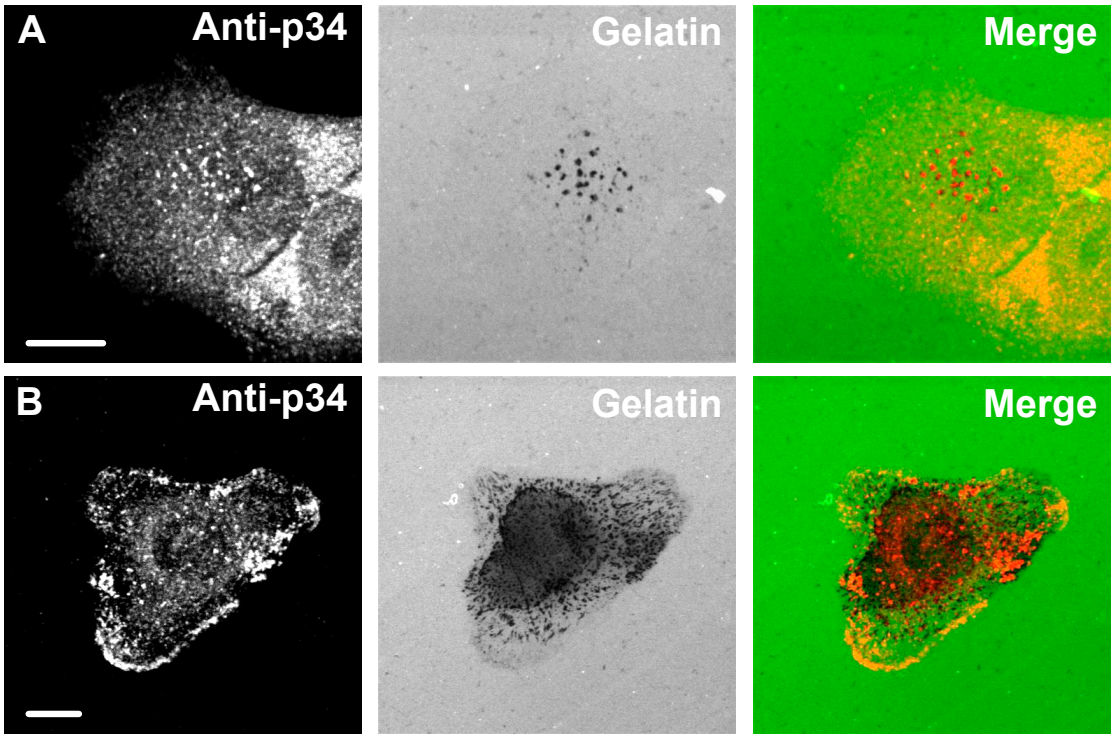

Figure 3.11. Comparison of invadopodia formation by A375MM and CHL-1 melanoma cells
(A)A375MM or (B) CHL-1 human melanoma cells were plated on Oregon Green 488 gelatin matrix for 16 h. Cells were fixed and stained with anti-p34. Scale bar is 10μm.

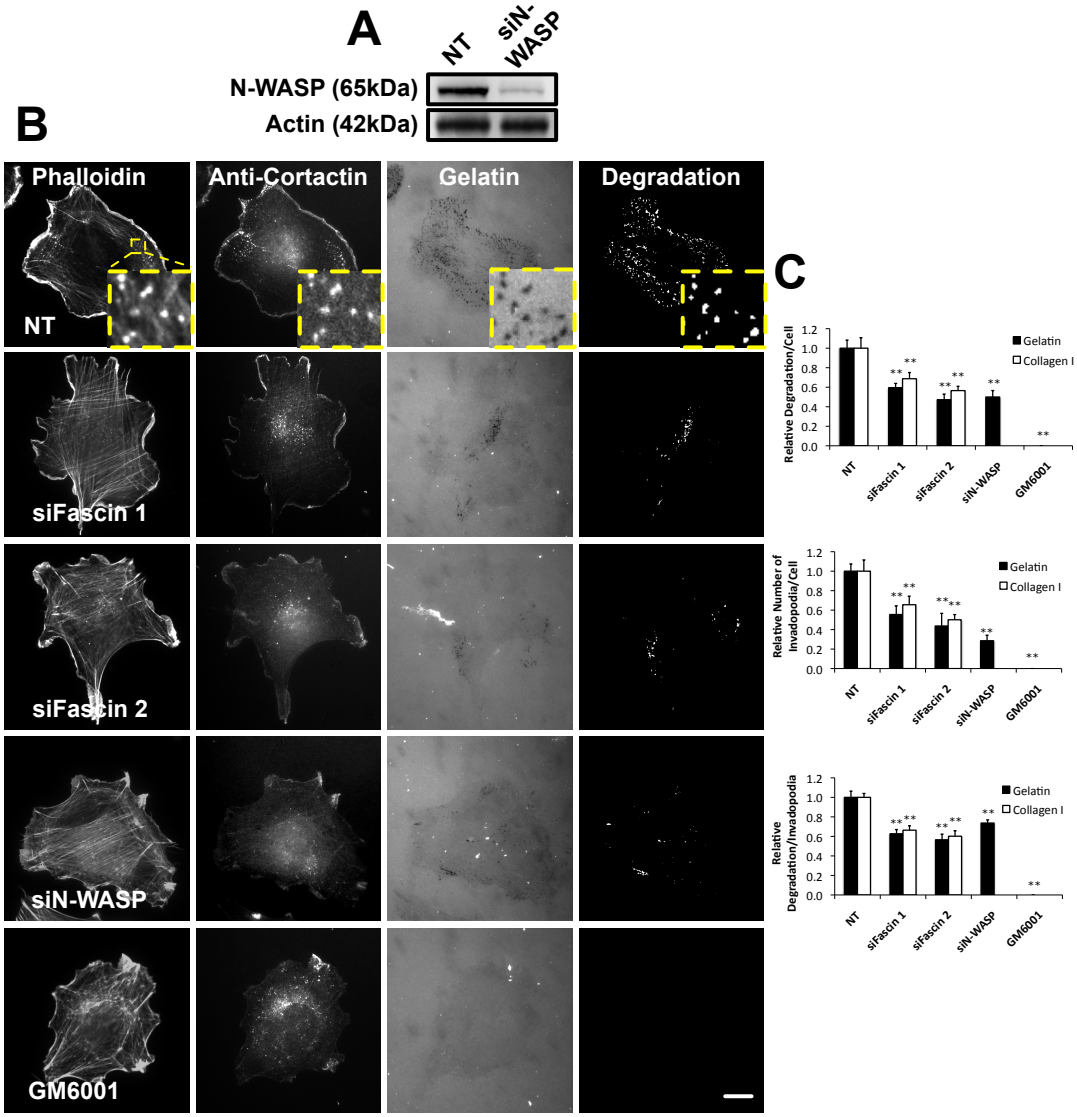

Figure 3.12. Fascin is required for the formation of invadopodia in CHL-1 cells. (A) Cell lysates from CHL-1 human melanoma cells transiently transfected with non-targeting pool control siRNA (NT) or N-WASP siRNA were analyzed by immunoblotting and probed for N-WASP. Membranes were also probed with actin antibody as a loading control. (B)Representative images from in vitro matrix degradation assay. Cells transfected with NT control, fascin siRNAs (siFascin 1 and siFascin 2), N-WASP siRNA or treated with 5μM GM6001 on Oregon Green 488 matrix (shown as grey) and stained with rhodamine phalloidin and anti-cortactin to localize invadopodia. the scale bar is 10μm. (B) Top: relative area of degradation per cell on gelatin (black) and collagen I (white). Middle: number of invadopodia per cell on gelatin (black) and collagen I (white). Bottom: area of degradation per invadopod of the ten biggest degradations per cell on crosslinked gelatin (black) and collagen I (white). All error bars indicate mean ± standard error of the mean (SEM). **p < 0.01 by t test. Invadopodia were defined as puncta enriched for actin, cortactin, and gelatin degradation.

3.3.9 Fascin localized at invadopodia in SCC9 human head and neck squamous cell carcinoma cells and MDA-MB-231 human breast adenocarcinoma cells.

We have shown that fascin is important for invadopodia formation in melanoma cells. We next investigated if fascin is important for invadopodia formation in cells derived from cancer types other than melanoma. SCC9 human head and neck squamous cell carcinoma cells (HNSCC) form invadopodia when cultured on crosslinked ECM (Lucas et al., 2010). We found that endogenous fascin co-localizes nicely with actin or Arp2/3 complex at invadopodia (Figure 3.13). Similarly, endogenous fascin or exogenous fascin-GFP co-localize with gelatin degradations (Figure 3.14A) in MDA-MB-231 human breast adenocarcinoma cells, a cell type that is very commonly used for invadopodia study. In addition, transient or stable knockdown of fascin significantly reduce invadopodia degradation in MDA-MB-231 cells (Figure 3.14B-E). Furthermore, siRNA against p34-Arc (ARPC2) in MDA-MB-231 cells also reduced invadopodia degradation. Similar to other cell types, we found that fascin knockdown did not affect MDA-MB-231 cell proliferation (Figure 3.15). Together, these results demonstrate a general importance of fascin for invadopodia formation on various matrices and cells from different cancer types.

3.3.10 Filopodia formation depends on fascin phosphorylation

Phosphorylation of fascin at serine 39 is important for its actin bundling activity in vitro (Ono et al., 1997; Yamakita et al., 1996). To examine the roles of serine 39 phosphorylation in filopodia formation, A375MM cells were transiently transfected with GFP-fascin, or two different phosphorylation-state mutants of fascin, GFP-fascin S39A, an active dephosphomimic that retains its actin-bundling activity, or GFP-fascin S39E, an inactive phosphomimic that has lost its actin-bundling activity but that retains PKC-binding activity (Vignjevic et al., 2006). Interestingly, A375MM cells expressing *H. sapiens* GFP-fascin, GFP-fascin S39A showed similar morphology with formation

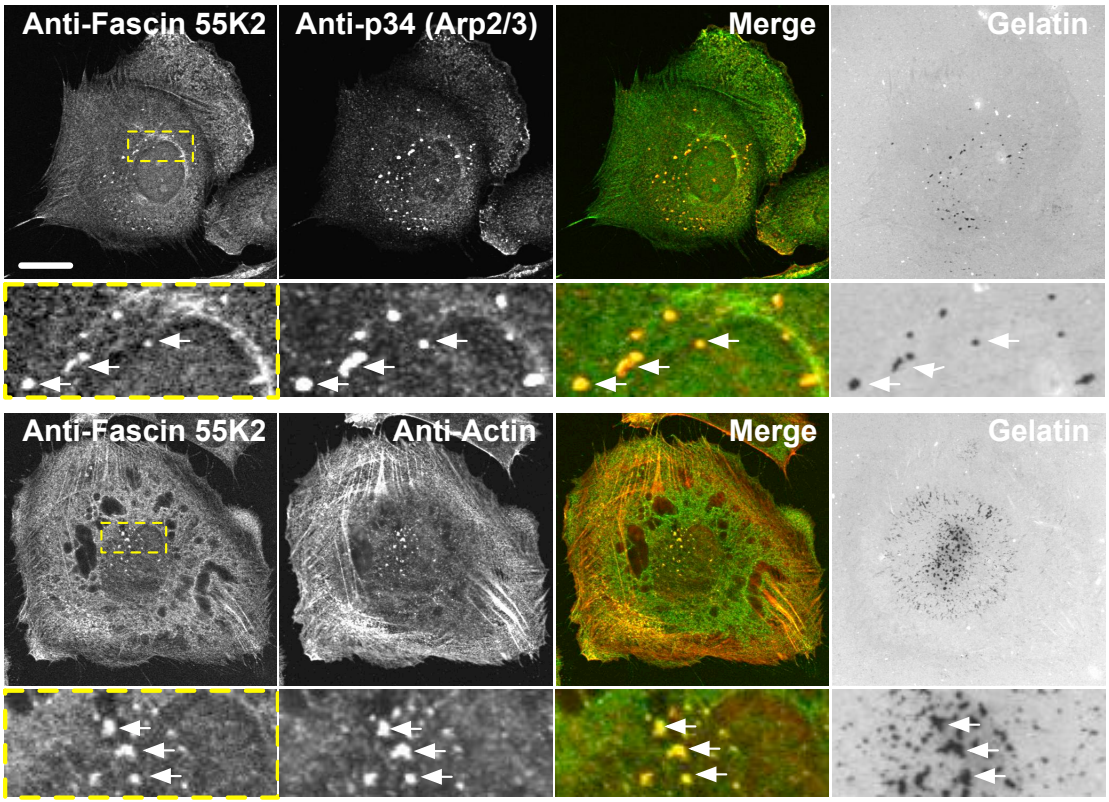

Figure 3.13. Fascin localize to invadopodia in SCC9 human squamous cell carcinoma cells
(A) SCC9 cells on Oregon Green 488 gelatin matrix (gray) with anti-fascin (55K2) and (A) anti-p34-Arc and (B) anti-actin. Arrows show individual invadopodia. .Scale bar is 10μm.

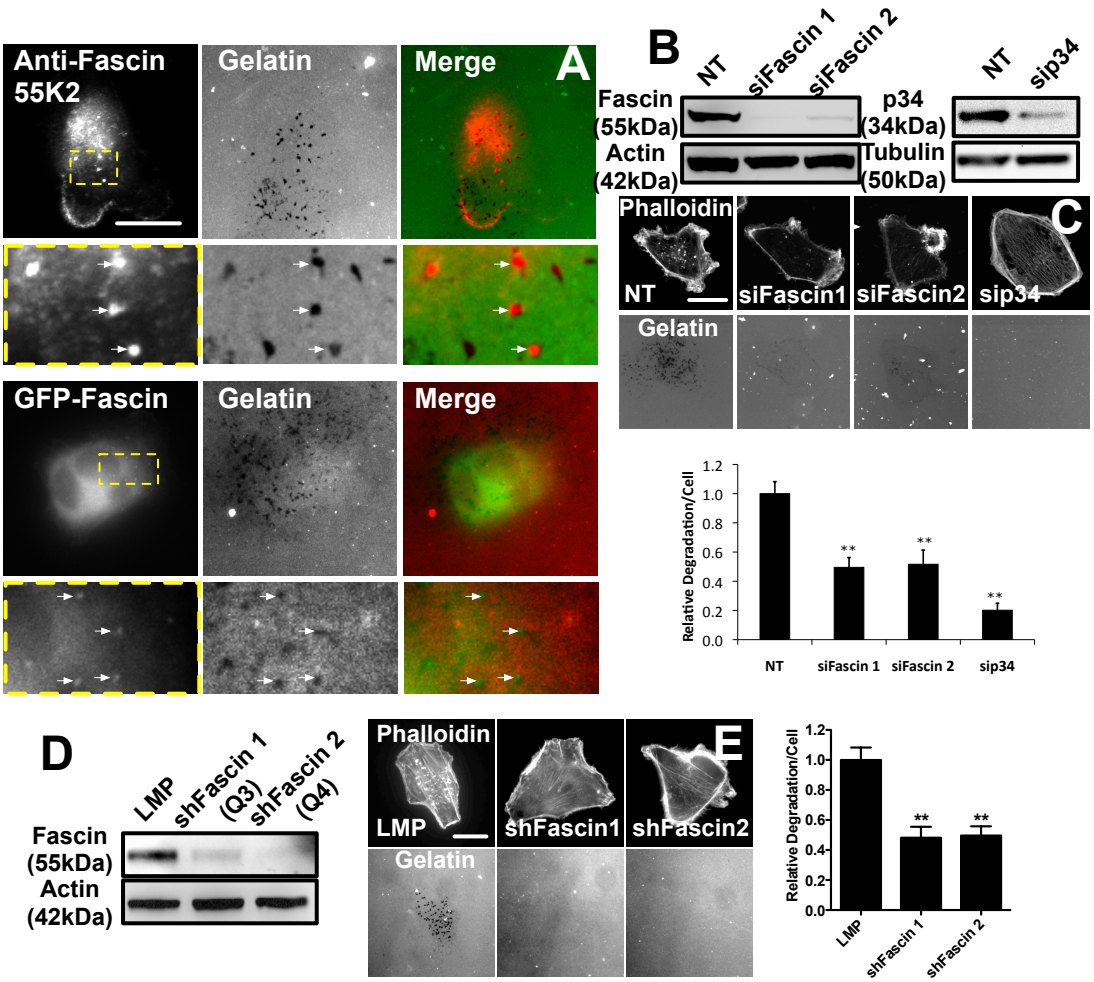

Figure 3.14. Fascin is required for the formation of invadopodia in MBA-MB-231 human breast adenocarcinoma cells. (A) Top: MDA-MB-231 cell on Oregon Green 488 gelatin matrix (gray) with anti-fascin (55K2). Bottom: MDA-MB-231 cell expressing GFP-fascin on Alexa594 gelatin matrix (gray) Arrows show individual invadopodia. (B) Cell lysates from MDA-MB-231 cells transiently transfected with NT, fascin or p34-ARC siRNA were analyzed by immunoblotting and probed with antibodies as indicated. Membranes were also probed with actin antibody as a loading control. (C)Representative images from in vitro matrix degradation assay. Cells transfected with NT control, fascin siRNAs or p34-ARC siRNA on Oregon Green 488 matrix (shown as grey) and stained with rhodamine phalloidin. Relative area of degradation per cell on gelatin. (D) Cell lysates from MDA-MB-231 cells expressing empty LMP vector or vectors contain fascin shRNA were analyzed by immunoblotting and probed with antibodies as indicated. (E) Representative images from in vitro matrix degradation assay. Cells expressing empty LMP vector or vectors contain fascin shRNA on Oregon Green 488 matrix (shown as grey) and stained with Alexa350 phalloidin. Relative area of degradation per cell on gelatin. All error bars indicate mean ± standard error of the mean (SEM). **p < 0.01 by t test. All scale bars are 10μm.

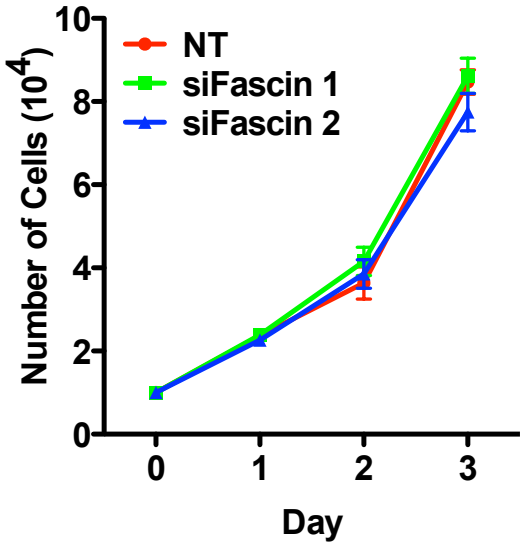

Figure 3.15 Fascin knockdown does not alter cell growth rate in MDA-MB-231 breast cancer adenocarcinoma cells

$1x10^4$ MBA-MD-231 cells express NT or fascin siRNA were plated in each well of 6 well plates, and number of cells was counted every day for 3 days. Each point (Mean ± SEM) is derived from the mean of hemocytometer count of cells from three replicate dishes from two independent experiments.

numerous microspikes on the dorsal surface of the cells (Figure 3.16A). However, expression of GFP-fascin S39E inhibits the formation of microspikes on the surface of the cells (Figure 3.16A). To further confirm this effect, *X. tropicalis* GFP-fascin (Xtfascin), GFP- Xtfascin S33A (Serine 33 in *X. tropicalis* is equivalent to serine 39 in *H. sapiens* fascin. Also see (Hashimoto et al., 2007) or GFP- Xtfascin S33D were transiently expressed in A431 epithelial carcinoma cells and cells were plated on glass coverslips overnight and fixed. Consistent with data for *H. sapiens* GFP-fascin, cells expressing GFP- Xtfascin or GFP-Xtfascin S33A in A431 cell showed formation of filopodia (Figure 3.16B). Expression of GFP-Xtfascin S33D, however, suppresses the formation of filopodia (Figure 3.16B). Together, these data indicate that Serine 39 phosphorylation regulates fascin activity and formation of filopodia. These also suggest that the inactive phosphomimic mutant of fascin has a dominant-negative effect on filopodia formation.

3.3.11 Phosphorylation of fascin regulates formation of invadopodia in CHL-1 cells

We have shown that the phosphorylation of fascin at serine 39 regulates the formation filopodia. To determine whether fascin phosphorylation is likely to regulate invadopodia formation, we made fascin knockdown cells with expression of GFP, GFP-Xtfascin, GFP-Xtfascin S33A or GFP-Xtfascin S33D. Knockdown of fascin in CHL-1 cells did not alter the expression of Xtfascin (Figure 3.17). Knockdown of endogenous fascin strongly reduced the total area of degradation per cell; area of degradation of single invadopodia and number of invadopodia per cell as compared to control and this cannot be rescued by expressing GFP in the cells (Figure 3.18). Invadopodia formation can be fully restored by express of wild type GFP-Xtfascin or GFP-Xtfascin S33A (Figure 3.18). In addition, both of these proteins localized to invadopodia together with cortactin (Figure 3.19). Although there was no defect on cell spreading, expression of GFP-Xtfascin S33D in fascin knockdown CHL-1 cells failed to rescue the formation of invadopodia with the

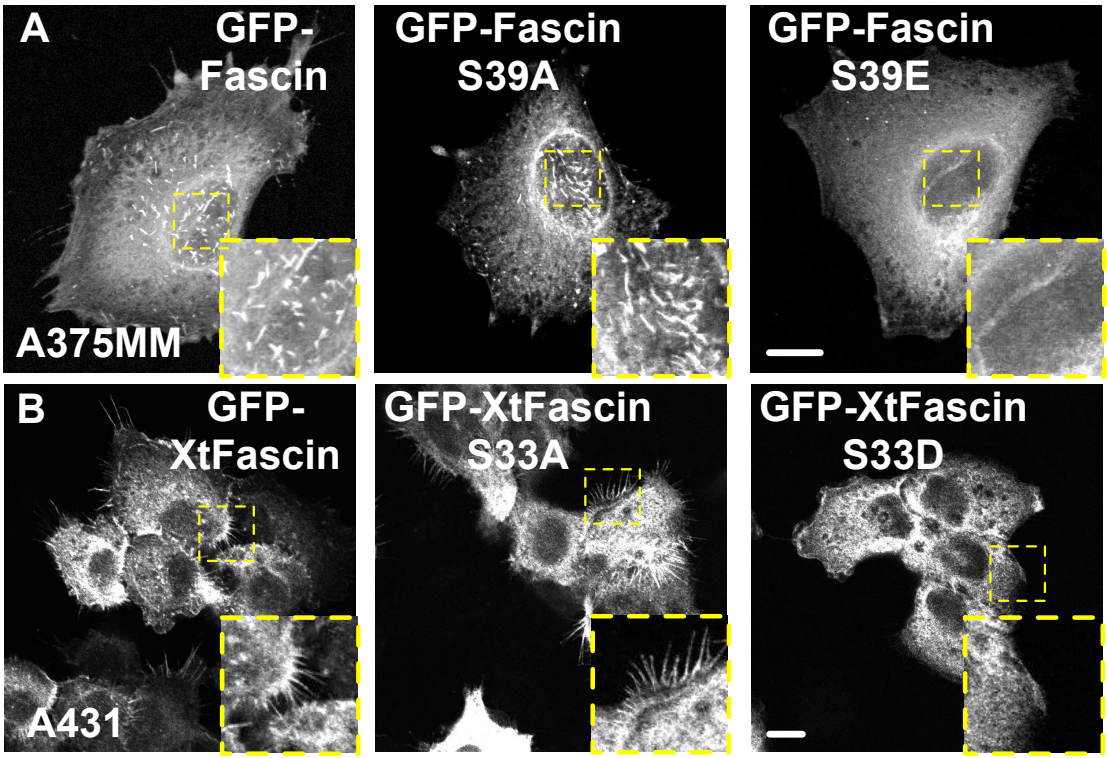

Figure 3.16. Effects of fascin mutants on filopodia formation in A375MM and A431 cells

(A) Combined Z-stack images (1µm) of A375MM melanoma cells expressing *H. sapiens* GFP-fascin, GFP-fascin S39A or GFP-fascin S39E were spreaded on glass coverslip overnight. (B) A431 epithelial carcinoma cells expressing GFP-*X. tropicalis* fascin, GFP-*X. tropicalis* fascin S33A or GFP- *X. tropicalis* fascin S33D were spreaded on glass coverslip overnight and fixed. Inserts show formation of filopodia. Scale bar is 10µm.

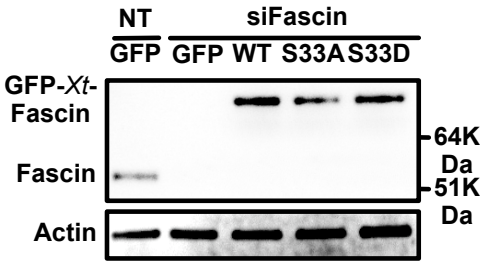

Figure 3.17. Expression of *X.tropicalis* fascin in fascin knockdown CHL-1 cells.
Western blot showing CHL-1 cells stably expressing GFP, GFP-X. tropicalis fascin, GFP-X. tropicalis fascin S33A, and GFP-X. tropicalis fascin S33D were transfected with non-targeting (NT) control siRNA or fascin siRNA (siFascin 1). Immunoblots were probed with anti-fascin and anti-actin as loading control.

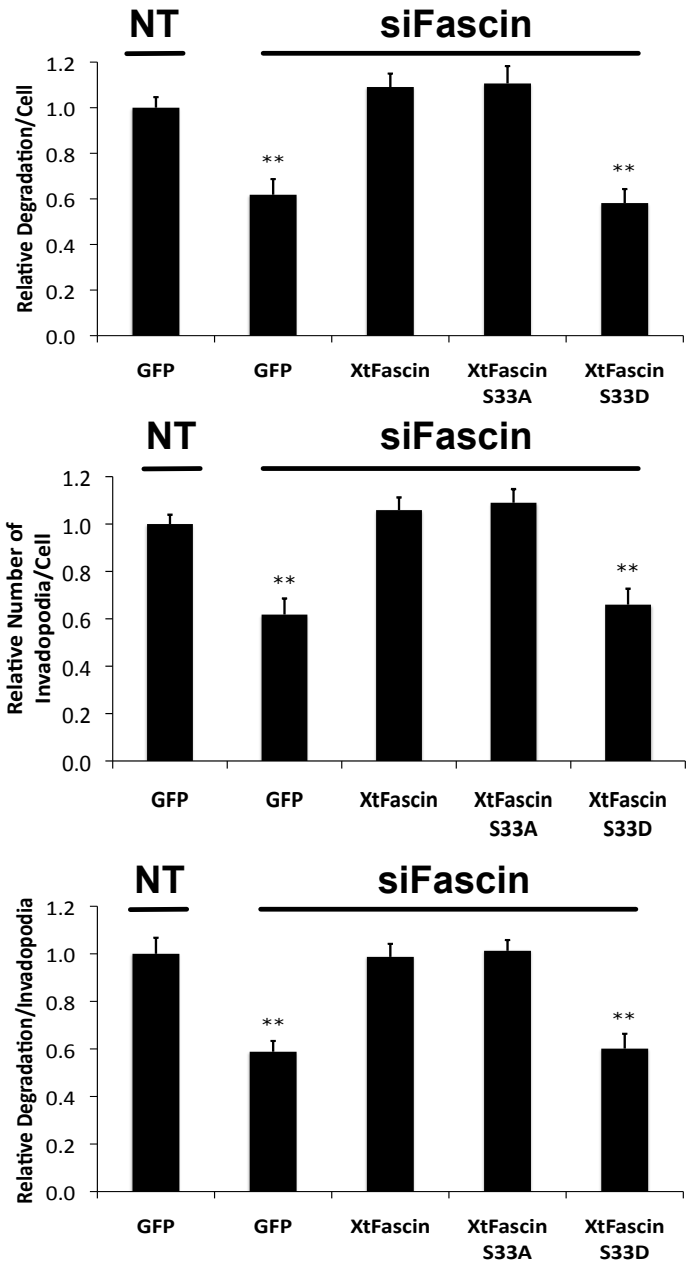

Figure 3.18. Fascin Regulation at Serine 39 Is Important for Invadopodia Formation in CHL-1 cells(C) Top: relative area of degradation on gelatin per cell. Middle: number of invadopodia per cell. Invadopodia were defined as puncta enriched for actin, cortactin, and gelatin degradation. Bottom: area of degradation per invadopod of the ten biggest degradations per cell on crosslinked gelatin.; Error bars show mean ±SEM. ** $p < 0.01$ by t test.

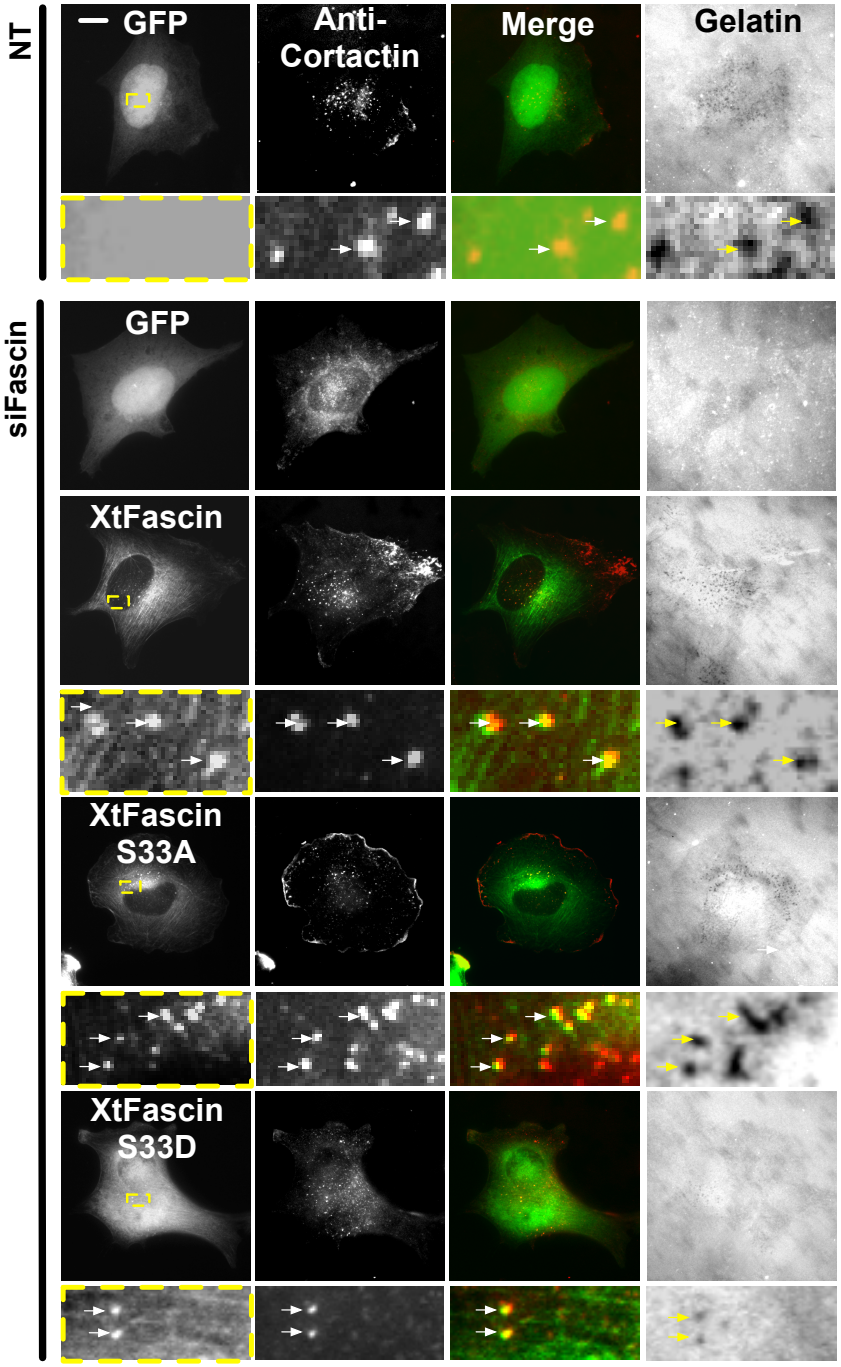

Figure 3.19. Localization of fascin mutants in fascin knockdown CHL-1 cells

CHL-1 cells stably expressing GFP, GFP-X. tropicalis fascin, GFP-X. tropicalis fascin S33A, and GFP-X. tropicalis fascin S33D were transfected with non-targeting (NT) control siRNA or fascin siRNA (siFascin 1), cultured on Alexa594 gelatin matrix, and labeled with anti-cortactin. Arrows show invadopodia. Scale bars represent 10 μm.

total area of degradation per cell, area of degradation of single invadopodia and number of invadopodia per cell remaining similar to the fascin knockdown cells (Figure 3.18). Furthermore, GFP-Xtfascin S33D appeared diffuse with weak localization to residual invadopodia (Figure 3.19).

3.3.12 Phosphorylation of fascin regulates formation of invadopodia in A375MM cells

We have shown that fascin phosphorylation at serine 39 is very important for invadopodia formation in CHL-1 cells. To further confirm these results, A375MM cells expressing GFP, GFP-Xtfascin, GFP-Xtfascin S33A or GFP-Xtfascin S33D were transfected with NT or fascin siRNA. Western blotting indicated that GFP-Xtfascin, GFP-Xtfascin S33A and GFP-Xtfascin S33D was not susceptible to the human fascin siRNA (Figure 3.20A). Similar to CHL-1 cells, invadopodia formation was fully restored by expression of GFP-Xtfascin or GFP-Xtfascin S33A in fascin knockdown A375MM cells (Figure 3.21). Both of these proteins localized to invadopodia together with cortactin (Figure 3.20B). GFP-Xtfascin S33D failed to rescue invadopodia formation (Figure 3.21). In a few of GFP-Xtfascin S33D expressing cells with recognizable invadopodia-like staining, GFP-Xtfascin S33D was also weakly localized at invadopodia together with cortactin, although appeared diffuse with weak localization to invadopodia (Figure 3.20B). In addition, expression of *H. sapiens* GFP-fascin S39E in wild-type A375MM cells significantly decreased matrix degradation (Figure 3.22). However, expression of human GFP-fascin or GFP-fascin S39A did not significantly affect extracellular matrix (ECM) degradation (Figure 3.22). Together, these data suggest that the actin-bundling activity of fascin may be required for invadopodia formation and that the inactive phosphomimic mutant of fascin has a dominant-negative effect.

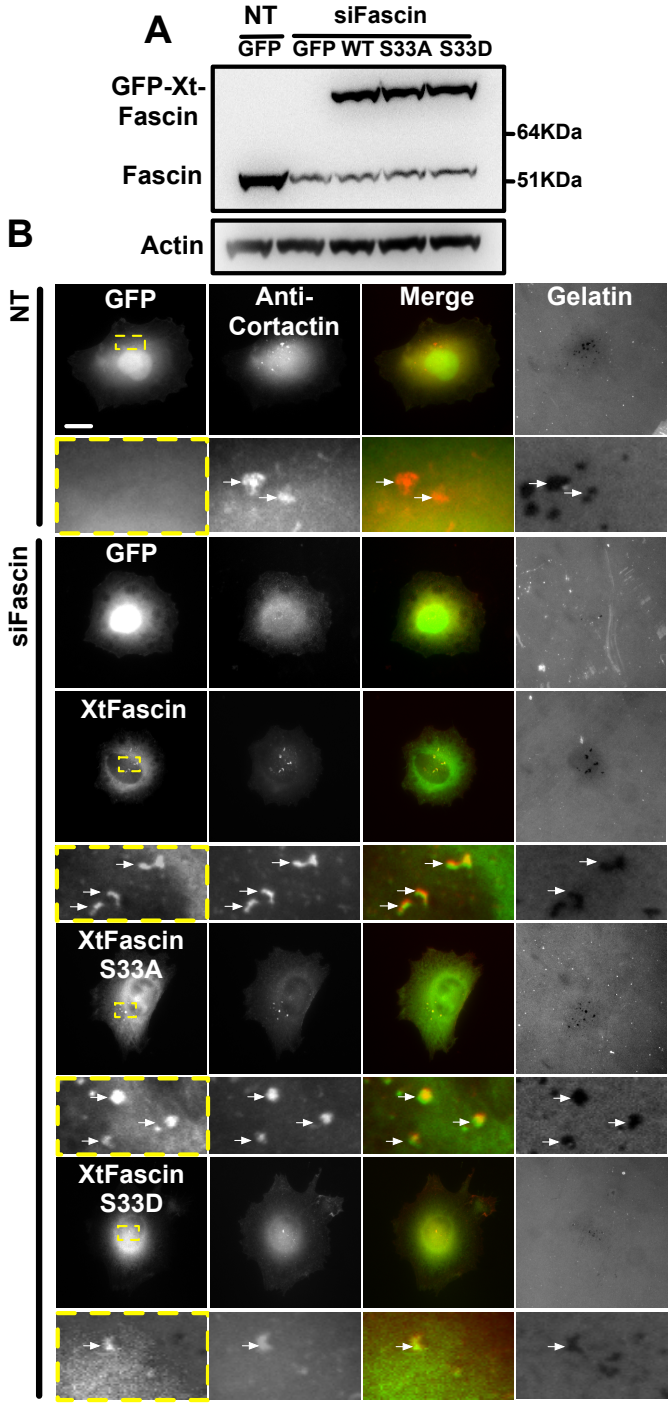

Figure 3.20. Localization of fascin mutants in fascin knockdown A375MM cells
Western blot showing A375 cells stably expressing GFP, GFP-X. tropicalis fascin, GFP-X. tropicalis fascin S33A, and GFP-X. tropicalis fascin S33D were transfected with non-targeting (NT) control siRNA or fascin siRNA (siFascin 1). Immunoblots were probed with anti-fascin and anti-actin as loading control. (B) A375 cells expressing GFP, GFP-X. tropicalis fascin, GFP-X. tropicalis fascin S33A, and GFP-X. tropicalis fascin S33D were transfected with non-targeting (NT) control siRNA or fascin siRNA (siFascin 1), cultured on Alexa594 gelatin matrix, and labeled with anti-cortactin. Arrows show invadopodia. Scale bars represent 10 μm.

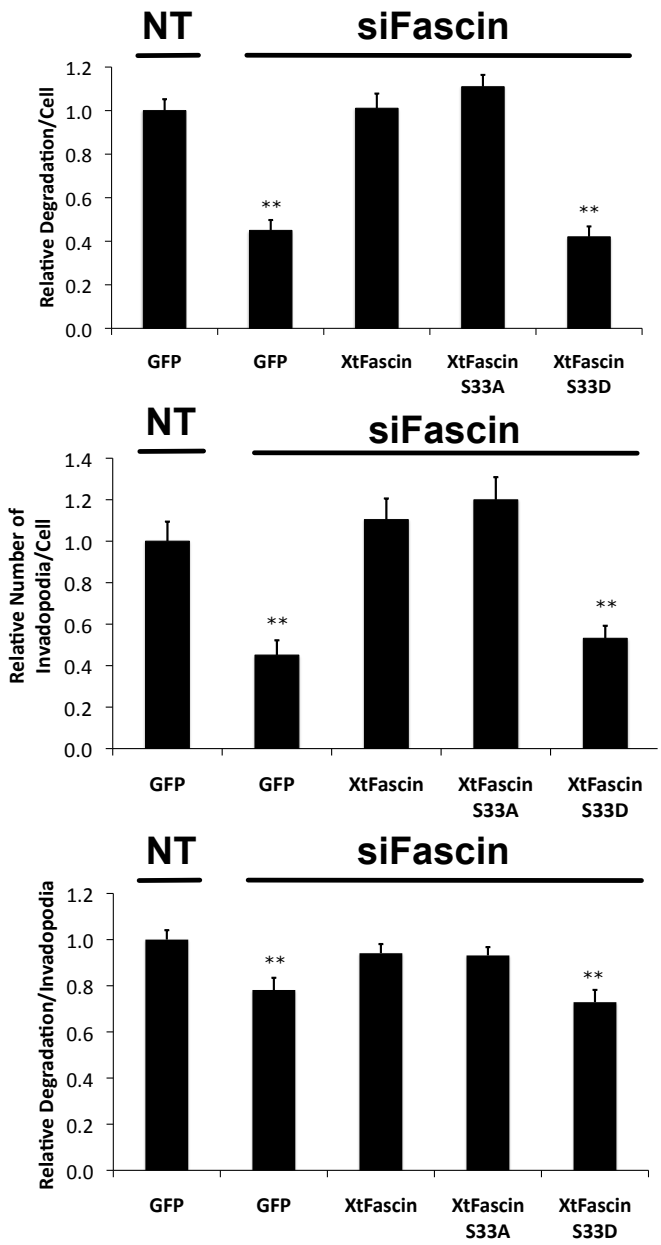

Figure 3.21. Fascin Regulation at Serine 39 Is Important for Invadopodia Formation in A375MM cells Top: relative area of degradation on gelatin per cell. Middle: number of invadopodia per cell. Invadopodia were defined as puncta enriched for actin, cortactin, and gelatin degradation. Bottom: area of degradation per invadopod of the ten biggest degradations per cell on crosslinked gelatin.; error bars show mean ±SEM. ** $p < 0.01$ by t test.

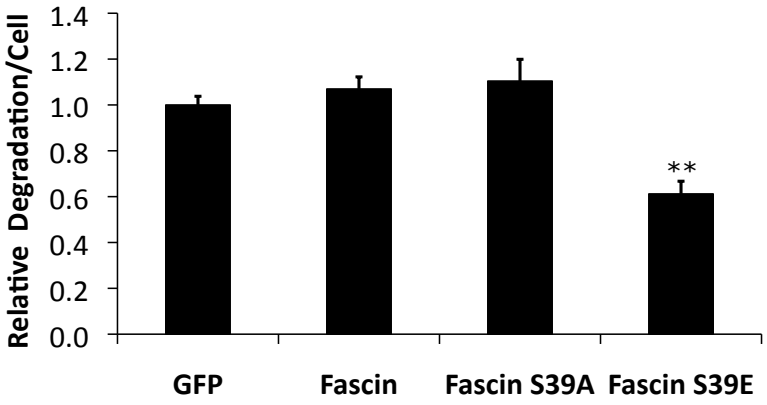

Figure 3.22. Expression of GFP-Fascin S39E Suppresses Invadopodia Formation in A375MM Cells

A375MM cells transiently transfected with GFP, H. sapiens GFP-fascin, H. sapiens GFP-fascin S39A and H. sapiens GFP-fascin S39E were cultured on crosslinked Alexa594 conjugated gelatin matrix for 16 hours. Quantifications of invadopodia on gelatin from three independent experiments in duplicate as described in Figure 1. (Mean ± SEM). **, P< 0.01 compared to control cells by t-test.

3.3.13 Fascin regulates actin stability at invadopodia

To understand how fascin controls actin dynamics at invadopodia, the turnover rates of GFP-tagged actin, cortactin, N-WASP, p21-Arc (ARPC3), and fascin at invadopodia was examined (Figure 3.23) via FRAP. Although invadopodia persisted for hours, cortactin, N-WASP, and p21-Arc all rapidly recovered to more than 80% of prebleach values, and the recovery kinetics agree fairly closely with previously published values for turnover of actin, cortactin, and Arp2/3 complex in lamellipodia (Lai et al., 2008). Actin, however, only recovered to about 70% prebleach level, suggesting that 30% of actin is trapped (Figure 3.23 and Movie 2). Although fascin at invadopodia recovered to nearly prebleach level, the recovery rate of fascin was >10-fold slower than that of actin, cortactin, N-WASP, and p21-Arc with half time of recovery of about 65 seconds (Figure 3.23 and Movie 2). Fascin turnover in filopodia was more rapid, with a half-time of recovery of about 9 seconds (Figure 3.23 in agreement with (Aratyn et al., 2007; Vignjevic et al., 2006) and 96% recovery. Together, these results indicate that rather than form a stable complex fascin, actin, cortactin, N-WASP, p21-Arc (ARPC3) at invadopodia undergo a constant association/dissociation cycle and majority of the proteins are dynamic. Fascin is particularly stable at invadopodia, perhaps to provide a platform for force production.

Previous reports implicated fascin in stabilization of membrane protrusions and alteration of the equilibrium of actin polymerization (Yamakita et al., 2009; Yamashiro et al., 1998). In order to study whether the level of fascin in cells could change the actin dynamics at invadopodia, the actin dynamics were compared in fascin-depleted and -overexpressing cells via FRAP (Figure 3.24A). The mobile fraction of actin at invadopodia was significantly increased in fascin knockdown cells and decreased in GFP-fascin-overexpressing cells (Figure 3.24B). However, the bulk turnover rates of actin at invadopodia were almost unaffected (Figure 3.24B, recovery half-time). Thus, the amount of actin trapped at invadopodia is at least partially dependent on fascin, but rapidly cycling actin may not be bundled by fascin. This is consistent with the

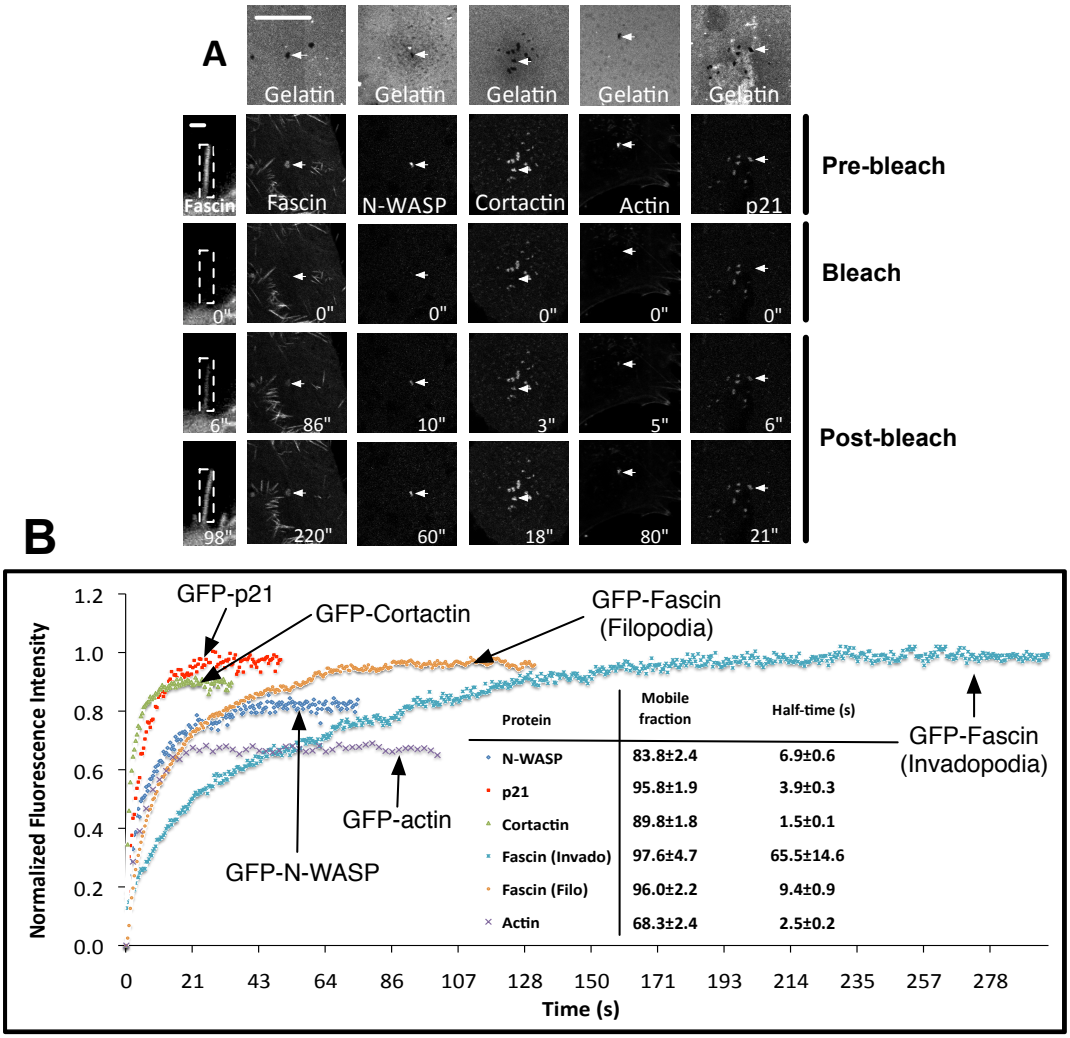

Figure 3.23. Fascin is Stably Associated with Invadopodia
(A) A375MM cells transiently transfected with GFP-cortactin, GFP-p21, GFP-N- WASP, GFP-actin and GFP-fascin were cultured on crosslinked Alexa594 gelatin matrix for 16 hr and analyzed by confocal microscope at 37°C. Invadopodia were defined as colocalization of GFP tagged protein with gelatin matrix degradation. Images from time-lapse movies of FRAP experiments before and after photobleaching on GFP- cortactin, GFP-actin, GFP-p21, GFP-N-WASP at invadopodia (arrowed) and GFP- fascin at invadopodia (arrowed) and filopodia (boxed). Bars, right, 10μm, left, 1μm. Time in sec. (A) The recovery kinetics of GFP-cortactin (green triangles) (n = 28), GFP-actin (purple crosses) (n = 31), GFP-p21-Arc (red squares) (n = 30), GFP-N-WASP (blue diamond) (n = 30) at invadopodia, GFP-fascin at invadopodia (light blue x symbols) (n = 22), and filopodia (orange dots) (n = 25) after photobleaching. Mobile fraction and half-time of recovery are indicated as mean ± SEM.

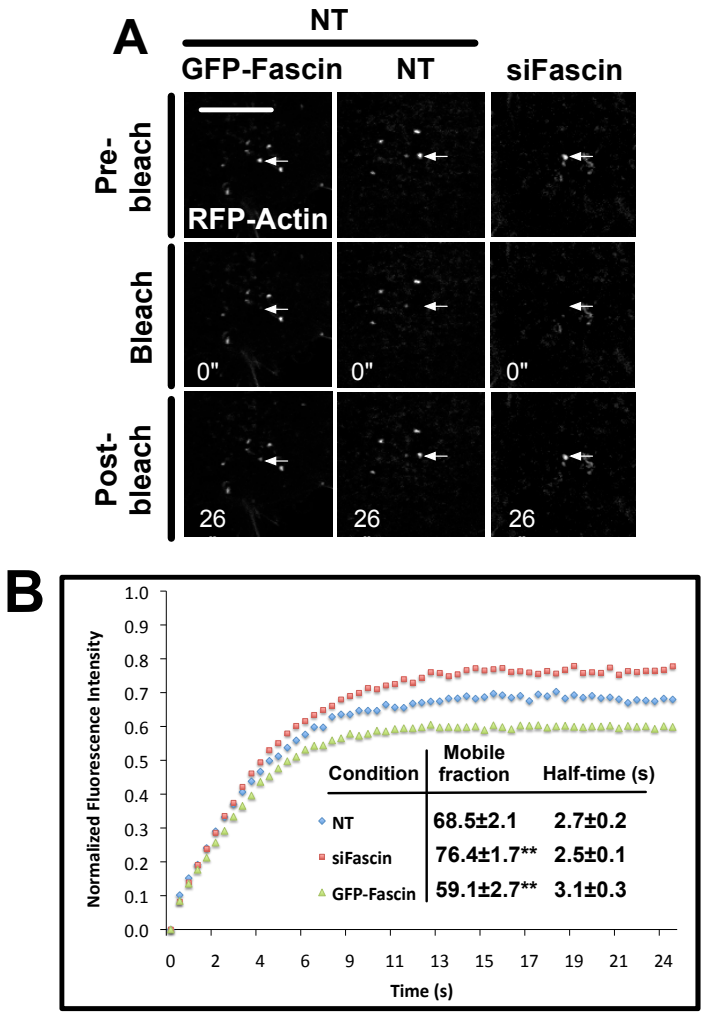

Figure 3.24. Fascin Knockdown Reduces Actin Recovery in Invadopoda
(A) A375MM cells expressing control or fascin siRNA transiently cotransfected with EGFP-fascin and mRFP-actin or transfected with mRFP-actin were cultured on crosslinked gelatin matrix for 16 hours. Images represented time-lapse sequence of FRAP experiments before and after photobleaching of mRFP-actin at invadopodia (arrowed). (B) Recovery kinetics of mRFP-actin at invadopodia in cells expressing NT control siRNA (blue diamond) (n = 50), GFP-fascin and control siRNA (EGFP- fascin) (green triangles) (n = 47), or fascin siRNA (siFascin) (red squares) (n = 45). Percentage of mobile fraction and half-time of recovery for each condition are indicated as mean ± SEM; **p < 0.01 by t test.

presence of unbundled highly dynamic actin, which is likely being rapidly turned over to produce force for motility and more stable actin in association with fascin to provide longevity of protrusions.

Because fascin stabilizes the filamentous actin at invadopodia and itself exchanges slowly at invadopodia, this suggests that fascin might function at invadopodia to provide a more stable platform for degradation of matrix. To test this, the dynamics of invadopodia in control and fascin depleted A375MM cells were compared by time-lapse microscopy. Most (>50%) invadopodia in A375MM cells persisted for up to and beyond 6 to 8 hr (Figure 3.25 and Movie 3). Fascin knockdown cells formed fewer invadopodia, and invadopodia were generally smaller and shorter lived (approximately 50% of invadopodia persisted for less than 2 hr) (Figure 3.25 and Movie 3). Together, these data indicate that fascin is important for invadopodia stability and function, by regulating the number and size of invadopodia, as well as their lifetime.

3.3.14 Fascin and metalloproteases are not required for A375MM melanoma cell invasion

We have shown that fascin stabilizes actin at invadopodia. We investigated the role for fascin in invasion of melanoma cells into 3D Collagen I/Matrigel matrix, a process that takes place over the timescale of days and which might require long-lived invasive protrusions. Consistent with previous reports, migrating A375MM cells in collagen I-Matrigel appeared rounded, characteristic of the so-called amoeboid type of migration (Figure 3.26A) (Gadea et al., 2008; Sanz-Moreno et al., 2008). Fascin protein levels were depleted by siRNA and the resulting cells were assayed in the inverse invasion assay. Surprisingly, The invasion of A375MM cells was found not to be dependent on endogenous fascin (Figure 3.26B). In addition, fascin knockdown had no apparent effect on the rounded shape of A375MM cells in 3D Collagen I/Matrigel matrix (Figure 3.26A). Furthermore, fascin knockdown in A375MM cells had no effect on cell migration cross the filter in transwell

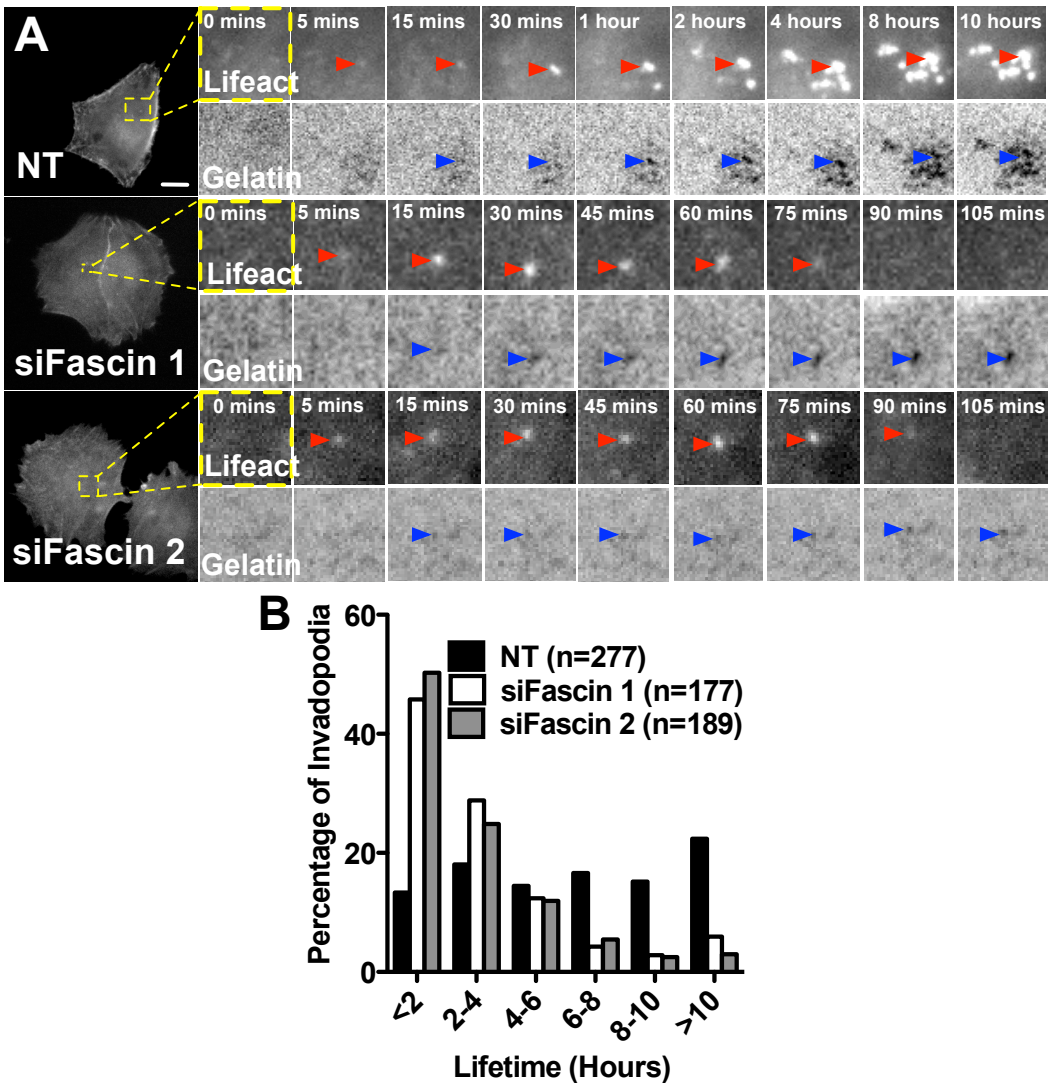

Figure 3.25. Fascin Knockdown reduces Lifetime of Invadopoda
(A) Time-lapse image sequence of A375MM cells stably expressing RFP-Lifeact were transfected with control or fascin siRNA and cultured on Oregon Green 488-conjugated crosslinked gelatin overnight in presence of 5μM GM6001 MMP inhibitor. Time-lapse image was taken within 1 hour after washout of the inhibitor. Scale bars represent 10 μm. Red arrowheads show invadopodia and blue arrowheads show gelatin degradation. (B) Time-lapse lifetime of invadopodia was calculated with data from 30 cells from at least three independent experiments. n represents the total number of invadopodia analyzed.

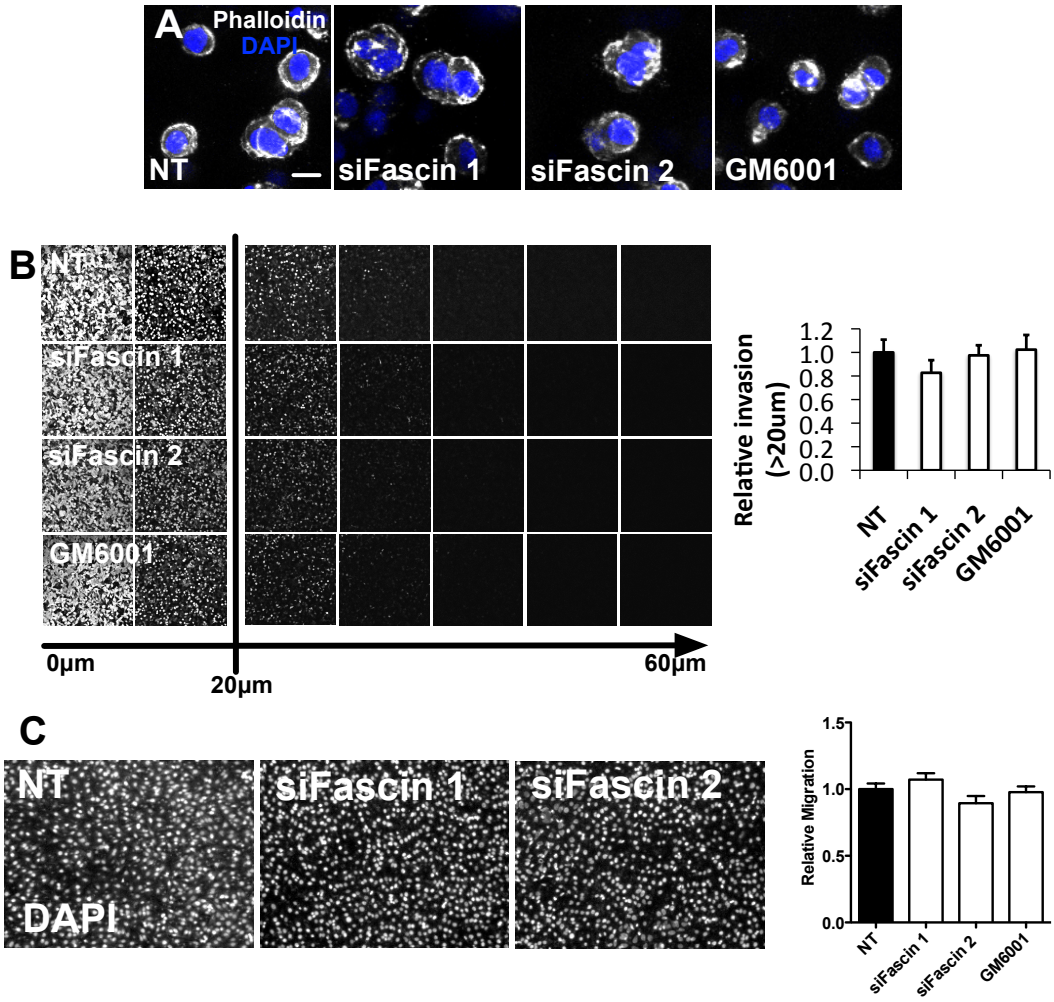

Figure 3.26. A375MM cells migration and invasion is fascin and MMP independent
(A) A375MM cells in collagen I-Matrigel matrix treated with NT, fascin siRNA or 5μM GM6001 were fixed and stained with rhodamine phalloidin and DAPI. Serial of z-stack images were taken with 0.5 μm interval and combined. (B) Representative images of A375MM cells invading into 3D collagen I-Matrigel matrix. Quantification of relative invasion >20 μM into collagen I-Matrigel. Error bars show mean ± SEM. ** $p < 0.01$ by t test. (C) Representative images of transfilter migration assay. A375MM cells expressing NT or fascin siRNA crossed the filter were fixed and stained with DAPI. Quantification of relative migration of A375MM cells crossed filter. Scale bars represent 10 μm.

migration assay. Metalloprotease and matrix degradation have been showed previously to be not required for cell invade using amoeboid type of migration (Wyckoff et al., 2006). Treatments to inhibit protease activity did not affect invasion, migration and morphology of A375MM cells. Together, these results demonstrate that fascin and metalloproteases do not contribute to the invasion of A375MM melanoma cells and that amoeboid type cells may be less dependent on invadopodia for invasion.

3.3.15 Mesenchymal-type cancer cells require fascin during cell invasion in a 3D environment

In contrast to A375MM cells which use an amoeboid type migration for invasion, CHL-1 melanoma cells have been shown to use a more elongated lamellipodia-driven mesenchymal type of migration in 3D (Sanz-Moreno et al., 2008). In addition, during invasion into collagen I-Matrigel matrix, CHL-1 cells appeared elongated and very spiky, with many long, fine actin-rich protrusions, many of which showed abundant fascin (Figure 3.27B). To investigate the effect of fascin on invasion and migration of CHL-1 cells, fascin was depleted using either siRNA transient or shRNA stable knockdown (Figure 3.27E), and invasiveness of resulting cells was measured using inverse invasion assay and transwell migration assay. The invasion and migration of CHL-1 cells were significantly reduced when fascin was depleted (Figure 3.27G, D). I also examined whether fascin is required for cell invasion in 3D matrix using another melanoma cell line: MV3 and MDA-MB-231 human breast adenocarcinoma cell line in which both cell displayed mesenchymal type of migration (Friedl et al., 1997; Wolf et al., 2007). Fascin knockdown in both cell lines resulted in significant reduction in cell invasion through the 3D Collagen I/Matrigel matrix and migration through the filter (Figure 3.28 and 3.29). Collectively, these findings suggest that cells, which use a mesenchymal type of migration for invasion into 3D matrix may selectively require fascin.

To test if fascin is required for collagen degradation in 3D, the ability of NT or

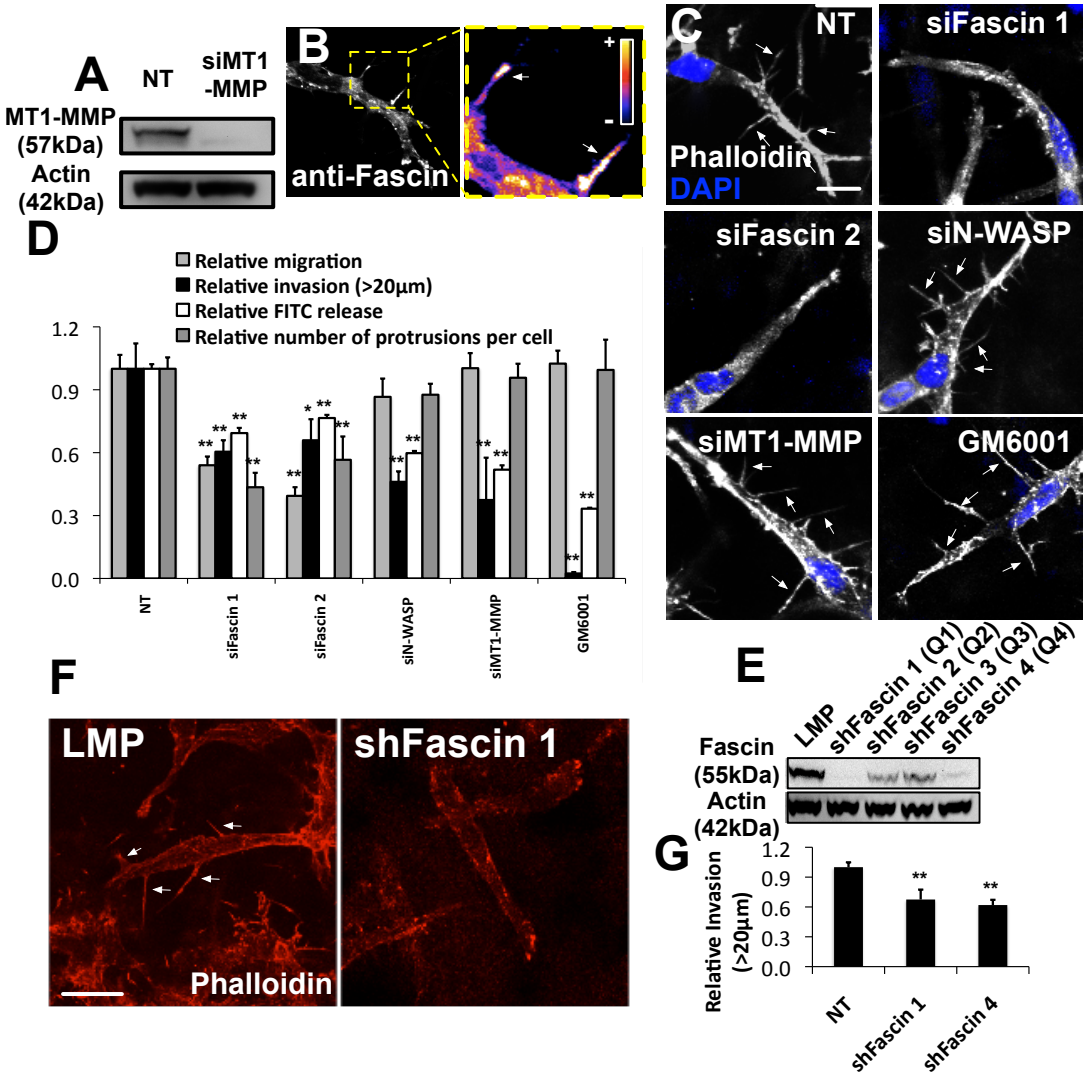

Figure 3.27. Fascin is required for efficient mesenchymal-type invasion in 3D
(A) Western blot of CHL-1 cells expressing NT control siRNA, MT1-MMP siRNA probed with anti-MT1-MMP, and anti-actin loading control. (B) Left: CHL-1 in collagen I-Matrigel matrix fixed and stained with anti-fascin (55K2). Serial Z stack images (0.5 μm) were combined and shown here. Scale bars represent 10 mm. Right: densitometric analysis of fascin signal with arrows at peak fascin intensities.
(C) CHL-1 cells in 3D collagen I-Matrigel matrix treated with siRNA or inhibitor (as indicated) were fixed and stained with rhodamine phalloidin and DAPI. Serial Z stack images (0.5 μm interval) were combined. Filopod-like protrusions were arrowed.
(D) Relative migration cross the filter (light grey), relative invasion >20 mM into collagen I-Matrigel (black), relative release of soluble fluorescein isothiocyanate (FITC) from collagenolysis caused by CHL-1 cells within 3D FITC-collagen lattices (white), and relative number of filopod-like protrusions per cell (dark gray). (E) Western blot of CHL-1 cells stably express LMP vector or fascin shRNA probed with anti-fascin, and anti-actin loading control. (F) CHL-1 cells in 3D collagen I-Matrigel matrix stably express LMP vector or fascin shRNA fixed and stained with rhodamine phalloidin. Filopod-like protrusions were arrowed. Scale bars represent 10 μm. (G) Relative invasion >20 μM into collagen I-Matrigel. All error bars show mean ± SEM. **p < 0.01 and *p < 0.05 by t test.

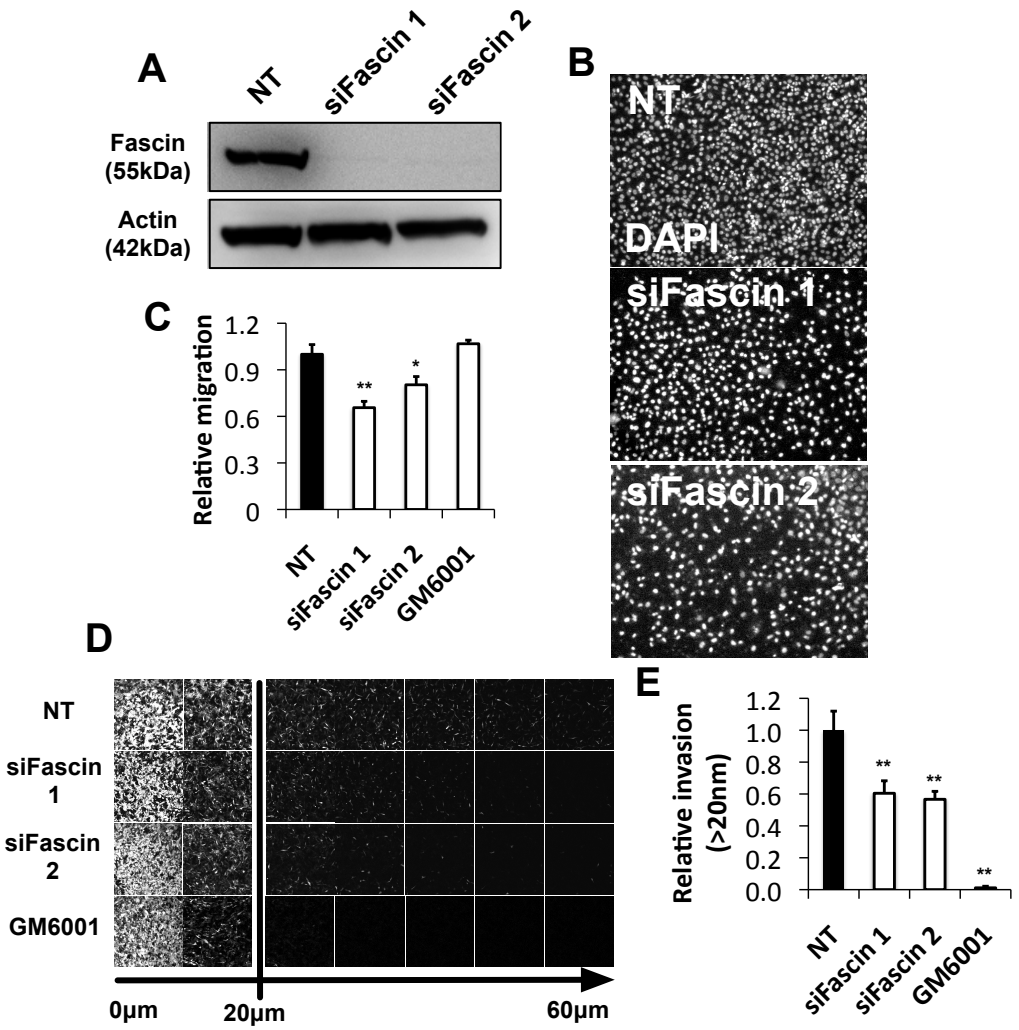

Figure 3.28. Fascin is required by MV3 Melanoma cells for efficient migratin and invasion
(A) Western blot of MV3 melanoma cells expressing NT control siRNA or fascin siRNA probed with anti-fascin, and anti-actin as loading control. (B) Representative images of transfilter migration assay. MV3 cells expressing NT or fascin siRNA crossed the filter were fixed and stained with DAPI. (C) Quantification of relative migration of MV3 crossed filter. (D) Representative images of MV3 cells invading into 3D collagen I-Matrigel matrix. (E) Quantification of relative invasion >20 µM into collagen I-Matrigel. Error bars show mean ± SEM. ** $p < 0.01$, * $p < 0.05$ by t test.

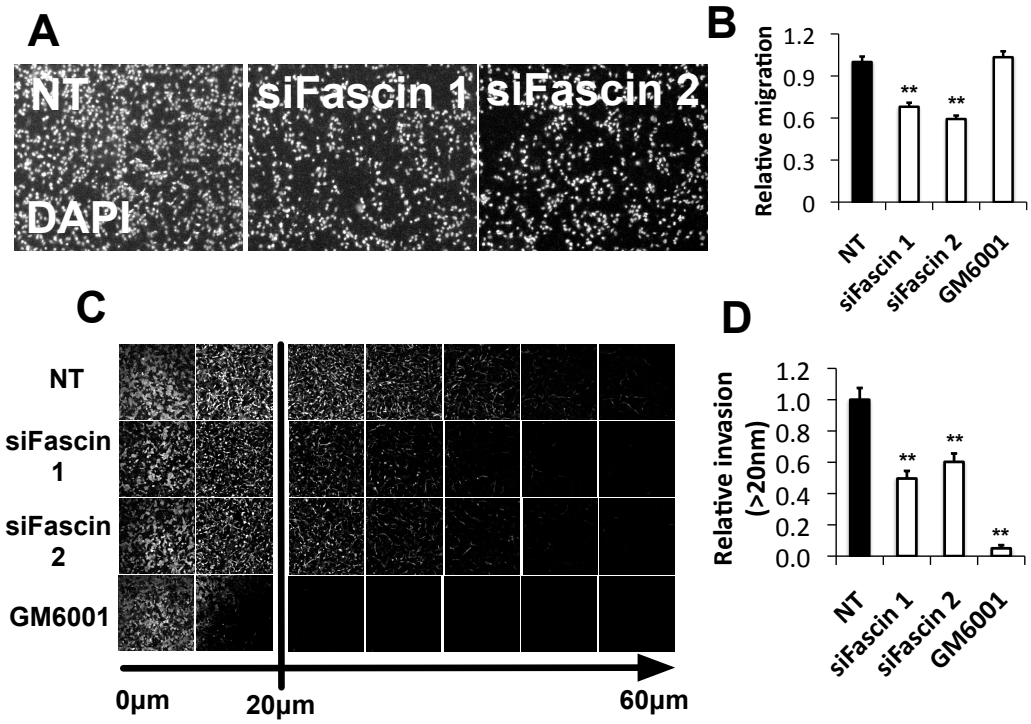

Figure 3.29. Fascin is required by MDA-MB-231 for efficient migratin and invasion
(A) Representative images of transfilter migration assay. MDA-MB-231 cells expressing NT or fascin siRNA crossed the filter were fixed and stained with DAPI. (B) Quantification of relative migration of MBA-MB-231 cell crossed filter. (C) Representative images of MDA-MB-231 cells invading into 3D collagen I-Matrigel matrix. (D) Quantification of relative invasion >20 μM into collagen I-Matrigel. Error bars show mean ± SEM. ** $p < 0.01$ by t test.

Fascin siRNA expressing CHL-1 cells to degradate 3D collagen matrix was measured using FITC collagen release assay as previously described (Wolf et al., 2003a; Wolf et al., 2007). 3D collagen degradation was significantly deceased upon fascin knockdown (Figure 3.27D). In addition, the shape of CHL-1 cells were changed by either transient or stable fascin knockdown, with a decrease in filopod-like protrusions and some remaining small puncta and stubby protrusions (Figure 3.27C, D, F and Movie 4). I postulated that finger-like protrusions in CHL-1 cells could be invasive filopodia and aid the movement of mesenchymal-type cells in 3D matrix. The requirements for other components of invadopodia, including N-WASP, which organizes Arp2/3 complex mediated actin assembly, and the transmembrane matrix metalloprotease MT1-MMP, which controls matrix degradation at invadopodia were probed. Knockdown of N-WASP, which causes a reduction of invadopodia (Figure 3.12) but no change in the filopod-like protrusions in 3D (Figure 3.27C, D), reduced both invasion collagen I-Matrigel matrix and 3D collagen degradation (Figure 3.27D). Likewise, the MMP inhibitor GM6001 or siRNA reduction of MT1-MMP (Figure 3.27A) did not affect filopod-like protrusions in 3D matrix but significantly reduced invasion of mesenchymal-type cells and 3D collagen degradation (Figure 3.27A, C, D; 3.28D, E and 3.29C, D and Movie 4). These results show that filopod-like protrusions alone are not sufficient for 3D invasion and suggest that invadopodia or their equivalents in 3D are required for mesenchymal-type cells to degrade the matrix during 3D invasion.

3.3.16 Fascin phosphorylation regulates mesenchymal-type cancer cell invasion, degradation in 3D environment

In order to examine the effect of fascin bundling activity on cell invasion, Xtfascin S33A and Xtfascin S33D were used to rescue fascin knockdown in CHL-1 cells. Wild type Xtfascin or Xtfascin S33A restored the normal number of protrusions, relative invasion, migration and 3D collagen degradation, whereas Xtfascin S33D did not (Figure 3.30).

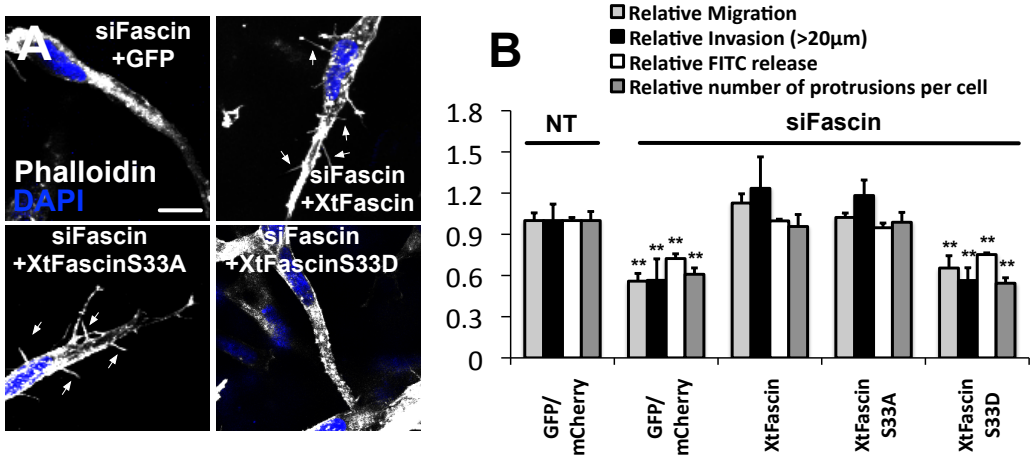

Figure 3.30. Fascin dephosphorylation at Serine 39 is required for efficient migration and mesenchymal-type invasion.
(A) CHL-1 cells in 3D collagen I-Matrigel matrix treated with siRNA were rescued with Xtfascin constructs (as indicated) were fixed and stained with rhodamine phalloidin and DAPI. Serial Z stack images (0.5 µm interval) were combined. Scale bars represent 10 µm. Filopod-like protrusions were arrowed. (B) Quantification of relative migration cross the filter (light grey), relative invasion >20 µm into collagen I-Matrigel (black), relative release of soluble fluorescein isothiocyanate (FITC) from collagenolysis caused by CHL-1 cells within 3D FITC-collagen lattices (white), and relative number of filopod-like protrusions per cell (dark gray) in cells expressing GFP/RFP and NT siRNA, GFP/ RFP and siFascin, or GFP/RFP-Xtfascin and mutants, as indicated in the figure. All error bars show mean ± SEM. **p < 0.01 by t test.

Taken together, these data suggest that actin bundling activity fascin is important for the formation of stable actin-based degradative structures (invadopodia on 2D matrix and their equivalent in 3D) and for filopod-like protrusions that contribute to invasion in 2D and in 3D. Formation of filopodia alone was not sufficient for optimal migration in 3D because knockdown of N-WASP and MT1-MMP reduced invasion but didn't reduce the formation of filopod-like protrusions.

3.4 Discussion

3.4.1 Fascin localize with actin at invaodpodia actin comet structures

Invadopodia have been most closely compared with podosomes, which are dot-shaped F-actin containing structures found in cells such as osteoclasts, endothelial cells and macrophages (Buccione et al., 2004). Unlike podosomes, however, invadopodia appear as highly dynamic actin comet structures similar to those previously described on intracellular pathogens such as *Listeria monocytogenes* or other bacteria and viruses (Baldassarre et al., 2006; Lambrechts et al., 2008). These comet-like structures also have been described on endocytic vesicles in various cells (Fehrenbacher et al., 2003) and are thought to function in trafficking. We provide new insight into the mechanism of actin dynamics at these comet-like structures. We show that invadopodia comets appear to be tethered and the tail spins somewhat reminiscent of a corkscrew (Movie 1 part 1). We found that Arp2/3 complex and cortactin localized largely throughout the actin comet structure, together with fascin, whilst N-WASP was localized primarily at the head. This agrees with a model whereby N-WASP orchestrates the activation of Arp2/3 complex in association with a PIP2-rich membrane surface (Caldieri and Buccione, 2010; Yamaguchi and Oikawa, 2010), forming an actin tail consisting of a branched network. The role of fascin seems to be to stabilize some of the actin in the tail of the comet to provide a platform for force production and possibly also to aid in the secretion of metalloproteases.

3.4.2 Fascin and filopodia proteins are required for invadopodia formation

Our studies suggest that invadopodia contain not only branched actin, but also longer straight networks found in fascin microspikes and in filopodia. Diaphanous related formins were shown to be important players in invadopodia assembly (Lizárraga et al., 2009) also supporting the role of unbranched actin at these structures. Knockdown of DRFs1-3 greatly reduced matrix degradation and invadopodia formation in MDA-MB-231 breast cancer cells and that this also affected invasion of these cells into Matrigel. We find that DRF proteins, IRSp53 and the related IRTKS also localize to invadopodia, although knockdown of IRSp53 did not prevent invadopodia formation in our experiments (Data not shown). It is interesting to note that once a network is initiated by Arp2/3 complex, the actin bundling activity of fascin can drive *Listeria monocytogenes* propulsion in vitro, producing actin tails with long straight actin filaments (Brieher et al., 2004). This implies that actin bundling activity can contribute to protrusive force and motility in cells. In addition, recent study using EM revealed a dense array of thin filaments resembling actin bundles at the very tip of the protrusions or at the sides during elongation of invadopodia (Schoumacher et al., 2010). Moreover, fascin depleted cells form much shorter invadopodia (Schoumacher et al., 2010), which strongly support our idea that fascin may bind to parallel bundles of slowly exchanging actin filaments that can generate force and structural stability for invadopodia over long periods of time. Although invadopodia have properties of invasive filopodia, since several filopodia-inducing proteins are found to have an important role in their formation and stability, they are clearly different from filopodia, as they contain actin comet structures not seen in typical filopodia.

3.4.3 Fascin stablizes actin at invadopodia

In vitro, fascin forms parallel-polarized bundles of actin filaments and shows a very slow exchange rate compared with other bundling proteins such as

alpha-actinin (Tseng and Wirtz, 2004). Fascin also formed side-branched networks in vitro, which is interesting in light of the localization of fascin to lamellipodia and the effects of fascin knockdown on mesenchymal type motility (Adams et al., 1999). We found that fascin overexpression increased the amount of actin trapped at invadopodia in photobleaching experiments, while a decrease in fascin expression increased the mobile fraction of actin filaments. This suggests that in invadopodia, at least some fraction of the fascin forms stable actin bundles that do not exhange on the time scale of minutes. This observation is consistent with our observation that most single invadopodia persist for more than 10 hours in cultured cells (supplementary movies and our unpublished observations). These structures are distinct from what have previously been termed short-lived precursor structures in MTLn3 cells (Chan et al., 2009; Cortesio et al., 2008; Yamaguchi et al., 2005). Many types of actin puncta have been reported in cultured cells including what appear to be small surface ruffles and also endocytic events, so we only counted invadopodia as degradative structures. Myosin-II and myosin V can drive the sliding of actin-fascin bundles (Ishikawa et al., 2003) suggesting that in filopodia, myosins may drive retrograde flow of filopodial actin bundles (Kovar, 2007). Myosin-X is an actin-based motor, which uses its motor activity to move forward along actin filaments to the tips of filopodia. Intersetly, myosin-X has been shown to be required for invadopodia formation (Schoumacher et al., 2010). This suggests that myosin-X could work as a molecular motor transporting molecule such as VASP (Tokuo and Ikebe, 2004) and possibly MMPs to the tip of invadopodia. Since we found that fascin is required for the degradative function of invadopodia, we speculate that fascin bundles may also serve as a platform for cargo transport and the secretion of metalloproteases at invadopodia.

3.4.4 Fascin is selectively required for invasion of mesenchymal-type cancer cells

We found that not only was fascin required for invadopodia assembly and matrix degradation, but it also impacted significantly on the ability of some cancer cells to migrate into collagen/matrigel 3D plugs. Our studies have

raised the question of whether mesenchymal cells need invadopodia more than amoeboid cells for invasion into 3D matrix. This is interesting in light of other studies showing that cells use a combination of rounded acto-myosin based motility termed “amoeboid” and elongated protrusive motility termed “mesenchymal” (Sahai, 2005; Sahai and Marshall, 2003; Wolf et al., 2003a). Mesenchymal motility is defined in some studies as requiring protease activity and involving Rac1 induced lamellipodial protrusions. We find that, in general, loss of fascin impairs invasion of cells that use primarily mesenchymal motility. Thus, our data suggest that amoeboid cells might not need invadopodia for their invasion and agree with a role for fascin in protrusions as well as matrix invasion and degradation. Interestingly, Huttenlocher and colleagues also published that they observed a separation between enhanced invadopodia formation and the invasive capacity of cancer cells (Chan et al., 2009). They showed that FAK deficient MTLn3 cells showed impaired invasion across Matrigel coated filters, yet had enhanced capacity to form invadopodia. This likely reflects the complex nature of invasion, which requires a fine balance of adhesion, migration and matrix remodeling, as well as perhaps that MTLn3 cells use a primarily amoeboid mode of motility in 3D gels (Wyckoff et al., 2006).

Previous studies suggest that cell leading edges are not necessarily major places of matrix degradation but rather that degradation happens at lateral points where the matrix restricts the cell movement and at structures that have been called ‘‘lytic protrusions’’ (Wolf and Friedl, 2009). Some of the filopod-like protrusions in CHL-1 cells may be involved in matrix remodeling because they all contained GFP-MT1-MMP (data not shown). However, our data strongly suggest that matrix remodeling promoted by ‘‘invadopodia equivalents’’ is more important for efficient cell invasion than filopod-like protrusions. Attempt to identify "invadopodia equivalents" in 3D was unsuccessful as most of antibodies that we use to label invadopodia (anti-cortactin, anti-p34) in 2D do not work in 3D collagen I-matigel matrix. ‘‘Invadopodia equivalents’’ may be smaller and more transient in 3D than in 2D on very stiff matrix, analogous to focal adhesions (Cukierman et al., 2001). Moreover, invadopodia formation in cells grown on a 3D dense matrix based

on cell-free dermis suggest a different morphology of invadopodia in 2D and 3D and matrix-degrading activity of invadopoida is localized to the base of invadopodia rather than at matrix-penetrating protrusions (Tolde et al., 2010). Historically, invadopodia were first described as invasive finger-like protrusions into gelatin beads (Chen, 1989; Mueller and Chen, 1991), but invadopodia with obvious actin comet tails have not yet been visualized in 3D gels. We find that fascin promotes long protrusions in 3D and stabilizes actin in invadopodia and that this enhanced stability allows for more efficient invasion by mesenchymal cells, both in 2D and in 3D.

Chapter IV
Rac1 drives melanoblast organization during mouse development by orchestrating pseudopod-driven motility and cell cycle progression.

4.1 Summary

During embryogenesis, melanoblasts proliferate and migrate ventrally through the developing dermis and epidermis as single cells. I demonstrate here that targeted deletion of Rac1 in the melanoblasts of developing mice causes defects in migration, cell cycle progression and cytokinesis. Rac1 null cells migrate markedly less efficiently, but global steering, crossing the dermal/epidermal junction and homing to hair follicles are normal. Melanoblasts navigate in the epidermis using two classes of protrusion: short stubs and long pseudopods. Short stubs are driven by actin assembly, but unexpectedly are independent of Rac1, Arp2/3 complex, myosin or microtubules. Rac1 positively regulates the frequency of initiation of long pseudopods, which promote migration speed and directional flexibility. Scar/WAVE and Arp2/3 complex drive actin assembly for long pseudopod extension, which is also microtubule dependent. Myosin contractility balances the extension of long pseudopods by effecting retraction and allowing force generation for movement through the complex 3D epidermal environment.

4.2 Introduction

Mammalian melanoblasts are the precursor cells of melanocytes; they emerge from the neural tube during embryogenesis, with other neural crest cells and migrate and proliferate to populate the skin and hair follicles. Genetic studies in the mouse have made a considerable contribution to our understanding of melanoblast development, identifying over 127 genes essential to normal pigmentation (Bennett and Lamoreux, 2003). Of the loci that have been cloned, over one third comprise genes that regulate melanocyte development. Mutations in these genes often manifest themselves as ‘white-spotting’ phenotypes, as a consequence of defects in melanocyte precursor proliferation, survival, migration and/or tissue invasion (Baxter et al., 2004). From these studies, several molecules involved in melanoblast pathfinding have been identified, including both receptor tyrosine

kinases (e.g. Kit) and G- protein-coupled receptors (e.g. Ednrb) and their ligands (KitL and Endothelin3, respectively). However, how melanoblasts migrate in during development and how these molecules affect melanoblast behaviour are still unknown. Recently, a high power ex-vivo microscopic method (Mort et al., 2010) became available so that we are now in a position to understand the mechanisms of migration of these fascinating cells.

Rac1 is the major ubiquitous isoform of Rac expressed in mammalian tissues, with Rac2 being primarily hematopoietic and Rac3 being expressed in some regions of the brain (Didsbury et al., 1989; Haataja et al., 1997). Rac1 controls assembly of the actin cytoskeleton via a number of signaling pathways, the major ones being activation of the Scar/WAVE complex leading to Arp2/3 complex mediated actin nucleation (Insall and Machesky, 2009) and activation of p21-activated kinase (PAK) and LIM kinase leading to changes in cofilin phosphorylation and actin turnover (Delorme *et al.*, 2007). Both of these pathways are thought to be important in normal and cancer cell migration. Loss of Rac1 in tissue culture and primary cells leads to a loss of lamellipodia and a general reduction of migration speed (Guo et al., 2006; McCarty et al., 2005a; Vidali et al., 2006). Rac1 depletion also reduces focal adhesions and stress fibers in mouse embryonic fibroblasts (Delorme et al., 2007; Guo et al., 2006; Vidali et al., 2006).

In vivo, we have limited knowledge of the role of Rac1 in migration. *Drosophila* oocyte border cells, which migrate through the egg chamber collectively as a small cluster, are unable to migrate when they express dominant negative Rac (Bianco et al., 2007; Duchek et al., 2001; Geisbrecht and Montell, 2004; Murphy and Montell, 1996; Wang et al., 2010) and their motility can be induced by photoactivation of a Rac analog (Wang et al., 2010). Border cells use cadherin-based adhesion to navigate among nurse cells and Rac triggers the generation of long protrusions made by leader cells during this migration (Bianco et al., 2007; Duchek et al., 2001; Geisbrecht and Montell, 2004; Murphy and Montell, 1996). Likewise, sequestration of Rac1 activity in zebrafish germ cells inhibits actin brush formation, cell polarity and migration (Kardash *et al.*, 2010). In zebrafish embryos, neural crest cell

migration toward SDF-1 is regulated by Rac1 (Theveneau et al., 2010). Mouse anterior visceral endoderm (AVE) cells also require Rac1 for protrusion formation and collective migration to the developing anterior side of the embryo between days E5.5-6.0 during body axis specification (Migeotte *et al.*, 2010). Surprisingly, mouse neural crest cells do not require Rac1 for homing to initial target structures, but Rac1 loss impairs proliferation (Fuchs *et al.*, 2009). Thus Rac1 emerges as an important controller of in vivo migration, but our mechanistic insight is limited.

Rac is activated downstream of Ras and can activate JNK1, possibly via Pak kinases to stimulate cell cycle progression (Olson *et al.*, 1995). Both cell-cell and cell-matrix adhesion transmit signals to increase cyclin D1 levels for progression through the cell cycle and Rac1, together with ERK regulates this signaling (Fournier *et al.*, 2008; Klein *et al.*, 2008). The mechanism by which Rac1 controls cyclin D1 mRNA levels is not known. Rac1 is tightly regulated in cytokinesis, both temporally and spatially and is inhibited at the cleavage furrow by centralspindlin, a GTPase activator (GAP) (Canman et al., 2008). No positive role for Rac1 in cytokinesis has been demonstrated to our knowledge.

In the present Chapter, I have described here an important role for Rac1 in migration, proliferation and cytokinesis in mouse embryonic melanoblasts in skin *ex vivo* and revealing an important role for Rac1 as a coordinator of the rate of protrusion generation during migration. In addition, Rac1 deletion in melanoblasts results inability of cells to mount a Rac – Scar/WAVE – Arp2/3 mediated protrusion response for migration. Surprisingly, though, Rac1 null melanoblasts can still use short stubby protrusions to migrate independently of this pathway by a novel actin-driven mechanism.

4.3 Results

4.3.1 Rac1 loss in melanoblasts causes coat color defects, indicating impaired migration and proliferation

To assess the functions of Rac1 in the melanocyte lineage *in vivo*, we crossed mice carrying a floxed allele of Rac1 (Corbetta et al., 2009; Walmsley et al., 2003) with mice expressing Cre recombinase under control of the tyrosinase promoter (Tyr::Cre) (Delmas et al., 2003) (Figure 4.1A) in a C57BL6/J background. Rac1 f/f Tyr::Cre$^{+/o}$ mice were born healthy at the expected Mendelian ratio, however, they were smaller than littermates and they exhibited tremor (Figure 4.2 and Methods). Recombination was confirmed by genomic PCR, amplifying distinct fragments for wild-type, floxed, or null alleles of Rac1, respectively (Corbetta et al., 2009). The Rac1 null allele was only observed together with Tyr::Cre (Figure 4.1B) indicating efficient recombination in the melanocytes.

Rac1 f/f Tyr::Cre$^{+/o}$ mice (n=15) exhibited a distinctive white patch of hair along their ventral region, ranging in size from half to whole the width of the mouse underside (Figure 4.3). In addition, more than 80% of the mice had at least one white patch along the dorsal midline (Figure 4.3, white arrows) as well as white hairs among the black dorsal fur. The limbs and tail in all Rac1 f/f Tyr::Cre$^{+/o}$ mice were also hypopigmented (Figures 4.3B and C). Dopachrome tautomerase (Dct), is involved in the biosynthesis of melanin (Tsukamoto et al., 1992). Dct is first expressed in embryonic melanoblasts (E10) and is still expressed later in melanocytes and stem cellsin adults (Nishimura et al., 2002) thus can be used as melanocyte specific marker. Histological analysis of P14 control skin or black areas of the Rac1 f/f Tyr::Cre$^{+/o}$ mice with DCT antibody showed melanocytes in hair follicles (Figures 4.4A and C), indicating that some melanocytes lacking Rac1 can still home correctly. Whereas, no melanocytes were present in dorsal white patches or ventral skin of Rac1 f/f Tyr::Cre$^{+/o}$ mice (Figure 4.4B). Thus, Rac1 deficiency in melanocytes causes a pigmentation defect resulting from a lack of melanocytes in areas distal to their migration origin near the neural tube.

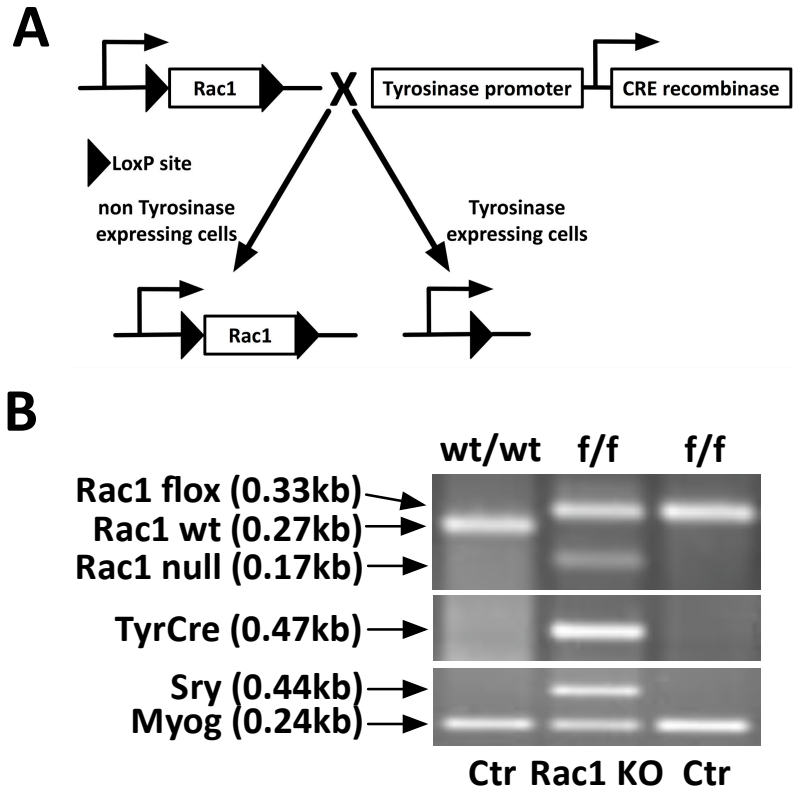

Figure 4.1 Rac1 conditional knockout in melanocytes

(A) Gene targeting strategy for generating Rac1 f/f Tyr::Cre$^{+/o}$ mice. Cre recombinase, under control of the tyrosinase promoter, mediates the excision of Rac1 in the melanocyte lineage. (B) A representative genotyping assay using DNA extracted from melanocyte-rich ear skin for: wild-type (left lane), Rac1 f/f Tyr::Cre$^{+/o}$ (middle lane) and Rac1 f/f Tyr::Cre$^{o/o}$ (right lane). Sex of mice is determined using male-specific maker Sry and universal maker Myog.

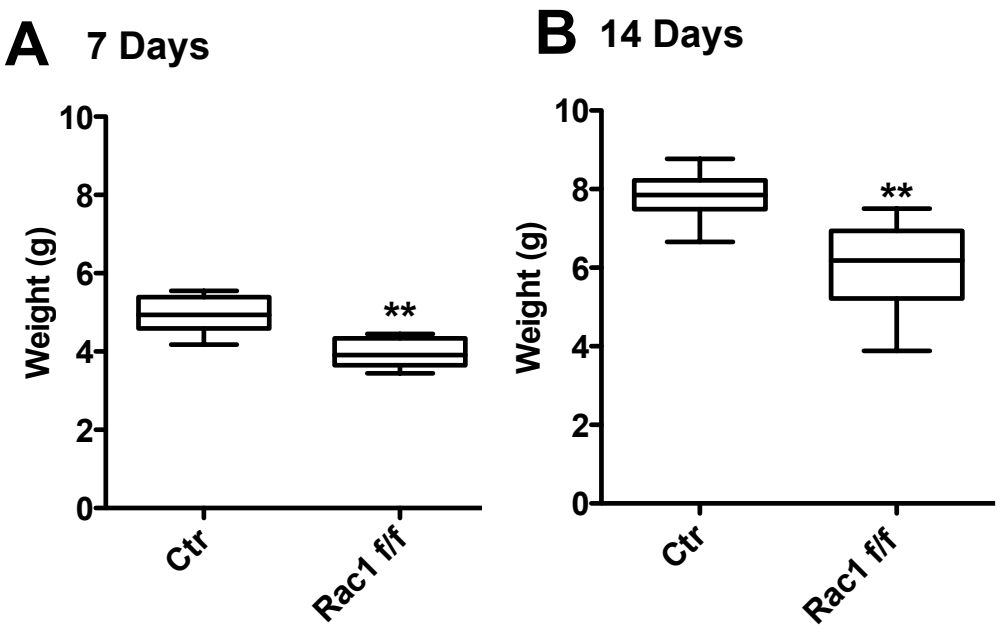

Figure 4.2 Rac1 f/f Tyr::Cre$^{+/o}$ mice show decreased body size compared to control litter mates.
Box plot of quantification of body weight of mice at day 7 (A) and day 14(B). Lower quartile, median, and upper quartile are shown. At least 6 mice from 3 different litters were quantified. **, P< 0.01 compared to control by t-test.

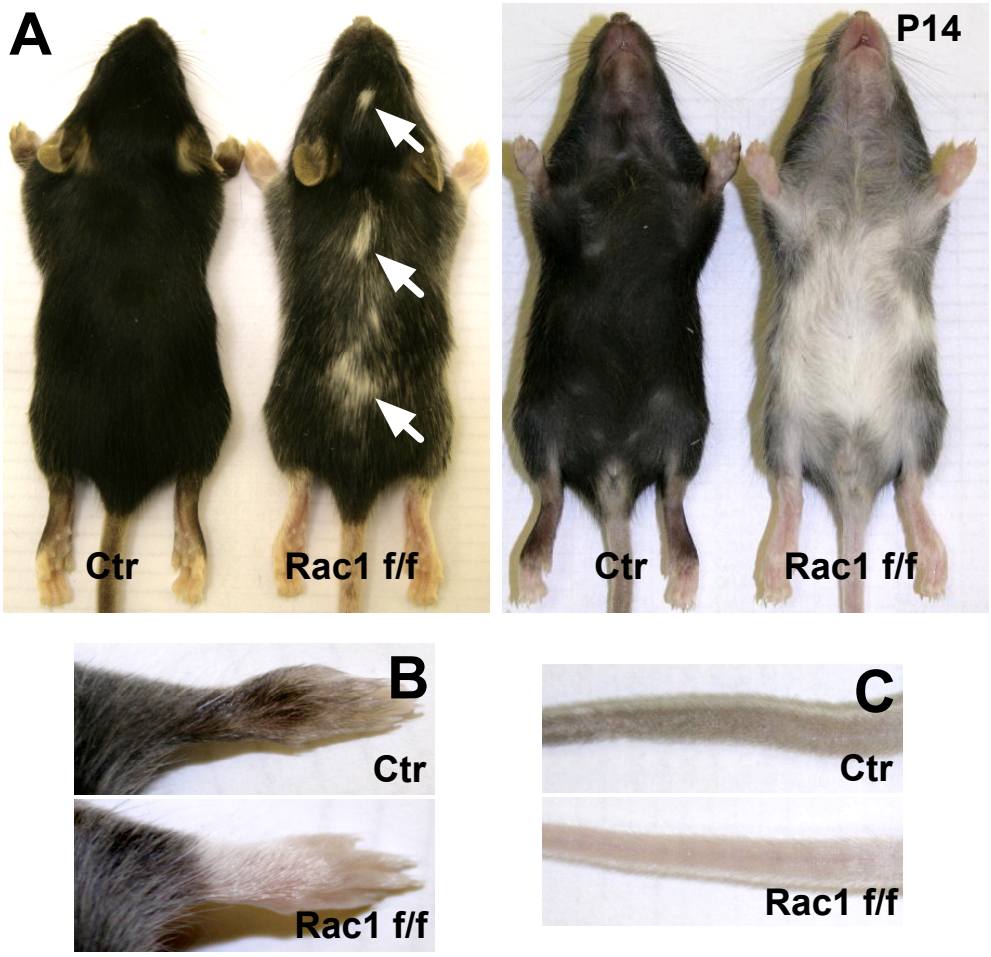

Figure 4.3 Rac1 specific deletion in melanocytic cells results in hypopigmentation in C57BL6 mice.

(A) Coat-color of P14 Rac1 f/f Tyr::Cre$^{+/o}$ (Rac1 f/f) mouse with control littermate (Ctr). Left: dorsal side. Right: Ventral side. White arrows point to typical dorsal white patches. (B) Forelimb of P14 Rac1 f/f Tyr::Cre$^{+/o}$ mouse with control littermate. (C) Tails of control and Rac1 f/f Tyr::Cre$^{+/o}$.

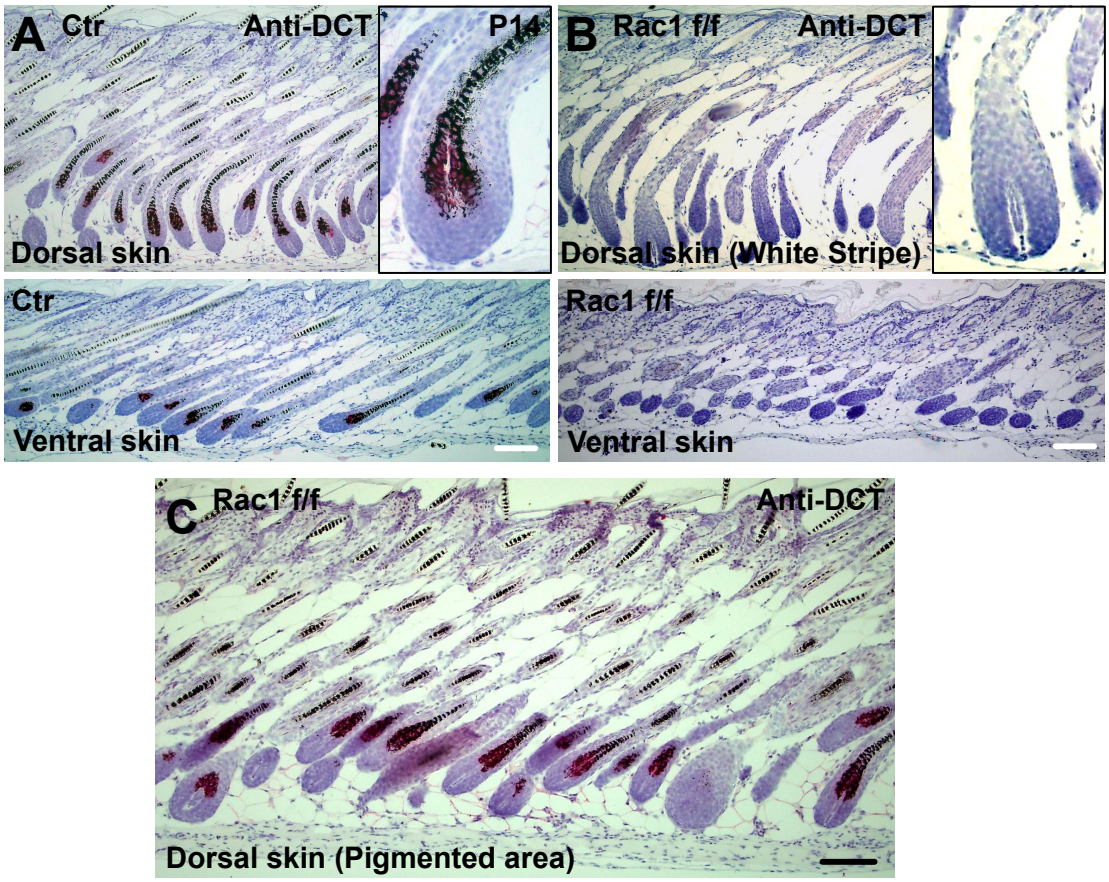

Figure 4.4 Rac1 f/f Tyr::Cre$^{+/o}$ show absence of melanoblasts in dorsal and ventral patches. (A) Dorsal and ventral skin of P14 control and (B) Rac1 f/f Tyr::Cre$^{+/o}$; dorsal skin from white patch and ventral skin with anti-DCT (melanocyte). Insets show hair follicles. (C) Dorsal skin (pigmented region) of P14 of Rac1 f/f Tyr::Cre$^{+/o}$ were subjected to immunohistochemical analysis with antibody against DCT to detect melanocytes. Scale bars 100μm.

4.3.2 Rac1 null melanoblasts progress towards the normal target areas of the embryo, but fail to complete population of the embryo skin

Mouse melanoblasts migrate out of the neural tube around E10 and continue to proliferate and migrate to fill the skin by the time of birth. The melanoblast distribution was examined to determine whether loss of Rac1 affected number and position of melanoblasts between E11.5 and E15.5 using a DCT::LacZ transgene (Mackenzie et al., 1997). On E11.5, when the Tyr::Cre is expressed (Delmas et al., 2007; Delmas et al., 2003), the number and distribution of melanoblasts were similar in control and Rac1 f/f Tyr::Cre$^{+/o}$ embryos (Figures 4.5A, E). In E13.5 control embryos, the melanoblast population started to expand ventrally (Figures 4.5B, E). By E15.5, melanoblasts colonized almost the entire embryo (Figures 4.5C, E). However, by E13.5, there were fewer melanoblasts in Rac1 f/f Tyr::Cre$^{+/o}$ embryos than controls and this difference increased by E15.5 (Figures 4.5B, C, E). The E15.5 Rac1 f/f Tyr::Cre$^{+/o}$ embryos also displayed a notable absence of melanoblasts on both the ventral region and limbs corresponding to the future unpigmented region (Figures 4.5C, D). Additionally, Rac1 depleted melanoblasts appeared less elongated than controls (Figure 4.6). Melanoblasts in Rac1 f/f Tyr::Cre$^{+/o}$ failed to cover the entire dorsal midline region on E15.5 accounting for the future dorsal white patches (Figure 4.7). Furthermore, Rac1 f/f Tyr::Cre$^{+/o}$ showed half the normal number of melanoblasts at P0.5 after birth (Figure 4.8). Thus, Rac1 is important for melanoblast position and number during embryogenesis. However, it is also clear that melanoblasts lacking Rac1 can still proliferate, migrate, home to hair follicles and produce and secrete melanin to pigment the hair, albeit less efficiently than those expressing Rac1.

4.3.3 Melanoblasts migrate in embryo epidermis with Rac1 driven long pseudopods and Rac1 independent short stubs

To investigate the functions of Rac1 in melanoblast migration in vivo, mice

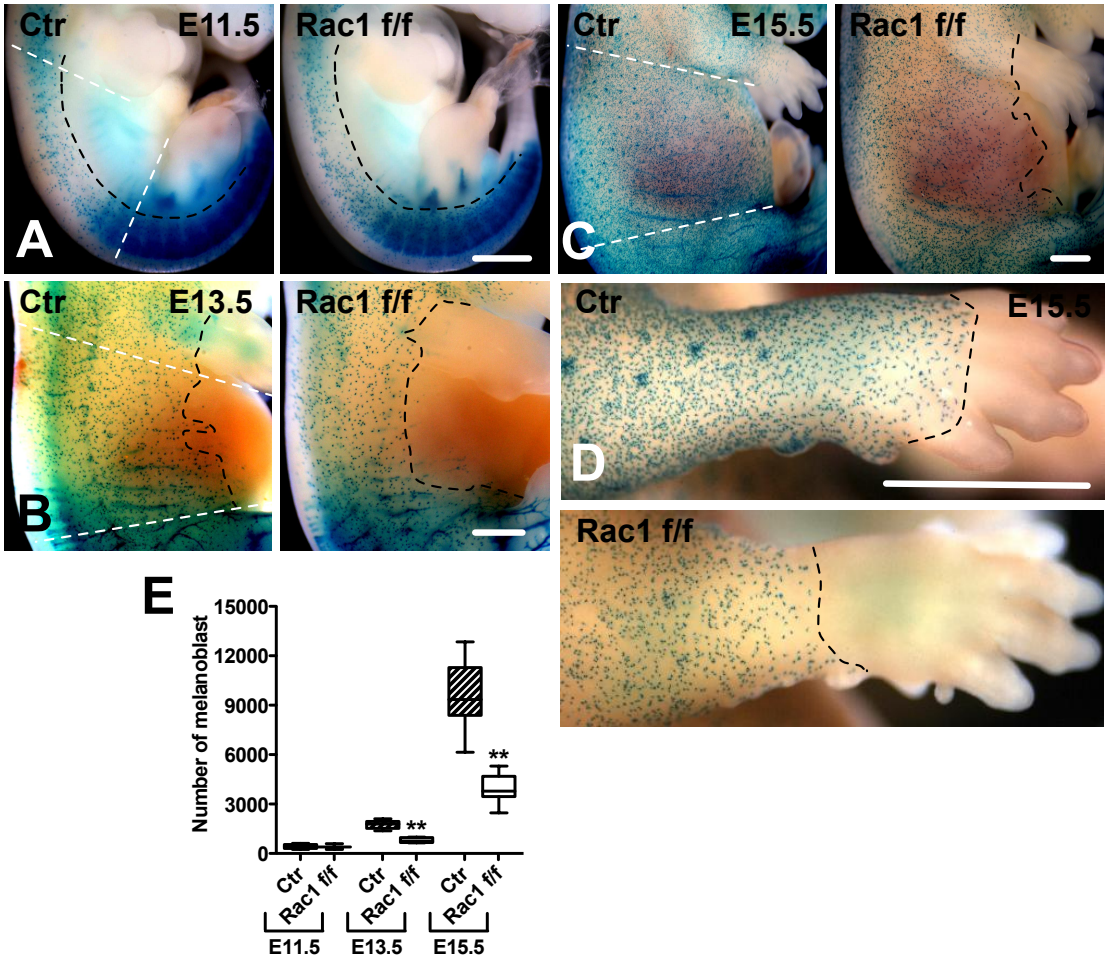

Figure 4.5 Loss of Rac1 alters melanoblast number and position from E13.5. (A-C) β-galactosidase stained whole mount DCT::LacZ control and Rac1 f/f Tyr::Cre$^{+/o}$ embryos at E11.5, E13.5 and E15.5. White dot lines in A, B and C indicate the trunk regions in which melanoblasts were quantified in box plot as shown in (E). Each image is representative of at least 5 embryos from four different litters. (D) Enlarged images of forelimb from E15.5 DCT::LacZ control and Rac1 f/f Tyr::Cre$^{+/o}$ embryos. (E) Quantification of melanoblasts in DCT::LacZ control and Rac1 f/f Tyr::Cre$^{+/o}$ littermate embryos at E11.5, 13.5 and 15.5 from (>=5 embryos, 4 litters). Lower quartile, median, and upper quartile are shown. **, P< 0.01 by t-test Scale bars are 1mm.

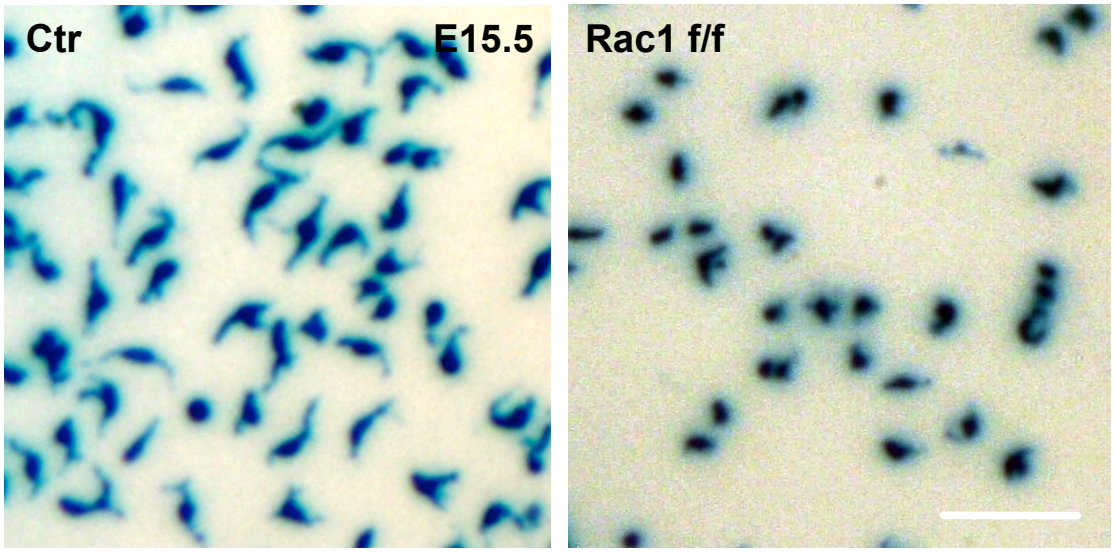

Figure 4.6 Loss of Rac1 alters melanoblast morphology in vivo. Enlarged images of β-galactosidase stained whole mount E15.5 DCT::LacZ control (left) and Rac1 f/f Tyr::Cre$^{+/o}$ (right) embryos trunk regions showing individual melanoblasts. Scale bar is 50μm.

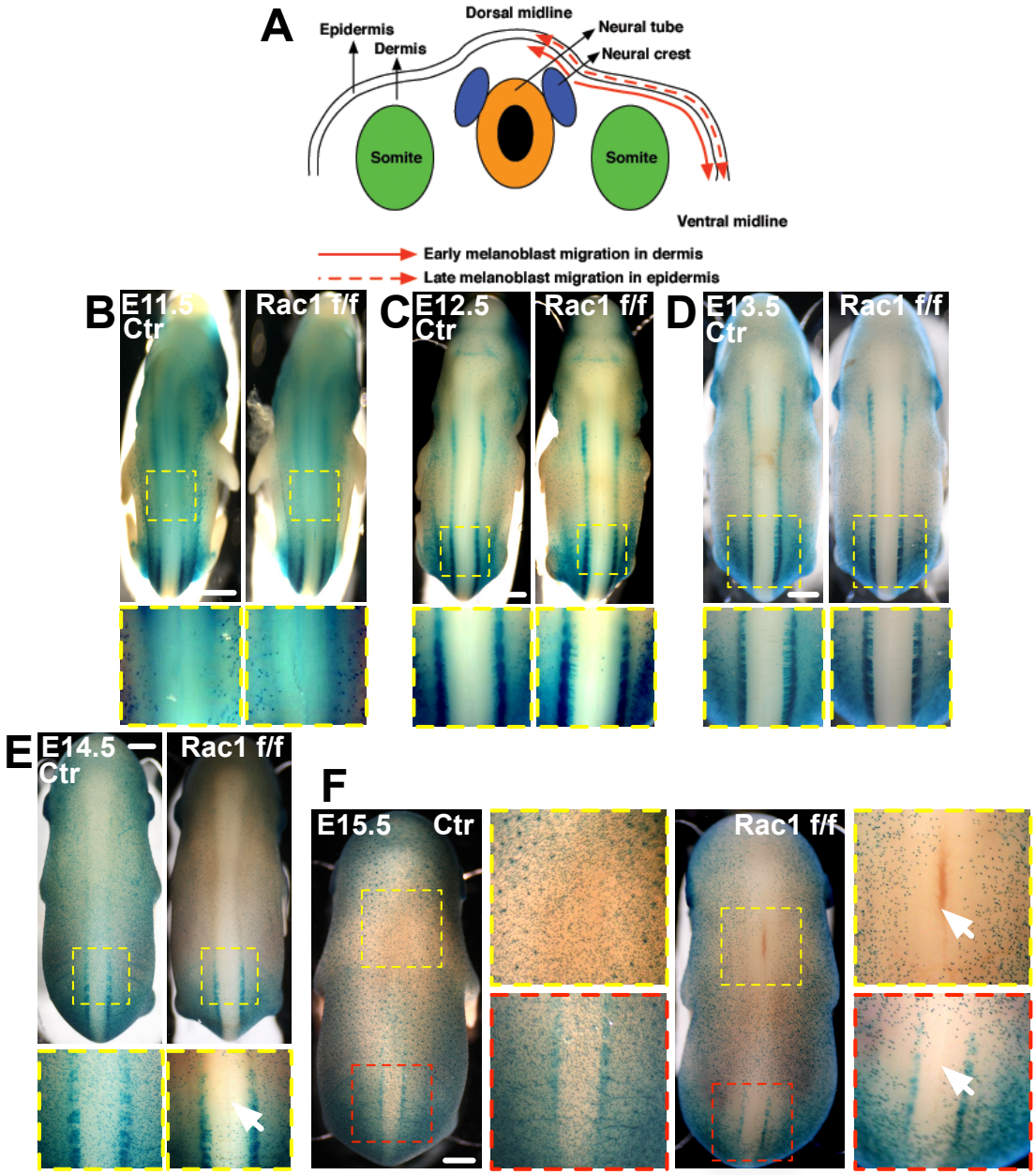

Figure 4.7 Rac1 f/f Tyr::Cre$^{+/o}$ mice show paucity of melanoblasts at the dorsal midline. (A) Diagram showing where melanoblasts emerge from the neural tube into the neural crest area (also called migration staging area) leaving the dorsal midline devoid of melanoblasts until they commence both dorsal (red arrows) and ventral migration (black arrows). (B-F) Images of dorsal side of DCT::LacZ control and Rac1 f/f Tyr::Cre+/o embryos at (B) 11.5 (C) E12.5, (D) E13.5, (E) E14.5 and (F) E15.5. Note that at E11.5-13.5, melanoblasts were absent from the dorsal midline in both control and Rac1 f/f Tyr::Cre+/o embryos. From E14.5 to E15.5, melanoblasts start to migrate into the dorsal midline and eventually cover the whole area. However, fewer melanoblasts migrate into dorsal midline in Rac1 f/f Tyr::Cre+/o embryos at E14.5, which results in unpopulated patches by E15.5 (white arrowed). Scale bars are (B-F) 1mm.

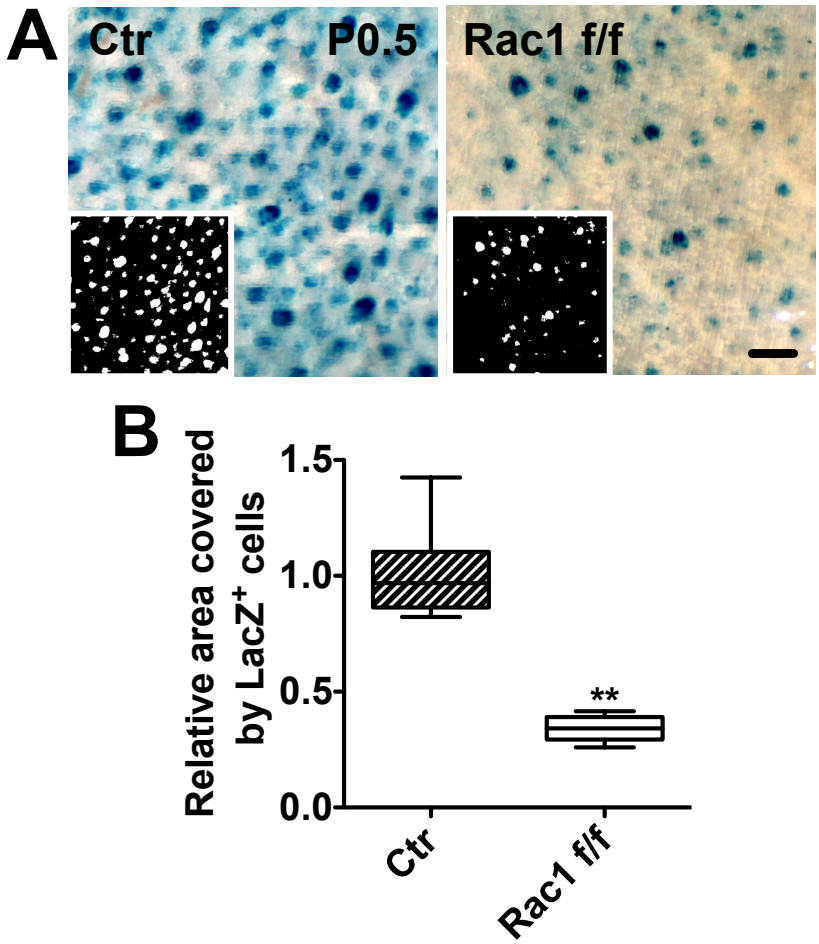

Figure 4.8. Loss of Rac1 alters melanocytes number in new born pups. (A) Representative images of β-galactosidase stained dorsal skin samples DCT::LacZ control (left) and Rac1 f/f Tyr::Cre$^{+/o}$ (right) pups at P0.5. Each image is from (>= 3 pups, 3 litters). Insets show representative thresholded images used in quantification. (B) Relative area covered by melanocytes per image for control and Rac1 f/f Tyr::Cre$^{+/o}$. Data derived from (5 images each from >=3 pups, 3 litters). Lower quartile, median, and upper quartile are shown. **, P< 0.01 by t-test. Scale bar is 100μm.

carrying a Z/EG double reporter transgene (Novak et al., 2000) were crossed onto the Rac1 f/f Tyr::Cre$^{+/o}$ background to allow specific GFP-expression in the melanoblast lineage. E15.5 embryonic trunk skin was then imaged as previously described (Mort et al., 2010). Skin explants consisted of epidermis, developing hair follicles and part of the dermis with most melanoblasts in the epidermis above the basement membrane among the keratinocytes (Movie 5). GFP-labelled melanoblasts in whole mounted skin explants exhibited an elongated morphology. They showed long cellular protrusions (>cell body width) traversing the regions in between adjacent keratinocytes that had microtubule cores with several actin rich tips (Figure 4.9 and Movie 5). 3D reconstructions revealed a rounded cell body with frequently one or two long protrusions, one of which was in the direction of migration (Figure 4.10, Movie 5). Melanoblasts and keratinocytes express E-cadherin and use E-cadherin to contact each other in the developing mouse embryo epidermis (Figures 4.9 and 4.11). Loss of Rac1 did not detectably alter E-cadherin localization in Rac1 f/f Tyr::Cre+/o melanoblasts or melanoblast position relative to keratinocyte neighbors (Figure 4.11). Keratinocytes also do not require Rac1 for adherence junctions in vivo (Benitah et al., 2005; Chrostek et al., 2006). It is likely that loss of Rac1 in melanoblasts didn't completely disrupt their cell-cell contacts. In summary, melanoblasts exhibit elongated shape and long protrusions between neighboring keratinocytes, which are rich in tubulin and actin and may use E-cadherin to contact the neighboring keratinocytes. Loss of melanoblast Rac1 gives cells a more rounded shape, but does not cause any detectable defects in melanoblast positioning in contact with keratinocytes.

Live time-lapse imaging of embryo skin explants revealed severe motility defects in Rac1 null melanoblasts. At any one time, nearly every normal melanoblast had at least one long protrusion (average 0.9 per cell) compared with average 0.2 per cell for Rac1 nulls (Figure 4.12A white arrows long protrusions, yellow arrows short stub protrusions and Figure 5.12B, Movie 5). Around 35% of the Rac1 depleted melanoblasts and only 4% of normal melanoblasts showed no protrusions (Figure 4.12C). Long protrusions were

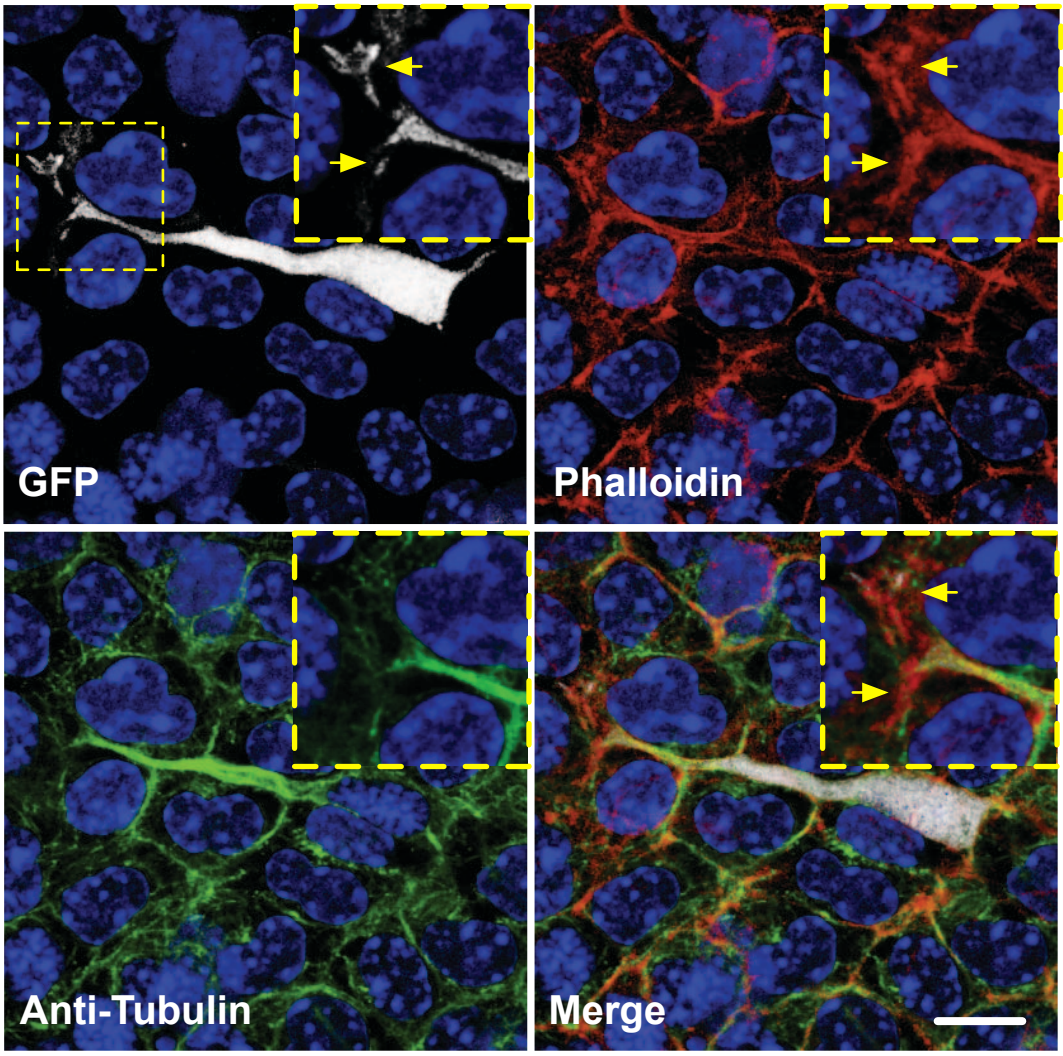

Figure 4.9. Epidermal melanoblasts display an elongated shape with long protrusions. Combined Z-stack image (1μm depth) of E13.5 Z/EG Tyr::Cre$^{+/o}$ control embryo stained with phalloidin, anti-tubulin and DAPI. Insets show distal tips (yellow arrowed). All scale bars are 10μm

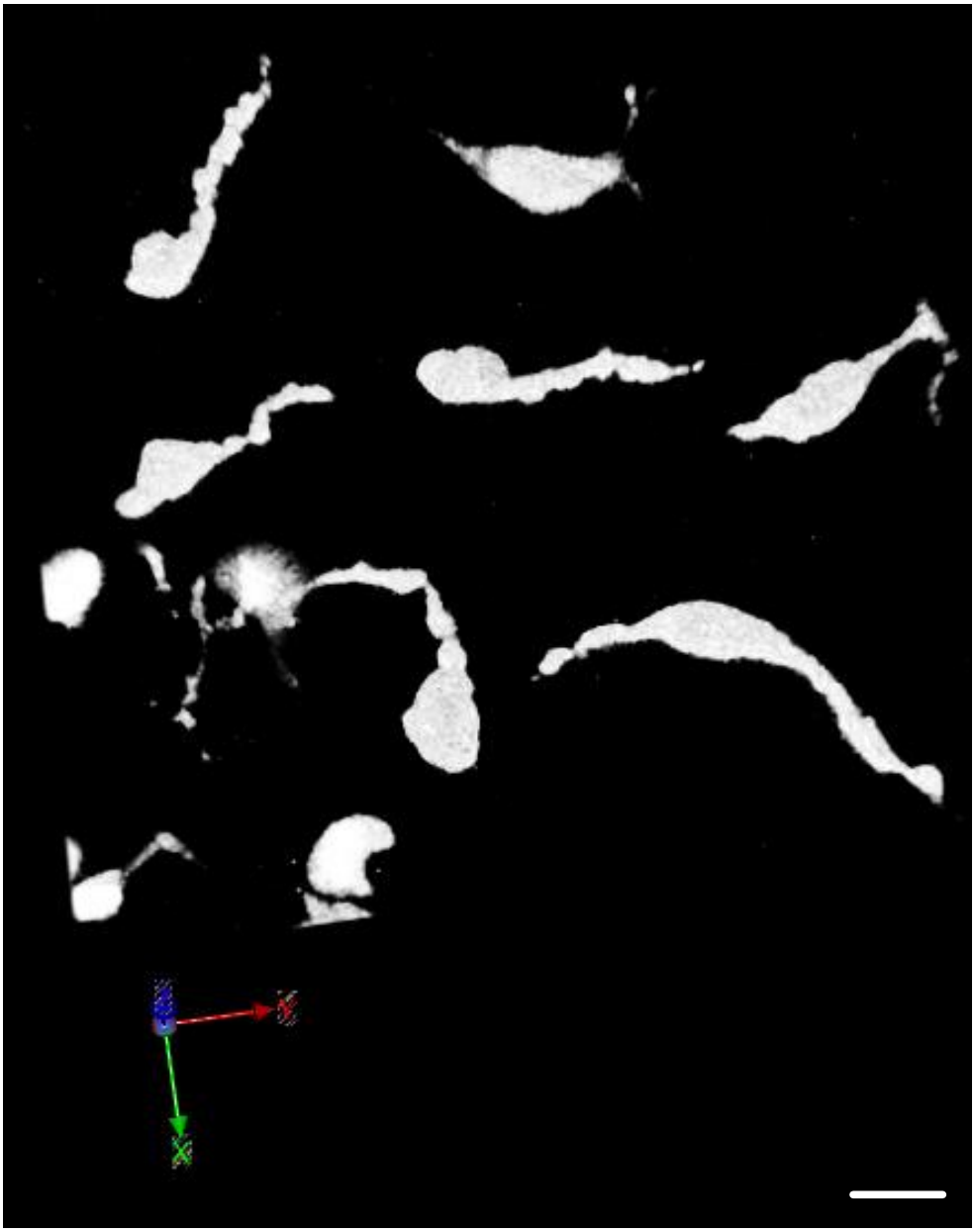

Figure 4.10. Epidermal melanoblasts forms long protrusions in skin explants. 3D reconstruction of E15.5 GFP-melanoblasts. Scale bars are 10μm

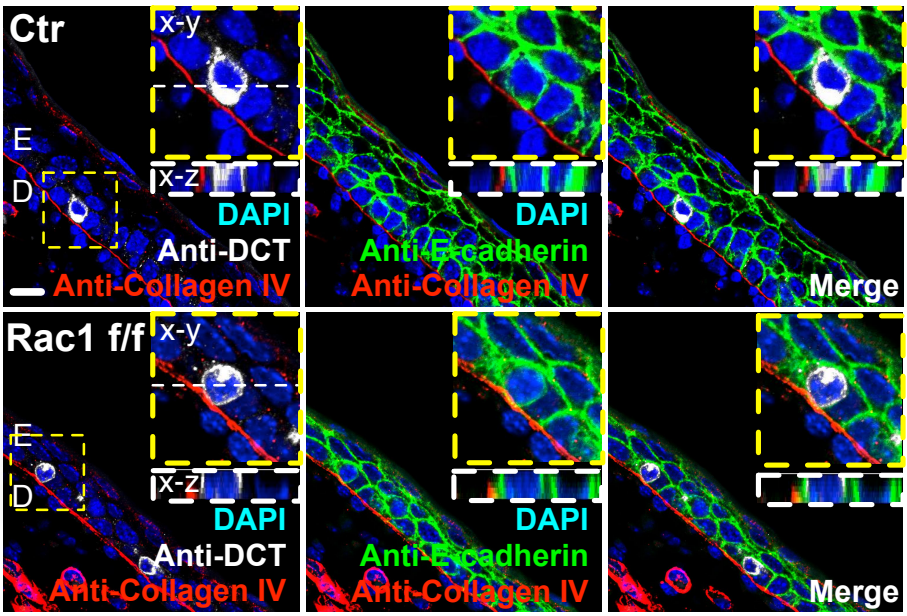

Figure 4.11. Rac1 depleted melanoblast showed normal E-cadherin localization. Representative combined Z-stack images (1μm depth) of sections from E15.5 control and Rac1 f/f Tyr::Cre+/o embryos stained for Collagen IV, E- cadherin, DCT and DAPI. “E” denotes epidermis and “D” denotes dermis above and below the red line of collagen IV staining that delineates the basement membrane. The insets are shown as X-Y and X-Z projections to view the melanoblasts relative to surrounding keratinocytes. Scale bar is 10μm.

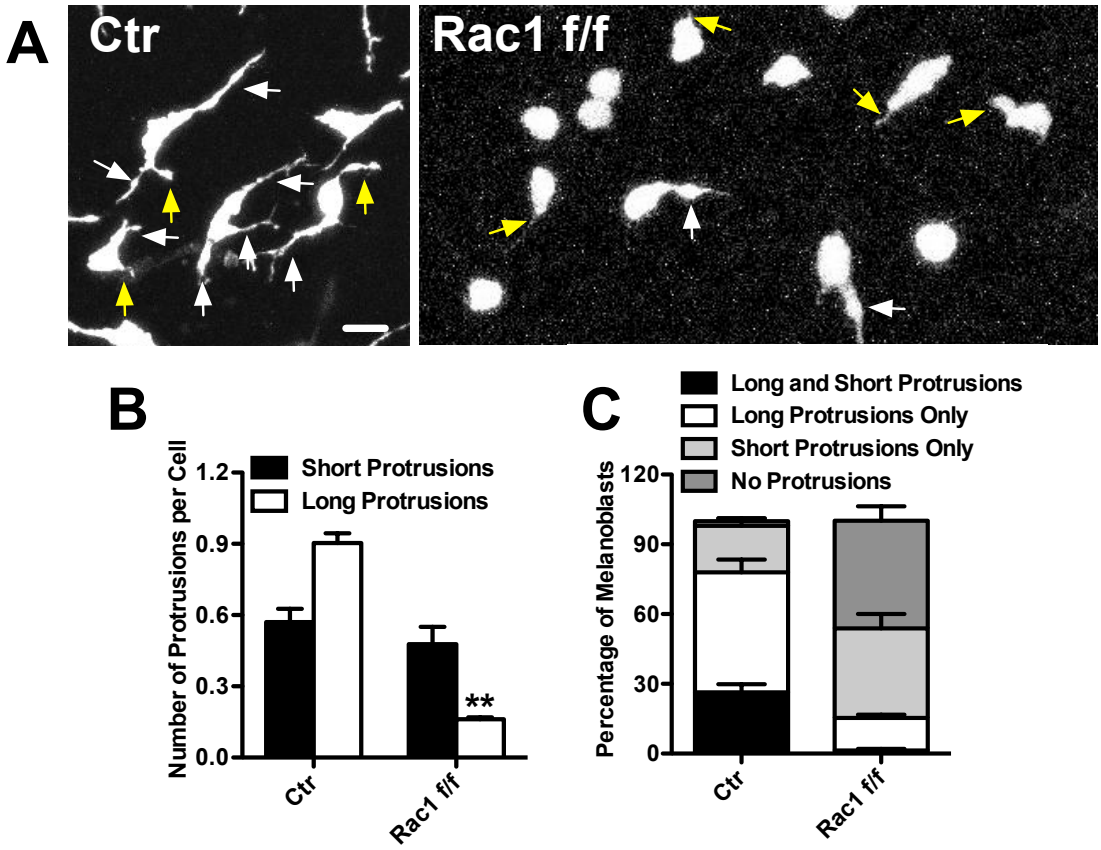

Figure 4.12. Loss of Rac1 in melanoblasts reduces the number of long protrusions. (A) Combined Z-stack images (1µm depth) of melanoblasts in skin explants from Z/EG$^{+/o}$ Tyr::Cre$^{+/o}$ and Z/EG$^{+/o}$ Rac1 f/f Tyr::Cre$^{+/o}$ embryos. Long protrusions and short protrusions are white and yellow arrowed respectively. (B) Number of long/short protrusions per melanoblast n>60 cells per explant >= 3 explants per genotype. (C) Proportion of melanoblasts with long/short protrusions. Error bars indicate Mean ± SEM. **, P< 0.01, by t-test. Scale bar is 10µm.

long-lived, with an average lifetime of 1h (Figure 4.13A and B). The protrusions in Rac1 depleted cells were much shorter-lived (Figure 4.13A and B) and the rate at which Rac1 depleted cells initiated long protrusions was nearly 3-fold decreased (Figure 4.13C, Movie 6). In contrast to *Drosophila* embryos or mouse AVE cells where Rac1 was required for movement (Migeotte et al., 2010; Murphy and Montell, 1996) around 90% of Rac1 depleted melanoblasts migrated despite having only short stubs (Figure 4.14B), although the average speed was around 50% slower than controls (Figures 4.14A, C and Movie 6). The formation of short stubs was always followed directly by the translocation of the cell body in Rac1 null melanoblasts, unlike in controls where short stubs elongated into long pseudopods and cells frequently changed direction, making them less persistent than Rac1 null cells (Figures 4.14D and Movies 6). Thus Rac1 null cells were impaired in long pseudopod generation leading to a reduction in speed and protrusion lifetime. Rac1 loss also decreased the frequency of protrusion initiation, indicating a role for Rac1 as an initiator and potentiator of protrusion.

4.3.4 The actin dynamics of Rac1 knockout melanoblasts migrate in embryo epidermis

Short stub protrusion formation occurred completely independently of Rac1 (Figure 4.13 B, C). To distinguish short protrusions from blebs, we created a conditional Lifeact expressing mouse where we could monitor F-actin dynamics specifically in melanoblasts ex-vivo. Blebs arise by a dissociation between the cell cortex and plasma membrane, followed by a gradual recruitment of actin and myosin and bleb retraction (Charras and Paluch, 2008). Live time-lapse video of melanoblasts expressing lifeact driven by Tyr::Cre expression revealed bright flashes of F-actin near the
tips and in the bodies of both long and short protrusions (Figure 4.15A yellow arrows and Movies 7). In contrast, when we added 50μM LY294002, a PI-3-kinase inhibitor, to skin explants, we induced blebbing, which could be followed with the lifeact probe (Figure 4.15A and Movie 7). Blebs were clearly

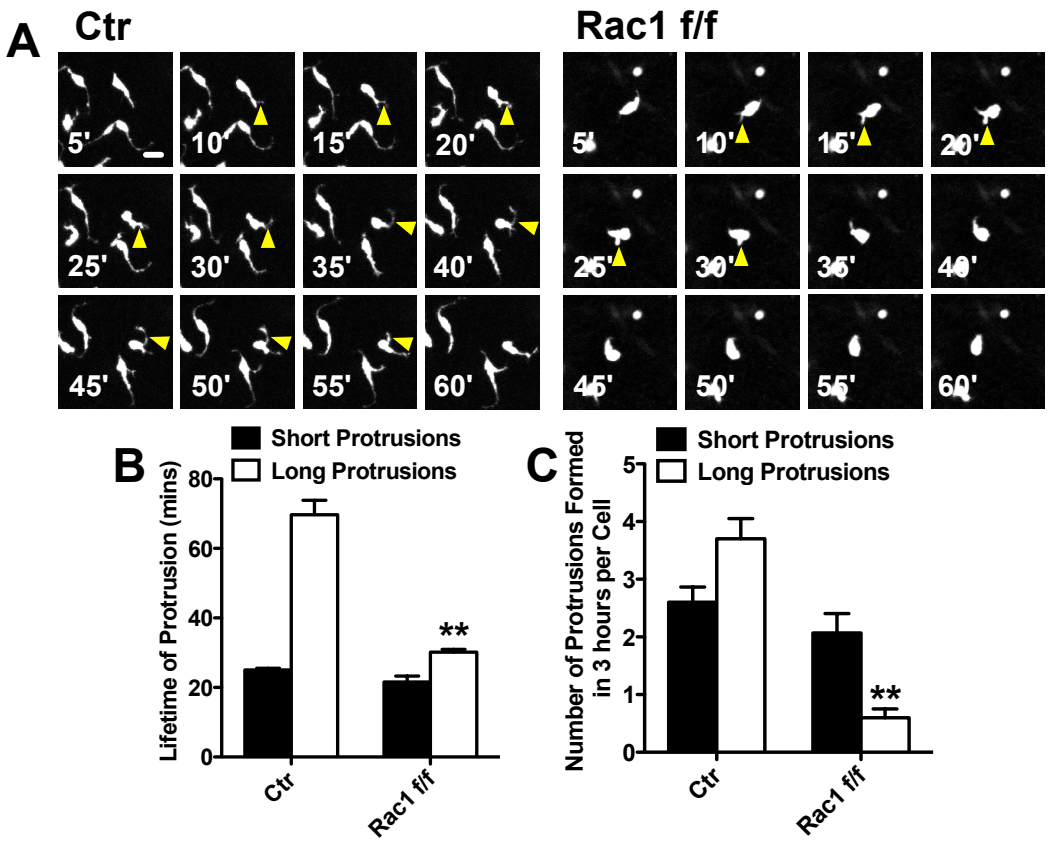

Figure 4.13. Loss of Rac1 in melanoblasts reduces lifetime and frequency of long protrusions. (A) Live cell imaging of protrusion dynamics in explants. Images captured every 5 min, yellow arrows - protrusions. (B) Lifetime of actively growing short/long protrusions formed in 20 cells per explant from >= 3 explants. (C) Frequency of short and long protrusion formation. Error bars indicate Mean ± SEM. **, P< 0.01, by t-test. Scale bar is 10μm.

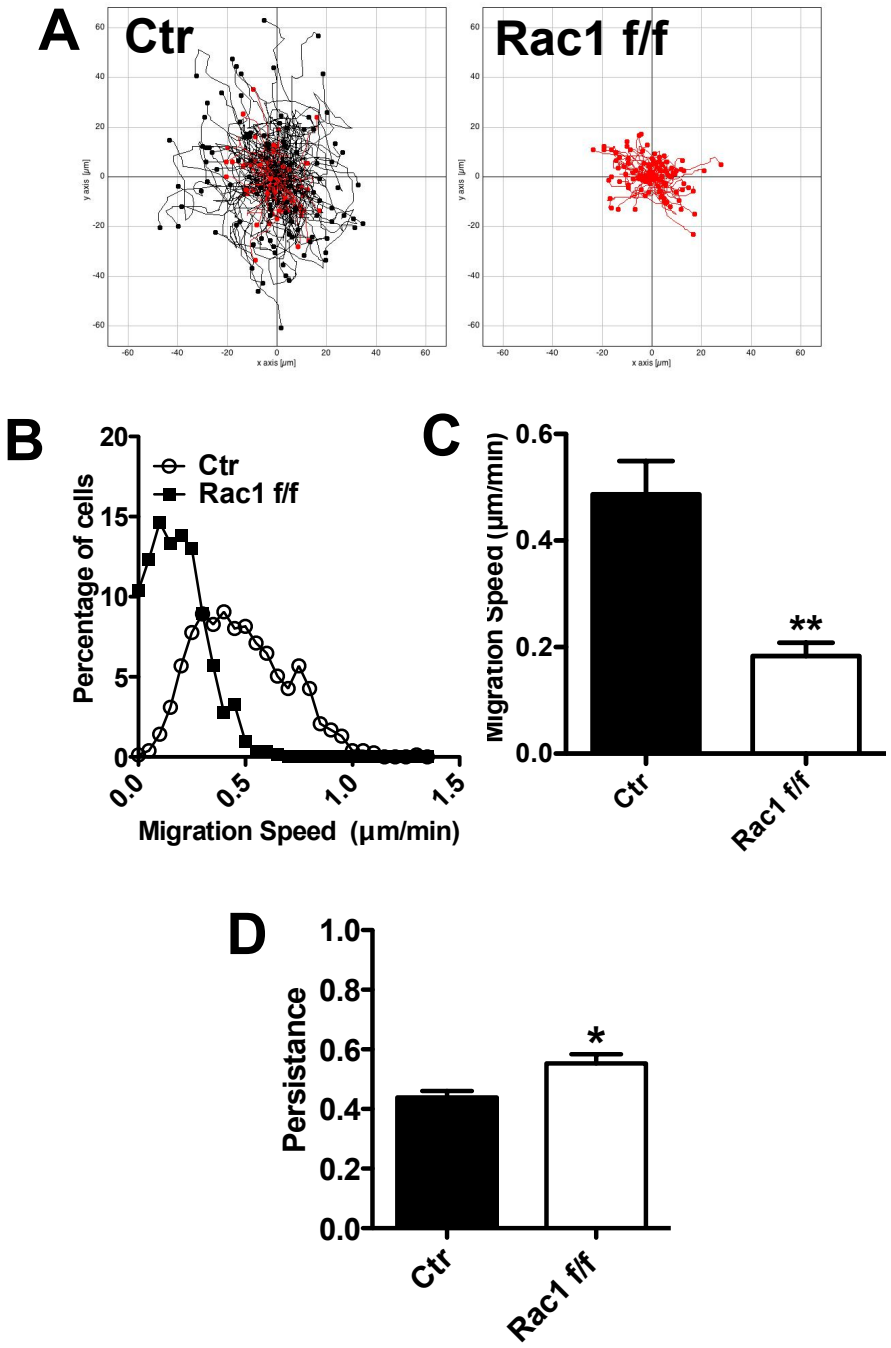

Figure 4.14. Loss of Rac1 in melanoblasts decreases the migration speed but increases in persistence (A) 3 hr tracks of individual melanoblast migration in skin explants, black tracks indicated migrated faster than average control, red indicates slower. (B) Speed distribution. >300 melanoblasts from three explants were randomly selected and mean migration speed over 3hr was plotted according to frequency in the population. (C) Migration speed. (D) Persistance. Error bars indicate Mean ± SEM. **, P< 0.01. *, P< 0.05 by t-test.

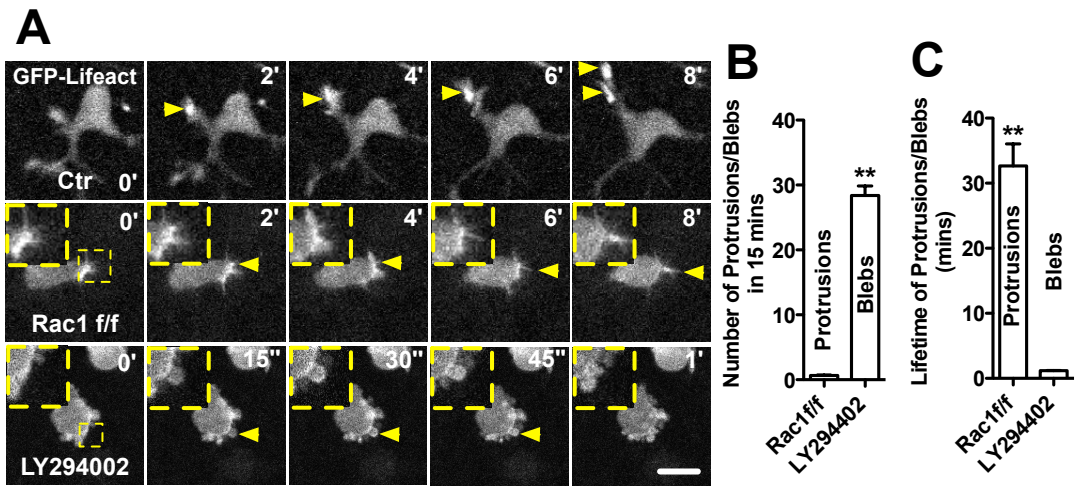

Figure 4.15. The actin dynamics of control and Rac1 depleted melanoblasts in E15.5 skin explants. (A) Live cell imaging of F-actin dynamics in GFP- Lifeact f/f Tyr::Cre+/o control or GFP-Lifeact f/f Rac1 f/f Tyr::Cre+/o explants or control explant treated with 50μM Ly294002. Yellow arrows - protrusions/blebs. (B) Frequency of blebs and short protrusions (C) Lifetime of blebs and protrusions. Error bars indicate Mean ± SEM. **, P< 0.01, by t-test. Scale bars are 10μm.

distinct in shape, as short stubs in Rac1 null melanoblasts often included spiky protrusions (Figure 4.15A, yellow arrows, Movie 7). They also had distinct actin distribution; Actin accumulated at the neck region (Figure 4.15A, 15") and then later as they began to retract actin accumulated near the periphery of blebs (Figure 4.15A, 30"), while it was distributed throughout short protrusions (Figure 4.15A and Movie 7). Furthermore blebs occurred with high frequency (Figure 4.15B) and were much shorter-lived than short protrusions (Figure 4.15C). Thus Rac1 null cells were impaired in long but not short pseudopod generation leading to a reduction in speed and protrusion lifetime. Rac1 loss also decreased the frequency of long but not short protrusion initiation, indicating a role for Rac1 as an initiator and potentiator of long protrusions that drive migration. Short stub protrusions are distinct from classical blebs and thus emerge as a novel Rac1-independent form of actin-based pseudopod. In addition, protusions formed by Rac1 depleted melanoblasts also contain tubulin rich core (Figure 4.16), indicated that tubulin orientation is not affected by Rac1 deletion.

4.3.5 Rac1 contributes to focal adhesion formation in vitro, but is not required for melanoblast contact with the basement membrane in vivo.

It was unclear whether melanoblasts in skin required Rac1 for long protrusions because of the environment of the skin or because melanoblasts are somehow different from fibroblasts, which require Rac1 for wide fan-shaped lamellipodia in culture (Delorme et al., 2007; Guo et al., 2006; Vidali et al., 2006). Cultured immortalized primary melanocytes from 1-day pups were examined using conditional inducible Rac1 deletion. Rac1 deletion was induced with tamoxifen analog 4-hydroxytamoxifen (OHT), using Tyr::CreERT2$^{+/o}$ Ink4a-Arf$^{-/-}$ Rac1 f/f melanocytes plated on fibronectin (Ackermann et al., 2005; Serrano et al., 1996). Anti-DCT staining confirmed that our cultures were nearly purely melanocytes (Figure 4.17A) and Rac1 was lost during 4 days of OHT treatment (Figure 4.17B and 4.18A) without

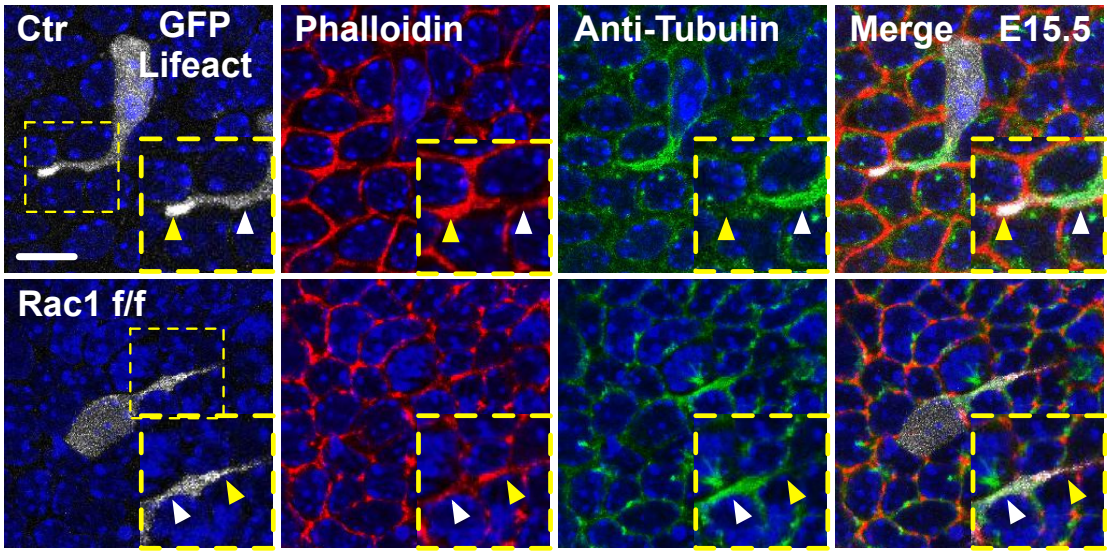

Figure 4.16. The actin and tubulin localization is not affected by Rac1 depletion in melanoblasts. Combined Z-stack image (1µm depth) of E15.5 GFP-Lifeact f/f Tyr::Cre $^{+/o}$ control embryo stained with phalloidin, anti-tubulin and DAPI. Insets show distal tips (yellow arrowed) and tubulin riched core (white arrowed). (B) Sections from E15.5 control and Rac1 f/f Tyr::Cre$^{+/o}$ embryo stained with anti-Rac1-GTP, anti-DCT and DAPI. All scale bars are 10µm.

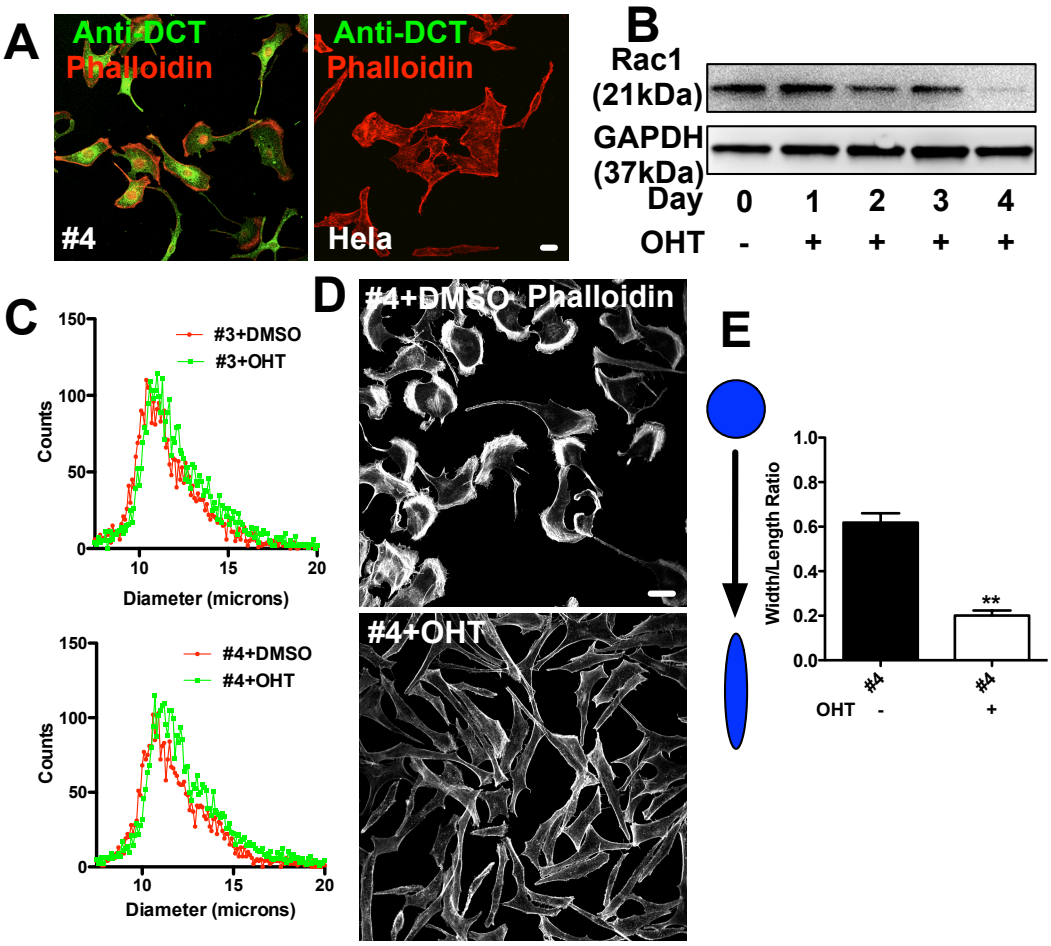

Figure 4.17. Induced Rac1 deletion affects melanocytes morphology. (A) Rac1 f/f Tyr::CreERT2$^{+/o}$ Ink4a-Arf$^{-/-}$ primary melanocyte cells (clone#4) on fibronectin coated glass coverslips were fixed and stained with rhodamine phalloidin and anti-DCT to confirm the purity of melanocytes. Hela human cervical cancer cells were used as negative control for DCT antibody. (B) Immunoblots of cell lysates extracted from OHT treated Rac1 f/f Tyr::CreERT2$^{+/o}$ Ink4a-Arf$^{-/-}$ primary melanocyte cells (#4) as indicated were probed with antibody against Rac1 and GAPDH (loading control), which showed deletion of Rac1 after 4 days. (C) DMSO or OHT treated Rac1 f/f Tyr::CreERT2$^{+/o}$ Ink4a-Arf$^{-/-}$ primary melanocyte cells (#3 and #4) on dished were trypsined and subjected to cell size analysis using CASY Cell Counter according to manufacture's instruction. (D) DMSO or OHT treated Rac1 f/f Tyr::CreERT2$^{+/o}$ Ink4a-Arf$^{-/-}$ primary melanocyte cells (#4) on fibronectin coated glass coverslips were fixed and stained with rhodamine phalloidin. (E) Qantification of cell body width/length ratio. Error bars indicate Mean ± SEM from 50 cells **, P< 0.01. by t-test. All scale bars are 10μm.

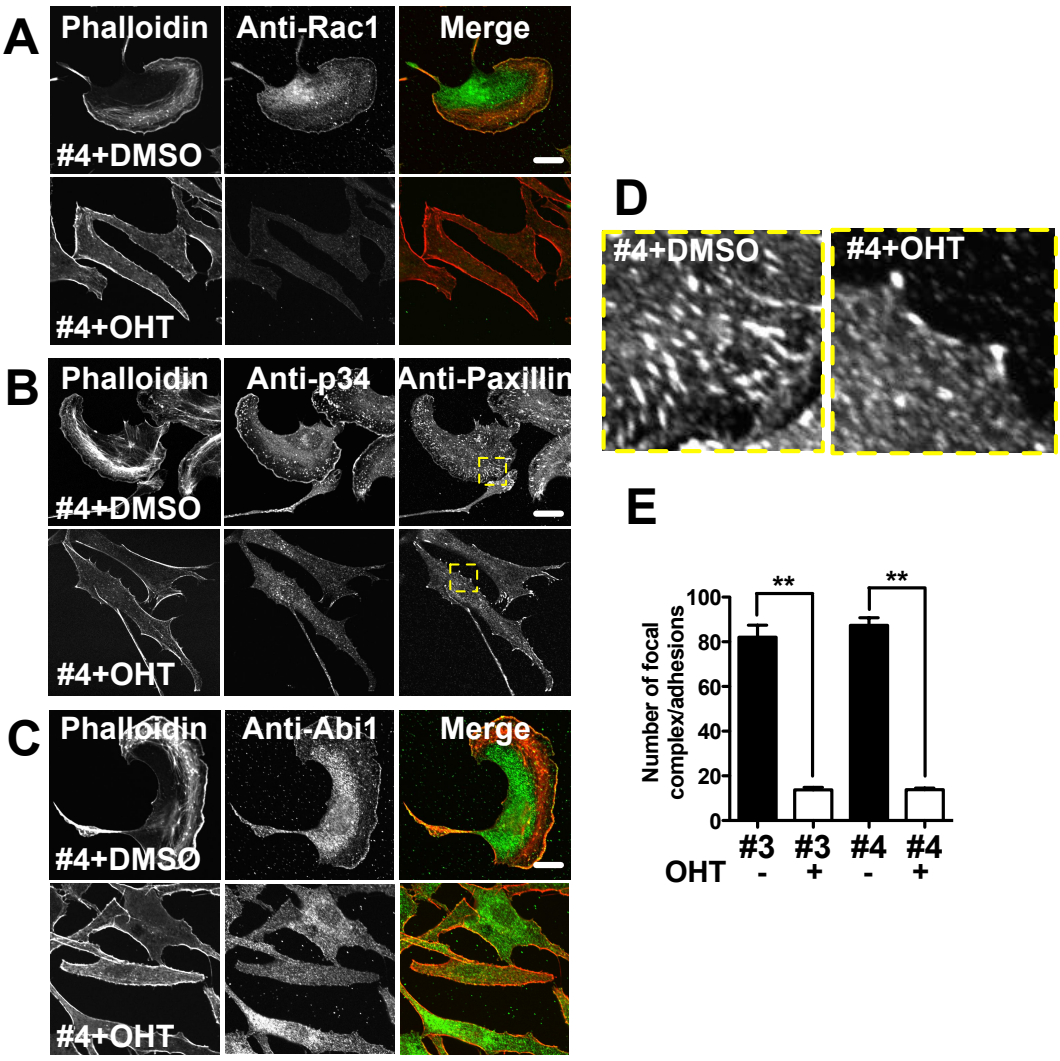

Figure 4.18. Rac1 controls lamellipodia and stress fiber formation, focal adhesion density in primary mouse melanocytes. (A) DMSO or OHT treated Rac1 f/f Tyr::CreERT2$^{+/o}$ Ink4a-Arf$^{-/-}$ primary melanocyte cells (#4) on fibronectin coated glass coverslips were fixed and stained with rhodamine phalloidin and anti-Rac1 as indicated. (B) DMSO or OHT treated Rac1 f/f Tyr::CreERT2$^{+/o}$ Ink4a-Arf$^{-/-}$ primary melanocyte cells (#4) on fibronectin coated glass coverslips were fixed and stained with rhodamine phalloidin, anti-p34 and anti-paxillin as indicated. (C) DMSO or OHT treated Rac1 f/f Tyr::CreERT2$^{+/o}$ Ink4a-Arf$^{-/-}$ primary melanocyte cells (#4) on fibronectin coated glass coverslips were fixed and stained with rhodamine phalloidin and anti-Abi1 as indicated. (D) Enlarged picture of focal adhesion (anti-paxillin) from inserts of figure B. (E) Number of focal adhesions in two independent primary melanocyte cell lines. More than 50 cells were scored per experiment and experiments repeated three times. All error bars indicate Mean ± SEM. **, P< 0.01 by t-test. All scale bars are 10μm.

affecting the size of melanocytes (Figure 4.17C). DMSO treated control melanocytes continuously formed lamellipodia during migration (Figure 4.17D and Movie 8) and Arp2/3 complex and Scar/WAVE complex strongly localized to lamellipodia protrusions (Figures 4.18B and C). In contrast, Rac1-deleted melanocytes displayed elongated cell morphology that lacked lamellipodia (Figures 4.17D, E and 4.18). Expression levels of WAVE complex (WAVE1, WAVE2 and Nap1) and Arp2/3 complex (p34) remained unchanged in OHT treated melanocytes (Figure 4.19). No upregulation of other Rac family members (Rac2 and Rac3) (Figure 4.19A) and no alteration of activity of Cdc42 and RhoA were observed (Figure 4.20). Rac1 depleted cells failed to form any lamellipodia during migration with absence Arp2/3 or WAVE complex localization at the periphery (Figure 4.18B, C and Movie 8), they also had fewer focal complex/adhesions (Figure 4.18B, D and E), but expression of paxillin, vinculin and β1-integrin was unchanged (Figure 4.19A). Migration was severely impaired following Rac1 loss (Figure 4.21). However, in vivo the same number of control and Rac1 deleted melanoblasts contacted the basement membrane (BM) at E15.5 (Figures 4.22) indicating that the ability to recognize and contact this structure is intact (Figure 4.22). Furthermore, expression levels of E-cadherin and ZO-1 (Figure 4.19A) and surface expression of E-cadherin were normal in cultured Rac1 depleted melanocytes (Figure 4.19B). Thus, loss of Rac1 in cultured melanocytes parallels observations in fibroblasts that lamellipodia and focal adhesions are affected (Guo et al., 2006), but Rac1 depleted melanoblasts can still position themselves relative to the basement membrane in vivo. The specific nature of Rac1 involvement in adhesion in vivo requires further study, as these interactions are complex.

4.3.6 Melanoblasts migrate individually in developing skin using a novel form of long protrusion based on microtubules and Arp2/3 complex

We further analysed the motility of melanoblasts in live skin explants to

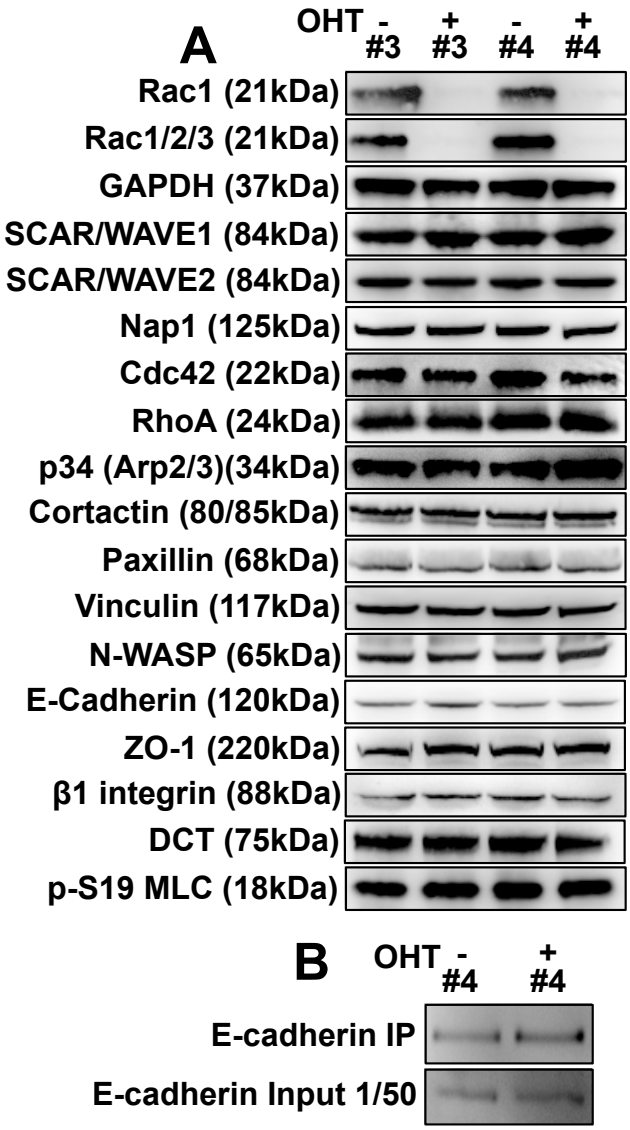

Figure 4.19. Levels of various cytoskeletal proteins in melanocytes or skin explants following loss of Rac1 or treatment with inhibitors. (A) Cell lysates from two independent Rac1 f/f Tyr::CreERT2$^{+/o}$ Ink4a-Arf$^{-/-}$ primary melanocyte cell lines (#3 and #4) treated with DMSO or OHT were separated by SDS-PAGE, transferred to PVDF membranes and probed with antibodies as indicated. (B) Cell surface protein from Rac1 f/f Tyr::CreERT2$^{+/o}$ Ink4a-Arf$^{-/-}$ primary melanocyte cell lines (#4) treated with DMSO or OHT were biotinylated for 15 mins on ice. Surface E-cadherin and total E-cadherin were probed with E-cadherin antibody.

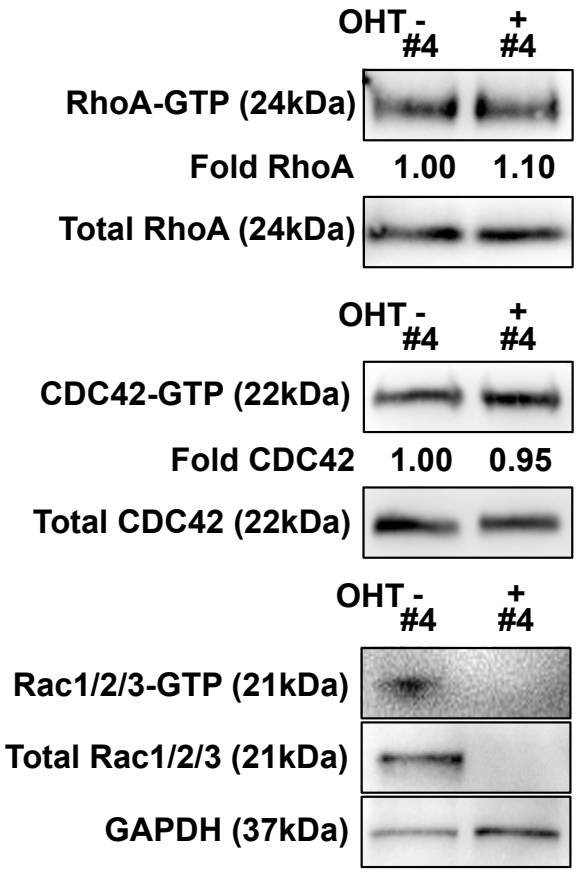

Figure 4.20. Rac1 depletion in mouse primary melanocyte had not effect on level of active RhoA and Cdc42. Relative levels of active GTP-bound RhoA, Cdc42 and Rac from primary melanocyte cell line (#4) treated with DMSO or OHT were measured by use of Rhotekin (for RhoA) or Pak1-PBD (for Cdc42 and Rac) domain. Relative levels were quantified and the relative intensity of active Rho GTPase (GTP bound) signal was normalised to total Rho GTPase. The results shown are the means of three independent experiments.

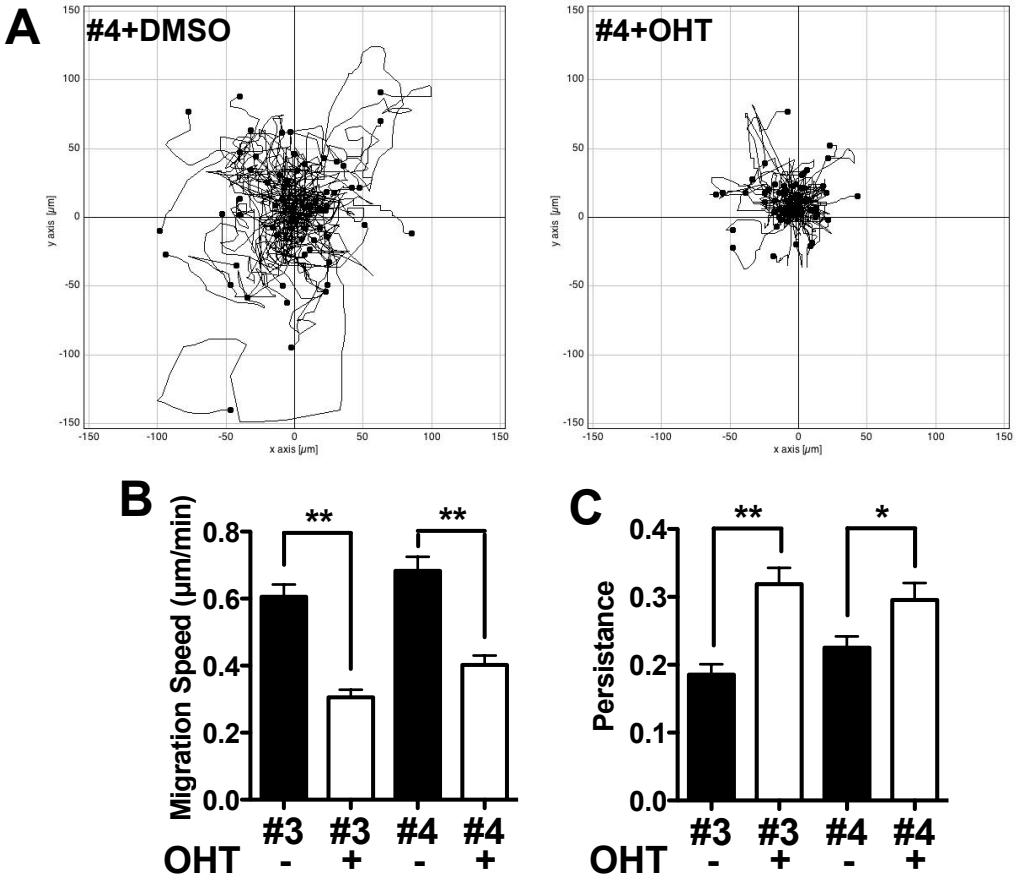

Figure 4.21. Rac1 controls migration speed in primary mouse melanocytes. (A) 10 hr tracks of individual melanocytes (#4) treated with DMSO or OHT migrate on fibronectin coated dish. (B) Random migration speed and (C) Persistance of two independent Rac1 f/f Tyr::CreERT2$^{+/o}$ Ink4a-Arf$^{-/-}$ primary melanocyte cell lines (#3 and #4) on fibronectin coated glass bottomed dish treated with DMSO or OHT. More than 50 cells were scored per experiment and experiments repeated three times. All error bars indicate Mean ± SEM. **, P< 0.01, *, P< 0.05 by t-test.

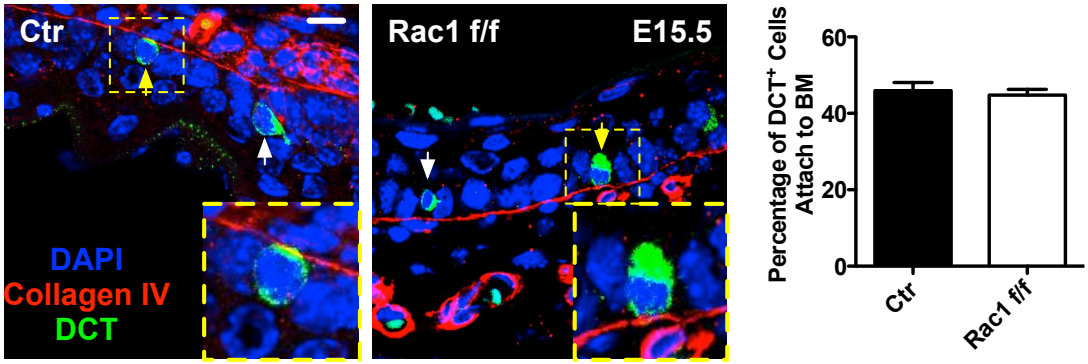

Figure 4.22. Rac1 knockout does not affect the proportion of melanoblasts contacting the basement membrane Representative combined Z-stack images (1µm depth) of sections from E15.5 control and Rac1 f/f Tyr::Cre$^{+/o}$ embryos stained for Collagen IV to visualize basement membrane, DCT (melanoblasts) and DAPI (DNA). Melanoblasts contacting the basement membrane were yellow arrowed, which those contacting the basement membrane were white arrowed. Percentage of melanoblasts attached to the basement membrane in control and Rac1 f/f Tyr::Cre$^{+/o}$ embryos. More than 200 cells were examined per embryo from at least three embryos for each genotype.

understand more about the molecular mechanism of movement within the keratinocyte layer. Inhibition of actin polymerization (latrunculin A) or tubulin polymerization (nocodazole) nearly completely stopped migration (Figure 4.23 and 4.24 and Movie 9). Microtubule stabilization with taxol slowed migration (Figure 4.24 and Movie 9). In addition, latrunculin A severely inhibited formation in both long and short stub protrusions, whereas nocodazole or taxol only inhibited formation of long protrusions (Figures 4.23 and 4.24 and Movie 9). Long protrusions formed by melanoblasts in skin are thus fundamentally different from lamellipodia, in that microtubule dynamics are required for normal protrusion extension and subsequent cell translocation (Ballestrem et al., 2000; Verkhovsky et al., 1999). However, the mechanism by which microtubules act is likely to be complex, as previous studies showed that microtubules sequester RhoGEFs, such as GEFH1 and their depolymerization can alter Rho activity and contractility in cells (Redd et al., 2006; Takesono et al., 2010; Zhou et al., 2010). We therefore tested whether inhibiting myosin-II mediated contractility in nocodazole treated melanoblasts could compensate for a possible increase in Rho activity caused by microtubule depolymerization. Indeed, the Rho-kinase inhibitor Y27632 restored the formation of protrusions in melanoblasts in nocodazole treated explants and cells cultured in vitro back to the levels seen in wild-type cells but did not restore the migration speed (Figures 4.24 and Movie 9). Furthermore, long protrusions formed in the presence of Y27632 and nocodazole were devoid of visible microtubules (Figure 4.24G) indicating that microtubules do not perform an essential structural role in long protrusions. Together, these data indicate that actin and tubulin dynamics are very important for melanoblast migration in epidermis, and that microtubule depolymerization may trigger RhoA activation in melanoblasts in vivo.

Myosin-II mediated contraction is important for cell body translocation, but not for Rac1 mediated lamellipodia assembly in cultured cells (Ponti et al., 2004; Vidali et al., 2006). We investigated the role of myosin-II in melanoblast migration and long protrusion formation using ROCK (Y27632) or myosin II inhibitor (Blebbistatin). At the concentrations we used, Y27632 treated skin

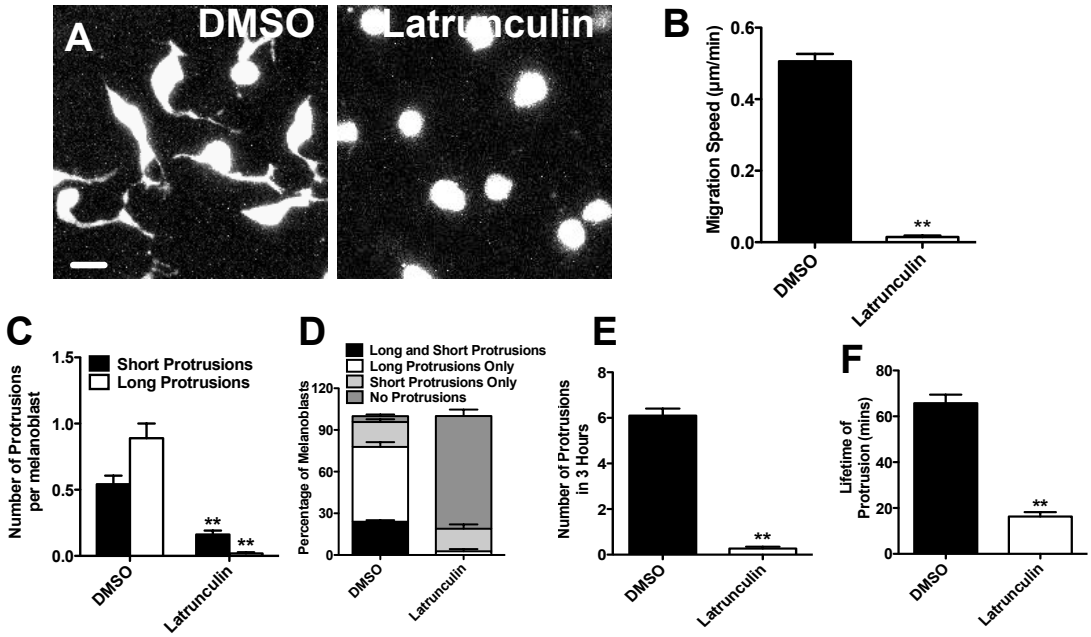

Figure 4.23. Melanoblast migration and protrusions are regulated by actin.

(A) Combined Z-stack images (1µm depth) of Z/EG$^{+/o}$ Tyr::Cre$^{+/o}$ melanoblasts in skin explants treated with inhibitor as indicated. (B) Migration speed. (C) Number of long and short protrusions per melanoblast for > 60 cells per explant from >= 3 explants per genotype. (D) Proportion of melanoblasts with short or long protrusions. (E) Lifetime of actively growing protrusions. (F) Frequency of protrusions formed in 20 cells per explant from >= three explants per condition. Error bars indicate Mean ± SEM. **, P< 0.01. *, P<0.05 by t-test. Scale bar 10µm.

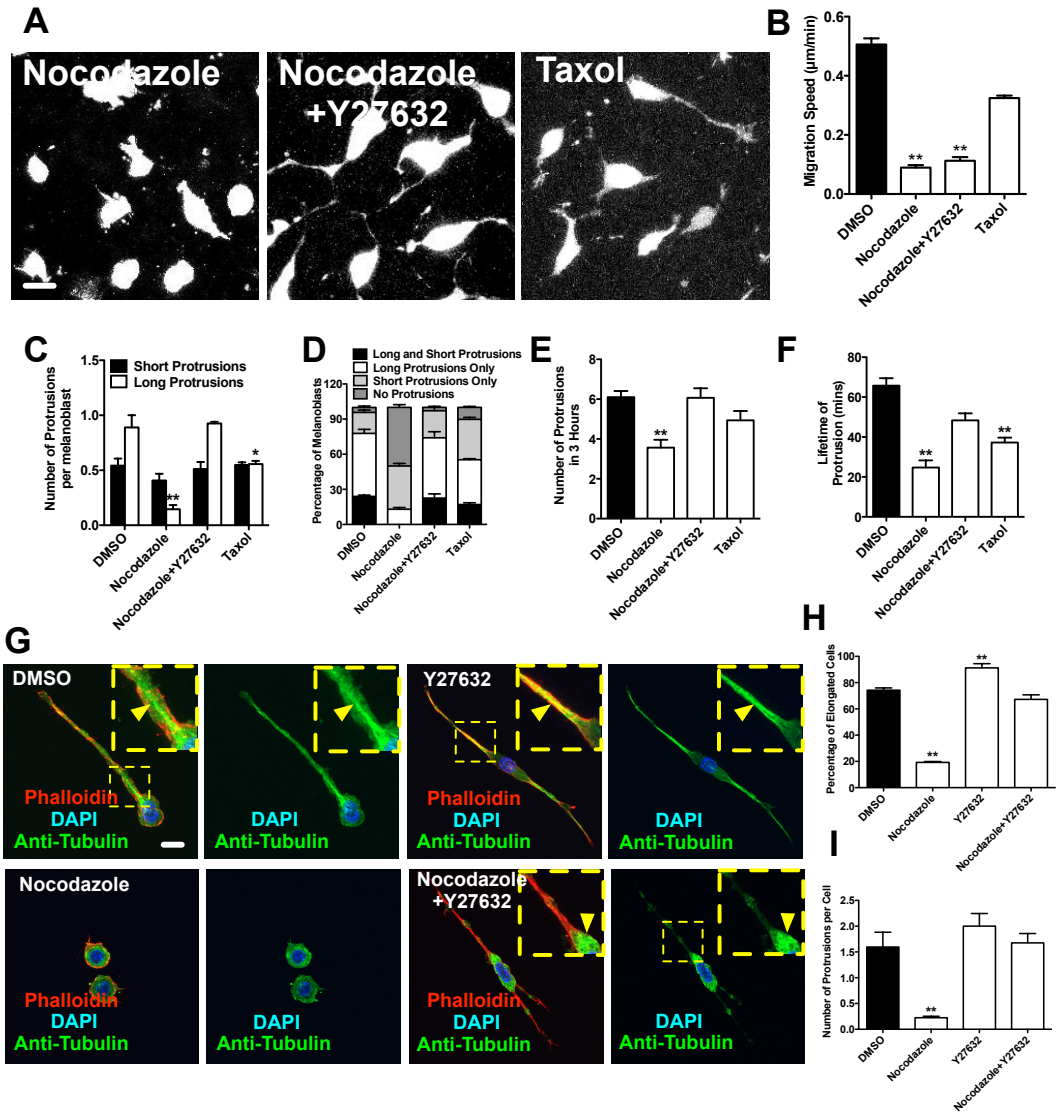

Figure 4.24. Melanoblast migration and protrusions are regulated by microtubules

(A) Combined Z-stack images (1μm depth) of Z/EG$^{+/o}$ Tyr::Cre$^{+/o}$ melanoblasts in skin explants treated with inhibitor as indicated. (B) Migration speed. (C) Number of long and short protrusions per melanoblast for > 60 cells per explant from >= 3 explants per genotype. (D) Proportion of melanoblasts with short or long protrusions. (E) Lifetime of actively growing protrusions. (F) Frequency of protrusions formed in 20 cells per explant from >= three explants per condition. (G) Rac1 f/f Tyr::CreERT2+/o Ink4a-Arf-/- (#4) primary melanocytes treated with DMSO or Y27632 or nocodazole or both Y27632 and nocodazole were plated on 3D collagen I matrix. Cells were stained with rhodamine phalloidin, anti-tubulin and DAPI. Yellow arrows indicate accumulation of tubulin in protruions (for DMSO and Y27632) or in cell body (Y27632+nocodazole). (H) % cells with elongated morphology and (I) Number of protrusions per cell for >300 cells x 3 repeats. Error bars indicate Mean ± SEM. **, P< 0.01, *, P< 0.05 by t-test. Scale bar 10μm.

explants exhibited a reduction in myosin light chain phosphorylation (Figure 4.25A) without any obvious change in keratinocyte actin structure or tissue integrity (Figure 4.25B). Both Y27632 and Blebbistatin caused a near halt in melanoblast migration (Figures 4.25D), but a significant increase in the number of both short stubs and long apparently thinner protrusions (Figures 4.25C, E, F and Movie 9). Protrusion formation occurred with the same frequency as in controls (Figure 4.25G) but protrusions were about 2-fold longer lived (Figure 4.25H). Thus, myosin II activity is not required for the initiation of protrusions but is important for the retraction dynamics of protrusions and for melanoblast translocation among keratinocytes in epidermis.

To test whether high contractility in Rac1 depleted melanoblasts might be inhibiting protrusion formation, we inhibited Rho-kinase with Y27632. These cells showed even slower migration than untreated Rac1 depleted or Y27632 treated control explants (Figure 4.25D, Movie 9), but they displayed a similar number of long protrusions to control cells with Rac1 (Figure 4.25C, D and E). These protrusions were around 2-fold longer-lived than controls (Figure 5E). Cell migration was mostly halted (Figure 4.25H, Movie 9). Importantly, long protrusions in Rac1 depleted cells formed with a 3-fold lower frequency than controls, regardless of myosin inhibition (Figure 4.25G, Movie 9) and inhibiting myosin didn't increase the frequency of protrusion formation in normal melanoblasts (Figure 4.25G). We also did not see any obvious difference in myosin light chain phosphorylation between normal and Rac1 null melanocytes *in vitro* (Figure 4.19A). Thus, Rac and myosin are not apparently opposing each other, but rather when Rac is active, myosin-based contractility mediates protrusion retraction and enables long protrusions to generate force for movement. When Rac is not present, long protrusions rarely form and if they do form, they are weaker and less resistant to contractile forces. Thus Rac controls the rate of protrusion formation and myosin controls contractility that mediates retraction as well as generating pulling and squeezing forces for motility.

Pak kinases have been implicated in motility downstream of Rac1 (Edwards

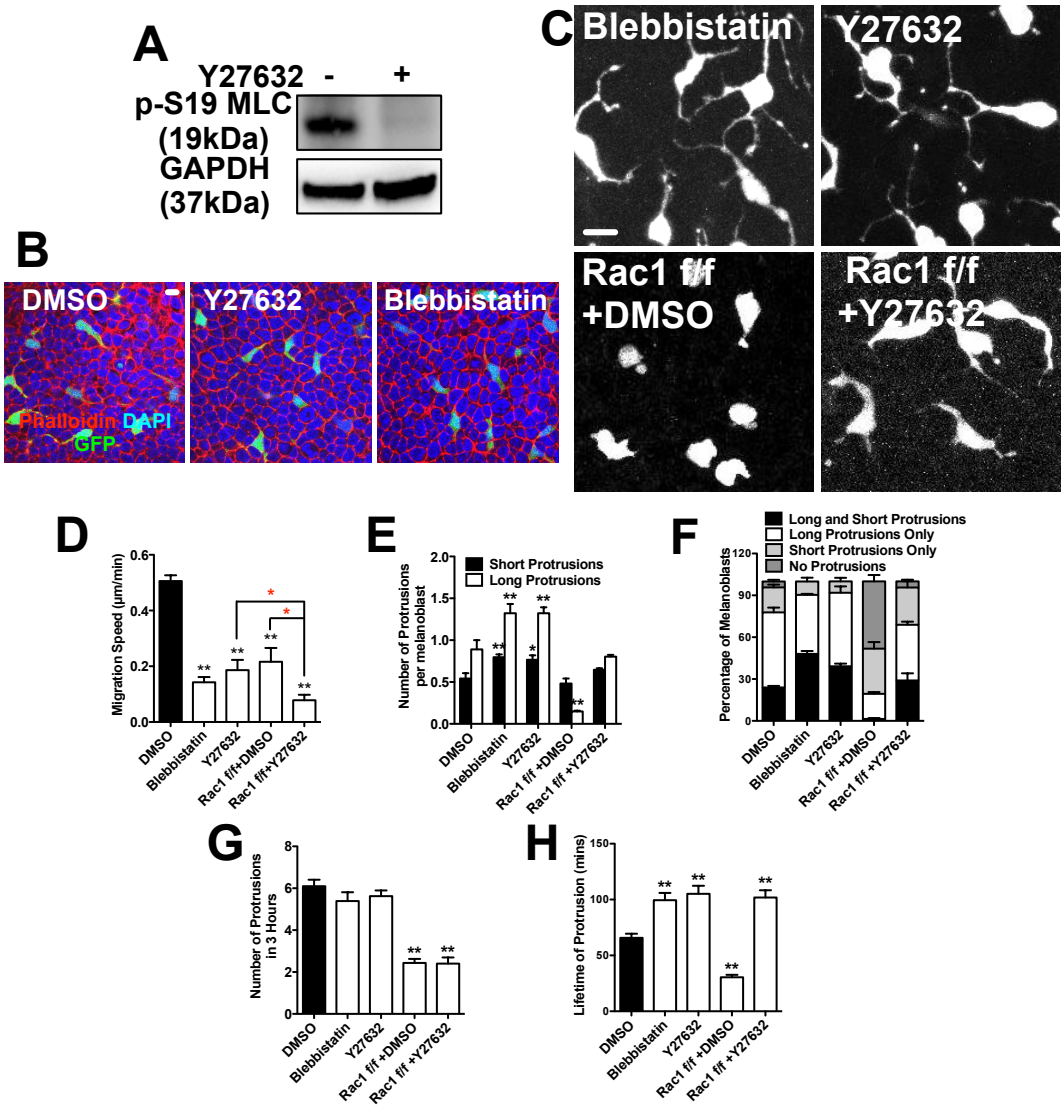

Figure 4.25. Melanoblast migration and protrusions are regulated myosin (A) Western blots of lysates extracted from skin explants treated with either DMSO or drug as indicated. Blots were then probed with antibody as indicated. (B) Confocal images of E15.5 epidermis from Z/EG$^{+/o}$ Tyr::Cre$^{+/o}$ explants treated with drugs as indicated for 5 hr. the explants were fixed and stained with rhodamine phalloidin and DAPI. (C) Combined Z-stack images (1μm depth) of Z/EG$^{+/o}$ Tyr::Cre$^{+/o}$ control or Z/EG$^{+/o}$ Rac1 f/f Tyr::Cre$^{+/o}$ (Rac1 f/f) melanoblasts in skin explants treated with inhibitor as indicated. (D) Migration speed. (E) Number of long and short protrusions per melanoblast for > 60 cells per explant from >= 3 explants per genotype. (F) Proportion of melanoblasts with short or long protrusions. (G) Frequency of protrusions formed in 20 cells per explant from >= three explants per condition. (H) Lifetime of actively growing protrusions. Error bars indicate Mean ± SEM. **, P< 0.01. *, P<0.05 by t-test. Scale bar 10μm.

et al., 1999; Smith et al., 2008; Yang et al., 1998), so we explored the role of the conventional PAKs 1-3 (group I Paks) and their downstream targets in migration. Treatment of skin explants with Pak inhibitor (IPA-3) (Deacon et al., 2008) and its downstream targets LIM kinase (LIMKi) (Scott et al., 2010) and ERK (U0126, a MEK1/2 inhibitor that inhibits ERK1/2 activation) showed no effect on melanobast motility despite reducing phosphorylation of their targets in skin explants (Figure 4.26, Movie 9 and data not shown). In addition, siRNA knockdown of Pak2, the only group I Pak isoform expressed in melanocytes (Figures 4.27A and B), did not change melanocyte morphology on 3D collagen I matrix (Figure 4.27C and Movie 10). Furthermore, despite the decrease in Pak2 and ERK phosphorlyation in our melanocyte cell lines (#3 and #4) in vitro (Figure 4.27D), we found no detectable changes in phosphorlylation of LIMK effector cofilin between DMSO and OHT treated melanocytes (Figure 4.27F). Thus, Rac1 regulates melanoblast migration in epidermis and formation of long protrusions through pathways other than Pak or its downstream targets.

The main effector of actin nucleation downstream of Rac is the Scar/WAVE complex; it activates Arp2/3 complex to induce branched actin assembly. Since we could not use a pharmacological inhibitor of Scar/WAVE, RNA interference was used to knock down Arp2/3 complex (p34 siRNA), WAVE complex (Nap1 siRNA) in primary melanocytes *in vitro*. Knockdown of p34 or Nap1, which, for Nap1, also caused significant reduction of expression of other WAVE complex constituents (Figures 4.28A and B), however, caused a dramatic morphological change similar to loss of Rac1 or Arp2/3 complex (Figures 4.28C Movie 10) in 3D. We also investigated the function of Arp2/3 complex in melanoblast migration by treating skin explants with inhibitor against Arp2/3 complex (CK-869) (Nolen et al., 2009). CK-869 reduced melanoblast migration in explants without affect keratinocyte actin organization (Figure 4.29A and C). The control compound CK-312 had no effect (Figure 4.29B-G and Movie 9). In addition, melanoblasts in CK-869 treated explants resembled Rac1 deleted cells with significant reduction in the formation of long but not short stub protrusions (Figures 4.29B, D and E). The frequency of protrusion initiation and lifetime of each protrusion was also

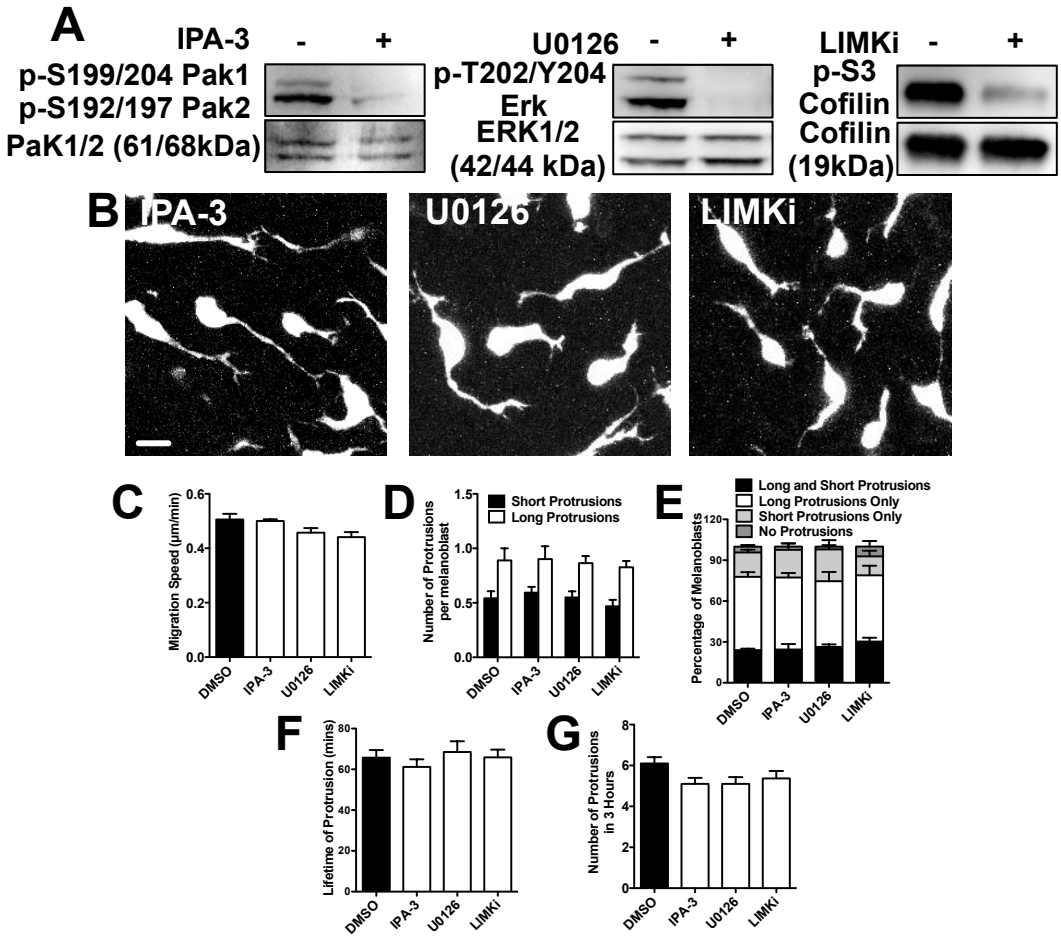

Figure 4.26. PAK signaling is not required for melanoblast migration and formation of protrusions (A) Western blots of lysates extracted from skin explants treated with either DMSO or drug as indicated. Blots were then probed with antibody as indicated. (B) Combined Z-stack images (1μm depth) of Z/EG$^{+/o}$ Tyr::Cre$^{+/o}$ control or Z/EG$^{+/o}$ Rac1 f/f Tyr::Cre$^{+/o}$ (Rac1 f/f) melanoblasts in skin explants treated with inhibitor and/or of genotype as indicated. (C) Migration speed. (D) Number of long and short protrusions per melanoblast for > 60 cells per explant from >= 3 explants per genotype. (E) Proportion of melanoblasts with short or long protrusions. (F) Lifetime of actively growing protrusions. (G) Frequency of protrusions formed in 20 cells per explant from >= three explants per condition. Error bars indicate Mean ± SEM. Scale bar 10μm.

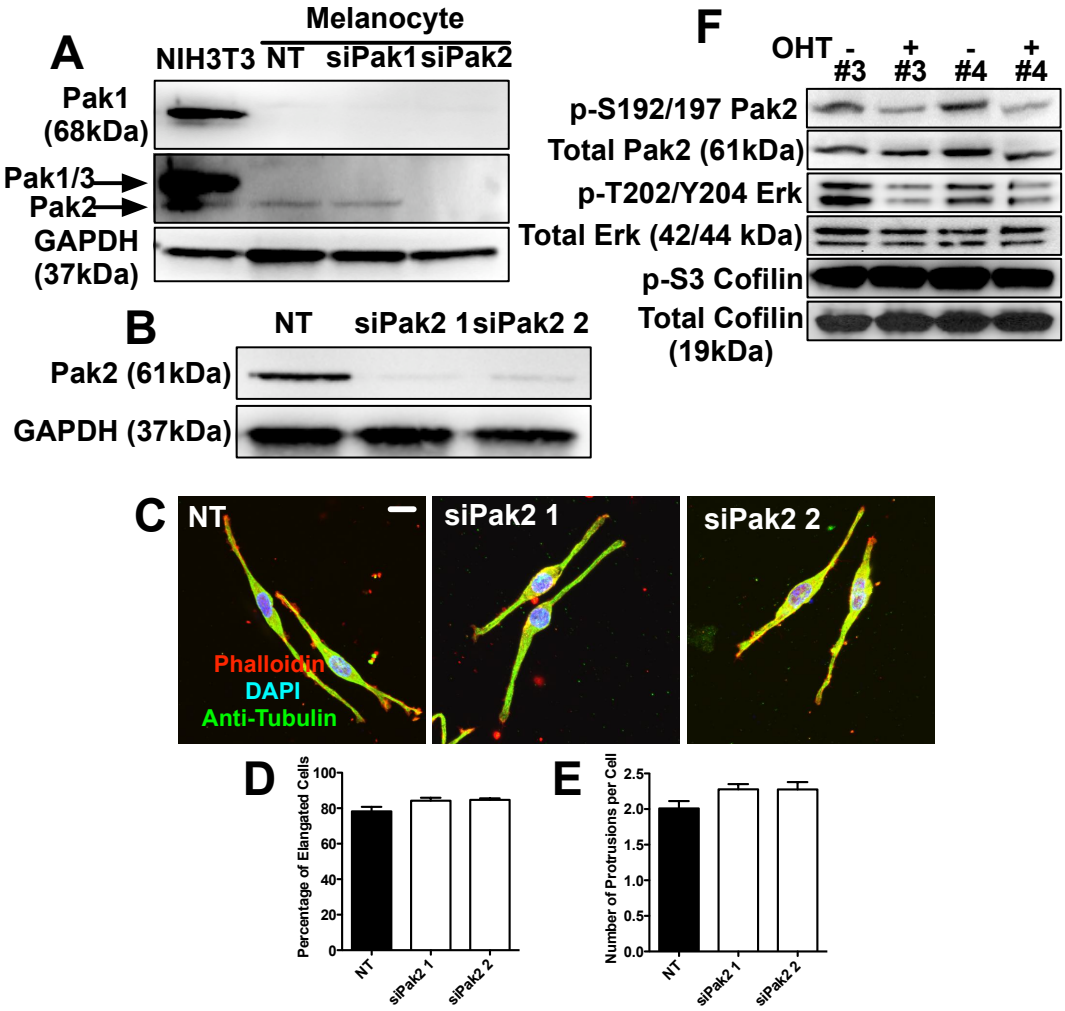

Figure 4.27. Pak2 is not required for formation of long protrusions of primary murine melanocytes (A) Immunoblots of primary mouse melanocytes transfected with NT, Pak1 and Pak2 siRNA. The same blot was probed with anti-Pak1, anti-Pak1/2/3 and anti-GAPDH as loading control. NIH3T3 mouse fibroblast lysate was used as positive control for Pak1. (B) Immunoblots of Pak2 siRNA treated melanoblasts probed with anti-Pak2 and anti-GAPDH as loading. (C) Rac1 f/f Tyr::CreERT2$^{+/o}$ Ink4a-Arf$^{-/-}$ (#4) primary melanocytes treated siRNA as indicated on collagen I, showing actin (phalloidin), microtubules (anti-tubulin) or DNA (DAPI) (D) % cells with elongated morphology and (E) Number of protrusions per cell for >300 cells x 3 repeats. Error bars indicate Mean ± SEM. (F) Cell lysates from two independent Rac1 f/f Tyr::CreERT2$^{+/o}$ Ink4a-Arf$^{-/-}$ primary melanocyte cell lines (#3 and #4) treated with DMSO or OHT were separated by SDS-PAGE, transferred to PVDF membranes and probed with antibodies as indicated. Scale bar 10μm.

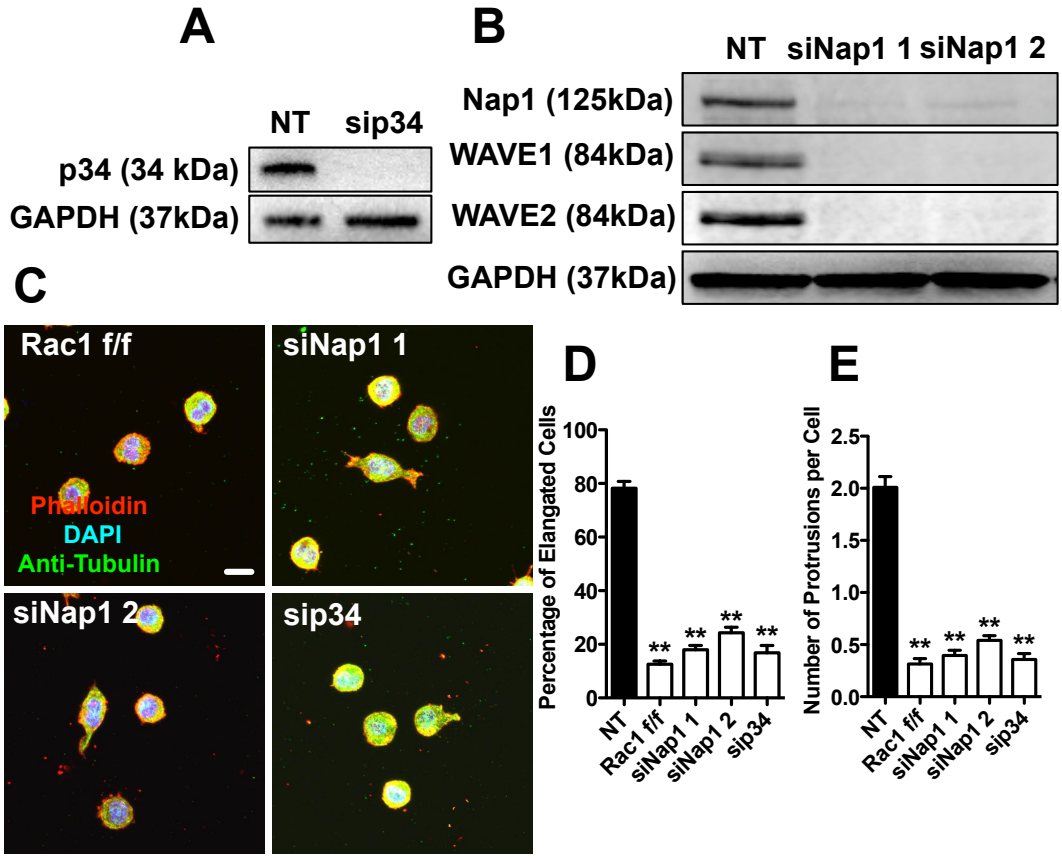

Figure 4.28. Primary murine melanocytes cultured on collagen require the Rac1-WAVE-Arp2/3 pathway for long protrusions. (A) Immunoblots of NT or p34-Arc.siRNA treated melanoblasts probed with p34-Arc and GAPDH antibody. (B) Immunoblots showing knockdown of Nap1 in melanocytes; anti-WAVE1 and anti-WAVE2 show the loss of WAVE complex. GAPDH was probed as loading control. (C) Rac1 f/f Tyr::CreERT2$^{+/o}$ Ink4a-Arf$^{-/-}$ (#4) primary melanocytes treated with OHT or siRNA as indicated on collagen I, showing actin (phalloidin), microtubules (anti-tubulin) or DNA (DAPI) (D) % cells with elongated morphology and (E) Number of protrusions per cell for >300 cells x 3 repeats. Error bars indicate Mean ± SEM. **, P< 0.01 by t-test. Scale bar 10μm.

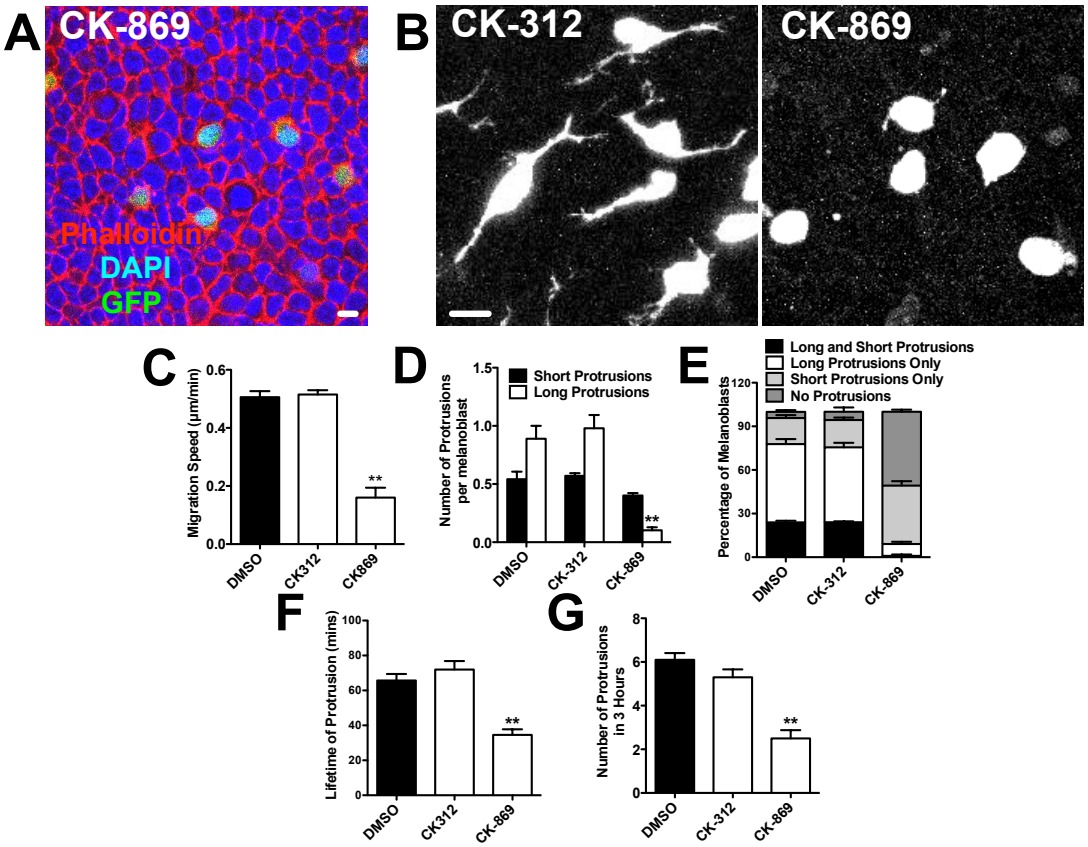

Figure 4.29. Arp2/3 complex is required for melanoblast migration and formation of protrusions (A) Confocal images of E15.5 epidermis from Z/EG$^{+/o}$ Tyr::Cre$^{+/o}$ explants treated with drugs as indicated for 5 hr. the explants were fixed and stained with rhodamine phalloidin and DAPI. (B) Combined Z-stack images (1μm depth) of Z/EG$^{+/o}$ Tyr::Cre$^{+/o}$ melanoblasts in skin explants treated with inhibitor as indicated. (C) Migration speed. (D) Number of long and short protrusions per melanoblast for > 60 cells per explant from >= 3 explants per genotype. (E) Proportion of melanoblasts with short or long protrusions. (F) Lifetime of actively growing protrusions. (G) Frequency of protrusions formed in 20 cells per explant from >= three explants per condition. Error bars indicate Mean ± SEM. **, P< 0.01. Scale bar 10μm.

decreased (Figures 4.29F and G). Surprisingly, this indicates that short stub protrusions form independently of Arp2/3 complex, but that Scar/WAVE and Arp2/3 are the major effectors driving actin dynamics in long protrusions.

In addition to Scar/WAVE, Arp2/3 complex can also be activated by N-WASP to drive efficient invasive cell migration (Insall and Machesky, 2009; Machesky, 2008) and N-WASP is robustly expressed in primary melanocytes (Figure 4.19A). Surprisingly, melanoblasts lacking N-WASP in Z/EG$^{+/o}$ N-WASP f/f Tyr::Cre$^{+/o}$ explants (Snapper et al., 2001) showed no difference in migration and formation of long protrusions as compared with melanoblasts in Z/EG$^{+/o}$ Tyr::Cre$^{+/o}$ control explants (Figure 4.30 and Movie 9). Additionally, the Tyr::Cre deletion of N-WASP revealed no coat color changes in a C57Bl6/J background (Figure 4.31A) and the number and position of melanoblasts in E15.5 DCT::LacZ N-WASP f/f Tyr::Cre$^{+/o}$ embryos showed no differences to control (Figure 4.30B-E), indicating normal melanocyte lineage function in the absence of N-WASP. Furthermore, depletion of N-WASP in melanocytes *in vitro* did not alter melanocyte morphology in 3D (Figures 4.32 and Movie 10). In summary, Rac1 regulates melanoblast migration in epidermis and formation of long protrusions through Scar/WAVE and Arp2/3 mediated actin assembly and independently of N-WASP.

4.3.7 Melanoblast motility across the basement membrane and in skin is not invasive

We were surprised that loss of N-WASP did not produce any apparent defects in melanoblast migration in the skin and it raised the question of whether melanoblasts use invasive matrix degrading migration during embryogenesis. N-WASP and Rac are essential for the formation of invadopodia by melanoma cells and for invasion of cultured cells into collagen gels (Li et al., 2010; Nakahara et al., 2003; Yamaguchi et al., 2005). To further explore the idea that melanoblast migration in skin is not invasive, we examined if metalloprotease (MMP) is required for the formation of long protrusions and migration of melanoblasts by treating the Z/EG$^{+/o}$ Tyr::Cre$^{+/o}$ control skin

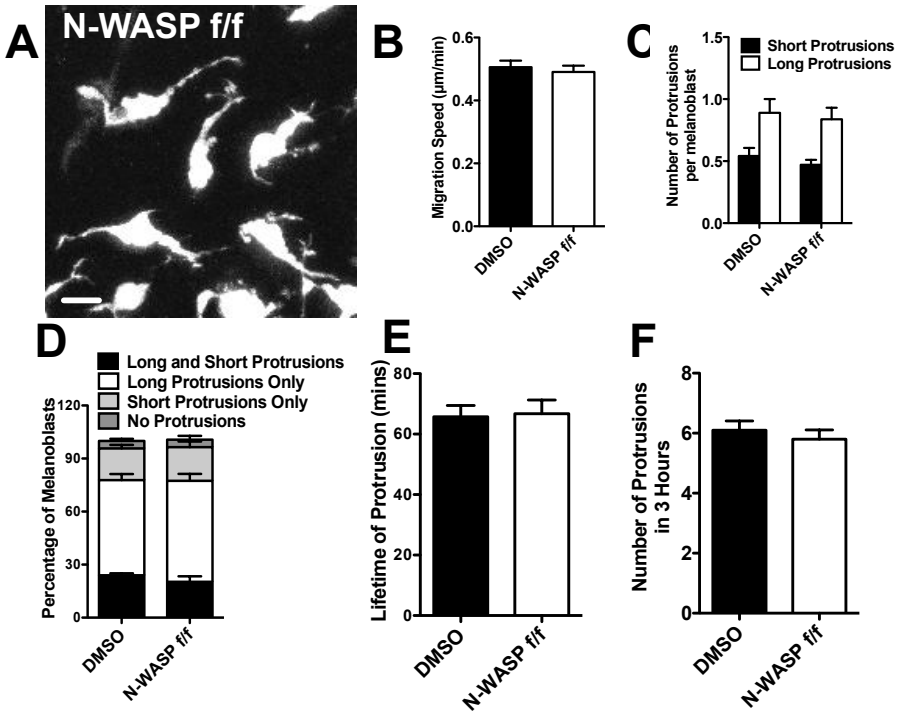

Figure 4.30. N-WASP is not required for melanoblast migration and formation of protrusions (A) Combined Z-stack images (1µm depth) of Z/EG$^{+/o}$ N-WASP f/f Tyr::Cre$^{+/o}$ melanoblasts in skin explants (B) Migration speed. (C) Number of long and short protrusions per melanoblast for > 60 cells per explant from >= 3 explants per genotype. (D) Proportion of melanoblasts with short or long protrusions. (E) Lifetime of actively growing protrusions. (F) Frequency of protrusions formed in 20 cells per explant from >= three explants per condition. Error bars indicate Mean ± SEM. Scale bar 10µm.

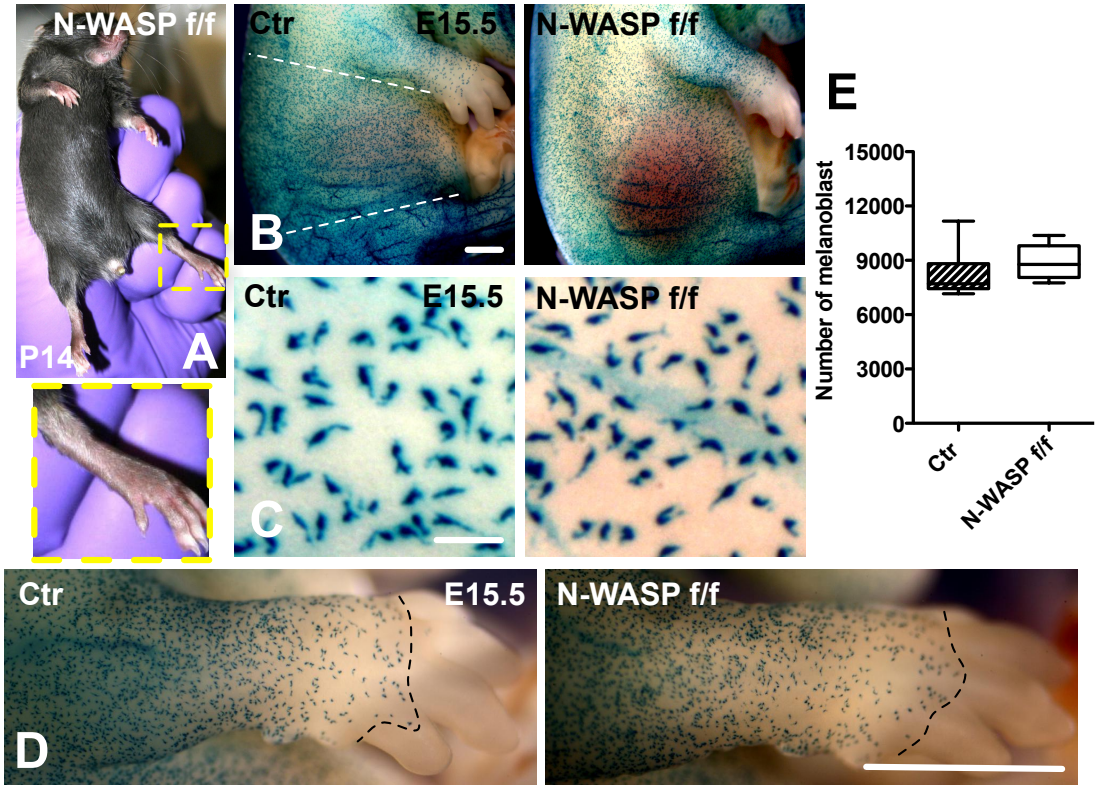

Figure 4.31. N-WASP f/f Tyr::Cre$^{+/o}$ mice revealed normal coat colour and distribution of melanoblasts (A) Ventral coat-color of P14 N-WASP f/f Tyr::Cre$^{+/o}$ mouse. Inset shows hind limb. (B) β-galactosidase stained whole mount DCT::LacZ control (left) and N-WASP f/f Tyr::Cre$^{+/o}$ (right) embryos at E15.5. White dot lines in B indicate the trunk regions in which melanoblasts were quantified in box plot as shown in (E). Each image is representative of 4 embryos from two different litters. (C) Enlarged images of E15.5 trunk regions showing individual melanoblasts. (D) Enlarged images of forelimb from E15.5 DCT::LacZ control (left) and N-WASP f/f Tyr::Cre$^{+/o}$ (right) embryos. (E) Quantification of melanoblasts in DCT::LacZ control and N-WASP f/f Tyr::Cre$^{+/o}$ littermate embryos at E15.5 from 4 embryos from 2 different litters. Lower quartile, median, and upper quartile are shown. Scale bars are (B, D) 1mm, (C) 50μm.

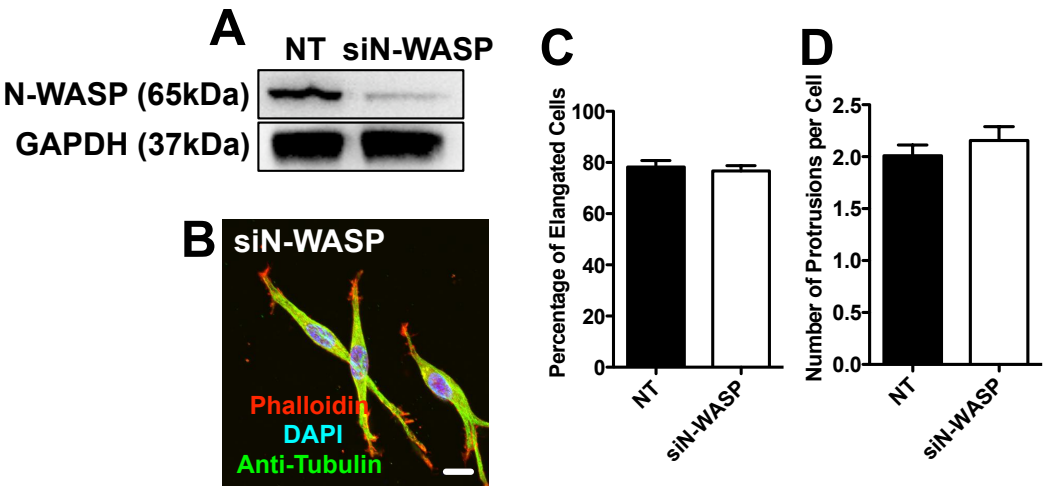

Figure 4.32. N-WASP is not required for formation of long protrusions in primary murine melanocytes (A) Immunoblots showing knockdown of N-WASP in primary mouse melanocytesGAPDH - loading control. (B) Rac1 f/f Tyr::CreERT2$^{+/o}$ Ink4a-Arf$^{-/-}$ (#4) primary melanocytes treated N-WASP siRNA as indicated on collagen I, showing actin (phalloidin), microtubules (anti-tubulin) or DNA (DAPI) (C) % cells with elongated morphology and (D) Number of protrusions per cell for >300 cells x 3 repeats. Error bars indicate Mean ± SEM. **, P< 0.01 by t-test. Scale bar 10μm.

explants with MMP inhibitor (GM6001). However, long protrusions and cell migration speed were not affected (Figures 4.33 and Movie 9), indicating that MMPs are not required for melanoblast migration in the epidermis.

During mouse embryogenesis, melanoblasts migrate from dermis to epidermis between E11.5 and E13.5 and this involves crossing the embryonic epidermal BM (Figure 4.34A). This is potentially a step in migration where melanoblasts would need to use invasive migration. However, the lack of a pigmentation defect (Figure 4.30) in the Tyr::Cre$^{+/o}$ N-WASP f/f mouse suggests that melanoblasts do not need invadopod-like structures mediated by N-WASP either for migration or for crossing the embryonic BM. To confirm this, the trunk region of X-gal stained Dct::LacZ control, Rac1 f/f Tyr::Cre$^{+/o}$ and N-WASP f/f Tyr::Cre$^{+/o}$ embryos were sectioned and the proportion of melanoblasts in the three distinct skin layers: dermis, epidermis and epidermal/dermal junction of the skin tissue sections was determined. On E13.5 and E15.5, the relative distribution of melanoblasts within each of the skin layers did not differ significantly between Rac1 depleted or N-WASP depleted or control embryos (Figures 4.34B, C). Thus, melanoblast migration from dermis to epidermis is unaffected by loss of Rac1 or N-WASP.

4.3.8 Rac1 is required for normal cell cycle progression of melanoblasts during embryogenesis

It was clear that melanoblast position in developing embryos was affected by the loss of Rac1 due to defects in migration, but we also observed a decrease in the number of melanoblasts that required further investigation. The number of melanoblasts undergoing the cell-cycle or apoptosis were determined by co-expression of DCT (melanoblast) and Ki67 (proliferation) or cleaved caspase3 (CC3, apoptosis) in E15.5 control or Rac1 f/f Tyr::Cre$^{+/o}$ embryos. The average percentage of melanoblasts expressing either Ki67 or CC3 between control and Rac1 depleted sections was not significantly changed (Figure 4.35A and data not shown), indicating that melanoblast reduction in

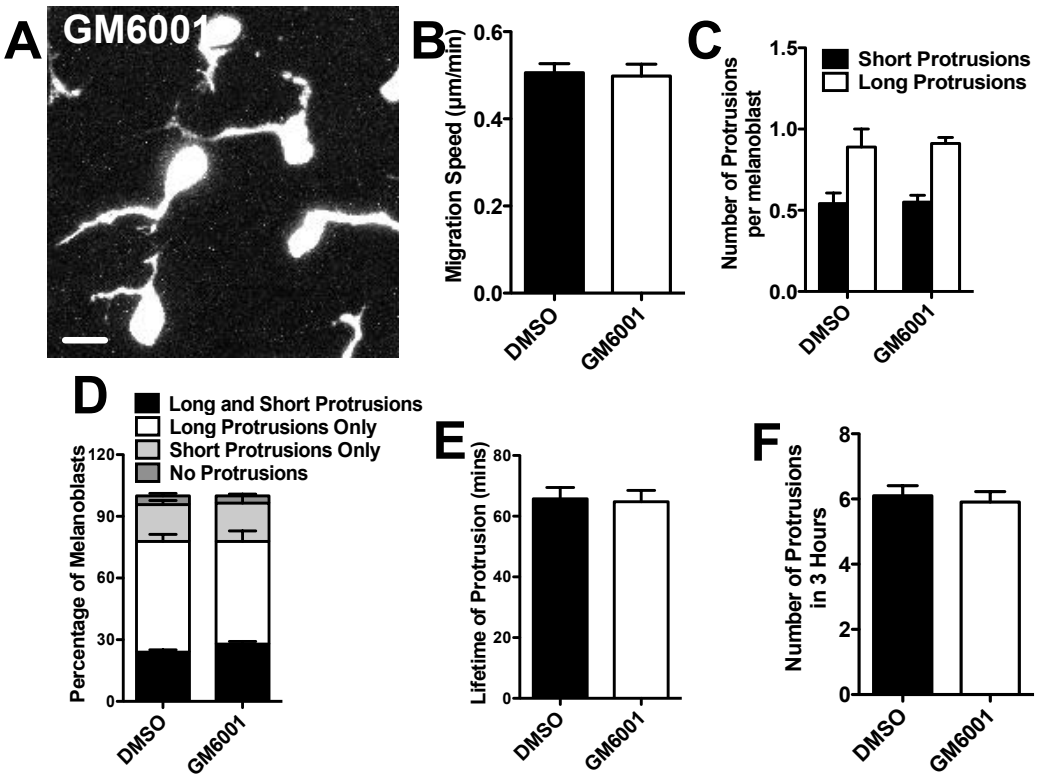

Figure 4.33. Metalloproteases is not required for melanoblast migration and formation of protrusions (A) Combined Z-stack images (1µm depth) of Z/EG$^{+/o}$ Tyr::Cre$^{+/o}$ melanoblasts in skin explants treated with 10µM GM6001. (B) Migration speed. (C) Number of long and short protrusions per melanoblast for > 60 cells per explant from >= 3 explants per genotype. (D) Proportion of melanoblasts with short or long protrusions. (E) Lifetime of actively growing protrusions. (F) Frequency of protrusions formed in 20 cells per explant from >= three explants per condition. Error bars indicate Mean ± SEM. Scale bar 10µm.

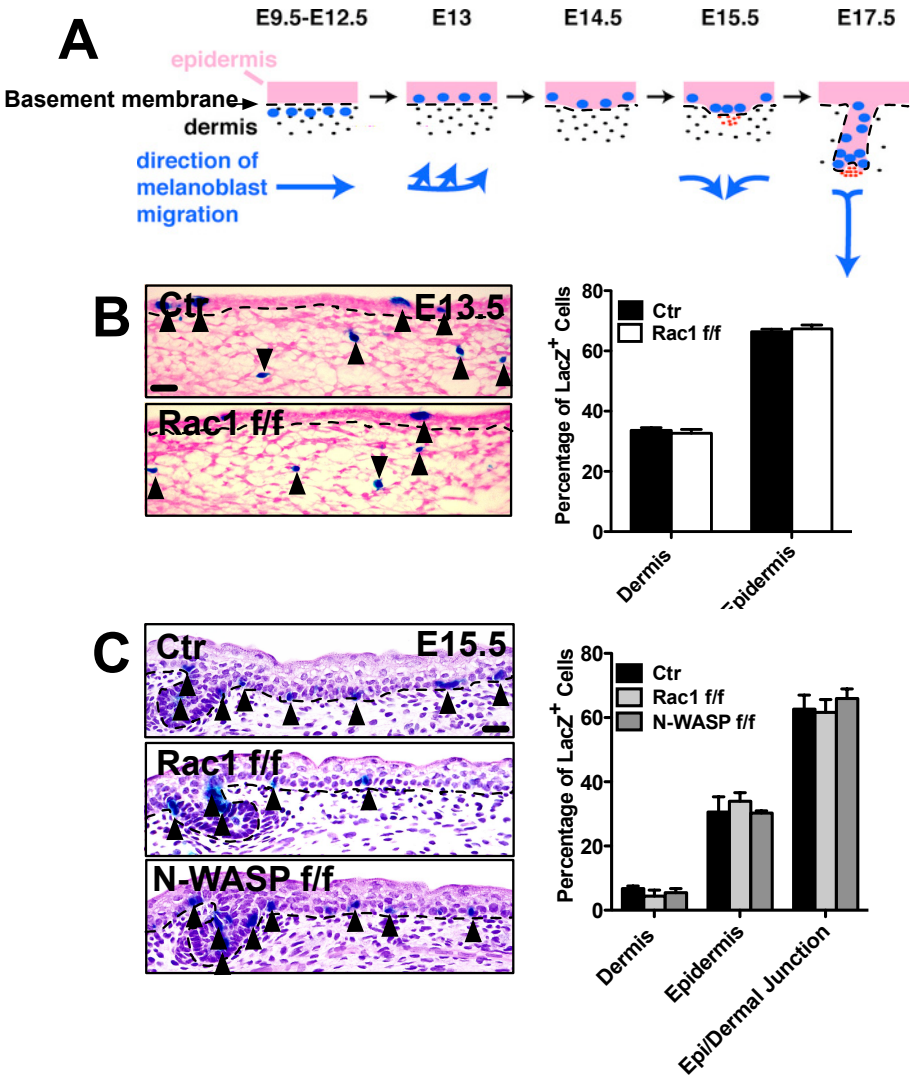

Figure 4.34. Rac1 or N-WASP knockout does not affect melanoblast migration from dermis to epidermis (A) Dorsolateral pathway Melanoblasts migrate from dermis to epidermis and finally hair follicles from E9.5 to E17.5. Image adapted from http:// php.med.unsw.edu.au/embryology/index.php?title=Neural_Crest_Development. (B) Images of sections and quantification of localization of melanoblasts in E13.5 DCT::LacZ control and Rac1 f/f Tyr::Cre$^{+/o}$ embryos. (C) Images of stains and quantification of localization of melanoblasts in E15.5 DCT::LacZ control, , Rac1 f/f Tyr::Cre$^{+/o}$ and N-WASP f/f Tyr::Cre$^{+/o}$ embryos. More then 200 cells were examined per embryo from at least three embryos for each genotype. Melanoblasts are black arrowed. Black dot lines in each picture represent the epi/dermal junction. Scale bars are (B and C) 20μm.

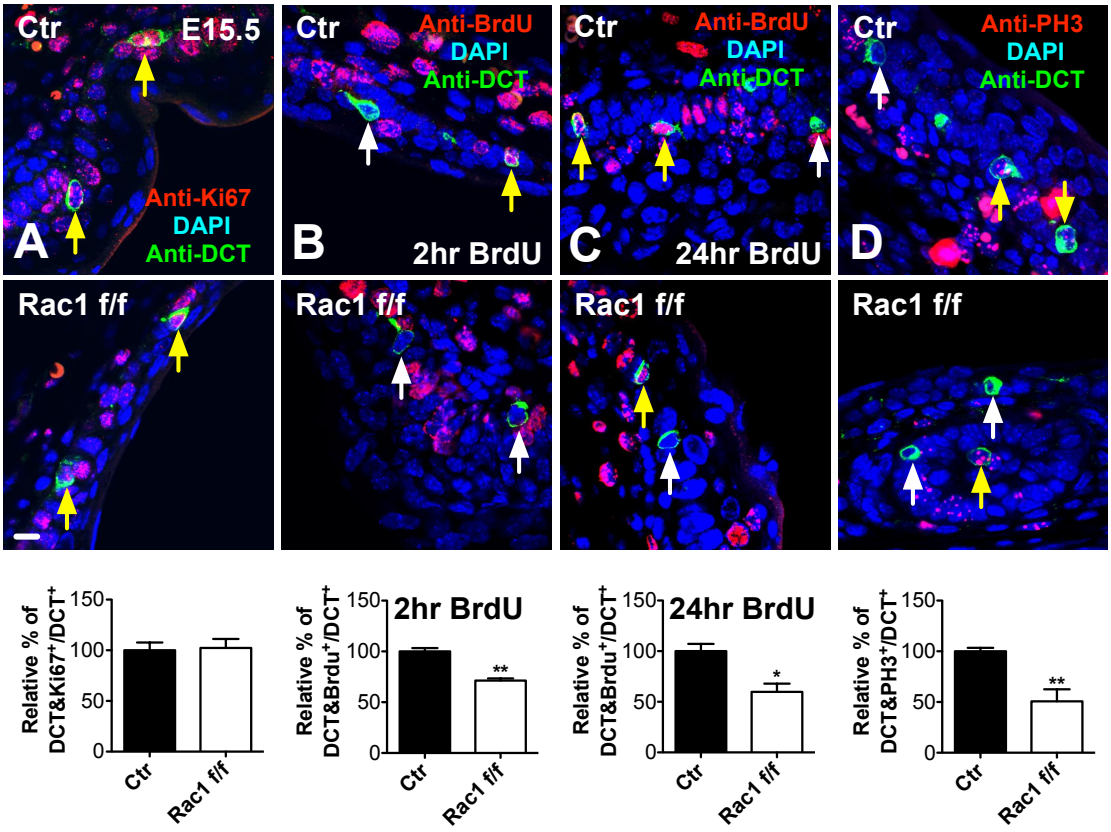

Figure 4.35. Rac1 is required for melanoblast cell cycle progression in vivo. (A-D) Representative images of sections from E15.5 control (left) and Rac1 f/f Tyr::Cre$^{+/o}$ (right) embryos stained for anti-Ki67 (proliferation) (A), anti-BrdU (proliferation) (B and C) or anti-PH3 (phospho-histone 3, mitosis) (D) with anti-DCT (melanoblast) and DAPI (DNA). The DCT-positive cells expressing Ki67, BrdU or PH3 are yellow arrowed and DCT-positive cells that do not co-localize with Ki67, BrdU or PH3 are white arrowed. Proportions of DCT and Ki67, BrdU or PH3 positive cells are shown. At least 3 embryos per genotype and 200 cells per embryo analyzed. Error bars indicate Mean ± SEM. **, P< 0.01 *, P<0.05 by t-test. Scale bar 10μm.

Rac1 f/f Tyr::Cre$^{+/o}$ embryos is not a consequence of reduced numbers of cells undergoing the cell cycle or apoptosis. Next, we examined whether loss of Rac1 induced a cell cycle progression defect in melanoblasts. We observed a significant decrease in BrdU incorporation into Rac1 depleted melanoblasts when animals were given either a 2hr or 24hr pulse before sacrifice (Figures 4.35B and C). Furthermore, there was a significant reduction in the percentage of phospho-histone 3 (PH3, mitosis) positive melanoblasts in Rac1 f/f Tyr::Cre$^{+/o}$ embryos (Figure 4.35D). Consistent with in vivo observations, the growth rate of OHT treated melanocyte cell lines #3 and #4 (Tyr::CreERT2$^{+/o}$ Ink4a-Arf$^{-/-}$ Rac1 f/f) was significant decreased compared to their DMSO treated control. Whereas, growth rate and cell morphology of OHT treated control melanocyte cell line #2 (Tyr::CreERT2$^{o/o}$ Ink4a-Arf$^{-/-}$ Rac1 f/f) was unaffected (Figures 4.36A, B and data not shown). Flow cytometry analysis of Rac1 knockout melanocytes showed shifting to the G1 phase with a significant reduction of cells in S phase as compared to control (Figures 4.36C, D). Thus, Rac1 is required for normal G1-S phase cell cycle progression but not cell cycle entry or prevention of apoptosis in melanoblasts in vivo.

4.3.9 Rac1 is required for efficient cytokinesis of melanoblasts during embryogenesis

Time-lapse videos revealed alterations in cytokinesis of Rac1 deficient melanoblasts that likely also contribute to growth rate slowing. Normal melanoblasts in Z/EG$^{+/o}$ Tyr::Cre$^{+/o}$ control explants undergo very efficient cytokinesis in skin explants , taking about 10 minutes to first show a cleavage furrow and about 30min from the initiation of furrowing to the separation of two daughter cells (Figures 4.37A, B). Interestingly, Rac1 depleted melanoblasts formed a furrow with normal timing, but exhibited a 3- fold delay in time to separation (Figures 4.37A, B and Movie 11) and the two daughter cells migrated apart more slowly (Figure 4.37C). Despite the strong delay in cytokinesis, Rac1 f/f Tyr::Cre+/o melanoblasts did not become multinucleate (data not shown) indicating that Rac1 is not essential for cytokinesis but

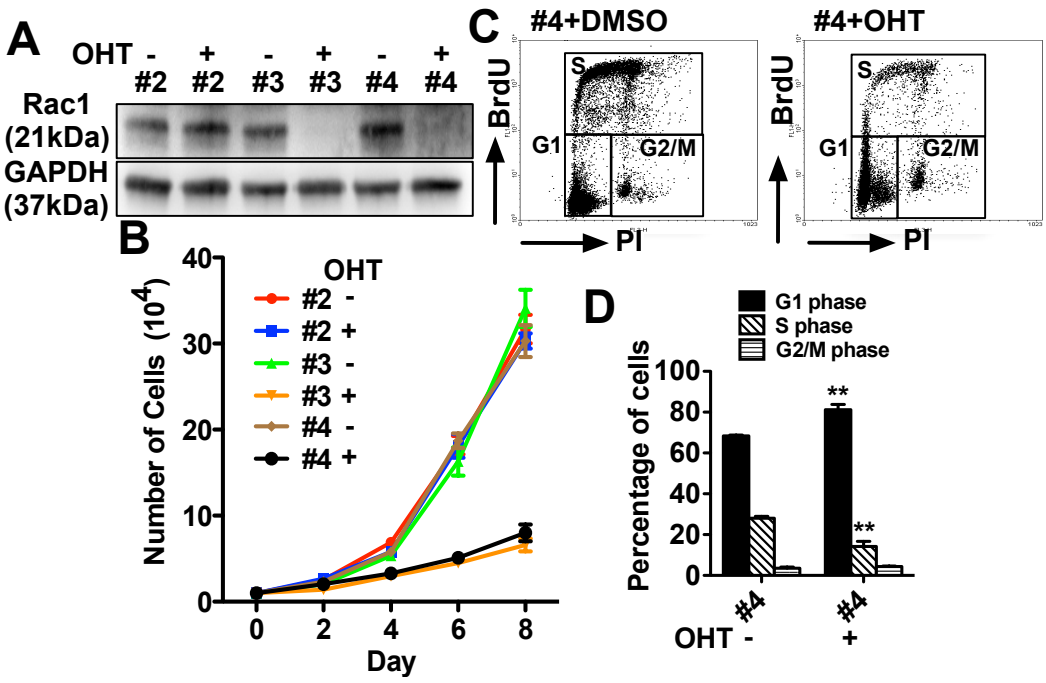

Figure 4.36. Rac1 is required for melanocyte cell cycle progression in vitro. (A) Western blots of lysates from Rac1 f/f Tyr::CreERT2$^{o/o}$ Ink4a-Arf$^{-/-}$ (#2) and two independent Rac1 f/f Tyr::CreERT2$^{+/o}$ Ink4a-Arf$^{-/-}$ primary melanocyte cell lines (#3 and #4) treated with DMSO or OHT probed with anti-Rac1 and anti-GAPDH (loading control). (B) Growth curve of melanocyte cell lines (#2, #3 and #4) treated with DMSO or OHT. Each point (Mean ± SEM) is derived from 3 replicate dishes from 3 independent experiments. (C) Representative experiment from Rac1 f/f Tyr::CreERT2$^{+/o}$ Ink4a-Arf$^{-/-}$ (#4) melanocytes treated with DMSO or OHT were pulse-labeled for 2 h with BrdU, and analyzed by flow cytometry for BrdU incorporation and propidium iodide (PI) labeling. Cells in the different states are indicated. (D) % cells in each phase as calculated from (C). Results are from 3 independent experiments. Error bars: Mean ± SEM. **, P< 0.01 by t-test. Scale bar 10μm.

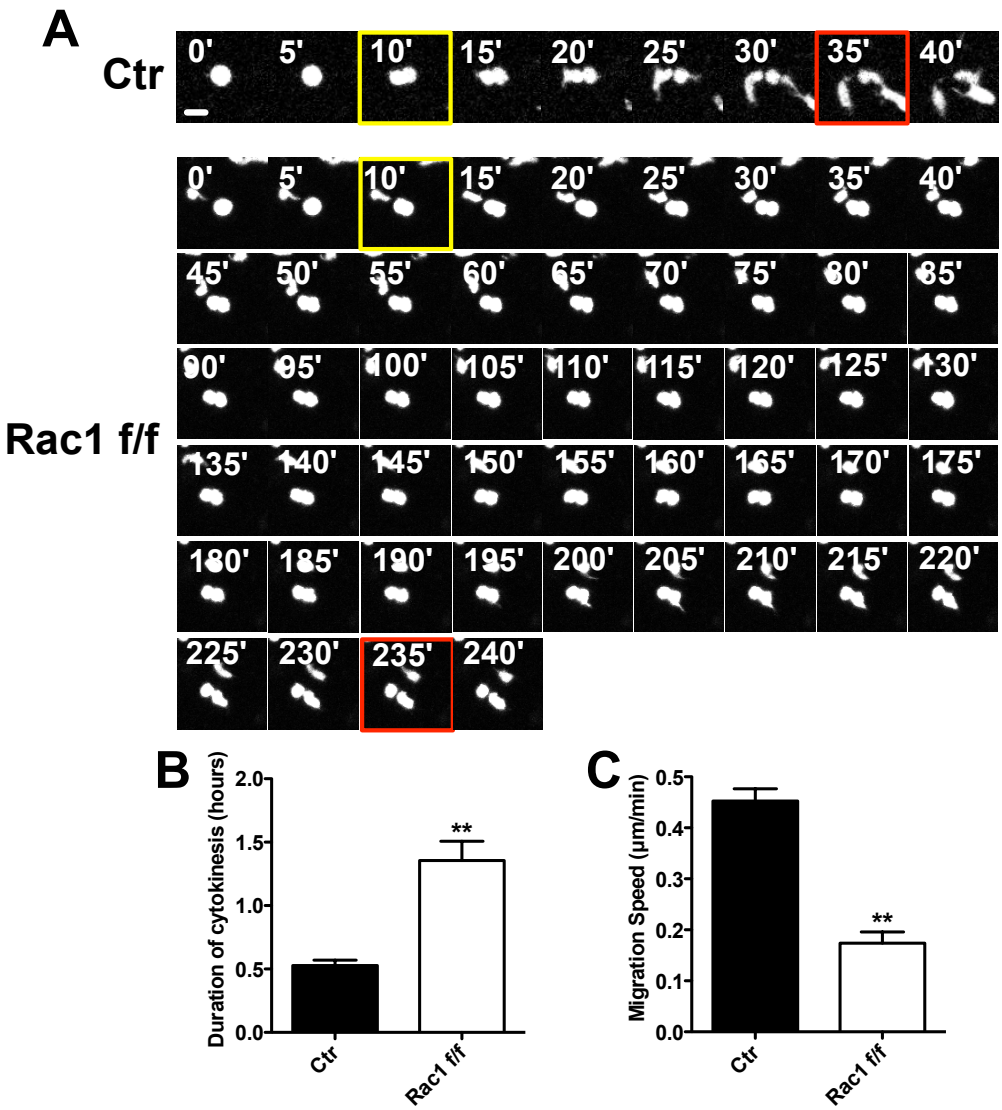

Figure 4.37. Rac1 knockout in melanoblasts delays cytokinesis in skin explants. (A) Representative live-cell imaging of melanoblasts in Z/EG$^{+/o}$ Tyr::Cre$^{+/o}$ control, Z/EG$^{+/o}$ Rac1 f/f Tyr::Cre$^{+/o}$ skin explants undergo cytokinesis. Images were captured every 5 min. Time-point of the initiation of furrowing was yellow squared, Time-point in which two daughter cells separated was red squared. (B) The duration or cytokinesis, from initiation of furrowing to separation of two daughter cells. Error bars indicate Mean ± SEM of 20 cells from 10 divisions. **, P< 0.01 by t-test. (C) Quantification of migration speed of daughter melanoblasts in the skin explants for 1 hr after cytokinesis. 20 daughter melanoblasts from 10 divisions were examined. All error bars indicate Mean ± SEM **, P< 0.01 by t-test. Scale bar 10μm.

required for efficient daughter cell separation in vivo. To see if the cytokinesis defect also exists in vitro, control and Rac1 depleted melanocytes were subjected for live time imaging. Interestingly, no obvious delay of cytokinesis was found in Rac1 depleted melanocytes on 2D cell culture dish (Figure 4.38). Together, these data suggest a more significant requirement for Rac to control cytokinesis in the tissue environment than in culture dishes.

4.4 Discussion

4.4.1 Melanoblasts move using a mixture of short Rac1-independent and long Rac1-dependent protrusions.

Melanoblasts extend a mixture of long and short protrusions in skin and short protrusions mature into long ones. Short stubby protrusions require actin assembly but not microtubules, myosin or components of the Rac-Scar/WAVE-Arp2/3 pathway. They might initiate by stochastic actin assembly reactions that are normally cycling in the melanoblasts (Betz et al., 2009; Michelot et al., 2007) or by some form of signaling. A candidate to signal short protrusion initiation might be Rho, which was found to precede Rac in motile cultured cells (Pertz et al., 2006) and downstream might lie diaphanous related formins (DRFs), to initiate formation of unbranched actin networks that could later serve as a platform for Arp2/3 mediated actin assembly. DRFs are attractive candidates, since they also coordinate actin and microtubule assembly and dynamics (Palazzo et al., 2001). Indeed, expression of GFP-mDia1 or GFP- mDia2 in normal and Rac1 null melanocytes on 3D collagen I matrix showed localization at tips of long and short protrusions (Figure 4.39). However, further studies are required to elucidate the role of formins in melanoblast motility. Treatment of skin explants with broad formin inhibitor (SMIFH2) (Rizvi et al., 2009) resulted in massive cell death within half hour incubation even at 100nM inhibitor (Data not shown), indicating that formin function may be crucial for melanoblast survival or that this inhibitor is toxic to our skin explants. In the future, we hope to understand the role of individual

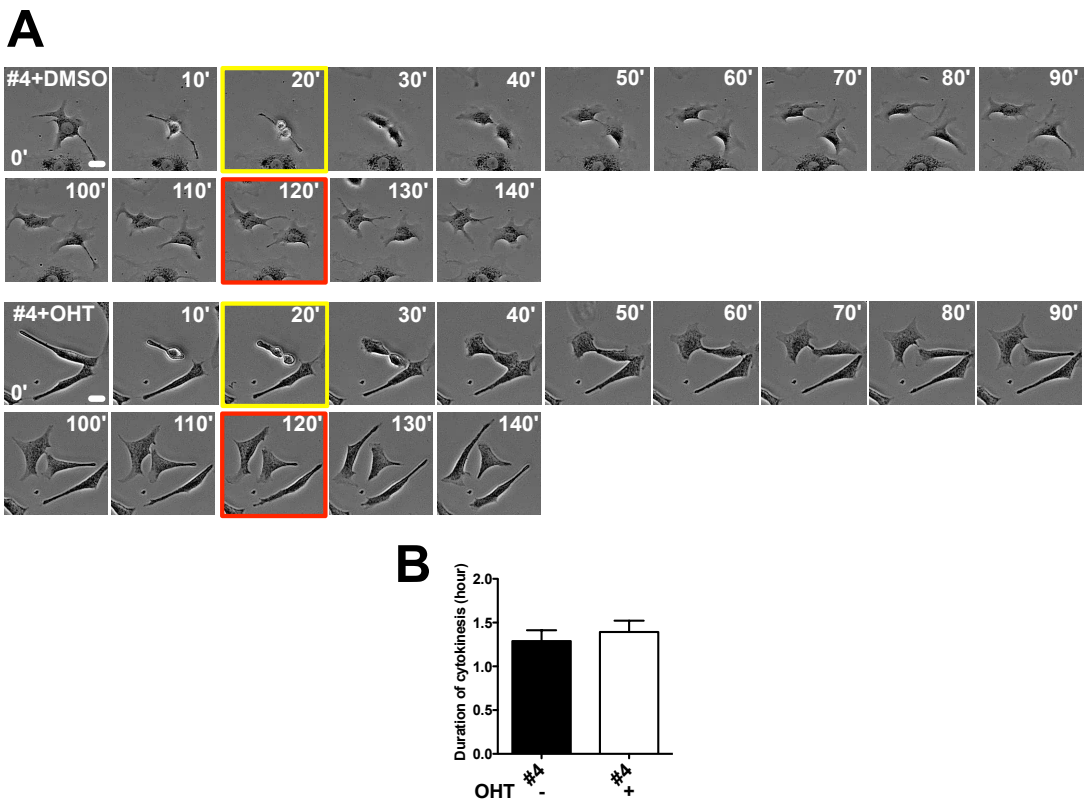

Figure 4.38. Rac1 deletion in mouse primary melanoblasts does not affect cytokinesis *in vitro.* (A) Representative stills from live-cell imaging of DMSO or OHT treated Rac1 f/f Tyr::CreERT2+/o Ink4a-Arf-/- primary melanocyte cells (#4) in culture on fibronectin coated coverslips undergoing cytokinesis. Images were captured every 10 min. Initiation of furrowing is yellow squared; Daughter cell separation point is red squared. (B) Quantification of the duration of cytokinesis from initiation of furrowing to separation of two daughter cells. Error bars indicate Mean ± SEM of 20 cells from 10 divisions. Scale bars 10μm.

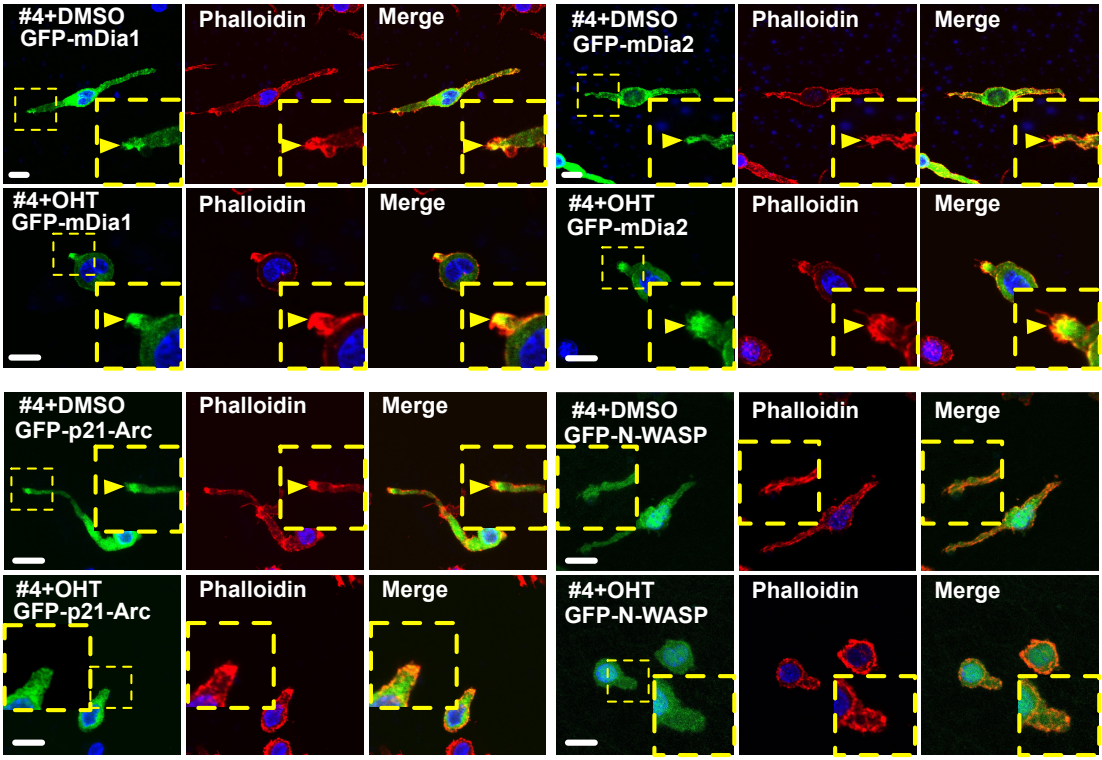

Figure 4.39 Localization of mDia2 to short protrusions. Rac1 f/f Tyr::CreERT2+/o Ink4a-Arf-/- (#4) primary melanocytes expressing GFP- mDia1, GFP-mDia2, GFP-p21-Arc or GFP-N-WASP treated with DMSO or OHT as indicated were plated on 3D collagen I matrix. Cells were stained with rhodamine phalloidin and DAPI. Yellow arrows indicate co-localization of GFP- tagged protein and actin at tips of protrusions. Scale bar is 10μm.

formins in melanoblast motility using mouse genetic experiments. Additionally, Small and colleagues propose that lamellipodial protrusions can be driven by proteins such as Mena/VASP, which can support extension of actin-based unbranched networks (Urban et al., 2010). It remains to be determined the relative roles of other actin network inducing proteins in stub protrusions. Our data suggest that short stubs are distinct from blebs (Fackler and Grosse, 2008), as they generally are thin and spiky or jagged in shape (rather than lobule-shaped like blebs) and they are rich in dynamic filamentous actin, similar to longer protrusions. Short stubs are thus novel Rac1 independent actin structures that can act as precursors to long pseudopods and might not occur on rigid flat substrates, where lamellipodia dominate.

Melanoblast long protrusions required on actin, microtubules and the Rac-Scar/WAVE-Arp2/3 pathway, but not myosin. Long protrusions traversed between keratinocytes, often spanning the length of 2 or 3 keratinocytes and existing in multiple planes, appearing to contact keratinocytes all over their surfaces. Melanoblast long protrusions have in common with neurite processes that they are microtubule-rich and have actin-rich tips. However, while Rac1 and the Scar/WAVE complex are important for lamellipodia of neuronal growth cones, the growth of long microtubule-rich processes from neuronal cells in culture wasn't ablated by loss of Rac1 or inhibition of Arp2/3 complex (Strasser et al., 2004; Tahirovic et al., 2010). A cell type that might be comparable to melanoblasts for migration in vivo is chick embryo muscle precursor, which migrates from somites into the limb bud. Horwitz and colleagues showed that these cells extend long stable protrusions similar in lifetime to melanoblasts (50 min vs 60 min in our study) and migrate with similar average speed (37μm/hr vs 30μm/hr in our study). They also found that dominant negative Rac stopped migration and limited protrusion (Knight et al., 2000).

4.4.2 Rac1 controls the frequency of long pseudopod extension

We were surprised that overall migration and directional steering of melanoblasts occurred normally in the majority of dorsal areas of the mouse skin. It was also unexpected that when myosin was inhibited, Rac1 was no longer required for long pseudopod generation; but it still strongly controlled the frequency of generation of long pseudopods. This only became apparent when we inhibited myosin activity in skin explants by adding Y27632 or blebbistatin, so it might be interesting to apply these compounds to *Drosophila* border cells or Rac1 deficient AVE cells. Scar/WAVE and Arp2/3 complex might be able to generate long pseudopodia in a Rac-independent manner in the case where cortical tension and contractility is low enough to be permissive for this. This may depend on other signaling, such as via phosphorylation (Lebensohn and Kirschner, 2009) or phospholipid or adapter protein interactions (Chen et al., 2010). While Rac1 is a major controller, it is likely that multiple signal inputs modulate the Scar/WAVE complex.

4.4.3 Loss of Rac1 affects focal adhesion formation but not contact with BM or cell-cell adhesion structures

Adhesion to extracellular matrix was likely affected by loss of Rac1, since in culture, melanocytes depleted for Rac1 showed reduced focal adhesions. This could alter the lifetime of long protrusions and their ability to adhere for force generation towards translocation. However, we could not find any change in the percentage of melanoblasts contacting the basement membrane in embryo skin, indicating that cells didn't likely completely lose contact between integrins and extracellular matrix. E-cadherin and actin surrounding the melanoblasts and neighboring keratinocytes in skin explant whole mounts appeared normal, as did levels of E-cadherin or ZO-1 expressed by cultured melanocytes following Rac1 depletion. We can't be sure that melanoblasts are making E-cadherin junctions with keratinocytes, but the extension of long protrusions into the spaces between keratinocytes, coupled with the precedent in other systems (Geisbrecht and Montell, 2002;

Kardash et al., 2010) suggests that E-cadherin is a good candidate to mediate interactions between these cells. This requires further study, such as with E-cadherin depleted melanoblasts or cadherin-blocking reagents.

4.4.4 Melanoblast motility across the basement membrane and in skin is not invasive

Melanoblasts traverse at least three very different tissue environments on their journey from the neural tube to the epidermis and hair follicles. They first emerge in the dermis, a complex matrix of collagen and proteoglycans and they migrate in the dermis until around E13.5, when they cross what appears as a collagen-rich BM into the epidermis. At E13.5, the epidermis is only ~1 cell-layer thick (Figure 4.34B) but by E15.5, multiple keratinocyte layers are present and around half of melanoblasts are touching the BM, but ~70% have crossed over and are above the BM (Figure 4.34C). We can find no evidence that this motility depends on either N-WASP or Rac, which are important for the assembly of invadopodia (Li et al., 2010; Nakahara et al., 2003; Yamaguchi et al., 2005) and for the invasion of cancer cells into 3D matrix (Kurisu et al., 2004; Li et al., 2010). Furthermore, migration of melanoblasts within the skin was not affected by inhibition of MMPs. Thus early dermal ECM and epidermal BM are likely permissive to cell transmigration independent of pericellular proteolysis, whch is similar to lymphatic endothelial BM and dendritic cells (Pflicke and Sixt, 2009). During melanoma formation, the acquisition of a BM degrading ability is thus unlikely to be a simple reversion to the normal melanoblast genetic programme. Melanoma cells require N-WASP for efficient invasion in vitro and use MT1-MMP to make invadopodia (Li et al., 2010), but melanoblasts do not appear to depend on similar invasive behavior during embryogenesis.

4.4.5 Rac1 is required for normal cell cycle progression and cytokinesis of melanoblasts during embryogenesis

Rac1 is important for G1 progression of melanoblasts during normal development. A major controller of melanoblast proliferation is c-kit, a tyrosine kinase receptor, which signals to Ras and activates entry into the cell cycle via PI3-kinase, Akt and MEK pathways (Smalley, 2009). Rac1 is well documented to act downstream of Ras in concert with PI3-kinase and to regulate G1 progression in vitro (Olson et al., 1995). However, unlike melanoblasts, anterior visceral endoderm cells can dispense with Rac1 for proliferation (Migeotte et al., 2010). Murine neural crest cells have increased apoptosis with loss of Rac1 induced by wnt-1 cre, unlike melanoblasts with Tyr::Cre (Thomas et al., 2010). We wonder if Rac1 loss affects stem cell survival of melanocytes in hair follicles, as was the case for keratinocytes (Benitah et al., 2005; Chrostek et al., 2006), but some expression of Tyr::Cre in the nervous system (Tonks et al., 2003) caused a shakiness of Rac1 deleted mice that required culling before they could be aged over several hair cycles.

There is little precedent for the positive involvement of Rac in control of cytokinesis, so it was surprising to find a 3-fold increase in time to divide in Rac1 null cells. However, Rac drives the assembly of the cortexillin-actin networks in dividing *Dictyostelium* cells (Faix, 2002) and recently Insall and colleagues found that Scar/WAVE proteins enabled cells to repolarize and crawl apart following cleavage, suggesting a late requirement for Rac at opposite poles of the dividing cells (King et al., 2010). In *C. elegans* early cleavage furrow formation, Rac1 inhibited by a complex containing the RacGEF CYK4 and centralspindlin, so that Rho can effect contractility (Canman et al., 2008). Rac1 depleted melanoblasts dividing in skin could still round up with the normal timing, but took far longer to divide, indicating a likely requirement for Rac1 in adhesion of the dividing cell to the surrounding milleu and repolarization of the dividing cells to then crawl apart. This defect wasn't seen in cultured cells, indicating that it was specific to the epidermal environment. So while in early cytokinesis, Rac1 may be inhibited at the

furrow, later cytokinesis may in some tissue environments utilize activation of Rac for adhesion, polarization and migration of the two daughter cells.

Chapter V

The role of Rac1 downstream of activated N-Ras^{Q61K} in melanocyte survival

5.1 Summary

Rac1 is important for Ras-mediated transformation in vitro, but its role downstream of Ras, especially N-Ras, is not fully understood. The aim of this chapter was to characterise the role of Rac1 in mice with melanocyte specific expression activated N-Ras transgene. This work led to the identification that Rac1 is required for activated N-Ras induced dermal melanocytes survival *in vivo*. In addition, melanoblast migration and proliferation in conditional Rac1 knockout mouse embryos cannot be compensated by expression of activated N-Ras.

5.2 Introduction

By switches between inactive GDP- and active GTP-bound states, small GTPases function as critical relays in communicating signals from outside of the cell to the nucleus. Ras subfamily small GTPases is activated upon ligand engagement of membrane receptors and mediates cell growth, differentiation and survival (Downward, 2003). Such pleiotropic effects depend on the ability of Ras-GTP to activate multiple signaling pathways through direct binding to effector proteins. Mutations in the Ras proto-oncogene family (H-Ras, N-Ras and K-Ras) are amongst the most frequently mutated genes in human cancers, being found in 20% to 30% of all human tumours (Downward, 2003). The most common mutations are found at residue G12 in the phosphate-binding loop and the catalytic residue Q61 (Malumbres and Barbacid, 2003). Constitutively Active N-Ras^{Q61K} are frequently found in nevi and early-stage melanomas (Platz et al., 2008). Expression of dominant-active human N-Ras^{Q61K} to the melanocyte lineage by tyrosinase regulatory sequences in mice results hyperpigmented skin (Ackermann et al., 2005), which can develop cutaneous metastasizing melanoma on an INK4a-Deficient background at 6 months .

Growing evidence have identified that the MAPK pathway as a key effector in Ras signaling (Cook and McCormick, 1994; Marshall, 1995). However, the recruitment of many other Ras targets is indispensable to elicit a full Ras

biological response. Among these Ras-dependent, Raf-independent pathways are those connecting Ras to the Rho family of small GTPases. In contrast to the relatively frequent incidence of activating mutations in Ras genes, there are no published reports of activating Rho mutations in human tumors. However, numerous lines of research indicate that Rho proteins do indeed contribute to cancer (Sahai and Marshall, 2002).

Rac1 small Rho GTPase has been known for over 15 years to be essential for Ras-induced transformation, at least in vitro (Qiu et al., 1995b), but relatively little is known about its role in cancer *in vivo*. Rac is essential for transformation in a K-Ras^{G12D} activated lung cancer model (Kissil et al., 2007a). In addition, Samuel at al, showed that Rac1 is required for K-Ras ^{G12D} driven epithelial cell hyperproliferation and that Rac1 activity is elevated in tissues expressing mutant oncogenic K-Ras (Samuel et al., 2011). Rac is activated downstream of Ras and can activate 70 kDa ribosomal S6 kinase (Chou and Blenis, 1996) and JNK1, which for JNK1, possibly via Pak kinases to stimulate cell cycle progression (Olson et al., 1995).

The aim of this Chapter was to identify of role of Rac1 downstream of active N-Ras^{Q61K} in melanocytes *in vivo*. I demonstrate here that Rac1 is required for activated N-Ras induced dermal melanocytes survival *in vivo*. Activated N-Ras does not play a role within melanoblast migration and proliferation during embryogenesis.

5.3 Results

5.3.1 Activated N-Ras doesn't compensate for loss of Rac1 in either melanoblast migration or proliferation

I have demonstrated in the last Chapter that Rac1 loss in melanoblasts causes coat colour defects in mice, which is due to impaired migration and proliferation. It has been shown that expression of dominant-active human N-Ras^{Q61K} under control of tyrosinase promoter in mice results in

hyperpigmented skin (Ackermann et al., 2005), which is due to hyperproliferation of melanocytes. To investigate whether hypopigmentation resulting from Rac1 knockout can be overcome by activated N-Ras expression, mice carrying a Tyr::N-Ras^{Q61K} transgene were crossed onto Rac1 f/f or Dct::LacZ background. Tyr::N-Ras$^{Q61K+/o}$ control and Tyr::N-Ras$^{Q61K+/o}$ Rac1 f/f Tyr::Cre$^{+/o}$ mice were born healthy at the expected Mendelian ratio. Consistent with the previous report (Ackermann et al., 2005), Tyr::N-Ras$^{Q61K+/o}$ control mice have much darkened skin compared to wild-type mice (Figure 5.1A, D). Histological analysis of P14 Tyr::N-Ras$^{Q61K+/o}$ control ventral skin revealed presence of increased number of melanocytes not just in hair follicles but also the dermis below the epidermis and throughout the fatty tissue (Figure 5.2). Interestingly, Tyr::N-Ras$^{Q61K+/o}$ Rac1 f/f Tyr::Cre$^{+/o}$ mice revealed no effect on the pattern or colour of the areas of unpigmented skin (Figure 5.1A, B). This was further confirmed by the fact that the number of white patches on the dorsal skin between Dct::LacZ Tyr::N-Ras$^{Q61K+/o}$ Rac1 f/f Tyr::Cre$^{+/o}$ and Dct::LacZ Rac1 f/f Tyr::Cre$^{+/o}$ mice was similar (Figure 5.1C). Strikingly, despite the large increase in the numbers of melanocytes in skin in adult mice, quantification of number of melanoblasts in E15.5 embryos or P0.5 skin only showed a slight increase in the presence of activated N-Ras in a normal background (Figure 5.3 and 5.4), and a significant reduction in melanoblast number in Rac1 f/f Tyr::Cre$^{+/o}$ embryos regardless of the presence of activated N-Ras, indicating that activated N-Ras doesn't likely confer a hyperproliferation of melanoblasts during embryogensis. Indeed, we found that the coat colour was indistinguishable between control and Tyr::N-Ras$^{Q61K+/o}$ control mice just after birth (Figure 5.5A), and coat colour in Tyr::N-Ras$^{Q61K+/o}$ control mice become darker after day 3 (Figure 5.5B and C), suggesting that the melanocyte hyperproliferation phenotype in Tyr::N-Ras$^{Q61K+/o}$ mice was developed after birth.

In addition, we also noted that expression of activated N-Ras didn't affect the morphology, motility, protrusion dynamics, epidermal/dermal localization and cytokinesis of either normal or Rac1 depleted melanoblasts detectably (Figure 5.6, 5.7, 5.8, 5.9 and data not shown). In summary, the cell cycle or motility

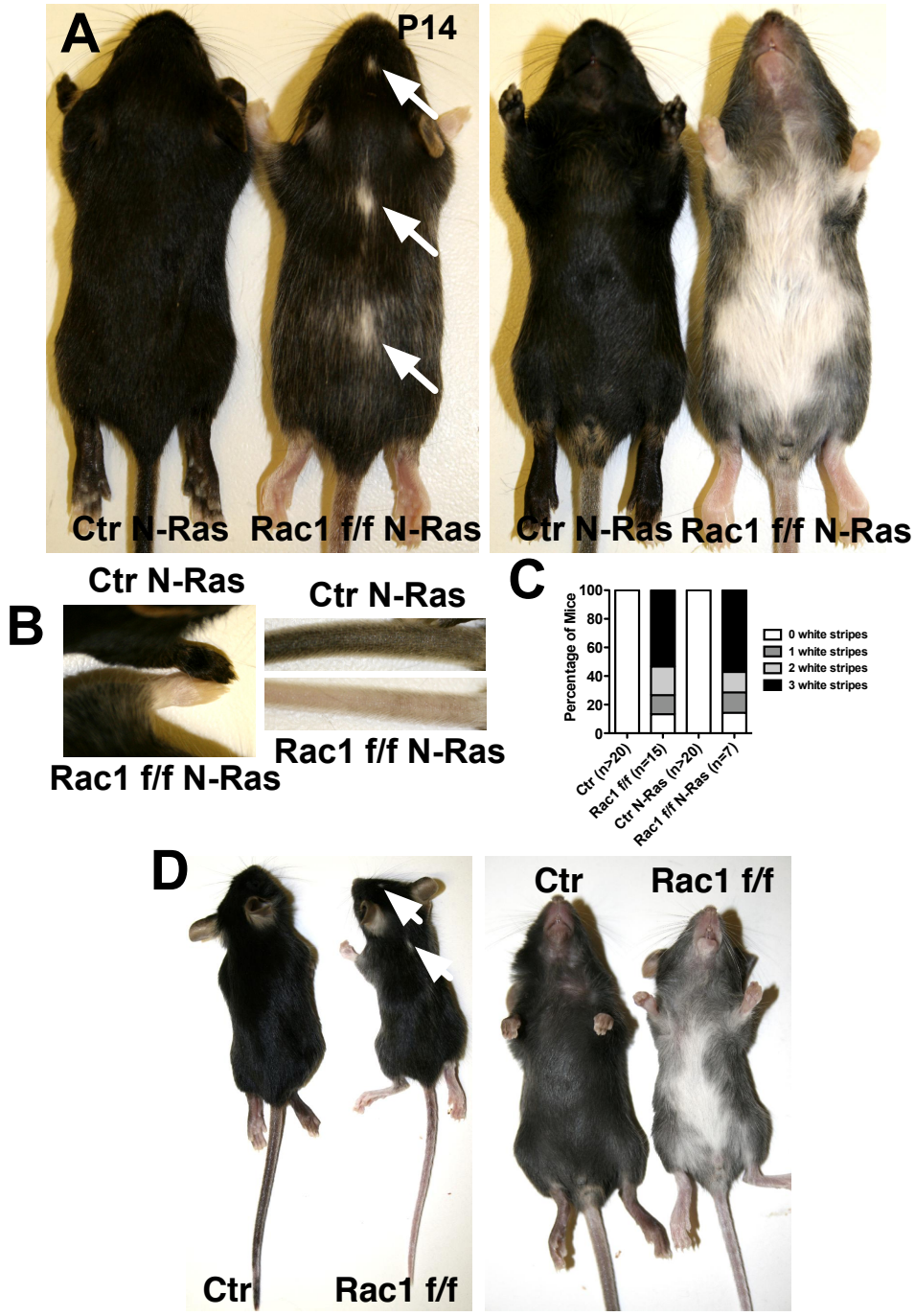

Figure 5.1 Expression of N-Ras^{Q61K} in the melanocyte lineage doesn't rescue the loss of Rac1. (A) Coat-color of dorsal side (left) and ventral side (right) of P14 Tyr::N-Ras$^{Q61K+/o}$ Rac1 f/f Tyr::Cre$^{+/o}$ (Rac1 f/f N-Ras) mouse with its Tyr::N-Ras$^{Q61K+/o}$ (N-Ras) control littermate. Three typical white patches on the dorsal side of the Rac1 f/f N-Ras mouse were white arrows. (B) Coat-color of forelimb and tail of P14 Rac1 f/f N-Ras mouse with its Ctr N-Ras control littermate. (C) Quantification of number of white patches on dorsal surface for genotypes of number of mice as indicated. (D)Coat-color of dorsal side (left) and ventral side (right) of P14 Rac1 f/f Tyr::Cre$^{+/o}$ (Rac1 f/f) mouse with its control littermate. Typical white patches on the dorsal side of the Rac1 f/f mouse were white arrowed.

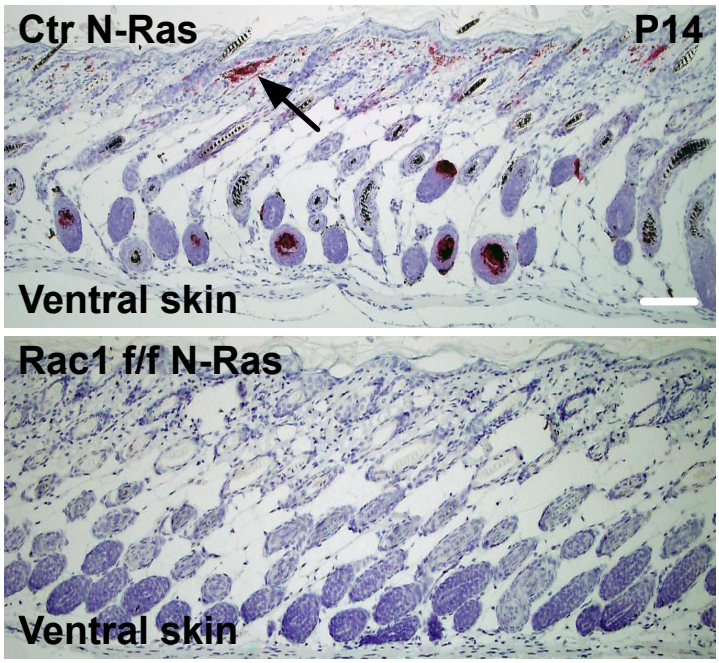

Figure 5.2 Melanocytes were absent in ventral white patches of Tyr::N-Ras$^{Q61K+/o}$ Rac1 f/f Tyr::Cre$^{+/o}$. Immunohistochemical analysis of ventral skin from P14 Ctr N-Ras and Rac1 f/f N-Ras mice with anti-DCT to detect melanocytes. Example of typical pocket of excess dermal melanocytes in Ctr N-Ras mouse is black arrowed. Scale bars 100μm.

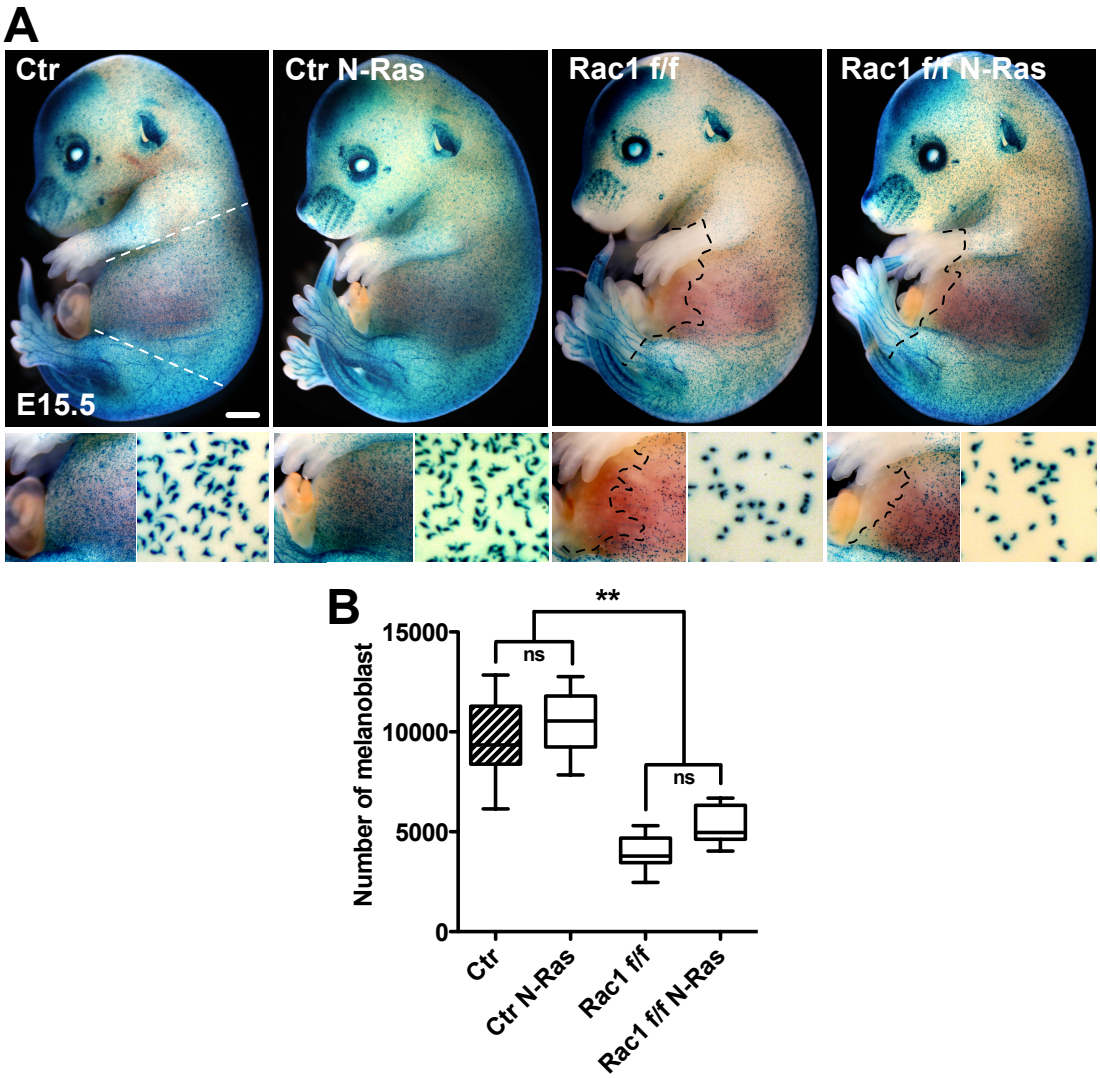

Figure 5.3 Expression of N-Ras^{Q61K} in the melanocyte lineage doesn't rescue the effect of loss of Rac1 on melanoblast number and distribution. (A) Images of β-galactosidase stained whole mount DCT::LacZ embryos: control, Tyr::N-Ras$^{Q61K+/o}$ control, Rac1 f/f Tyr::Cre$^{+/o}$ and Tyr::N-Ras$^{Q61K+/o}$ Rac1 f/f Tyr::Cre$^{+/o}$ embryos at E15.5. Each image is representative of at least 5 embryos from four different litters. Insets show higher magnification of belly area and cell shpae. White dot lines in A indicate the trunk regions in which melanoblasts were quantified in box plot as shown in (B). (B) Number of melanoblasts in DCT::LacZ embryos including control, Tyr::N-Ras$^{Q61K+/o}$ control, Rac1 f/f Tyr::Cre$^{+/o}$ and Tyr::N-Ras$^{Q61K+/o}$ Rac1 f/f Tyr::Cre$^{+/o}$ at E15.5. At least 5 embryos from four different litters were examined. Lower quartile, median, and upper quartile are shown. **, P< 0.01 compared to control by t-test. The scale bar is 1mm.

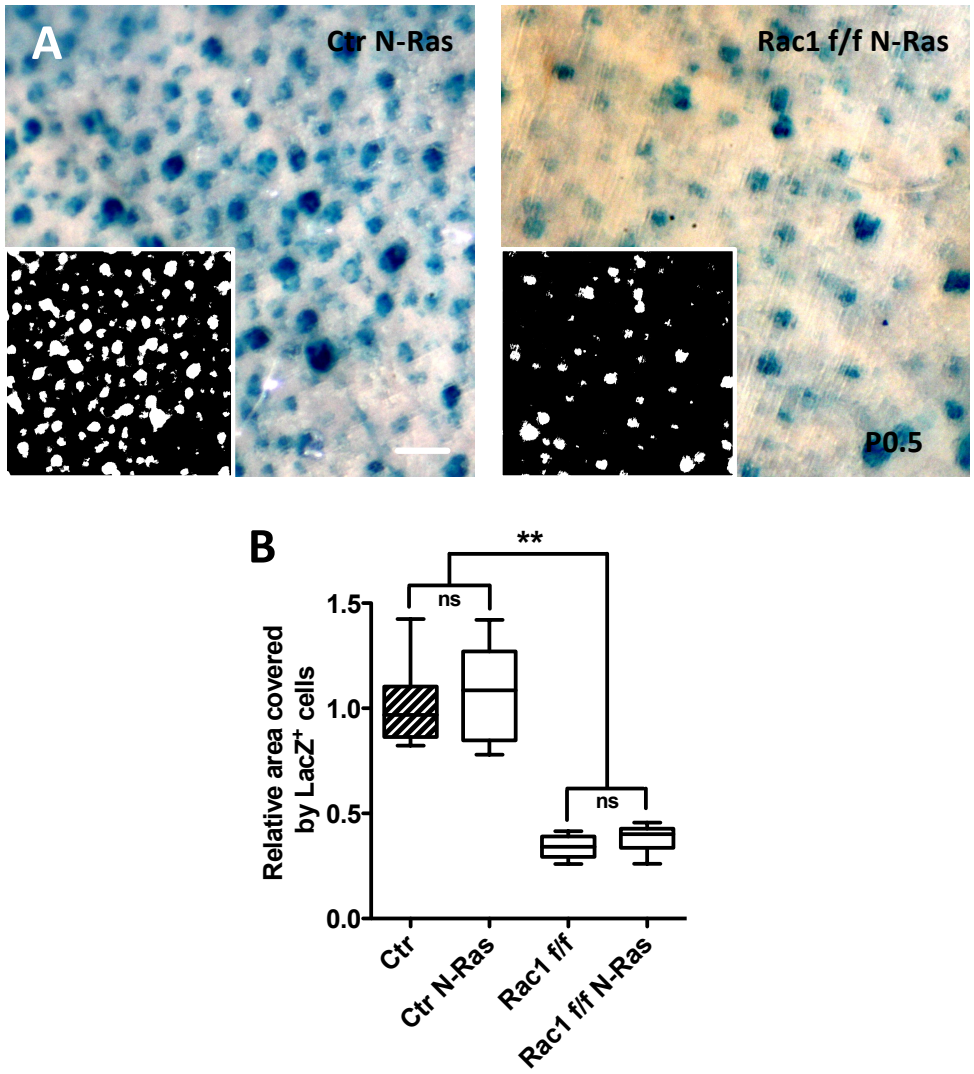

Figure 5.4 Expression of N-Ras^{Q61K} in the melanocyte lineage doesn't rescue the effect of loss of Rac1 on melanocytes number in new born pups. (A) Representative images of β-galactosidase stained skin samples taken from dorsal side of DCT::LacZ Tyr::N-Ras$^{Q61K+/o}$ control (left) and DCT::LacZ Tyr::N-Ras$^{Q61K+/o}$ Rac1 f/f Tyr::Cre$^{+/o}$ (right) newborn pups at P0.5. Representative images of threshold area covered by melanocytes (white squared). (H) Relative area covered by melanocytes per image for DCT::LacZ control, DCT::LacZ Tyr::N-Ras$^{Q61K+/o}$ control, DCT::LacZ Rac1 f/f Tyr::Cre$^{+/o}$ and DCT::LacZ Tyr::N-Ras$^{Q61K+/o}$ Rac1 f/f Tyr::Cre$^{+/o}$. Data derived from five images per skin sample from at least 3 pups from three different litters. Lower quartile, median, and upper quartile are shown. **, P< 0.01 by t-test. The scale bar is 100μm.

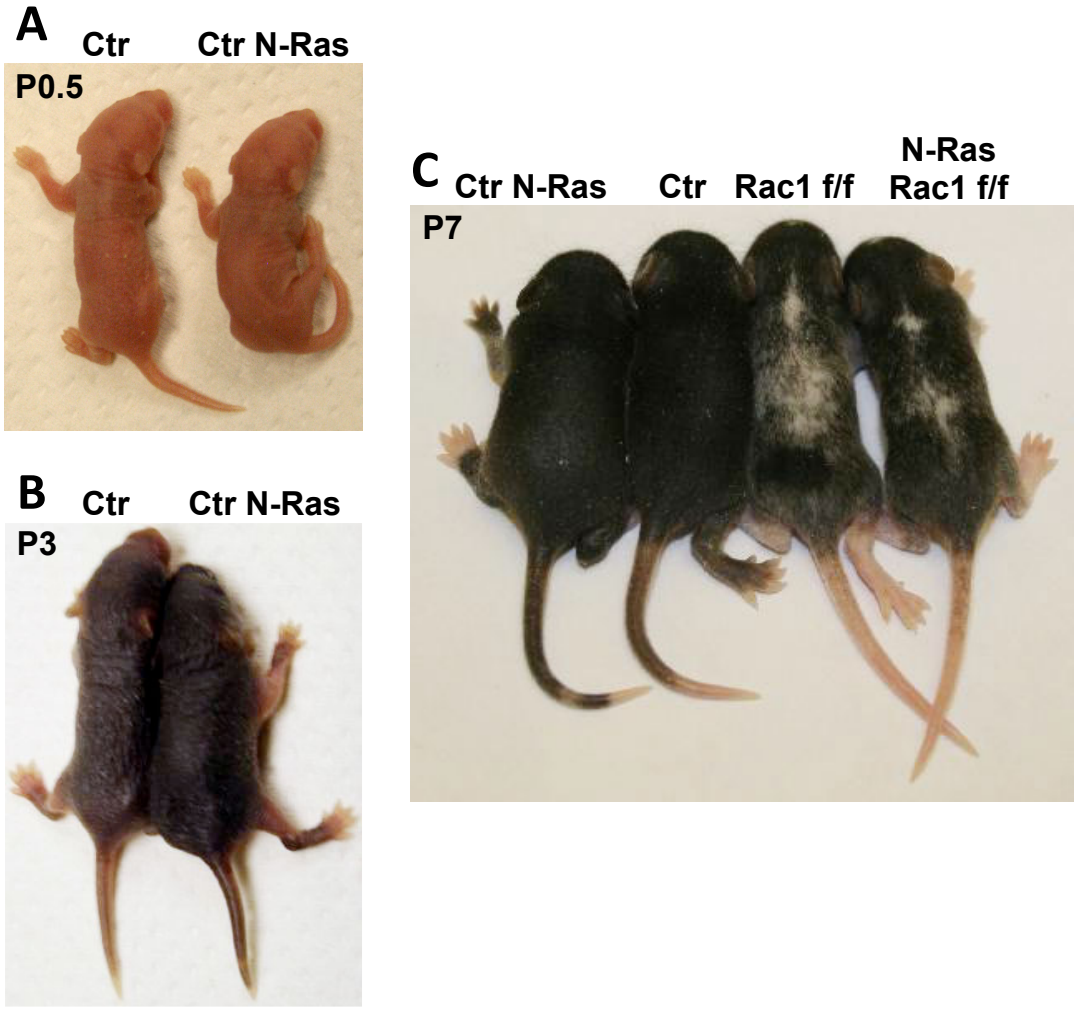

Figure 5.5 Expression of Tyr::N-Ras^{Q61K} in mice induce skin hyperproliferation after birth. Representative images of dorsal skin colour of control and Tyr::N-Ras$^{Q61K+/o}$ control mice on P0.5 (A) and P3 (B). (C) Representative images of dorsal skin of control and Tyr::N-Ras$^{Q61K+/o}$ control, Rac1 f/f Tyr::Cre$^{+/o}$ and Tyr::N-Ras$^{Q61K+/o}$ Rac1 f/f Tyr::Cre$^{+/o}$ mice on P7.

defects caused by loss of Rac1 are not compensated for by activated N-Ras and N-Ras hyperactivation in a normal or Rac-depleted background has no detectable effect on melanoblast motility during embryogenesis.

5.3.2 Rac1 is required for activated N-Ras induced hyperproliferation of epidermal/dermal melanocytes *in vivo*

I have demonstrated within this chapter that expression of activated N-Ras does not play a role within melanoblast migration and proliferation during embryogenesis and Tyr::N-Ras$^{Q61K+/o}$ Rac1 f/f Tyr::Cre$^{+/o}$ mice revealed no rescue on hypopigmentation. However, careful inspection of pigmented area of P14 Tyr::N-Ras$^{Q61K+/o}$ Rac1 f/f Tyr::Cre$^{+/o}$ mice revealed that the coat colour were lighter than Tyr::N-Ras$^{Q61K+/o}$ control mice (Figure 5.1), indicating a possible growth defect of melanocytes. Histological analysis of distribution of melanocytes using pigmented dorsal skin from Tyr::N-Ras$^{Q61K+/o}$ Rac1 f/f Tyr::Cre$^{+/o}$ showed excess melanocytes in hair follicle (Figure 5.10B), which also found in Tyr::N-Ras$^{Q61K+/o}$ control mice (Figure 5.10A). However, In Tyr::N-Ras$^{Q61K+/o}$ control mice, melanocytes accumulated in epidermis/dermis and throughout the fatty tissue (Figure 5.10A). Interestingly, We did not see any melanocytes in the dermis in skin taken from Tyr::N-Ras$^{Q61K+/o}$ Rac1 f/f Tyr::Cre$^{+/o}$ mice (Figure 5.10B). Together, these data indicate that Rac1 is required for Tyr::N-Ras$^{Q61K+/o}$ induced epidermal/dermal localization of melanocytes.

5.3.3 Expression of N-Ras^{Q61K} promotes survival of epidermal/dermal melanocytes via Rac1

I have demonstrated that the melanocyte distribution in dermis/epidermis was not affected by expression active N-Ras^{Q61K} during embryogenesis, therefore the appearance of epidermal/dermal melanocytes in active N-Ras^{Q61K} control mice could either be due to better survival of residual epidermal melanocytes after birth, or migration of melanocytes from hair follicle to dermis during hair

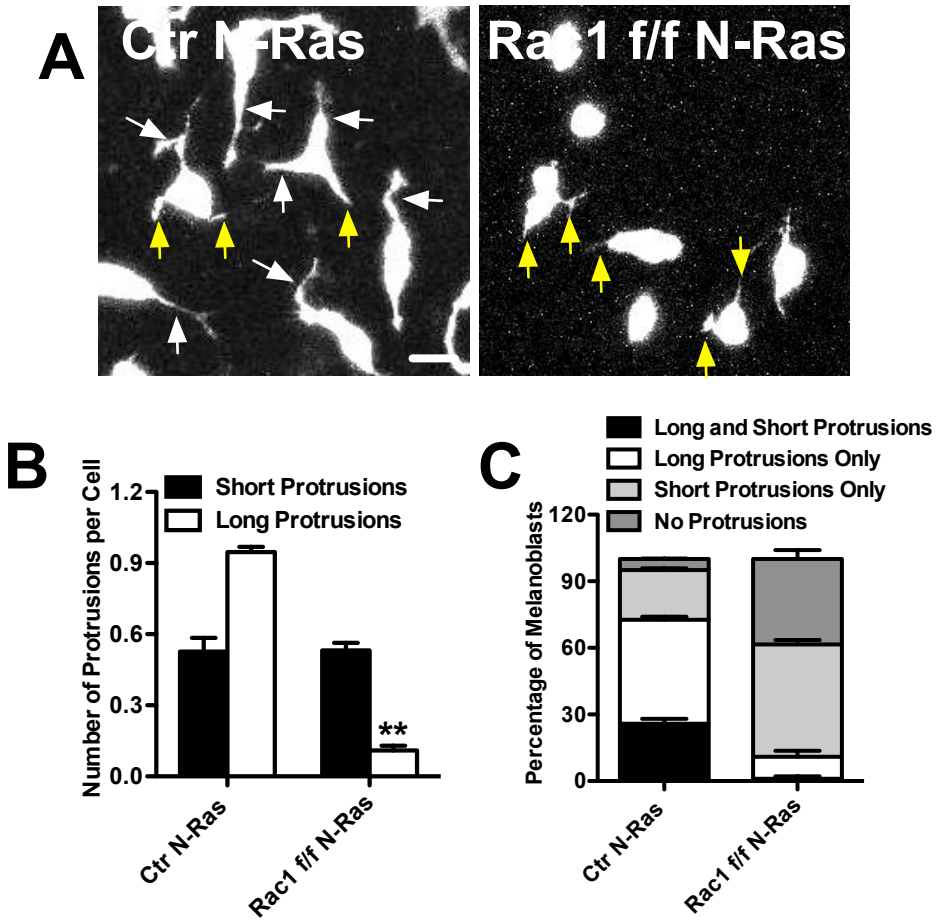

Figure 5.6. Expression of N-Ras^{Q61K} did not rescue protrusion defects caused by deletion of Rac1. (A) Combined Z-stack images (1µm depth) of melanoblasts in skin explants from Z/EG$^{+/o}$ Tyr::N-Ras$^{Q61K+/o}$ Tyr::Cre$^{+/o}$ control and Z/EG$^{+/o}$ Tyr::N-Ras$^{Q61K+/o}$ Rac1 f/f Tyr::Cre$^{+/o}$ embryos. Long protrusions and short protrusions are white and yellow arrowed respectively. (B) Number of long/short protrusions per melanoblast n>60 cells per explant >= 3 explants per genotype. (C) Proportion of melanoblasts with long/short protrusions. Error bars indicate Mean ± SEM. **, P< 0.01, by t-test. Scale bar is 10µm.

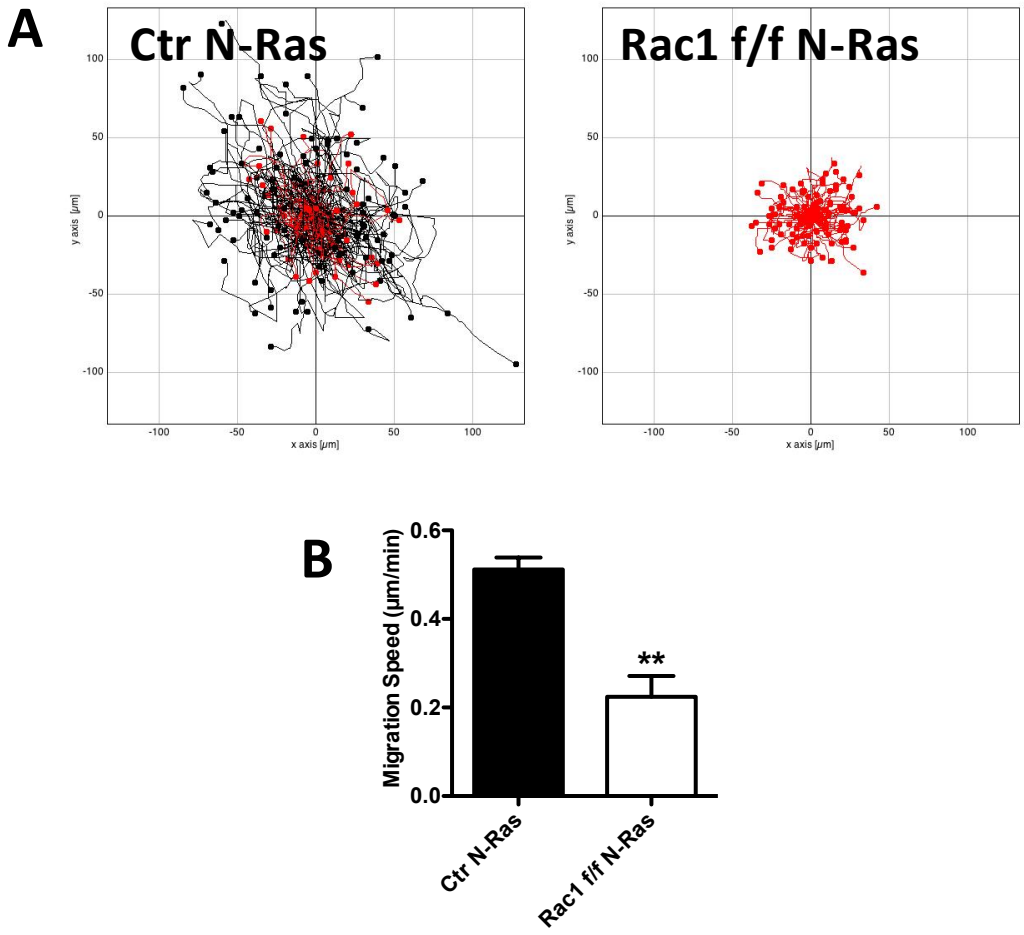

Figure 5.7. Expression of N-Ras^{Q61K} did not rescue migration defects caused by deletion of Rac1. (A) 3 hr tracks of individual melanoblast migration in skin explants, black tracks indicated migrated faster than average control, red indicates slower. (B) Migration speed. >300 melanoblasts from three explants were randomly selected. Error bars indicate Mean ± SEM. **, P< 0.01, by t-test.

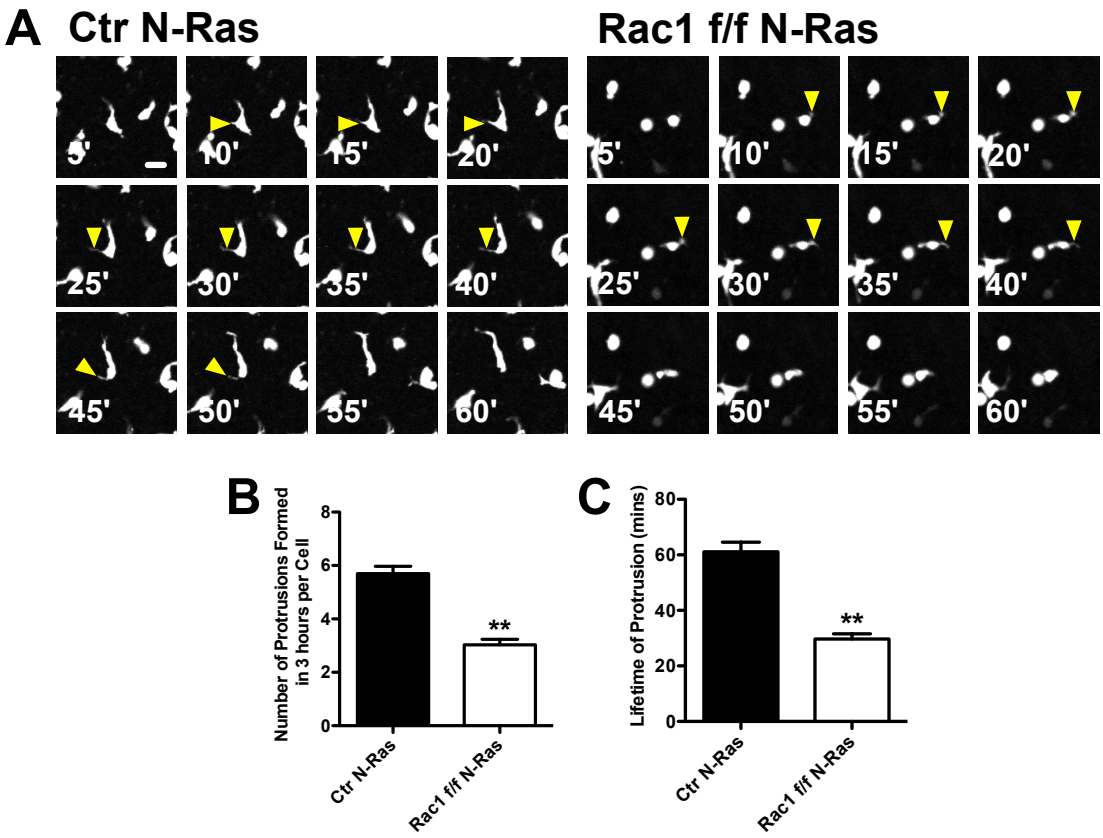

Figure 5.8. Expression of N-Ras^{Q61K} did not rescue lifetime and frequency of protrusion defects caused by deletion of Rac1.(A) Live cell imaging of protrusion dynamics in explants. Images captured every 5 min, yellow arrows - protrusions. (B) Frequency of protrusion formation. (C) Lifetime of actively growing protrusions formed in 20 cells per explant from >= 3 explants. Error bars indicate Mean ± SEM. **, P< 0.01, by t-test. Scale bar is 10μm.

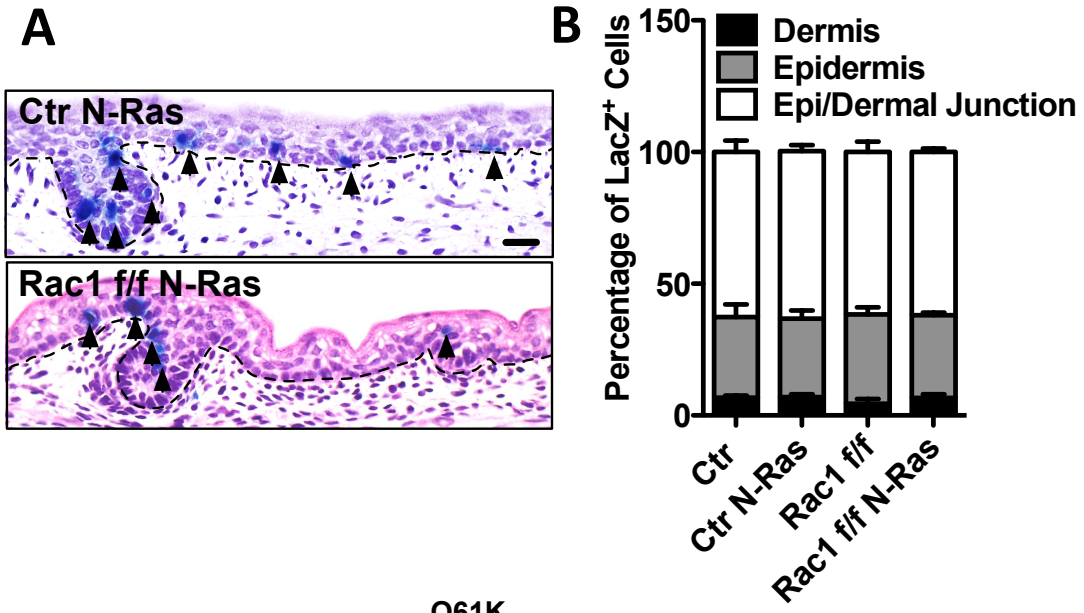

Figure 5.9 Expression of N-Ras^{Q61K} in the melanocyte does not affect melanoblast migration from dermis to epidermis. (A) Images show the localization of melanoblasts in E15.5 DCT::LacZ Tyr::N-Ras^{Q61K} control and Tyr::N-Ras^{Q61K}Rac1 f/f Tyr::Cre$^{+/o}$ embryos. (B) Quantification of localization of melanoblast in E15.5 DCT::LacZ control, Tyr::N-Ras^{Q61K} control, Rac1 f/f Tyr::Cre $^{+/o}$ and Tyr::N-Ras^{Q61K}Rac1 f/f Tyr::Cre$^{+/o}$ embryos. More then 200 cells were examined per embryo from at least three embryos for each genotype. Melanoblasts are black arrowed. Black dot lines in each picture represent the epi/dermal junction. Scale bar is 20μm.

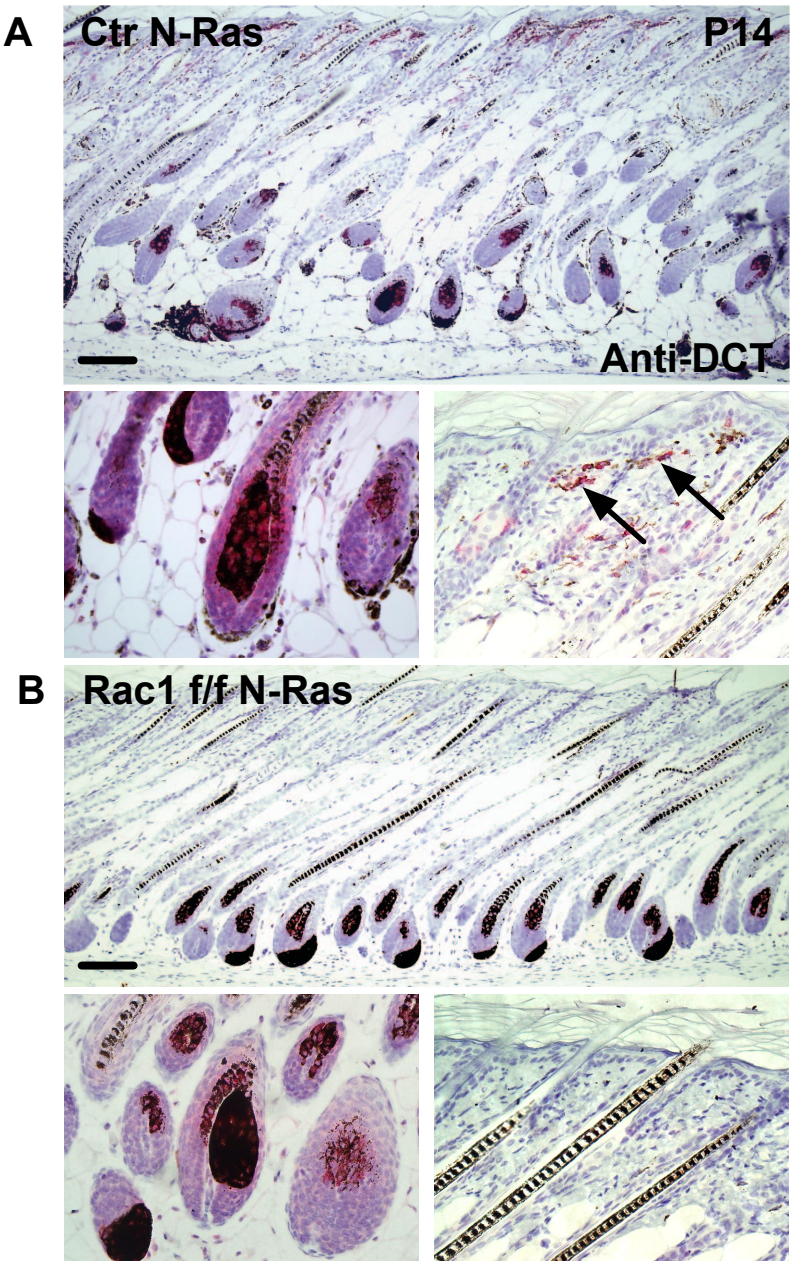

Figure 5.10 Rac1 is required for N-Ras^{Q61K} induced survival of dermal melanocytes in mice. Immunohistochemical analysis of dorsal skin from P14 Tyr::N-Ras^{Q61K} control (A) and Tyr::N-Ras^{Q61K}Rac1 f/f Tyr::Cre$^{+/o}$ (B) mice with anti-DCT to detect melanocytes. High magnification images of hair follicle and dermis were shown Example of typical pocket of excess dermal melanocytes in Ctr N-Ras mouse is black arrowed. Scale bars 100μm.

follicle morphogensis. In order to study how active N-Ras^{Q61K} induces melanocyte localization in dermis and how Rac1 deletion affects this, the first hair follicle cycle was tracked by taking dorsal skin from control, Tyr::N-Ras$^{Q61K+/o}$ control and Tyr::N-Ras$^{Q61K+/o}$ Rac1 f/f Tyr::Cre$^{+/o}$ mice at day 0.5, 3, 5, 14, and 21. The skin were then sectioned and stained with DCT antibody to analyse the distribution of melanocytes (Figure 5.11 and 5.12). In both control and Tyr::N-Ras$^{Q61K+/o}$ Rac1 f/f Tyr::Cre$^{+/o}$ mice, melanocytes in the epidermis gradually disappeared from day 0.5 to day 3 (Figure 5.11A and 5.12). However, in Tyr::N-Ras$^{Q61K+/o}$ control mice, melanocytes in epidermis survived from day 0.5 and number of melanocytes in epidermis increased as the mouse getting older (5.11B), indicating that expression of N-Ras^{Q61K} promotes melanocyte survival in epidermis/dermis and Rac1 is required for this.

Although Rac1 is required for N-Ras^{Q61K} promoted melanocyte survival in the epidermis/dermis, melanocytes hyperproliferation during anagen phase was found in the hair follicle of both Tyr::N-Ras$^{Q61K+/o}$ control mice and Tyr::N-Ras$^{Q61K+/o}$ Rac1 f/f Tyr::Cre$^{+/o}$ mice. This suggest that expression of Tyr::N-Ras$^{Q61K+/o}$ promotes melanocyte proliferation in hair follicles and Rac1 has a very little role during this process.

It has been shown that the transition from anagen to telogen is an apoptosis-driven process that leads to shortening of the hair follicle length by about 70% due to the well-coordinated apoptotic death of the vast majority of follicular keratinocytes, and during this process, most of the follicular melancytes undergo apoptosis (Sharov et al., 2005). Consistent with this, we found that in the telogen phase of the first hair follicle cycle (day 21), only the permanent part of the hair follicles remained in dorsal skin taken from control mice (Figure 5.11A). Although, the lower part of hair follicles in Tyr::N-Ras$^{Q61K+/o}$ control mouse have already degenerated, most of follicular melanocytes can still be found in the place corresponding to earlier hair bulbs, together with continuous accumulation of melanocytes in epidermis/dermis (Figure 5.11B). Interestingly, these follicular melanocytes can no longer be maintained if Rac1 is deleted (Figure 5.12). Together, these data suggest that active N-Ras

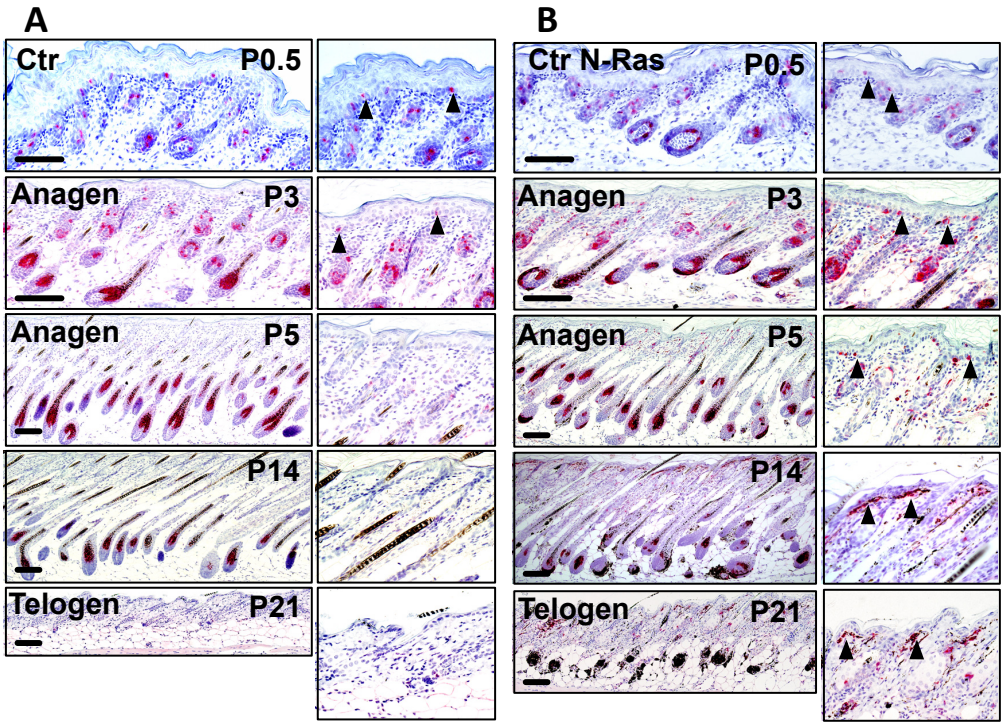

Figure 5.11. Expression of N-Ras^{Q61K} promote survival of dermal melanocytes in mice. Immunohistochemical analysis of dorsal skin from Ctr (A) and Ctr N-Ras (B) mice at P0.5, P3, P5, P14 and p21 with anti-DCT to detect melanocytes. Example of dermal melanocytes are black arrowed. Scale bars 100μm.

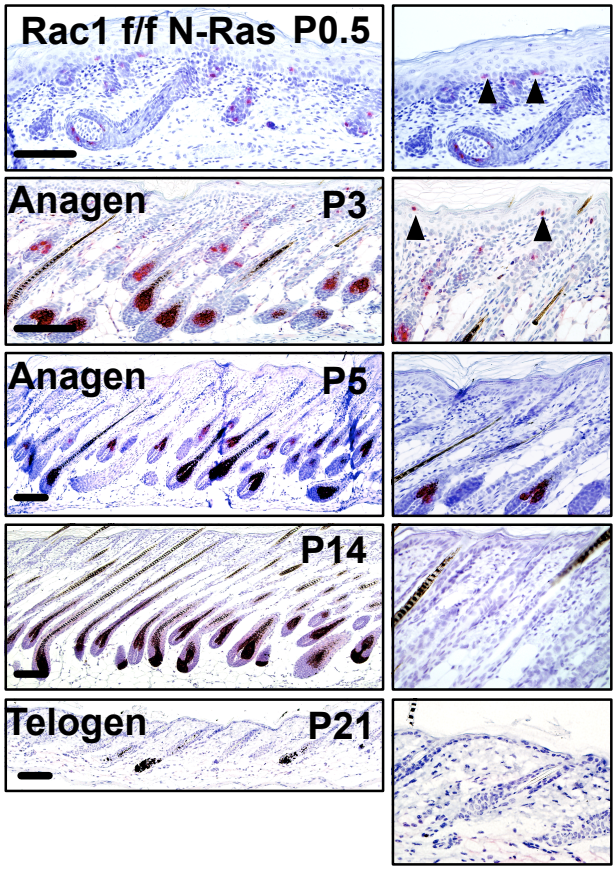

Figure 5.12. Deletion of Rac in meanocytes results gradually loss of dermal melanocytes in N-Ras^{Q61K} background. Immunohistochemical analysis of dorsal skin from Ctr and Ctr N-Ras mice at P0.5, P3, P5, P14 and p21 with anti-DCT to detect melanocytes. Example of dermal melanocytes are black arrowed. Scale bars 100μm.

protects follicular melanocytes from undergoing apoptosis during hair follicle degeneration, which is dependent on Rac1.

5.4 Discussion

5.4.1 Activated N-Ras doesn't compensate for loss of Rac1 in either migration or proliferation during embryogenesis

Since around 20% of human melanomas acquire N-Ras^{Q61K}, we wondered whether expression of activated N-Ras would compensate for loss of Rac1 for growth, motility defects. Knockdown of Rac1 in melanoma cells caused a block in NFkB activity that resulted in defective proliferation in vitro and in tumour xenografts (Bauer et al., 2007), suggesting that Rac1 might be important downstream of Ras in tumorigenesis. Additionally, in a K-Ras induced lung cancer model, loss of Rac1 prevented tumor formation (Kissil et al., 2007), indicating also the importance of Rac in mediating the downstream effects of Ras on proliferation. We were surprised that expression of activated N-Ras in melanoblasts didn't increase the number of melanoblasts and motility parameters during embryogenesis, indicating that these pathways are already running at a high level during embryogensis and Ras is likely already active during embryogenesis, so adding more active Ras doesn't greatly change proliferation rates.

5.4.2 Rac1 is required for activated N-Ras induced survival of dermal melanocytes

Animals expressing activated N-Ras under control of tyrosinase promoter accumulate more melanocytes in their dermis and in the hair follicles than normal mice. Interestingly, Rac1 deletion in melanocytes results in loss of dermal melanocytes in a similar fashion as normal mice, suggesting that Rac1 plays a very important role downstream of N-Ras in regulating melanocyte survival. However, it is still unclear how the epidermal/dermal melanocytes disappeared from skin during the first a few days after the mouse was born,

as we failed to detect any apoptotic melanocyte in dermis with cleaved caspase-3 antibody in both P0.5 and P3 skin sections (data not shown). It could be possible that the removal of epidermal/dermal melanocytes is due to infiltration of macrophages.

Kit signaling via KitL is known to trigger proliferation and survival via activation of Ras via MAPK/ERK signaling (Mackenzie et al., 1997) and PI3 kinase signaling. It has also been shown that KitL accumulated in the hair bulbs of anagen hair follicles with very little or no expression in the epidermis (Peters et al., 2003). This may explain why in normal mice, melanocytes cannot survive in the epidermis, which is probably due to the low concentration of KitL in epidermis. However, expression of activated N-Ras^{Q61K} in the melanocyte may overcome the requirement of KitL, thus promote melanocyte survival and proliferation by activating the downstream targets in a Kit independent manner, which is dependent on Rac1 (Figure 5.13 and 5.14). It will be of interest to see if the Rac1 function can be compensated by ectopic expression of KitL in epidermis (Kunisada et al., 1998).

Similar to Tyr::N-Ras^{Q61K} control mice, we observed more melanocyte accumulation in hair bulbs during anagen in Tyr::N-Ras$^{Q61K+/o}$ Rac1 f/f Tyr::Cre$^{+/o}$ mice. We think this is probably due to the fact that the transgenic mouse line we used has both ectopic expression of N-Ras^{Q61K} and endogenous expression of wildtype N-Ras. Therefore, in the presence of KitL in hair bulbs, the endogenous N-Ras and activated N-Ras^{Q61K} may work synergistically to promote the proliferation and survival of melanocytes (Figure 5.13 and 5.14). Rac1 deletion does seem to affect melanocytes in the hair bulbs, although it is unclear whether Rac1 is required for melanocyte proliferation in hair bulbs as it is impossible to determine the number of melanocytes in each hair bulb by skin sections. However, during the telogen of hair cycle, KitL concentration dropped and hair bulb degenerated (Peters et al., 2002; Sharov et al., 2005), which leads to turning off endogenous N-Ras pathway in melanocytes. Therefore, hair follicle melanocyte in Tyr::N-Ras^{Q61K} control mice would survived as they do in dermis and deletion of Rac1 in these hair follicle melanocyte may disrupt activated N-Ras^{Q61K} induced

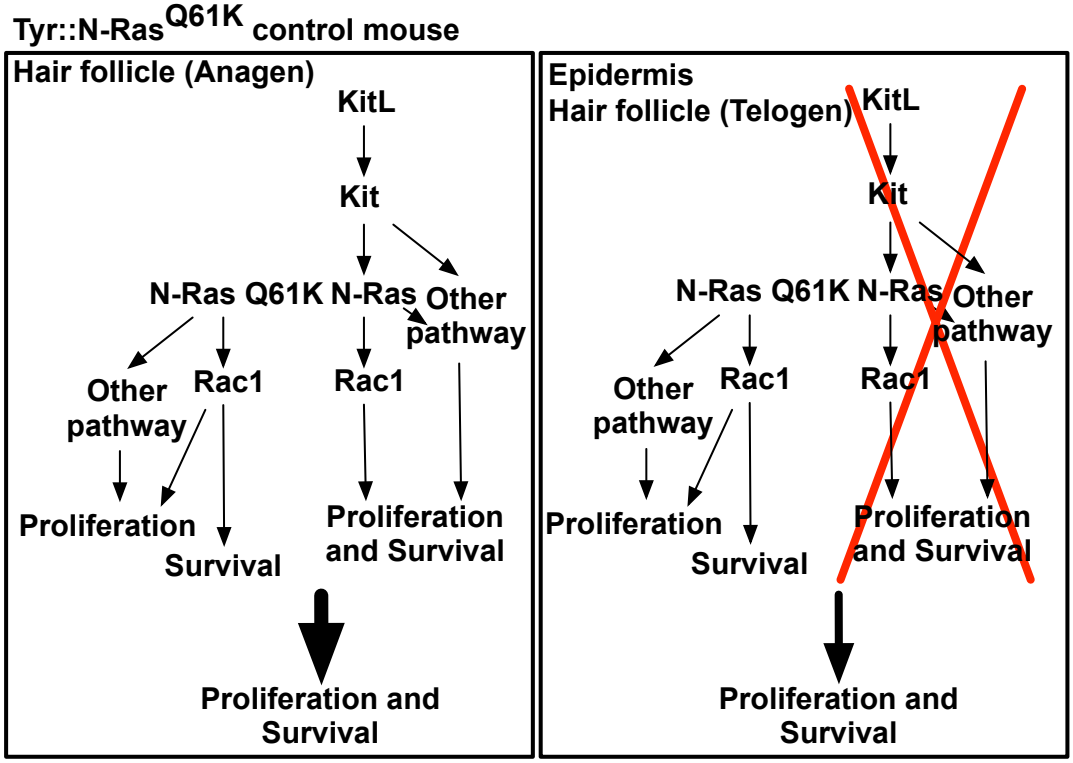

Figure 5.13. A predicted model for how Tyr::N-Ras^{Q61K} induces melanocyte survival in the Kit independent pathway. Left: Expression of KitL is concentrated in hair bulbs during anagen of hair cycle, which activate endogenous N-Ras signling pathway via Kit receptor. expression of activated N-Ras^{Q61K} work synergistically with endogenous N-Ras to promoter melanocyte hyperporliferation. Right: In epidermis/dermis or telogen of hair cycle, expression of KitL is very low or absent. The endogenous Kit pathway is off. The melanocytes are protected by expression of atcive N-Ras^{Q61K}.

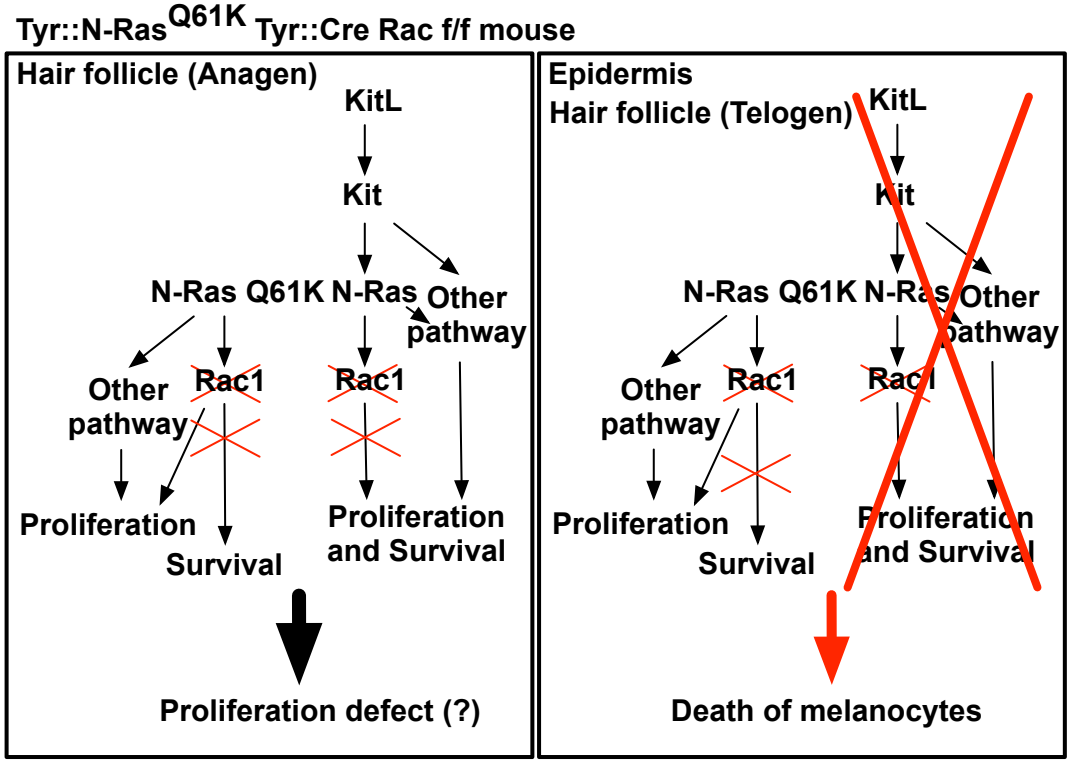

Figure 5.14. A predicted model for how Rac1 affects Tyr::N-Ras^{Q61K} induced melanocyte survival. Left: Expression of KitL is concentrated in hair bulbs during anagen of hair cycle, which activate endogenous N-Ras signling pathway via Kit receptor. Expression of activated N-Ras^{Q61K} work synergistically with endogenous N-Ras to promoter melanocyte hyperporliferation. Rac1 is dispensable for this process probably because another survival pathway can be activated by Kit signaling thus bypass the requirement for Rac1. Right: In epidermis/dermis or telogen of hair cycle, expression of KitL is very low or absent. The endogenous Kit pathway is off. The melanocytes are protected only by atcive N-Ras^{Q61K} induced survival pathway, which is probably through Rac1. Thus, deletion of Rac1 cause loss of melanocyte in dermis.

survival pathway, thus result loss of melanocytes in a similar fashion as wildtype mice (Figure 5.13 and 5.14).

In conclusion, Rac1 is important downstream target of activated N-Ras^{Q61K} for melanocyte survival in skin, but that N-Ras doesn't contribute detectably to migration or cytokinesis independently of Rac1 during embrogensis.

Chapter VI
Summary and future directions

6.1 Summary

One of the key aims of this thesis was to investigate the potential molecular mechanism for how fascin increases the invasiveness of cancer cells, which is mainly described in **Chapter 3**.

In order to address this question, I used immunofluorescence or expression of GFP-tagged fasicn to show for the first time that fascin is an integral component of invadopodia in multiple cancer cell types.

In addition, I have used siRNA or shRNA to successfully knockdown fascin in several different cancer cell lines. Consistent with previous studies, I showed that fascin is required for filopodia formation. Remarkably, I demonstrated that fascin is also required for the assembly of the actin cytoskeleton in invadopodia as well as for the degradation of matrix on different types of matrix.

I also confirmed the effect of phosphorylation of fascin S39 on filopodia formation and further demonstrated that phosphorylation of fascin at S39 also contributes to regulation at invadopodia.

Furthermore, I observed invadopodia similar to a comet-like organization resembling bacteria-propelling actin tails. I used immunofluorescence and 3D reconstruction to show that Arp2/3 complex, cortactin, and fascin localized throughout comet heads and tails, whereas N-WASP concentrated mostly in the head. In addition to these, I also found several other filopodia proteins (IRSP53, IRTKS and mDia2) at invadopodia. This implies the first time that invadopodia might be a hybrid structure containing both actin branches and bundles.

Next, I demonstrated that fascin is a very stable component of invadopodia and its presence enhance the stability of actin structures at invadopodia both in molecular level using FRAP or in cell level using live time imaging.

Finally, I implicate the important role of fascin in invasive migration into collagen I-Matrigel gels and 3D collagen degradation particularly in cell types

that use a degradation dependent, elongated mesenchymal type of motility (Figure 6.1). I demonstrated that fascin but not N-WASP or MT1-MMP is required for formation filopod-like protrusions in 3D. However, knockdown N-WASP or MT1-MMP which is required for invaopodia formation significantly reduce cell invasion and collagen degradation in 3D but not filopod-like protrusions, which implicate existence of two types of protrusion in 3D: the stable actin-based proteolytic structures similar to invadopodia in 2D and filopod-like protrusions. Therefore I have elucidated for the first time that fascin promotes long protrusions in 3D and stabilizes actin in invadopodia and that this enhanced stability allows for more efficient invasion by mesenchymal cells, both in 2D and in 3D.

Secondly, another aim of this thesis was to examine the role of Rac1 in melanoblast migration during mouse embryogenesis, which is mainly described in **Chapter 4.**

To assess the functions of Rac1 in the melanocyte lineage *in vivo*, I generated conditional Rac1 knockout mice by crossed mice carrying a floxed allele of Rac1 with mice expressing Cre recombinase under control of the tyrosinase promoter. I showed in the first time that Rac1 is required for normal pigmentation and melanocyte distribution in mice. Which is due to both migration and proliferation defect during embryogensis. In order to study the function of Rac1 in melanoblast migration in real time. I crossed mice carrying a Z/EG or GFP-Lifeact flox transgene onto the Tyr::Cre Rac1 f/f background. I showed that melanoblasts extend long dynamic pseudopodia containing both actin and microtubules and they squeeze between epidermal keratinocytes. In addition, I demonstrated that Rac1 is required for the formation of long pseudopodia in melanoblast, which also dependent on microtubules and Arp2/3 complex driven actin assembly.

In addition, I demonstrated here that Rac1 is not essential for melanoblast migration, which is different to previously published model with cells undergo collective migration (Murphy and Montell, 1996; Migeotte *et al.*, 2010).

I also implicated that melanoblasts can initiate short

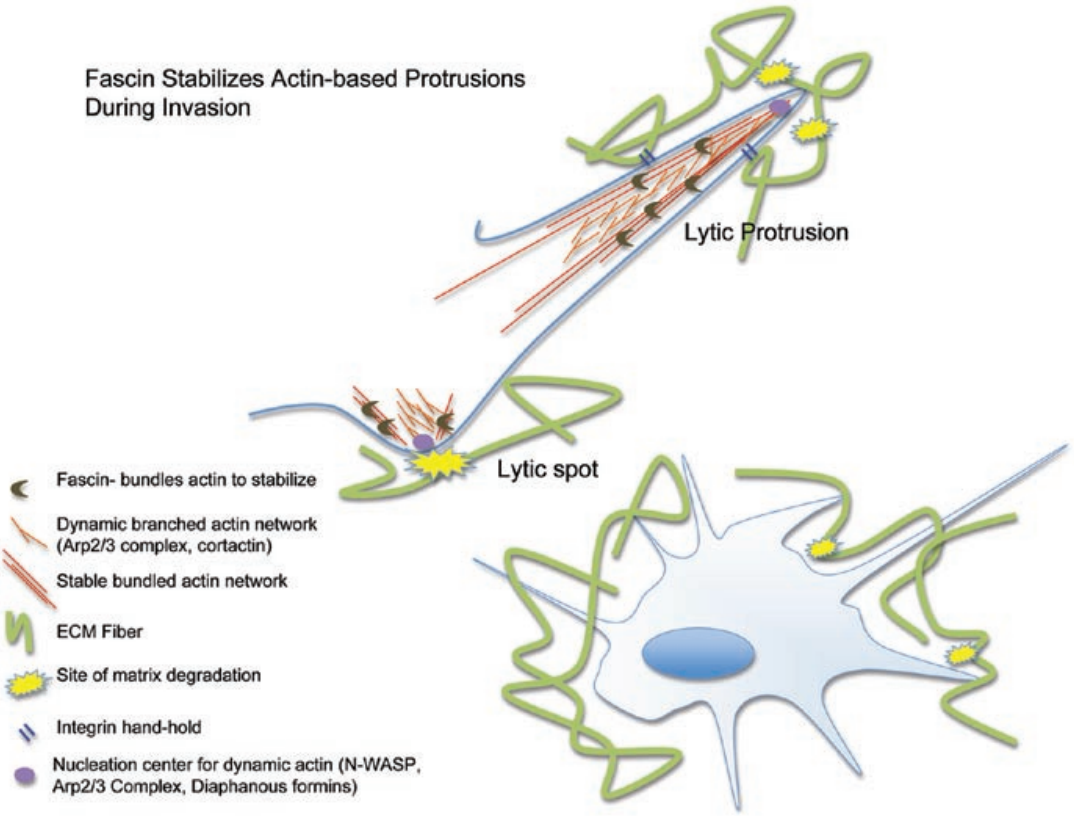

Figure 6.1. Model of fascin stabilizing actin bundles in an invasive cell migrating in the 3D environment of the tumor stroma. Sites of matrix remodeling can occur at protrusions or at other sites along the periphery of the cell, wherever the extracellular matrix (ECM) impedes cell migration and thus needs to be degraded for the cell to pass through. CHL-1 melanoma cells made both actin-rich spots and long thin filopod-like protrusions in matrigel-collagen gels. We have drawn fascin-actin bundles here close to the plasma membrane, but it is possible that they could form a core inside of the branched actin networks rather than or additional to a shell around them. arp2/3 complex and cortactin contribute to formation of branched actin networks and may also assist in membrane trafficking to and from sites of ECM remodeling. Integrins allow the cell to grab and pull against the ECM to aid migration.

actin-based protrusions independently of Rac1, Arp2/3 complex or myosin, suggest a novel form of actin dynamics, which drive melanoblast migration in a Rac1 independent manner in vivo.

Furthermore, I demonstrated that Rac1 is not absolutely required for long protrusion formation or polarized motility when myosin activity is suppressed. However, Rac1 controls the rate of protrusion initiation and the balance between myosin-based retraction and Rac-based pseudopod initiation governs translocation (Figure 6.2).

I further suggest that melanoblast migration across basement membrane from dermis to epidermis is not an invasive process. I demonstrated here that deletion of either Rac1 or N-WASP had no effect on melanoblast dermis/epidermis distribution, although both Rac1 and N-WASP play an important role formation of invadopodia and cell invasion.

Moreover, I investigated melanoblast growth defect both in vivo. I have shown that growth defect in Rac1 depleted melanoblast mainly due to defect in Brdu incorporation and proliferation, but not cell cycle exit or apoptosis. I also confirm this in vitro, and further suggested that the growth defect is mainly due defect in G1 to S phase transition.

Unexpectedly, I found that Rac1 depleted melanoblast undergo cytokinesis almost 3 fold slower then control melanoblast. However, in vitro, I did not notice any defects on Rac1 depleted melanocyte undergo cytokinesis, implicated a special requirements for Rac in cytokinesis in vivo than in culture dishes.

Overall my results here revealed a novel mode of in vivo migration controlled by Rac1 that is important for normal development and likely in melanoma.

Lastly, in **Chapter 5** I investigated the role of Rac1 downstream of active N-Ras^{Q61K} in melanoblast during embryogenesis and melanocytes proliferation in adult mice. I have shown that active N-Ras^{Q61K} did not contribute significantly to melanoblast migration and proliferation during embryogenesis.

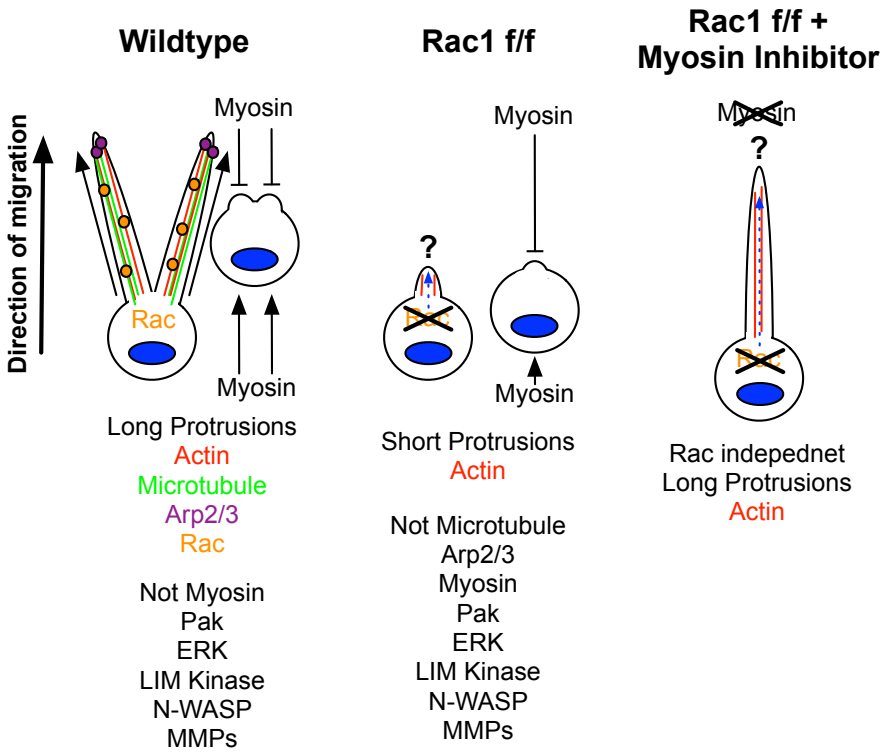

Figure 6.2. Model of melanoblast motility in epidermis.
In wild type melanoblasts, Rac1 positively regulates the frequency of initiation of long pseudopods, which promote migration speed and allow cells to change their direction of migration. Scar/WAVE and Arp2/3 complex drive actin assembly for long pseudopod extension, which also depends on microtubule dynamics. Myosin contractility balances the extension of long pseudopods by effecting retraction and allowing force generation for movement through the complex 3D epidermal environment. In absence of Rac1, melanoblasts mainly use short stubs for migration. the short stubs are distinct from blebs and are driven by actin assembly, but are independent of Rac1, Arp2/3 complex, myosin or microtubules. when myosin was inhibited in absence of Rac1, Rac1 was no longer required for long pseudopod generation; but it still strongly controlled the frequency of generation of long pseudopods.

I also demonstrate here that Rac1 is required for activated N-Ras ^{Q61K} induced dermal melanocytes survival *in vivo*, which implicated Rac1 as an important target downstream of activated N-Ras^{Q61K}.

6.2 Future directions

6.2.1 Function of fascin in pancreatic cancer formation and metastasis

Although the work present here clearly demonstrates that fascin is important for cancer cell invasion in vitro, it is still unclear whether fascin is required for tumour invasion and metastasis in vivo, and if it is, which stage of the metastasis is specially fascin dependent.

Pancreatic cancer is malignant neoplasm of the pancreas. The prognosis is relatively poor; the three-year survival rate is now about thirty percent, but less than 5 percent of those diagnosed are still alive five years after diagnosis and complete remission is still rather rare (Ghaneh et al., 2007). Pancreatic cancer is sometimes called a "silent killer" because early pancreatic cancer often does not cause symptoms and because of late diagnosis and frequent invading local structures or metastasizing makes the pancreatic cancer very difficult to be cured by surgery. Therefore, preventing pancreatic cancer metastasis is very important to improve the treatment and survival rate.

Fascin is upregulated in different types of invasive cancer, and its expression level often correlates with patient survival rate (Machesky and Li, 2010). My preliminary data using human pancreatic PDAC TMA revealed a strong correlation of high expression of fascin with poor survival (Figure 6.3), high tumour grade and high vascular invasion (Data not shown).

It has been shown that LSL-KrasG12D/+;LSL-Trp53R172H/+;Pdx-1-Cre transgenic mice model frequently develop metastatic pancreatic tumors (jen PNAS). I noticed that in this model, fascin is not expressed in normal

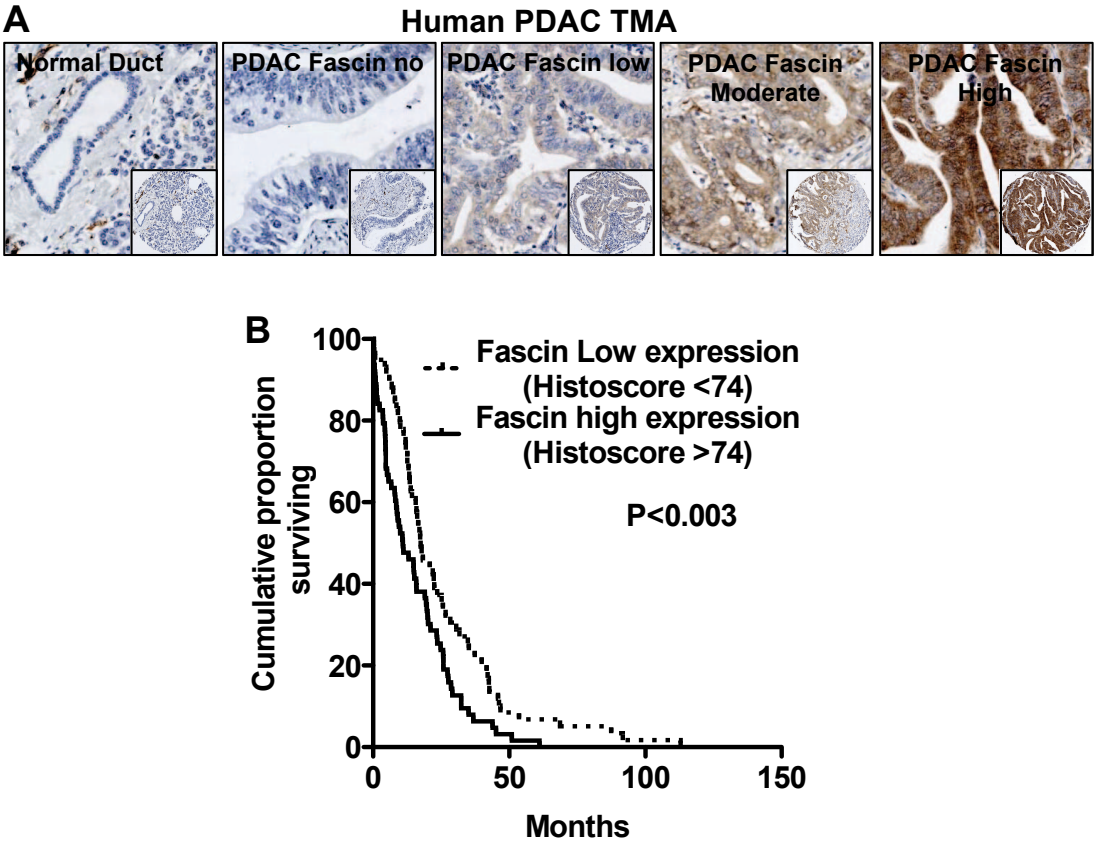

Figure 6.3. Fascin expression in human PDAC.
IHC analysis of tumour assay in human PDAC. representative images are shown for normal duct, PDAC with no, low, moderate and high staining (B) Kaplan&endashMeier analyses showing cases with high Fascin expression (n = 63) have poorer outcomes compared to those with low expression (n = 59; P < 0.003) Histoscore Median=74

pancreas (Figure. 6.4A) and PanINs (Figure 6.4B), but upregulated in both primary PDAC invasive front and metastatic PDAC to the liver (Figure 6.4C-H). Recently, fascin knockout mice have been generated, which develop normally with minor defect in neural development (Yamakita et al., 2009).

It would be interesting to see whether fascin is important for pancreatic cancer formation and metastasis in vivo by crossing the *LSL-Kras*G12D/+*;LSL-Trp53*R172H/+*;Pdx-1-Cre* transgenic mice into fascin null background. A recent paper showed that macroketone, the synthetic homologue of migrastatin can stop cancer cell becoming localized to lung in tail vein injection xenografts (Chen et al., 2010). Thus it will be interesting to see if macroketone can stop metastasis in this transgenic mice model.

In addition, fascin null PDAC cell lines derived from such genetically engineered mouse model could be used to significantly strengthen the role of fascin in tumour invasion. For example, typical invasion assay (without helping by fibroblast for invasion) (Li et al., 2010), organotypic assay (with help by fibroblast for invasion) (Gaggioli et al., 2007) with fascin null PDAC cell lines can be compared with wildtype, phospho-mimic and dephospho-mimic fascin rescued cell line to see if putting fascin back can promote invasion and if actin bundling activity of fascin is critical for this.

Furthermore, in vivo metastasis experiment by tail vein or intraspleen injection of cells into nude mice can be used to compare the metastatic ability of those cell line to localize to the lung or liver. Subcutaneous injection can be used to determine whether fascin also promote cancer cell growth and if this is dependent on actin bundling activity of fascin.

6.2.2 Function of Rac1 in melanoma progression and metastasis

Previous study showed that Tyr::N- $Ras^{Q61K+/o}$ $INK4a^{-/-}$ transgenic mice develop metastatic melanoma at about 6 months (Figure 6.5) (Ackermann et

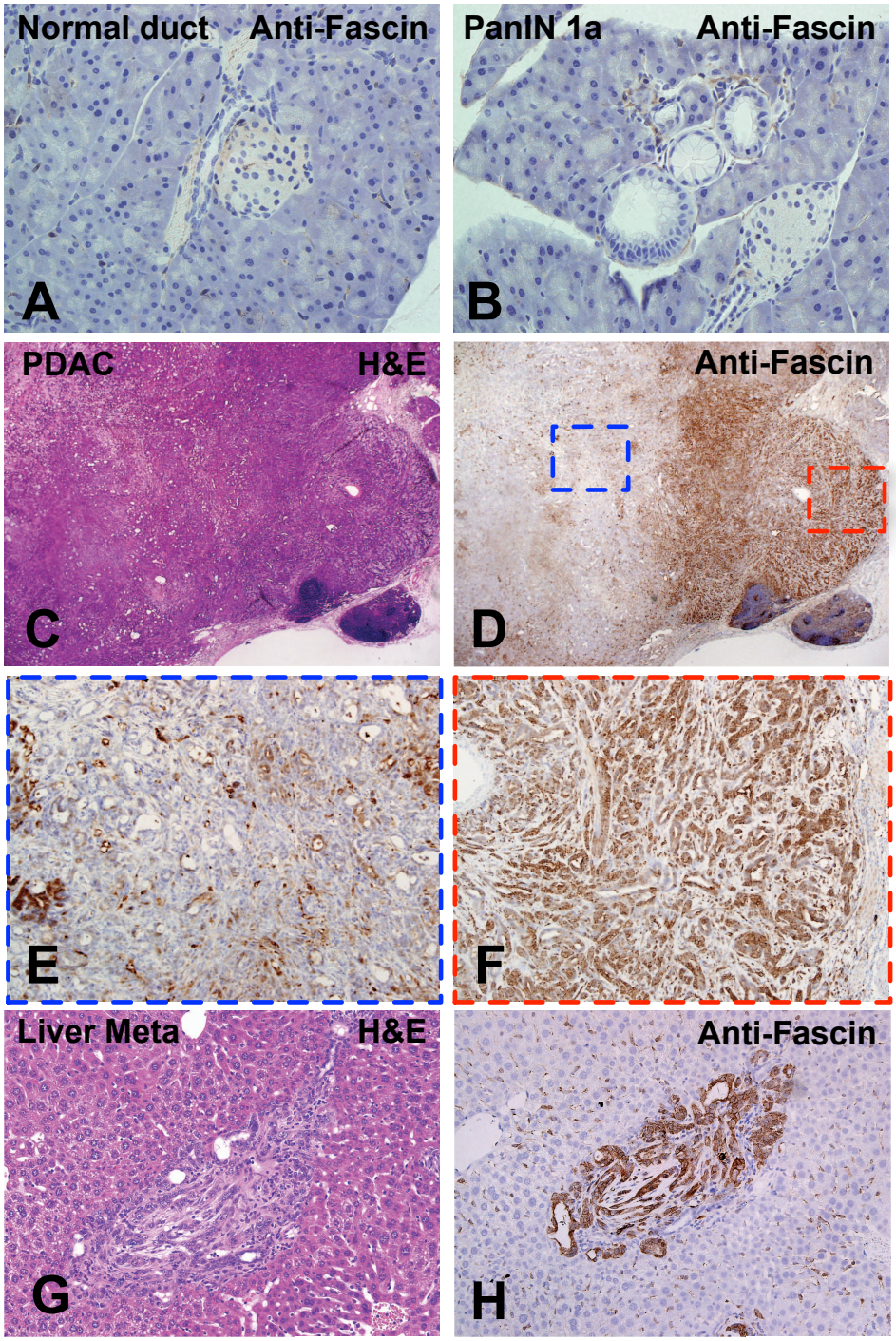

Figure 6.4. Fascin is upregulated in invasive front and metastasis in mouse PDAC
All sections from LSL-KrasG12D/+;LSL-Trp53R172H/+;Pdx-1-Cre pancreatic cancer mouse model. Fascin is not expressed in (A) normal duct and (B) PanIN 1a. In PDAC, fascin expression is strongly upregulated at invasive front (D and F) compared to centre of the tumour (D and E). The centre (E) and invasive front (F) of the tumour are enlarged. fascin upregulation also found in liver metastasis (G and H). Sections stained with H&E and fascin antibody as indicated.

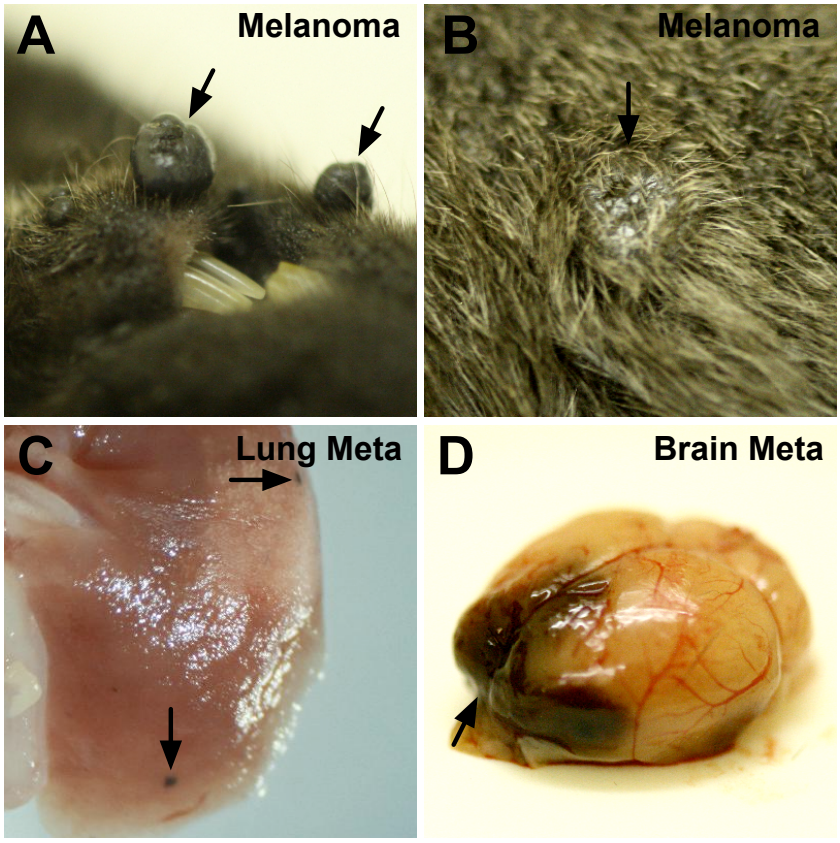

Figure 6.5.Tyr::N- Ras$^{Q61K+/o}$ INK4a-/- transgenic mice frequently develop metastatic melanoma.
Primary melanoma formed near mouth (A) and on the back (B) of the mouse. Lung metastasis (C) and brain metastasis (D) were detected frequently in these mice. melanoma cells are black arrowed.

al., 2005). In addition, Rac1 is required for initiation of lung cancer formation in a K-Ras^{G12D} activated lung cancer model (Kissil et al., 2007). However, whether Rac1 is required for cancer metastasis is still unknown. We would like to first confirm whether Rac1 would affect melanoma formation in our melanoma model, Two cohorts can be compared on melanoma formation: Tyr::N- Ras$^{Q61K+/o}$ INK4a$^{-/-}$ Tyr::CreER$^{+/o}$ Rac1 f/f and Tyr::N- Ras$^{Q61K+/o}$ INK4a$^{-/-}$ Tyr::CreER$^{o/o}$ Rac1 f/f treated with tamoxifen. In addition, we would like to further address whether Rac1 is required for melanoma progression and metastasis in vivo. In this case, tomoxifen or vehicle will be applied to Tyr::N- Ras$^{Q61K+/o}$ INK4a$^{-/-}$ Tyr::CreER$^{+/o}$ Rac1 f/f mice when melanoma is formed. Furthermore, in vitro or in vivo invasion and metastasis experiments (as discuss above) using melanoma cells derived from these tumours will be used to further confirm the role of Rac1 in tumour progression and metastasis.

6.3 Conclusion

The work presented here has further characterized the regulation of actin bundling protein fascin and has identified novel functional roles for this protein in regulation of invadopodia stability and matrix degradation during cancer cell invasion. Furthermore, this study has revealed a novel mode of in vivo migration by mouse melanoblast during embryogenesis, and identified a novel role of Rac1 as regulator of dynamics of protrusions that is important for normal melanoblast migration. Moreover, this study also shed some light on a novel mode of actin dynamics that drive melanoblast migration independent of Rac1 and implicated that melanoblast migration through basement membrane is not invasive. Finally, I provided evidence to show that Rac1 is important for melanoblast proliferation and cytokinesis, and Rac1 play a role in constitutively active N-Ras^{Q61K} induced melanocyte hyperproliferation in mice, which together suggested a important role of Rac1 in normal development and likely in melanoma. Together, these results add to the convincing body of evidence implying a significant role for Fascin and Rac1 in the regulation of cell morphology, motility and tumour cell invasion, embryogensis and tumourigenesis.

Reference

Ackermann, J., Frutschi, M., Kaloulis, K., McKee, T., Trumpp, A., and Beermann, F. (2005). Metastasizing Melanoma Formation Caused by Expression of Activated N-RasQ61K on an INK4a-Deficient Background. Cancer Research *65*, 4005-4011.

Adams, J.C. (2004a). Fascin protrusions in cell interactions. Trends Cardiovasc Med *14*, 221-226.

Adams, J.C. (2004b). Roles of fascin in cell adhesion and motility. Curr Opin Cell Biol *16*, 590-596.

Adams, J.C., Clelland, J.D., Collett, G.D.M., Matsumura, F., Yamashiro, S., and Zhang, L. (1999). Cell-Matrix Adhesions Differentially Regulate Fascin Phosphorylation. Mol Biol Cell *10*, 4177-4190.

Akin, O., and Mullins, R.D. (2008). Capping Protein Increases the Rate of Actin-Based Motility by Promoting Filament Nucleation by the Arp2/3 Complex. Cell *133*, 841-851.

Aratyn, Y.S., Schaus, T.E., Taylor, E.W., and Borisy, G.G. (2007). Intrinsic Dynamic Behavior of Fascin in Filopodia. Mol Biol Cell *18*, 3928-3940.

Artym, V.V., Zhang, Y., Seillier-Moiseiwitsch, F.o., Yamada, K.M., and Mueller, S.C. (2006). Dynamic Interactions of Cortactin and Membrane Type 1 Matrix Metalloproteinase at Invadopodia: Defining the Stages of Invadopodia Formation and Function. Cancer Research *66*, 3034-3043.

Ayala, I., Baldassarre, M., Caldieri, G., and Buccione, R. (2006). Invadopodia: A guided tour. European Journal of Cell Biology *85*, 159-164.

Ayala, I., Baldassarre, M., Giacchetti, G., Caldieri, G., Tete, S., Luini, A., and Buccione, R. (2008). Multiple regulatory inputs converge on cortactin to control invadopodia biogenesis and extracellular matrix degradation. J Cell Sci *121*, 369-378.

Baldassarre, M., Ayala, I., Beznoussenko, G., Giacchetti, G., Machesky, L.M., Luini, A., and Buccione, R. (2006). Actin dynamics at sites of extracellular matrix degradation. European Journal of Cell Biology *85*, 1217-1231.

Baldassarre, M., Pompeo, A., Beznoussenko, G., Castaldi, C., Cortellino, S., McNiven, M.A., Luini, A., and Buccione, R. (2003). Dynamin Participates in Focal Extracellular Matrix Degradation by Invasive Cells. Mol Biol Cell *14*, 1074-1084.

Bauer, N.N., Chen, Y.-W., Samant, R.S., Shevde, L.A., and Fodstad, O. (2007). Rac1 activity regulates proliferation of aggressive metastatic melanoma. Experimental Cell Research *313*, 3832-3839.

Baxter, L.L., Hou, L., Loftus, S.K., and Pavan, W.J. (2004). Spotlight on Spotted Mice: A Review of White Spotting Mouse Mutants and Associated Human Pigmentation Disorders. Pigment Cell Research *17*, 215-224.

Baynash, A.G., Hosoda, K., Giaid, A., Richardson, J.A., Emoto, N., Hammer, R.E., and Yanagisawa, M. (1994). Interaction of endothelin-3 with endothelin-B receptor is essential for development of epidermal melanocytes and enteric neurons. Cell *79*, 1277-1285.

Benitah, S.A., Frye, M., Glogauer, M., and Watt, F.M. (2005). Stem Cell Depletion Through Epidermal Deletion of Rac1. Science *309*, 933-935.

Bennett, D.C., and Lamoreux, M.L. (2003). The Color Loci of Mice – A Genetic Century. Pigment Cell Research *16*, 333-344.

Benvenuti, F., Hugues, S., Walmsley, M., Ruf, S., Fetler, L., Popoff, M., Tybulewicz, V.L.J., and Amigorena, S. (2004). Requirement of Rac1 and Rac2 Expression by Mature Dendritic Cells for T Cell Priming. Science *305*, 1150-1153.

Betz, T., Koch, D., Lim, D., and K‰s, J.A. (2009). Stochastic Actin Polymerization and Steady Retrograde Flow Determine Growth Cone Advancement. Biophysical Journal *96*, 5130-5138.

Bianco, A., Poukkula, M., Cliffe, A., Mathieu, J., Luque, C.M., Fulga, T.A., and Rorth, P. (2007). Two distinct modes of guidance signalling during collective migration of border cells. Nature *448*, 362-365.

Bowden, E.T., Barth, M., Thomas, D., Glazer, R.I., and Muelle, S.C. (1999). An invasion-related complex of cortactin, paxillin and PKC associates with invadopodia at sites of extracellular matrix degradation. Oncogene *18*, 4440-4449.

Bowden, E.T., Onikoyi, E., Slack, R., Myoui, A., Yoneda, T., Yamada, K.M., and Mueller, S.C. (2006). Co-localization of cortactin and phosphotyrosine identifies active invadopodia in human breast cancer cells. Experimental Cell Research *312*, 1240-1253.

Braga, V.M.M., Betson, M., Li, X., and Lamarche-Vane, N. (2000). Activation of the Small GTPase Rac Is Sufficient to Disrupt Cadherin-dependent Cell-Cell Adhesion in Normal Human Keratinocytes. Mol Biol Cell *11*, 3703-3721.

Braga, V.M.M., Del Maschio, A., Machesky, L., and Dejana, E. (1999). Regulation of Cadherin Function by Rho and Rac: Modulation by Junction Maturation and Cellular Context. Mol Biol Cell *10*, 9-22.

Braga, V.M.M., Machesky, L.M., Hall, A., and Hotchin, N.A. (1997). The Small GTPases Rho and Rac Are Required for the Establishment of Cadherin-dependent Cell‚ÄìCell Contacts. The Journal of Cell Biology *137*, 1421-1431.

Brieher, W.M., Coughlin, M., and Mitchison, T.J. (2004). Fascin-mediated propulsion of Listeria monocytogenes independent of frequent nucleation by the Arp2/3 complex. The Journal of Cell Biology *165*, 233-242.

Britsch, S., Goerich, D.E., Riethmacher, D., Peirano, R.I., Rossner, M., Nave, K.-A., Birchmeier, C., and Wegner, M. (2001). The transcription factor Sox10

is a key regulator of peripheral glial development. Genes & Development *15*, 66-78.

Bryan, J., Edwards, R., Matsudaira, P., Otto, J., and Wulfkuhle, J. (1993). Fascin, an echinoid actin-bundling protein, is a homolog of the Drosophila singed gene product. Proceedings of the National Academy of Sciences of the United States of America *90*, 9115-9119.

Buccione, R., Caldieri, G., and Ayala, I. (2009). Invadopodia: specialized tumor cell structures for the focal degradation of the extracellular matrix. Cancer and Metastasis Reviews *28*, 137-149.

Buccione, R., Orth, J.D., and McNiven, M.A. (2004). Foot and mouth: podosomes, invadopodia and circular dorsal ruffles. Nat Rev Mol Cell Biol *5*, 647-657.

Bugyi, B., and Carlier, M.-F. (2010). Control of Actin Filament Treadmilling in Cell Motility. Annual Review of Biophysics *39*, 449-470.

Cable, J., Jackson, I.J., and Steel, K.P. (1995). Mutations at the W locus affect survival of neural crest-derived melanocytes in the mouse. Mechanisms of Development *50*, 139-150.

Caldieri, G., and Buccione, R. (2010). Aiming for invadopodia: organizing polarized delivery at sites of invasion. Trends in Cell Biology *20*, 64-70.

Calle, Y., Burns, S., Thrasher, A.J., and Jones, G.E. (2006). The leukocyte podosome. European Journal of Cell Biology *85*, 151-157.

Campellone, K.G., and Welch, M.D. (2010). A nucleator arms race: cellular control of actin assembly. Nat Rev Mol Cell Biol *11*, 237-251.

Canman, J.C., Lewellyn, L., Laband, K., Smerdon, S.J., Desai, A., Bowerman, B., and Oegema, K. (2008). Inhibition of Rac by the GAP activity of centralspindlin is essential for cytokinesis. Science *322*, 1543-1546.

Cant, K., and Cooley, L. (1996). Single Amino Acid Mutations in Drosophila Fascin Disrupt Actin Bundling Function in Vivo. Genetics *143*, 249-258.

Caswell, P.T., Spence, H.J., Parsons, M., White, D.P., Clark, K., Cheng, K.W., Mills, G.B., Humphries, M.J., Messent, A.J., Anderson, K.I., et al. (2007). Rab25 associates with alpha5beta1 integrin to promote invasive migration in 3D microenvironments. Dev Cell 13, 496-510.

Chambers, A.F., Groom, A.C., and MacDonald, I.C. (2002). Metastasis: Dissemination and growth of cancer cells in metastatic sites. Nat Rev Cancer *2*, 563-572.

Chan, K.T., Cortesio, C.L., and Huttenlocher, A. (2009). FAK alters invadopodia and focal adhesion composition and dynamics to regulate breast cancer invasion. The Journal of Cell Biology *185*, 357-370.

Chang, H.Y., Sneddon, J.B., Alizadeh, A.A., Sood, R., West, R.B., Montgomery, K., Chi, J.-T., Rijn, M.v.d., Botstein, D., and Brown, P.O. (2004). Gene Expression Signature of Fibroblast Serum Response Predicts Human Cancer Progression: Similarities between Tumors and Wounds. PLoS Biol *2*, e7.

Charras, G., and Paluch, E. (2008). Blebs lead the way: how to migrate without lamellipodia. Nat Rev Mol Cell Biol *9*, 730-736.

Chen, L., Yang, S., Jakoncic, J., Zhang, J.J., and Huang, X.-Y. (2010a). Migrastatin analogues target fascin to block tumour metastasis. Nature *464*, 1062-1066.

Chen, W.-T. (1989). Proteolytic activity of specialized surface protrusions formed at rosette contact sites of transformed cells. Journal of Experimental Zoology *251*, 167-185.

Chen, Z., Borek, D., Padrick, S.B., Gomez, T.S., Metlagel, Z., Ismail, A.M., Umetani, J., Billadeau, D.D., Otwinowski, Z., and Rosen, M.K. (2010b). Structure and control of the actin regulatory WAVE complex. Nature *468*, 533-538.

Chiyomaru, T., Enokida, H., Tatarano, S., Kawahara, K., Uchida, Y., Nishiyama, K., Fujimura, L., Kikkawa, N., Seki, N., and Nakagawa, M. (2010). miR-145 and miR-133a function as tumour suppressors and directly regulate FSCN1 expression in bladder cancer. Br J Cancer *102*, 883-891.

Chou, M.M., and Blenis, J. (1996). The 70 kDa S6 Kinase Complexes with and Is Activated by the Rho Family G Proteins Cdc42 and Rac1. Cell *85*, 573-583.

Chou, S.-W., Hwang, P., Gomez, G., Fernando, C.A., West, M.C., Pollock, L.M., Lin-Jones, J., Burnside, B., and McDermott, B.M., Jr. (2011). Fascin 2b Is a Component of Stereocilia that Lengthens Actin-Based Protrusions. PLoS ONE *6*, e14807.

Christofori, G., and Semb, H. (1999). The role of the cell-adhesion molecule E-cadherin as a tumour-suppressor gene. Trends in Biochemical Sciences *24*, 73-76.

Chrostek, A., Wu, X., Quondamatteo, F., Hu, R., Sanecka, A., Niemann, C., Langbein, L., Haase, I., and Brakebusch, C. (2006). Rac1 Is Crucial for Hair Follicle Integrity but Is Not Essential for Maintenance of the Epidermis. Mol Cell Biol *26*, 6957-6970.

Clark, E.S., and Weaver, A.M. (2008). A new role for cortactin in invadopodia: Regulation of protease secretion. European Journal of Cell Biology *87*, 581-590.

Clark, E.S., Whigham, A.S., Yarbrough, W.G., and Weaver, A.M. (2007). Cortactin Is an Essential Regulator of Matrix Metalloproteinase Secretion and

Extracellular Matrix Degradation in Invadopodia. Cancer Research *67*, 4227-4235.

Cook, S., and McCormick, F. (1994). Ras blooms on sterile ground. Nature *369*, 361-362.

Corbetta, S., Gualdoni, S., Albertinazzi, C., Paris, S., Croci, L., Consalez, G.G., and de Curtis, I. (2005). Generation and Characterization of Rac3 Knockout Mice. Mol Cell Biol *25*, 5763-5776.

Corbetta, S., Gualdoni, S., Ciceri, G., Monari, M., Zuccaro, E., Tybulewicz, V.L.J., and de Curtis, I. (2009). Essential role of Rac1 and Rac3 GTPases in neuronal development. The FASEB Journal *23*, 1347-1357.

Cortesio, C.L., Chan, K.T., Perrin, B.J., Burton, N.O., Zhang, S., Zhang, Z.-Y., and Huttenlocher, A. (2008). Calpain 2 and PTP1B function in a novel pathway with Src to regulate invadopodia dynamics and breast cancer cell invasion. The Journal of Cell Biology *180*, 957-971.

Coso, O.A., Chiariello, M., Yu, J.-C., Teramoto, H., Crespo, P., Xu, N., Miki, T., and Silvio Gutkind, J. (1995). The small GTP-binding proteins Rac1 and Cdc42regulate the activity of the JNK/SAPK signaling pathway. Cell *81*, 1137-1146.

Croker, B.A., Tarlinton, D.M., Cluse, L.A., Tuxen, A.J., Light, A., Yang, F.-C., Williams, D.A., and Roberts, A.W. (2002). The Rac2 Guanosine Triphosphatase Regulates B Lymphocyte Antigen Receptor Responses and Chemotaxis and Is Required for Establishment of B-1a and Marginal Zone B Lymphocytes. The Journal of Immunology *168*, 3376-3386.

Cukierman, E., Pankov, R., Stevens, D.R., and Yamada, K.M. (2001). Taking Cell-Matrix Adhesions to the Third Dimension. Science *294*, 1708-1712.

Czuchra, A., Wu, X., Meyer, H., van Hengel, J., Schroeder, T., Geffers, R., Rottner, K., and Brakebusch, C. (2005). Cdc42 Is Not Essential for Filopodium Formation, Directed Migration, Cell Polarization, and Mitosis in Fibroblastoid Cells. Mol Biol Cell *16*, 4473-4484.

Darnel, A.D., Behmoaram, E., Vollmer, R.T., Corcos, J., Bijian, K., Sircar, K., Su, J., Jiao, J., Alaoui-Jamali, M.A., and Bismar, T.A. (2009). Fascin Regulates Prostate Cancer Cell Invasion and Is Associated with Metastasis and Biochemical Failure in Prostate Cancer. Clinical Cancer Research *15*, 1376-1383.

De Arcangelis, A., Georges-Labouesse, E., and Adams, J.C. (2004). Expression of fascin-1, the gene encoding the actin-bundling protein fascin-1, during mouse embryogenesis. Gene Expression Patterns *4*, 637-643.

Deacon, S.W., Beeser, A., Fukui, J.A., Rennefahrt, U.E.E., Myers, C., Chernoff, J., and Peterson, J.R. (2008). An Isoform-Selective, Small-Molecule Inhibitor Targets the Autoregulatory Mechanism of p21-Activated Kinase. Chemistry & biology *15*, 322-331.

Delmas, V., Beermann, F., Martinozzi, S., Carreira, S., Ackermann, J., Kumasaka, M., Denat, L., Goodall, J., Luciani, F., Viros, A.*, et al.* (2007). β-Catenin induces immortalization of melanocytes by suppressing p16INK4a expression and cooperates with N-Ras in melanoma development. Genes & Development *21*, 2923-2935.

Delmas, V., Martinozzi, S., Bourgeois, Y., Holzenberger, M., and Larue, L. (2003). Cre-mediated recombination in the skin melanocyte lineage. genesis *36*, 73-80.

Delorme, V., Machacek, M., DerMardirossian, C., Anderson, K.L., Wittmann, T., Hanein, D., Waterman-Storer, C., Danuser, G., and Bokoch, G.M. (2007). Cofilin activity downstream of Pak1 regulates cell protrusion efficiency by organizing lamellipodium and lamella actin networks. Dev Cell *13*, 646-662.

Didsbury, J., Weber, R.F., Bokoch, G.M., Evans, T., and Snyderman, R. (1989). Rac, a novel ras-related family of proteins that are botulinum toxin substrates. Journal of Biological Chemistry *264*, 16378-16382.

Diekmann, D., Abo, A., Johnston, C., Segal, A.W., and Hall, A. (1994). Interaction of Rac with p67phox and regulation of phagocytic NADPH oxidase activity. Science *265*, 531-533.

Dos Remedios, C.G., Chhabra, D., Kekic, M., Dedova, I.V., Tsubakihara, M., Berry, D.A., and Nosworthy, N.J. (2003). Actin Binding Proteins: Regulation of Cytoskeletal Microfilaments. Physiological Reviews *83*, 433-473.

Dovas, A., and Couchman, J.R. (2005). RhoGDI: multiple functions in the regulation of Rho family GTPase activities. Biochem J *390*, 1-9.

Downward, J. (2003). Targeting RAS signalling pathways in cancer therapy. Nat Rev Cancer *3*, 11-22.

Duchek, P., Somogyi, K., Jekely, G., Beccari, S., and Rorth, P. (2001). Guidance of cell migration by the Drosophila PDGF/VEGF receptor. Cell *107*, 17-26.

Edwards, D.C., Sanders, L.C., Bokoch, G.M., and Gill, G.N. (1999). Activation of LIM-kinase by Pak1 couples Rac/Cdc42 GTPase signalling to actin cytoskeletal dynamics. Nat Cell Biol *1*, 253-259.

Fackler, O.T., and Grosse, R. (2008). Cell motility through plasma membrane blebbing. The Journal of Cell Biology *181*, 879-884.

Faix, J. (2002). The actin-bundling protein cortexillin is the downstream target of a Rac1-signaling pathway required for cytokinesis. Journal of Muscle Research and Cell Motility *23*, 765-772.

Fehrenbacher, K., Huckaba, T., Yang, H.-C., Boldogh, I., and Pon, L. (2003). Actin comet tails, endosomes and endosymbionts. J Exp Biol *206*, 1977-1984.

Fournier, A.K., Campbell, L.E., Castagnino, P., Liu, W.F., Chung, B.M., Weaver, V.M., Chen, C.S., and Assoian, R.K. (2008). Rac-dependent cyclin D1 gene expression regulated by cadherin- and integrin-mediated adhesion. J Cell Sci *121*, 226-233.

Friedl, P., Maaser, K., Klein, C.E., Niggemann, B., Krohne, G., and Z√§nker, K.S. (1997). Migration of Highly Aggressive MV3 Melanoma Cells in 3-Dimensional Collagen Lattices Results in Local Matrix Reorganization and Shedding of Œ±2 and Œ≤1 Integrins and CD44. Cancer Research *57*, 2061-2070.

Friedl, P., and Wolf, K. (2003). Tumour-cell invasion and migration: diversity and escape mechanisms. Nat Rev Cancer *3*, 362-374.

Fuchs, S., Herzog, D., Sumara, G., Buchmann-Moller, S., Civenni, G., Wu, X., Chrostek-Grashoff, A., Suter, U., Ricci, R., Relvas, J.B.*, et al.* (2009). Stage-specific control of neural crest stem cell proliferation by the small rho GTPases Cdc42 and Rac1. Cell Stem Cell *4*, 236-247.

Gadea, G., Sanz-Moreno, V., Self, A., Godi, A., and Marshall, C.J. (2008). DOCK10-Mediated Cdc42 Activation Is Necessary for Amoeboid Invasion of Melanoma Cells. Current biology : CB *18*, 1456-1465.

Gaggioli, C., Hooper, S., Hidalgo-Carcedo, C., Grosse, R., Marshall, J.F., Harrington, K., and Sahai, E. (2007). Fibroblast-led collective invasion of carcinoma cells with differing roles for RhoGTPases in leading and following cells. Nat Cell Biol *9*, 1392-1400.

Garcia, R.J., Ittah, A., Mirabal, S., Figueroa, J., Lopez, L., Glick, A.B., and Kos, L. (2007). Endothelin 3 Induces Skin Pigmentation in a Keratin-Driven Inducible Mouse Model. J Invest Dermatol *128*, 131-142.

Gawden-Bone, C., Zhou, Z., King, E., Prescott, A., Watts, C., and Lucocq, J. (2010). Dendritic cell podosomes are protrusive and invade the extracellular matrix using metalloproteinase MMP-14. Journal of Cell Science *123*, 1427-1437.

Geisbrecht, E.R., and Montell, D.J. (2002). Myosin VI is required for E-cadherin-mediated border cell migration. Nat Cell Biol *4*, 616-620.

Geisbrecht, E.R., and Montell, D.J. (2004). A role for Drosophila IAP1-mediated caspase inhibition in Rac-dependent cell migration. Cell *118*, 111-125.

Geissler, E.N., Ryan, M.A., and Housman, D.E. (1988). The dominant-white spotting (W) locus of the mouse encodes the c-kit proto-oncogene. Cell *55*, 185-192.

Ghaneh, P., Costello, E., and Neoptolemos, J.P. (2007). Biology and management of pancreatic cancer. Gut *56*, 1134-1152.

Gimona, M., and Buccione, R. (2006). Adhesions that mediate invasion. The International Journal of Biochemistry & Cell Biology *38*, 1875-1892.

Gimona, M., Buccione, R., Courtneidge, S.A., and Linder, S. (2008). Assembly and biological role of podosomes and invadopodia. Curr Opin Cell Biol *20*, 235-241.

Grüneberg, H. (1953). The relations of microphthalmia and white in the mouse. Journal of Genetics *51*, 359-362.

Gu, Y., Filippi, M.-D., Cancelas, J.A., Siefring, J.E., Williams, E.P., Jasti, A.C., Harris, C.E., Lee, A.W., Prabhakar, R., Atkinson, S.J., *et al.* (2003). Hematopoietic Cell Regulation by Rac1 and Rac2 Guanosine Triphosphatases. Science *302*, 445-449.

Guo, F., Debidda, M., Yang, L., Williams, D.A., and Zheng, Y. (2006). Genetic Deletion of Rac1 GTPase Reveals Its Critical Role in Actin Stress Fiber Formation and Focal Adhesion Complex Assembly. Journal of Biological Chemistry *281*, 18652-18659.

Gupton, S.L., and Gertler, F.B. (2007). Filopodia: The Fingers That Do the Walking. Sci STKE *2007*, re5-.

Haataja, L., Groffen, J., and Heisterkamp, N. (1997). Characterization of RAC3, a Novel Member of the Rho Family. Journal of Biological Chemistry *272*, 20384-20388.

Hall, A. (1998). Rho GTPases and the Actin Cytoskeleton. Science *279*, 509-514.

Hashimoto, Y., Loftis, D.W., and Adams, J.C. (2009). Fascin-1 Promoter Activity Is Regulated by CREB and the Aryl Hydrocarbon Receptor in Human Carcinoma Cells. PLoS ONE *4*, e5130.

Hashimoto, Y., Parsons, M., and Adams, J.C. (2007). Dual Actin-bundling and Protein Kinase C-binding Activities of Fascin Regulate Carcinoma Cell Migration Downstream of Rac and Contribute to Metastasis. Mol Biol Cell *18*, 4591-4602.

Hashimoto, Y., Shimada, Y., Kawamura, J., Yamasaki, S., and Imamura, M. (2004). The prognostic relevance of fascin expression in human gastric carcinoma. Oncology *67*, 262-270.

Hashimoto, Y., Skacel, M., and Adams, J.C. (2005). Roles of fascin in human carcinoma motility and signaling: Prospects for a novel biomarker? The International Journal of Biochemistry & Cell Biology *37*, 1787-1804.

Hashimoto, Y., Skacel, M., Lavery, I.C., Mukherjee, A.L., Casey, G., and Adams, J.C. (2006). Prognostic significance of fascin expression in advanced colorectal cancer: an immunohistochemical study of colorectal adenomas and adenocarcinomas. BMC Cancer *6*, 241.

Heasman, S.J., and Ridley, A.J. (2008). Mammalian Rho GTPases: new insights into their functions from in vivo studies. Nat Rev Mol Cell Biol *9*, 690-701.

Hodgkinson, C.A., Moore, K.J., Nakayama, A., SteingrÌmsson, E., Copeland, N.G., Jenkins, N.A., and Arnheiter, H. (1993). Mutations at the mouse microphthalmia locus are associated with defects in a gene encoding a novel basic-helix-loop-helix-zipper protein. Cell *74*, 395-404.

Hosoda, K., Hammer, R.E., Richardson, J.A., Baynash, A.G., Cheung, J.C., Giaid, A., and Yanagisawa, M. (1994). Targeted and natural (piebald-lethal) mutations of endothelin-B receptor gene produce megacolon associated with spotted coat color in mice. Cell *79*, 1267-1276.

Hotary, K., Li, X.-Y., Allen, E., Stevens, S.L., and Weiss, S.J. (2006). A cancer cell metalloprotease triad regulates the basement membrane transmigration program. Genes & Development *20*, 2673-2686.

Hotchin, N.A., and Hall, A. (1995). The assembly of integrin adhesion complexes requires both extracellular matrix and intracellular rho/rac GTPases. The Journal of Cell Biology *131*, 1857-1865.

Hughes, M.J., Lingrel, J.B., Krakowsky, J.M., and Anderson, K.P. (1993). A helix-loop-helix transcription factor-like gene is located at the mi locus. Journal of Biological Chemistry *268*, 20687-20690.

Hwang, J.-H., Smith, C.A., Salhia, B., and Rutka, J. (2008). The role of fascin in the migration and invasiveness of malignant glioma cells. Neoplasia *10*.

Innocenti, M., Zucconi, A., Disanza, A., Frittoli, E., Areces, L.B., Steffen, A., Stradal, T.E.B., Fiore, P.P.D., Carlier, M.-F., and Scita, G. (2004). Abi1 is essential for the formation and activation of a WAVE2 signalling complex. Nat Cell Biol *6*, 319-327.

Insall, R.H., and Machesky, L.M. (2009). Actin Dynamics at the Leading Edge: From Simple Machinery to Complex Networks. Developmental cell *17*, 310-322.

Ishikawa, R., Sakamoto, T., Ando, T., Higashi-Fujime, S., and Kohama, K. (2003). Polarized actin bundles formed by human fascin-1: their sliding and disassembly on myosin II and myosin V in vitro. Journal of Neurochemistry *87*, 676-685.

Jayo, A., and Parsons, M. (2010). Fascin: A key regulator of cytoskeletal dynamics. The International Journal of Biochemistry & Cell Biology *42*, 1614-1617.

Jordan, S.n.A., and Jackson, I.J. (2000). MGF (KIT Ligand) Is a Chemokinetic Factor for Melanoblast Migration into Hair Follicles. Developmental Biology *225*, 424-436.

Jou, T.-S., and Nelson, J. (1998). Effects of Regulated Expression of Mutant RhoA and Rac1 Small GTPases on the Development of Epithelial (MDCK) Cell Polarity. The Journal of Cell Biology *142*, 85-100.

Kane, R.E. (1975). Preparation and purification of polymerized actin from sea urchin egg extracts. The Journal of Cell Biology *66*, 305-315.

Kano, M., Seki, N., Kikkawa, N., Fujimura, L., Hoshino, I., Akutsu, Y., Chiyomaru, T., Enokida, H., Nakagawa, M., and Matsubara, H. (2010). miR-145, miR-133a and miR-133b: Tumor-suppressive miRNAs target FSCN1 in esophageal squamous cell carcinoma. International Journal of Cancer *127*, 2804-2814.

Kardash, E., Reichman-Fried, M., Maitre, J.-L., Boldajipour, B., Papusheva, E., Messerschmidt, E.-M., Heisenberg, C.-P., and Raz, E. (2010). A role for Rho GTPases and cell-cell adhesion in single-cell motility in vivo. Nat Cell Biol *12*, 47-53.

Kelsh, R.N., Harris, M.L., Colanesi, S., and Erickson, C.A. (2009). Stripes and belly-spots--A review of pigment cell morphogenesis in vertebrates. Seminars in Cell & Developmental Biology *20*, 90-104.

King, J.S., Veltman, D.M., Georgiou, M., Baum, B., and Insall, R.H. (2010). SCAR/WAVE is activated at mitosis and drives myosin-independent cytokinesis. J Cell Sci *123*, 2246-2255.

Kissil, J.L., Walmsley, M.J., Hanlon, L., Haigis, K.M., Bender Kim, C.F., Sweet-Cordero, A., Eckman, M.S., Tuveson, D.A., Capobianco, A.J., Tybulewicz, V.L.*, et al.* (2007). Requirement for Rac1 in a K-ras induced lung cancer in the mouse. Cancer Res *67*, 8089-8094.

Klein, E.A., Campbell, L.E., Kothapalli, D., Fournier, A.K., and Assoian, R.K. (2008). Joint requirement for Rac and ERK activities underlies the mid-G1 phase induction of cyclin D1 and S phase entry in both epithelial and mesenchymal cells. J Biol Chem *283*, 30911-30918.

Knight, B., Laukaitis, C., Akhtar, N., Hotchin, N.A., Edlund, M., and Horwitz, A.R. (2000). Visualizing muscle cell migration in situ. Curr Biol *10*, 576-585.

Kovar, D.R. (2007). Intracellular Motility: Myosin and Tropomyosin in Actin Cable Flow. Current Biology *17*, R244-R247.

Kozlowski, J.M., Hart, I.R., Fidler, I.J., and Hanna, N. (1984). A human melanoma line heterogeneous with respect to metastatic capacity in athymic nude mice. Journal of the National Cancer Institute *72*, 913-917.

Kunda, P., Craig, G., Dominguez, V., and Baum, B. (2003). Abi, Sra1, and Kette Control the Stability and Localization of SCAR/WAVE to Regulate the Formation of Actin-Based Protrusions. Current biology : CB *13*, 1867-1875.

Kunisada, T., Yoshida, H., Yamazaki, H., Miyamoto, A., Hemmi, H., Nishimura, E., Shultz, L.D., Nishikawa, S., and Hayashi, S. (1998). Transgene

expression of steel factor in the basal layer of epidermis promotes survival, proliferation, differentiation and migration of melanocyte precursors. Development *125*, 2915-2923.

Kureishy, N., Sapountzi, V., Prag, S., Anilkumar, N., and Adams, J.C. (2002). Fascins, and their roles in cell structure and function. BioEssays *24*, 350-361.

Kurisu, S., Suetsugu, S., Yamazaki, D., Yamaguchi, H., and Takenawa, T. (2004). Rac-WAVE2 signaling is involved in the invasive and metastatic phenotypes of murine melanoma cells. Oncogene *24*, 1309-1319.

Kuriyama, S., and Mayor, R. (2008). Molecular analysis of neural crest migration. Philosophical Transactions of the Royal Society B: Biological Sciences *363*, 1349-1362.

Lai, F.P.L., Szczodrak, M., Block, J., Faix, J., Breitsprecher, D., Mannherz, H.G., Stradal, T.E.B., Dunn, G.A., Small, J.V., and Rottner, K. (2008). Arp2/3 complex interactions and actin network turnover in lamellipodia. EMBO J *27*, 982-992.

Lambrechts, A., Gevaert, K., Cossart, P., Vandekerckhove, J., and Van Troys, M. (2008). Listeria comet tails: the actin-based motility machinery at work. Trends in Cell Biology *18*, 220-227.

Larue, L., Dougherty, N., Porter, S., and Mintz, B. (1992). Spontaneous malignant transformation of melanocytes explanted from Wf/Wf mice with a Kit kinase-domain mutation. Proceedings of the National Academy of Sciences of the United States of America *89*, 7816-7820.

Le Clainche, C., and Carlier, M.-F. (2008). Regulation of Actin Assembly Associated With Protrusion and Adhesion in Cell Migration. Physiological Reviews *88*, 489-513.

Lebensohn, A.M., and Kirschner, M.W. (2009). Activation of the WAVE Complex by Coincident Signals Controls Actin Assembly. Molecular Cell *36*, 512-524.

Li, A., Dawson, J.C., Forero-Vargas, M., Spence, H.J., Yu, X., Kˆnig, I., Anderson, K., and Machesky, L.M. (2010). The Actin-Bundling Protein Fascin Stabilizes Actin in Invadopodia and Potentiates Protrusive Invasion. Current biology : CB *20*, 339-345.

Li, B., Yu, H., Zheng, W.-p., Voll, R., Na, S., Roberts, A.W., Williams, D.A., Davis, R.J., Ghosh, S., and Flavell, R.A. (2000). Role of the Guanosine Triphosphatase Rac2 in T Helper 1 Cell Differentiation. Science *288*, 2219-2222.

Linder, S. (2007). The matrix corroded: podosomes and invadopodia in extracellular matrix degradation. Trends in Cell Biology *17*, 107-117.

Liu, J., Yue, P., Artym, V.V., Mueller, S.C., and Guo, W. (2009). The Role of the Exocyst in Matrix Metalloproteinase Secretion and Actin Dynamics during Tumor Cell Invadopodia Formation. Mol Biol Cell *20*, 3763-3771.

Lizarraga, F., Poincloux, R., Romao, M., Montagnac, G., Le Dez, G., Bonne, I., Rigaill, G., Raposo, G., and Chavrier, P. (2009). Diaphanous-related formins are required for invadopodia formation and invasion of breast tumor cells. Cancer Res *69*, 2792-2800.

Lorenz, M., Yamaguchi, H., Wang, Y., Singer, R.H., and Condeelis, J. (2004). Imaging Sites of N-WASP Activity in Lamellipodia and Invadopodia of Carcinoma Cells. Current biology : CB *14*, 697-703.

Lozano, E., Betson, M., and Braga, V.M.M. (2003). Tumor progression: Small GTPases and loss of cell–cell adhesion. BioEssays *25*, 452-463.

Lucas, J.T., Jr., Salimath, B.P., Slomiany, M.G., and Rosenzweig, S.A. (2010). Regulation of invasive behavior by vascular endothelial growth factor is HEF1-dependent. Oncogene *29*, 4449-4459.

Machesky, L.M. (2008). Lamellipodia and filopodia in metastasis and invasion. FEBS Letters *582*, 2102-2111.

Machesky, L.M., Atkinson, S.J., Ampe, C., Vandekerckhove, J., and Pollard, T.D. (1994). Purification of a cortical complex containing two unconventional actins from Acanthamoeba by affinity chromatography on profilin-agarose. The Journal of Cell Biology *127*, 107-115.

Machesky, L.M., and Li, A. (2010). Fascin: Invasive filopodia promoting metastasis. Commun Integr Biol *3*, 263-270.

Mackenzie, M.A.F., Jordan, S.n.A., Budd, P.S., and Jackson, I.J. (1997). Activation of the Receptor Tyrosine Kinase Kit Is Required for the Proliferation of Melanoblasts in the Mouse Embryo. Developmental Biology *192*, 99-107.

Madri, J.A., and Graesser, D. (2000). Cell Migration in the Immune System: the Evolving Inter-Related Roles of Adhesion Molecules and Proteinases. Developmental Immunology *7*, 103-116.

Malumbres, M., and Barbacid, M. (2003). RAS oncogenes: the first 30 years. Nat Rev Cancer *3*, 459-465.

Marchisio, P.C., Bergui, L., Corbascio, G.C., Cremona, O., D'Urso, N., Schena, M., Tesio, L., and Caligaris-Cappio, F. (1988). Vinculin, talin, and integrins are localized at specific adhesion sites of malignant B lymphocytes. Blood *72*, 830-833.

Marchisio, P.C., Cirillo, D., Naldini, L., Primavera, M.V., Teti, A., and Zambonin-Zallone, A. (1984). Cell-substratum interaction of cultured avian osteoclasts is mediated by specific adhesion structures. The Journal of Cell Biology *99*, 1696-1705.

Marshall, C.J. (1995). Specificity of receptor tyrosine kinase signaling: Transient versus sustained extracellular signal-regulated kinase activation. Cell *80*, 179-185.

Mayer, T.C. (1973). The migratory pathway of neural crest cells into the skin of mouse embryos. Developmental Biology *34*, 39-46.

McCarty, O.J., Larson, M.K., Auger, J.M., Kalia, N., Atkinson, B.T., Pearce, A.C., Ruf, S., Henderson, R.B., Tybulewicz, V.L., Machesky, L.M.*, et al.* (2005). Rac1 is essential for platelet lamellipodia formation and aggregate stability under flow. J Biol Chem *280*, 39474-39484.

McClive, P.J., and Sinclair, A.H. (2001). Rapid DNA extraction and PCR-sexing of mouse embryos. Molecular Reproduction and Development *60*, 225-226.

McGough, A., Pope, B., Chiu, W., and Weeds, A. (1997). Cofilin Changes the Twist of F-Actin: Implications for Actin Filament Dynamics and Cellular Function. The Journal of Cell Biology *138*, 771-781.

Mertens, A.E.E., Rygiel, T.P., Olivo, C., van der Kammen, R., and Collard, J.G. (2005). The Rac activator Tiam1 controls tight junction biogenesis in keratinocytes through binding to and activation of the Par polarity complex. The Journal of Cell Biology *170*, 1029-1037.

Michaelson, D., Abidi, W., Guardavaccaro, D., Zhou, M., Ahearn, I., Pagano, M., and Philips, M.R. (2008). Rac1 accumulates in the nucleus during the G2 phase of the cell cycle and promotes cell division. The Journal of Cell Biology *181*, 485-496.

Michelot, A., Berro, J., GuÈrin, C., Boujemaa-Paterski, R., Staiger, C.J., Martiel, J.-L., and Blanchoin, L. (2007). Actin-Filament Stochastic Dynamics Mediated by ADF/Cofilin. Current biology : CB *17*, 825-833.

Migeotte, I., Omelchenko, T., Hall, A., and Anderson, K.V. (2010). Rac1-Dependent Collective Cell Migration Is Required for Specification of the Anterior-Posterior Body Axis of the Mouse. PLoS Biol *8*, e1000442.

Millard, T.H., Dawson, J., and Machesky, L.M. (2007). Characterisation of IRTKS, a novel IRSp53/MIM family actin regulator with distinct filament bundling properties. J Cell Sci *120*, 1663-1672.

Minden, A., Lin, A., McMahon, M., Lange-Carter, C., Derijard, B., Davis, R.J., Johnson, G.L., and Karin, M. (1994). Differential activation of ERK and JNK mitogen-activated protein kinases by Raf-1 and MEKK. Science *266*, 1719-1723.

Mizutani, K., Miki, H., He, H., Maruta, H., and Takenawa, T. (2002). Essential Role of Neural Wiskott-Aldrich Syndrome Protein in Podosome Formation and Degradation of Extracellular Matrix in src-transformed Fibroblasts. Cancer Research *62*, 669-674.

Moore, K.A., Sethi, R., Doanes, A.M., Johnson, T.M., Pracyk, J.B., Kirby, M., Irani, K., Goldschmidt-Clermont, P.J., and Finkel, T. (1997). Rac1 is required for cell proliferation and G2/M progression. Biochem J *326*, 17-20.

Mort, R.L., Hay, L., and Jackson, I.J. (2010). Ex vivo live imaging of melanoblast migration in embryonic mouse skin. Pigment Cell & Melanoma Research *23*, 299-301.

Mueller, S., and Chen, W. (1991). Cellular invasion into matrix beads: localization of beta 1 integrins and fibronectin to the invadopodia. J Cell Sci *99*, 213-225.

Mueller, S.C., Ghersi, G., Akiyama, S.K., Sang, Q.-X.A., Howard, L., Pineiro-Sanchez, M., Nakahara, H., Yeh, Y., and Chen, W.-T. (1999). A Novel Protease-docking Function of Integrin at Invadopodia. Journal of Biological Chemistry *274*, 24947-24952.

Murphy, A.M., and Montell, D.J. (1996). Cell type-specific roles for Cdc42, Rac, and RhoL in Drosophila oogenesis. The Journal of Cell Biology *133*, 617-630.

Nakahara, H., Mueller, S.C., Nomizu, M., Yamada, Y., Yeh, Y., and Chen, W.-T. (1998). Activation of β1 Integrin Signaling Stimulates Tyrosine Phosphorylation of p190 RhoGAP and Membrane-protrusive Activities at Invadopodia. Journal of Biological Chemistry *273*, 9-12.

Nakahara, H., Otani, T., Sasaki, T., Miura, Y., Takai, Y., and Kogo, M. (2003). Involvement of Cdc42 and Rac small G proteins in invadopodia formation of RPMI7951 cells. Genes to Cells *8*, 1019-1027.

Nishimura, E.K., Jordan, S.A., Oshima, H., Yoshida, H., Osawa, M., Moriyama, M., Jackson, I.J., Barrandon, Y., Miyachi, Y., and Nishikawa, S.-I. (2002). Dominant role of the niche in melanocyte stem-cell fate determination. Nature *416*, 854-860.

Nishimura, E.K., Yoshida, H., Kunisada, T., and Nishikawa, S.-I. (1999). Regulation of E- and P-Cadherin Expression Correlated with Melanocyte Migration and Diversification. Developmental Biology *215*, 155-166.

Nobes, C.D., and Hall, A. (1995). Rho, Rac, and Cdc42 GTPases regulate the assembly of multimolecular focal complexes associated with actin stress fibers, lamellipodia, and filopodia. Cell *81*, 53-62.

Nobes, C.D., Hawkins, P., Stephens, L., and Hall, A. (1995). Activation of the small GTP-binding proteins rho and rac by growth factor receptors. J Cell Sci *108*, 225-233.

Nodari, A., Zambroni, D., Quattrini, A., Court, F.A., D'Urso, A., Recchia, A., Tybulewicz, V.L.J., Wrabetz, L., and Feltri, M.L. (2007). β1 integrin activates Rac1 in Schwann cells to generate radial lamellae during axonal sorting and myelination. The Journal of Cell Biology *177*, 1063-1075.

Nolen, B.J., Tomasevic, N., Russell, A., Pierce, D.W., Jia, Z., McCormick, C.D., Hartman, J., Sakowicz, R., and Pollard, T.D. (2009). Characterization of two classes of small molecule inhibitors of Arp2/3 complex. Nature *460*, 1031-1034.

Novak, A., Guo, C., Yang, W., Nagy, A., and Lobe, C.G. (2000). Z/EG, a double reporter mouse line that expresses enhanced green fluorescent protein upon cre-mediated excision. genesis *28*, 147-155.

Nürnberg, A., Kitzing, T., and Grosse, R. (2011). Nucleating actin for invasion. Nat Rev Cancer *11*, 177-187.

Oldenbourg, R., Katoh, K., and Danuser, G. (2000). Mechanism of Lateral Movement of Filopodia and Radial Actin Bundles across Neuronal Growth Cones. Biophysical journal *78*, 1176-1182.

Olson, M.F., Ashworth, A., and Hall, A. (1995). An essential role for Rho, Rac, and Cdc42 GTPases in cell cycle progression through G1. Science (New York, NY) *269*, 1270-1272.

Ono, S., Yamakita, Y., Yamashiro, S., Matsudaira, P.T., Gnarra, J.R., Obinata, T., and Matsumura, F. (1997). Identification of an Actin Binding Region and a Protein Kinase C Phosphorylation Site on Human Fascin. Journal of Biological Chemistry *272*, 2527-2533.

Palamidessi, A., Frittoli, E., GarrÈ, M., Faretta, M., Mione, M., Testa, I., Diaspro, A., Lanzetti, L., Scita, G., and Di Fiore, P.P. (2008). Endocytic Trafficking of Rac Is Required for the Spatial Restriction of Signaling in Cell Migration. Cell *134*, 135-147.

Palazzo, A.F., Cook, T.A., Alberts, A.S., and Gundersen, G.G. (2001). mDia mediates Rho-regulated formation and orientation of stable microtubules. Nat Cell Biol *3*, 723-729.

Paňková, K., Rösel, D., Novotný, M., and Brábek, J. (2010). The molecular mechanisms of transition between mesenchymal and amoeboid invasiveness in tumor cells. Cellular and Molecular Life Sciences *67*, 63-71.

Parsons, M., and Adams, J.C. (2008). Rac regulates the interaction of fascin with protein kinase C in cell migration. J Cell Sci *121*, 2805-2813.

Pedersen, T.X., Leethanakul, C., Patel, V., Mitola, D., Lund, L.R., Dano, K., Johnsen, M., Gutkind, J.S., and Bugge, T.H. (2003). Laser capture microdissection-based in vivo genomic profiling of wound keratinocytes identifies similarities and differences to squamous cell carcinoma. Oncogene *22*, 3964-3976.

Perez-Losada, J., Sanchez-Martin, M., Rodriguez-Garcia, A., Sanchez, M.L., Orfao, A., Flores, T., and Sanchez-Garcia, I. (2002). Zinc-finger transcription factor Slug contributes to the function of the stem cell factor c-kit signaling pathway. Blood *100*, 1274-1286.

Perona, R., Montaner, S., Saniger, L., S√°nchez-P√©rez, I., Bravo, R., and Lacal, J.C. (1997). Activation of the nuclear factor-kappaB by Rho, CDC42, and Rac-1 proteins. Genes & Development *11*, 463-475.

Pertz, O., Hodgson, L., Klemke, R.L., and Hahn, K.M. (2006). Spatiotemporal dynamics of RhoA activity in migrating cells. Nature *440*, 1069-1072.

Peters, E.M.J., Maurer, M., Botchkarev, V.A., Jensen, K.d., Welker, P., Scott, G.A., and Paus, R. (2003). Kit Is Expressed by Epithelial Cells In Vivo. *121*, 976-984.

Peters, E.M.J., Tobin, D.J., Botchkareva, N., Maurer, M., and Paus, R. (2002). Migration of Melanoblasts into the Developing Murine Hair Follicle Is Accompanied by Transient c-Kit Expression. Journal of Histochemistry & Cytochemistry *50*, 751-766.

Pflicke, H., and Sixt, M. (2009). Preformed portals facilitate dendritic cell entry into afferent lymphatic vessels. The Journal of Experimental Medicine *206*, 2925-2935.

Philippar, U., Roussos, E.T., Oser, M., Yamaguchi, H., Kim, H.-D., Giampieri, S., Wang, Y., Goswami, S., Wyckoff, J.B., Lauffenburger, D.A.*, et al.* (2008). A Mena Invasion Isoform Potentiates EGF-Induced Carcinoma Cell Invasion and Metastasis. Developmental cell *15*, 813-828.

Pla, P., Moore, R., Morali, O.G., Grille, S., Martinozzi, S., Delmas, V., and Larue, L. (2001). Cadherins in neural crest cell development and transformation. Journal of Cellular Physiology *189*, 121-132.

Platz, A., Egyhazi, S., Ringborg, U., and Hansson, J. (2008). Human cutaneous melanoma; a review of NRAS and BRAF mutation frequencies in relation to histogenetic subclass and body site. Molecular Oncology *1*, 395-405.

Poincloux, R., Lizarraga, F., and Chavrier, P. (2009). Matrix invasion by tumour cells: a focus on MT1-MMP trafficking to invadopodia. J Cell Sci *122*, 3015-3024.

Pollard, T.D., and Cooper, J.A. (2009). Actin, a Central Player in Cell Shape and Movement. Science *326*, 1208-1212.

Ponti, A., Machacek, M., Gupton, S.L., Waterman-Storer, C.M., and Danuser, G. (2004). Two Distinct Actin Networks Drive the Protrusion of Migrating Cells. Science *305*, 1782-1786.

Price, L.S., Leng, J., Schwartz, M.A., and Bokoch, G.M. (1998). Activation of Rac and Cdc42 by Integrins Mediates Cell Spreading. Mol Biol Cell *9*, 1863-1871.

Qiu, R.-G., Chen, J., Kirn, D., McCormick, F., and Symons, M. (1995a). An essential role for Rac in Ras transformation. Nature *374*, 457-459.

Quintavalle, M., Elia, L., Condorelli, G., and Courtneidge, S.A. (2010). MicroRNA control of podosome formation in vascular smooth muscle cells in vivo and in vitro. The Journal of Cell Biology *189*, 13-22.

Redd, M.J., Kelly, G., Dunn, G., Way, M., and Martin, P. (2006). Imaging macrophage chemotaxis in vivo: Studies of microtubule function in zebrafish wound inflammation. Cell Motility and the Cytoskeleton *63*, 415-422.

Ridley, A.J. (2001). Rho GTPases and cell migration. J Cell Sci *114*, 2713-2722.

Ridley, A.J., Paterson, H.F., Johnston, C.L., Diekmann, D., and Hall, A. (1992). The small GTP-binding protein rac regulates growth factor-induced membrane ruffling. Cell *70*, 401-410.

Rizvi, S.A., Neidt, E.M., Cui, J., Feiger, Z., Skau, C.T., Gardel, M.L., Kozmin, S.A., and Kovar, D.R. (2009). Identification and Characterization of a Small Molecule Inhibitor of Formin-Mediated Actin Assembly. Chemistry & biology *16*, 1158-1168.

Roberts, A.W., Kim, C., Zhen, L., Lowe, J.B., Kapur, R., Petryniak, B., Spaetti, A., Pollock, J.D., Borneo, J.B., Bradford, G.B.*, et al.* (1999). Deficiency of the Hematopoietic Cell-Specific Rho Family GTPase Rac2 Is Characterized by Abnormalities in Neutrophil Function and Host Defense. Immunity *10*, 183-196.

Rossman, K.L., Der, C.J., and Sondek, J. (2005). GEF means go: turning on RHO GTPases with guanine nucleotide-exchange factors. Nat Rev Mol Cell Biol *6*, 167-180.

Sahai, E. (2005). Mechanisms of cancer cell invasion. Current Opinion in Genetics & Development *15*, 87-96.

Sahai, E., and Marshall, C.J. (2002). RHO-GTPases and cancer. Nat Rev Cancer *2*, 133-142.

Sahai, E., and Marshall, C.J. (2003). Differing modes of tumour cell invasion have distinct requirements for Rho/ROCK signalling and extracellular proteolysis. Nat Cell Biol *5*, 711-719.

Sakurai-Yageta, M., Recchi, C., Le Dez, G.I., Sibarita, J.-B., Daviet, L., Camonis, J., D'Souza-Schorey, C., and Chavrier, P. (2008). The interaction of IQGAP1 with the exocyst complex is required for tumor cell invasion downstream of Cdc42 and RhoA. The Journal of Cell Biology *181*, 985-998.

Samuel, M.S., Louren√ßo, F.C., and Olson, M.F. (2011). K-Ras Mediated Murine Epidermal Tumorigenesis Is Dependent upon and Associated with Elevated Rac1 Activity. PLoS ONE *6*, e17143.

Sanz-Moreno, V., Gadea, G., Ahn, J., Paterson, H., Marra, P., Pinner, S., Sahai, E., and Marshall, C.J. (2008). Rac Activation and Inactivation Control Plasticity of Tumor Cell Movement. Cell *135*, 510-523.

Schoumacher, M., Goldman, R.D., Louvard, D., and Vignjevic, D.M. (2010). Actin, microtubules, and vimentin intermediate filaments cooperate for elongation of invadopodia. The Journal of Cell Biology *189*, 541–556.

Scita, G., Confalonieri, S., Lappalainen, P., and Suetsugu, S. (2008). IRSp53: crossing the road of membrane and actin dynamics in the formation of membrane protrusions. Trends in Cell Biology *18*, 52-60.

Scott, R.W., Hooper, S., Crighton, D., Li, A., K√∂nig, I., Munro, J., Trivier, E., Wickman, G., Morin, P., Croft, D.R.*, et al.* (2010). LIM kinases are required for invasive path generation by tumor and tumor-associated stromal cells. The Journal of Cell Biology *191*, 169-185.

Sedeh, R.S., Fedorov, A.A., Fedorov, E.V., Ono, S., Matsumura, F., Almo, S.C., and Bathe, M. (2010). Structure, Evolutionary Conservation, and Conformational Dynamics of Homo sapiens Fascin-1, an F-actin Crosslinking Protein. Journal of Molecular Biology *400*, 589-604.

Serbedzija, G.N., Fraser, S.E., and Bronner-Fraser, M. (1990). Pathways of trunk neural crest cell migration in the mouse embryo as revealed by vital dye labelling. Development *108*, 605-612.

Serrano, M., Lee, H.-W., Chin, L., Cordon-Cardo, C., Beach, D., and DePinho, R.A. (1996). Role of the INK4a Locus in Tumor Suppression and Cell Mortality. Cell *85*, 27-37.

Shan, D., Chen, L., Njardarson, J.T., Gaul, C., Ma, X., Danishefsky, S.J., and Huang, X.-Y. (2005). Synthetic analogues of migrastatin that inhibit mammary tumor metastasis in mice. PNAS *102*, 3772-3776.

Sharov, A., Tobin, D.J., Sharova, T.Y., Atoyan, R., and Botchkarev, V.A. (2005). Changes in Different Melanocyte Populations During Hair Follicle Involution (Catagen). J Investig Dermatol *125*, 1259-1267.

Shin, M.K., Levorse, J.M., Ingram, R.S., and Tilghman, S.M. (1999). The temporal requirement for endothelin receptor-B signalling during neural crest development. Nature *402*, 496-501.

Silver, D.L., Hou, L., Somerville, R., Young, M.E., Apte, S.S., and Pavan, W.J. (2008). The Secreted Metalloprotease ADAMTS20 Is Required for Melanoblast Survival. PLoS Genet *4*, e1000003.

Small, J.V., Isenberg, G., and Celis, J.E. (1978). Polarity of actin at the leading edge of cultured cells. Nature *272*, 638-639.

Smalley, K.S.M. (2009). Understanding Melanoma Signaling Networks as the Basis for Molecular Targeted Therapy. J Invest Dermatol *130*, 28-37.

Smith, S.D., Jaffer, Z.M., Chernoff, J., and Ridley, A.J. (2008). PAK1-mediated activation of ERK1/2 regulates lamellipodial dynamics. J Cell Sci *121*, 3729-3736.

Snapper, S.B., Takeshima, F., Anton, I., Liu, C.-H., Thomas, S.M., Nguyen, D., Dudley, D., Fraser, H., Purich, D., Lopez-Ilasaca, M.*, et al.* (2001). N-WASP deficiency reveals distinct pathways for cell surface projections and microbial actin-based motility. Nat Cell Biol *3*, 897-904.

Sporn, M.B. (1997). The War on Cancer: A Reviewa. Annals of the New York Academy of Sciences *833*, 137-146.

Steel, K.P., Davidson, D.R., and Jackson, I.J. (1992). TRP-2/DT, a new early melanoblast marker, shows that steel growth factor (c-kit ligand) is a survival factor. Development *115*, 1111-1119.

Steffen, A., Faix, J., Resch, G.P., Linkner, J., Wehland, J., Small, J.V., Rottner, K., and Stradal, T.E.B. (2006). Filopodia Formation in the Absence of Functional WAVE- and Arp2/3-Complexes. Mol Biol Cell *17*, 2581-2591.

Steffen, A., Le Dez, G., Poincloux, R., Recchi, C., Nassoy, P., Rottner, K., Galli, T., and Chavrier, P. (2008). MT1-MMP-Dependent Invasion Is Regulated by TI-VAMP/VAMP7. Current biology *18*, 926-931.

Stradal, T.E.B., Rottner, K., Disanza, A., Confalonieri, S., Innocenti, M., and Scita, G. (2004). Regulation of actin dynamics by WASP and WAVE family proteins. Trends in Cell Biology *14*, 303-311.

Strasser, G.A., Rahim, N.A., VanderWaal, K.E., Gertler, F.B., and Lanier, L.M. (2004). Arp2/3 Is a Negative Regulator of Growth Cone Translocation. Neuron *43*, 81-94.

Sugihara, K., Nakatsuji, N., Nakamura, K., Nakao, K., Hashimoto, R., Otani, H., Sakagami, H., Kondo, H., Nozawa, S., Aiba, A.*, et al.* (1998). Rac1 is required for the formation of three germ layers during gastrulation. Oncogene *17*, 3427-3433.

Sviderskaya, E.V., Hill, S.P., Evans-Whipp, T.J., Chin, L., Orlow, S.J., Easty, D.J., Cheong, S.C., Beach, D., DePinho, R.A., and Bennett, D.C. (2002). p16Ink4a in Melanocyte Senescence and Differentiation. Journal of the National Cancer Institute *94*, 446-454.

Tahirovic, S., Hellal, F., Neukirchen, D., Hindges, R., Garvalov, B.K., Flynn, K.C., Stradal, T.E., Chrostek-Grashoff, A., Brakebusch, C., and Bradke, F. (2010). Rac1 Regulates Neuronal Polarization through the WAVE Complex. J Neurosci *30*, 6930-6943.

Takaishi, K., Sasaki, T., Kotani, H., Nishioka, H., and Takai, Y. (1997). Regulation of Cell-Cell Adhesion by Rac and Rho Small G Proteins in MDCK Cells. The Journal of Cell Biology *139*, 1047-1059.

Takesono, A., Heasman, S.J., Wojciak-Stothard, B., Garg, R., and Ridley, A.J. (2010). Microtubules Regulate Migratory Polarity through Rho/ROCK Signaling in T Cells. PLoS ONE *5*, e8774.

Tan, W., Palmby, T.R., Gavard, J., Amornphimoltham, P., Zheng, Y., and Gutkind, J.S. (2008). An essential role for Rac1 in endothelial cell function and vascular development. The FASEB Journal *22*, 1829-1838.

Tcherkezian, J., and Lamarche-vane, N. (2007). Current knowledge of the large RhoGAP family of proteins. Biology of the Cell *099*, 67-86.

Theveneau, E., Marchant, L., Kuriyama, S., Gull, M., Moepps, B., Parsons, M., and Mayor, R. (2010). Collective chemotaxis requires contact-dependent cell polarity. Dev Cell *19*, 39-53.

Thiery, J.P., Acloque, H., Huang, R.Y.J., and Nieto, M.A. (2009). Epithelial-Mesenchymal Transitions in Development and Disease. Cell *139*, 871-890.

Thomas, P.S., Kim, J., Nunez, S., Glogauer, M., and Kaartinen, V. (2010). Neural crest cell-specific deletion of Rac1 results in defective cell-matrix interactions and severe craniofacial and cardiovascular malformations. Developmental Biology *340*, 613-625.

Tolde, O., Rˆsel, D., Vesel˝, P., Folk, P., and Br·bek, J. (2010). The structure of invadopodia in a complex 3D environment. European Journal of Cell Biology *89*, 674-680.

Tokuo, H., and M. Ikebe. (2004). Myosin X transports Mena/VASP to the tip of filopodia. Biochem. Biophys. Res. Commun. *319*,214–220.

Tonks, I.D., Nurcombe, V., Paterson, C., Zournazi, A., Prather, C., Mould, A.W., and Kay, G.F. (2003). Tyrosinase-Cre mice for tissue-specific gene ablation in neural crest and neuroepithelial-derived tissues. genesis *37*, 131-138.

Tseng, Y., Fedorov, E., McCaffery, J.M., Almo, S.C., and Wirtz, D. (2001). Micromechanics and ultrastructure of actin filament networks crosslinked by human fascin: A comparison with [alpha]-actinin. Journal of Molecular Biology *310*, 351-366.

Tseng, Y., and Wirtz, D. (2004). Dendritic Branching and Homogenization of Actin Networks Mediated by Arp2/3 Complex. Physical Review Letters *93*, 258104.

Tsukamoto K, Jackson IJ, Urabe K, Montague PM, Hearing VJ. A second tyrosinase-related protein, TRP-2, is a melanogenic enzyme termed DOPAchrome tautomerase. Embo J 1992;11:519–526

Tubb, B., Mulholland, D.J., Vogl, W., Lan, Z.-J., Niederberger, C., Cooney, A., and Bryan, J. (2002). Testis Fascin (FSCN3): A Novel Paralog of the Actin-Bundling Protein Fascin Expressed Specifically in the Elongate Spermatid Head. Experimental Cell Research *275*, 92-109.

Urban, E., Jacob, S., Nemethova, M., Resch, G.P., and Small, J.V. (2010). Electron tomography reveals unbranched networks of actin filaments in lamellipodia. Nat Cell Biol *12*, 429-435.

Vidali, L., Chen, F., Cicchetti, G., Ohta, Y., and Kwiatkowski, D.J. (2006). Rac1-null Mouse Embryonic Fibroblasts Are Motile and Respond to Platelet-derived Growth Factor. Mol Biol Cell *17*, 2377-2390.

Vignjevic, D., Kojima, S., Aratyn, Y., Danciu, O., Svitkina, T., and Borisy, G.G. (2006). Role of fascin in filopodial protrusion. J Cell Biol *174*, 863-875.

Vignjevic, D., and Montagnac, G. (2008). Reorganisation of the dendritic actin network during cancer cell migration and invasion. Seminars in Cancer Biology *18*, 12-22.

Vignjevic, D., Schoumacher, M., Gavert, N., Janssen, K.-P., Jih, G., La√©, M., Louvard, D., Ben-Ze'ev, A., and Robine, S. (2007). Fascin, a Novel Target of β-Catenin-TCF Signaling, Is Expressed at the Invasive Front of Human Colon Cancer. Cancer Research *67*, 6844-6853.

Vignjevic, D., Yarar, D., Welch, M.D., Peloquin, J., Svitkina, T., and Borisy, G.G. (2003). Formation of filopodia-like bundles in vitro from a dendritic network. The Journal of Cell Biology *160*, 951-962.

Wada, Y., Abe, T., Itabashi, T., Sato, H., Kawamura, M., and Tamai, M. (2003). Autosomal Dominant Macular Degeneration Associated With 208delG Mutation in the FSCN2 Gene. Arch Ophthalmol *121*, 1613-1620.

Wada, Y., Abe, T., Takeshita, T., Sato, H., Yanashima, K., and Tamai, M. (2001). Mutation of Human Retinal Fascin Gene (FSCN2) Causes Autosomal Dominant Retinitis Pigmentosa. Investigative Ophthalmology & Visual Science *42*, 2395-2400.

Walmsley, M.J., Ooi, S.K.T., Reynolds, L.F., Smith, S.H., Ruf, S., Mathiot, A., Vanes, L., Williams, D.A., Cancro, M.P., and Tybulewicz, V.L.J. (2003). Critical Roles for Rac1 and Rac2 GTPases in B Cell Development and Signaling. Science *302*, 459-462.

Wang, W., Goswami, S., Sahai, E., Wyckoff, J.B., Segall, J.E., and Condeelis, J.S. (2005). Tumor cells caught in the act of invading: their strategy for enhanced cell motility. Trends Cell Biol *15*, 138-145.

Wang, X., He, L., Wu, Y.I., Hahn, K.M., and Montell, D.J. (2010) Light-mediated activation reveals a key role for Rac in collective guidance of cell movement in vivo. Nat Cell Biol *12*, 591-597.

Weaver, A. (2006). Invadopodia: Specialized Cell Structures for Cancer Invasion. Clinical and Experimental Metastasis *23*, 97-105.

Wehrle-Haller, B., and Weston, J.A. (1995). Soluble and cell-bound forms of steel factor activity play distinct roles in melanocyte precursor dispersal and survival on the lateral neural crest migration pathway. Development *121*, 731-742.

Wells, C.M., Walmsley, M., Ooi, S., Tybulewicz, V., and Ridley, A.J. (2004). Rac1-deficient macrophages exhibit defects in cell spreading and membrane ruffling but not migration. J Cell Sci *117*, 1259-1268.

Wennerberg, K., and Der, C.J. (2004). Rho-family GTPases: it's not only Rac and Rho (and I like it). J Cell Sci *117*, 1301-1312.

Wennerberg, K., Rossman, K.L., and Der, C.J. (2005). The Ras superfamily at a glance. J Cell Sci *118*, 843-846.

Westwick, J.K., Lambert, Q.T., Clark, G.J., Symons, M., Van Aelst, L., Pestell, R.G., and Der, C.J. (1997). Rac regulation of transformation, gene expression, and actin organization by multiple, PAK-independent pathways. Mol Cell Biol *17*, 1324-1335.

Wheeler, A.P., Wells, C.M., Smith, S.D., Vega, F.M., Henderson, R.B., Tybulewicz, V.L., and Ridley, A.J. (2006). Rac1 and Rac2 regulate macrophage morphology but are not essential for migration. Journal of Cell Science *119*, 2749-2757.

Wherlock, M., and Mellor, H. (2002). The Rho GTPase family: a Racs to Wrchs story. J Cell Sci *115*, 239-240.

Williams, L.M., Lali, F., Willetts, K., Balague, C., Godessart, N., Brennan, F., Feldmann, M., and Foxwell, B.M.J. (2008). Rac mediates TNF-induced cytokine production via modulation of NF-[kappa]B. Molecular Immunology *45*, 2446-2454.

Wilson, Y.M., Richards, K.L., Ford-Perriss, M.L., Panthier, J.-J., and Murphy, M. (2004). Neural crest cell lineage segregation in the mouse neural tube. Development *131*, 6153-6162.

Wolf, K., and Friedl, P. (2009). Mapping proteolytic cancer cell-extracellular matrix interfaces. Clinical and Experimental Metastasis *26*, 289-298.

Wolf, K., Mazo, I., Leung, H., Engelke, K., von Andrian, U.H., Deryugina, E.I., Strongin, A.Y., Br√∂cker, E.-B., and Friedl, P. (2003a). Compensation mechanism in tumor cell migration. The Journal of Cell Biology *160*, 267-277.

Wolf, K., Muller, R., Borgmann, S., Brocker, E.B., and Friedl, P. (2003b). Amoeboid shape change and contact guidance: T-lymphocyte crawling through fibrillar collagen is independent of matrix remodeling by MMPs and other proteases. Blood *102*, 3262-3269.

Wolf, K., Wu, Y.I., Liu, Y., Geiger, J., Tam, E., Overall, C., Stack, M.S., and Friedl, P. (2007). Multi-step pericellular proteolysis controls the transition from individual to collective cancer cell invasion. Nat Cell Biol *9*, 893-904.

Wyckoff, J.B., Pinner, S.E., Gschmeissner, S., Condeelis, J.S., and Sahai, E. (2006). ROCK- and Myosin-Dependent Matrix Deformation Enables Protease-

Independent Tumor-Cell Invasion In Vivo. Current biology : CB *16*, 1515-1523.

Wyckoff, J.B., Wang, Y., Lin, E.Y., Li, J.F., Goswami, S., Stanley, E.R., Segall, J.E., Pollard, J.W., and Condeelis, J. (2007). Direct visualization of macrophage-assisted tumor cell intravasation in mammary tumors. Cancer Res *67*, 2649-2656.

Yajima, I., Belloir, E., Bourgeois, Y., Kumasaka, M., Delmas, V., and Larue, L. (2006). Spatiotemporal gene control by the Cre-ERT2 system in melanocytes. genesis *44*, 34-43.

Yamaguchi, H., and Condeelis, J. (2007). Regulation of the actin cytoskeleton in cancer cell migration and invasion. Biochimica et Biophysica Acta (BBA) - Molecular Cell Research *1773*, 642-652.

Yamaguchi, H., Lorenz, M., Kempiak, S., Sarmiento, C., Coniglio, S., Symons, M., Segall, J., Eddy, R., Miki, H., Takenawa, T.*, et al.* (2005). Molecular mechanisms of invadopodium formation. The Journal of Cell Biology *168*, 441-452.

Yamaguchi, H., and Oikawa, T. (2010). Membrane lipids in invadopodia and podosomes: Key structures for cancer invasion and metastasis, Vol 1.

Yamaguchi, H., Pixley, F., and Condeelis, J. (2006). Invadopodia and podosomes in tumor invasion. European Journal of Cell Biology *85*, 213-218.

Yamakita, Y., Matsumura, F., Lipscomb, M.W., Chou, P.-c., Werlen, G., Burkhardt, J.K., and Yamashiro, S. (2011). Fascin1 Promotes Cell Migration of Mature Dendritic Cells. The Journal of Immunology.

Yamakita, Y., Matsumura, F., and Yamashiro, S. (2009). Fascin1 is dispensable for mouse development but is favorable for neonatal survival. Cell Motil Cytoskeleton.

Yamakita, Y., Ono, S., Matsumura, F., and Yamashiro, S. (1996). Phosphorylation of Human Fascin Inhibits Its Actin Binding and Bundling Activities. Journal of Biological Chemistry *271*, 12632-12638.

Yamashiro, S., Yamakita, Y., Ono, S., and Matsumura, F. (1998). Fascin, an Actin-bundling Protein, Induces Membrane Protrusions and Increases Cell Motility of Epithelial Cells. Mol Biol Cell *9*, 993-1006.

Yang, C., Czech, L., Gerboth, S., Kojima, S.-i., Scita, G., and Svitkina, T. (2007). Novel Roles of Formin mDia2 in Lamellipodia and Filopodia Formation in Motile Cells. PLoS Biol *5*, e317.

Yang, L., Wang, L., and Zheng, Y. (2006). Gene Targeting of Cdc42 and Cdc42GAP Affirms the Critical Involvement of Cdc42 in Filopodia Induction, Directed Migration, and Proliferation in Primary Mouse Embryonic Fibroblasts. Mol Biol Cell *17*, 4675-4685.

Yang, N., Higuchi, O., Ohashi, K., Nagata, K., Wada, A., Kangawa, K., Nishida, E., and Mizuno, K. (1998). Cofilin phosphorylation by LIM-kinase 1 and its role in Rac-mediated actin reorganization. Nature *393*, 809-812.

Yoshida, H., Kunisada, T., Grimm, T., Nishimura, E.K., Nishioka, E., and Nishikawa, S.-I. (2001). Review: Melanocyte Migration and Survival Controlled by SCF//c-kit Expression. J Investig Dermatol Symp Proc *6*, 1-5.

Yoshida, H., Kunisada, T., Kusakabe, M., Nishikawa, S., and Nishikawa, S.I. (1996). Distinct stages of melanocyte differentiation revealed by anlaysis of nonuniform pigmentation patterns. Development *122*, 1207-1214.

Zanet, J., Stramer, B., Millard, T., Martin, P., Payre, F.o., and Plaza, S. (2009). Fascin is required for blood cell migration during Drosophila embryogenesis. Development *136*, 2557-2565.

Zhang, F.-R., Tao, L.-H., Shen, Z.-Y., Lv, Z., Xu, L.-Y., and Li, E.-M. (2008). Fascin Expression in Human Embryonic, Fetal, and Normal Adult Tissue. Journal of Histochemistry & Cytochemistry *56*, 193-199.

Zhang, J., Fonovic, M., Suyama, K., Bogyo, M., and Scott, M.P. (2009). Rab35 Controls Actin Bundling by Recruiting Fascin as an Effector Protein. Science *325*, 1250-1254.

Zhao, Q., Shen, J.-H., Shen, Z.-Y., Wu, Z.-Y., Xu, X.-E., Xie, J.-J., Wu, J.-Y., Huang, Q., Lu, X.-F., Li, E.-M.*, et al.* (2010). Phosphorylation of Fascin Decreases the Risk of Poor Survival in Patients With Esophageal Squamous Cell Carcinoma. Journal of Histochemistry & Cytochemistry *58*, 979-988.

Zheng, J.Q., Wan, J.J., and Poo, M.M. (1996). Essential role of filopodia in chemotropic turning of nerve growth cone induced by a glutamate gradient. The Journal of Neuroscience *16*, 1140-1149.

Zhou, J., Kim, H.Y., Wang, J.H.C., and Davidson, L.A. (2010). Macroscopic stiffening of embryonic tissues via microtubules, RhoGEF and the assembly of contractile bundles of actomyosin. Development *137*, 2785-2794.

Appendix

Movie 1. Part 1 (Frame 1 to 45): Time-lapse confocal images of A375MM cells expressing GFP-actin show actin comets in invadopodia. Images were acquired every 4 sec. Elapsed time is indicated. Part 2 (Frame 46 to 95): Time-lapse confocal images of A375MM cells expressing GFP-fascin show localization throughout the entire actin comets at sites of gelatin degradation. Images were acquired every 0.428 sec. Elapsed time is indicated. Part 3 (Frame 96 to 199): 3D reconstruction of immunofluorescence of actin comets stained with anti-actin (red) and anti-fascin (green) antibody, which shows fascin localized throughout the actin comets. Part 4 (Frame 200 to 249): Time-lapse confocal images of A375MM cells expressing GFP-N-WASP and RFP-actin show N-WASP concentrated only at the head of the actin comet. Images were acquired every 10 sec. Elapsed time is indicated. Part 5 (Frame 250 to 354): 3D reconstruction of actin comets of invadopodia in A375MM cells expressing GFP-N-WASP (green) and stained with rhodamine phalloidin (red), which showed GFP-N-WASP localized only at the head of the comets.

Movie 2. Left: Photo-bleaching of GFP-fascin at invadopodia. Images were acquired every 0.428 seconds. Elapsed time is indicated. Right: Photo-bleaching of GFP-actin at invadopodia. Images were acquired every 4.28 sec. Elapsed time is indicated.

Movie 3. Control (Top) or Fascin (Bottom) siRNA-treated A375MM cells stably expressing RFP-Lifeact cultured on gelatin matrix onvernight in presence of 5μM GM6001. The timelapse was started within 1 hour after medium was replaced to remve GM6001. Formation of invadopodia, in which most of invadopodia had a lifetime exceeding 10 h. Images were acquired every 5 min. Elapsed time is indicated. Gelatin is shown to indicate degradation.

Movie 4. Time-lapse confocal images of NT, Fascin siRNA or 5μM GM6001-treated CHL-1 cells stably expressing GFP-Lifeact invading into collagen I-matrigel matrix displayed numerous filopodia-like protrusions. Images were acquired every 10 min. At each time point, a Z-stack images were taken with 0.5 μm Z-spacing and showed as a combined Z-stack. Elapsed time is also indicated.

Movie 5. Melanoblasts show long protrusions in E15.5 epidermis explants and 3D reconstruction of melanoblasts in control and Rac1 knockout explants. This movie shows the motility of melanoblasts in epidermal explants as well as a confocal z-stack through the epidermis showing melanoblast shape and position.

Movie 6. Melanoblasts in Rac1 depleted explants migrate slower and are more rounded than controls. This Movie shows a 3D reconstruction of the melanoblasts in the skin to demonstrate the shape differences between wt and Rac1 KO.

Movie 7. Melanoblasts migrating in epidermis show bright flashes of F-actin near the tips of protrusions, which are distinct from blebs. This movieshows Lifeact expressing melanoblasts migrating in skin explants.

Movie 8. Inhibtion of actin, tubulin or Arp2/3 complex, ablates long cellular protrusion formation of melanoblast in skin explants. This movie shows the cell motility data for Chapter 4, where we have shown quantification and still photos.

Movie 9. Deletion of Rac1, Arp2/3 or WAVE complex in primary mouse melanocytes reduces the formation of long protrusions. This movie shows the motility data for cells depleted of Rac1 or components of the WAVE complex in vitro.

Movie 10. Rac1 is required for lamellipodia formation and cell migration of melanocytes on fibronectin coated 2D surfaces. This movie shows the

dynamics of melanocytes depleted of Rac1.

Movie 11. Deletion of Rac1 in melanoblasts delays cytokinesis in skin explants but not in culture dishes. This movie shows that Rac1 deleted cells have delayed cytoskinesis in skin explants but not in a culture dish.